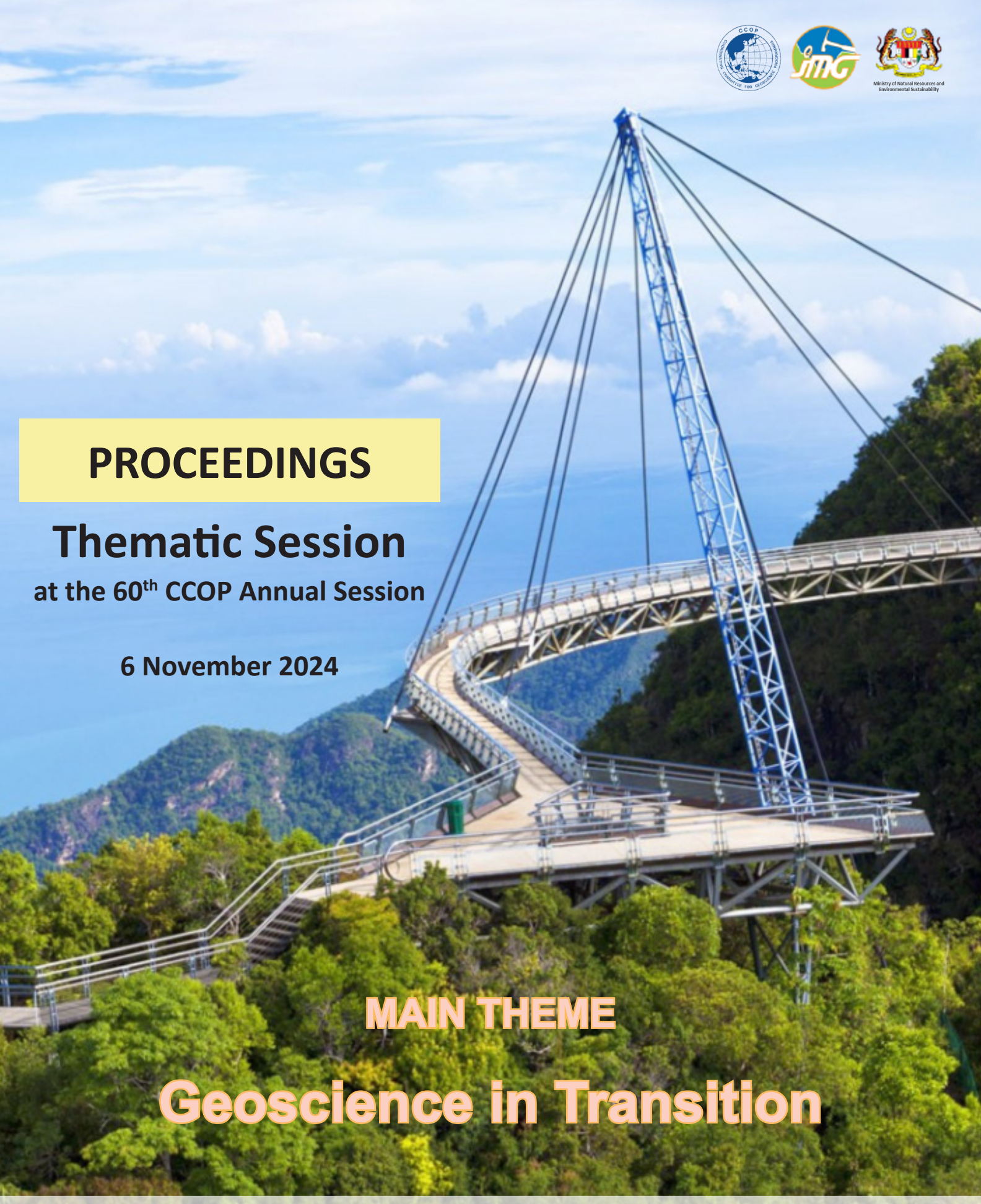

PROCEEDINGS

Thematic Session

at the 60th CCOP Annual Session

6 November 2024

MAIN THEME

Geoscience in Transition

Published by:

Coordinating Committee for Geoscience Programmes in East and Southeast Asia
CCOP Building. 75/10 Rama IV Road, Phayathai, Ratchathewi, Bangkok 10400, Thailand
https://www.ccop.asia/

June 2025

ISBN (e-book): 978-616-93191-3-9

PREFACE

The CCOP Thematic Session 2024 was held at the 60th CCOP Annual Session on 6 November 2024 in Langkawi, Malaysia, under the theme "Geoscience in Transition".

A total of 67 abstracts from seven CCOP Member Countries were submitted to the CCOP Technical Secretariat, leading to 67
in-person oral presentations. These were organized into three sub-sessions:

- Geoscience for Sustainable Future (24 oral presentations)
- Energy Transition (23 oral presentations)
- Climate Change and Disaster Resilience (20 oral presentations)

This proceedings volume includes 19 full papers showcasing the latest geoscience research from the region.
The CCOP Thematic Session 2024 successfully served as a platform for knowledge exchange, networking, and collaboration among CCOP delegates from Member Countries, Cooperating Countries, Cooperating Organizations, and other participants.

We sincerely appreciate the support of the Department of Mineral and Geoscience Malaysia (JMG), Petroliam Nasional Berhad (PETRONAS), Universiti Kebangsaan Malaysia (UKM), and the Geological Society of Malaysia (GSM) in organizing the event and preparing the abstract volume and proceedings.

At CCOP, we remain committed to supporting our Member Countries in accelerating progress toward the SDGs, with a strong focus on "Geoscience in Transition" — embracing innovation, digital transformation, and the energy transition. We will continue to strengthen our collective efforts to achieve sustainable development across the CCOP region.

Dr. Young Joo LEE
Director
CCOP Technical Secretariat

Contents

A review and discussion on the ground substrate research and application

Hongxing Hou[1], Hui Qin[1,*], Junhua Li[1], Bingzhang Ren[1], Peng Chen[1], Pengfei Shi[1], Guigang Zhang[2], Ming Li[2], Li Qi[3], Xin Du[3]

[1]Langfang Natural Resources Comprehensive Survey Center, China Geological Survey, Langfang, 065000, Hebei, China
[2]Department of Natural Resources Survey and Monitoring,
Ministry of Natural Resources of the People's Republic of China, Beijing, 100812, China
[3]Siping Academy of Modern Agricultural Sciences, Siping, 136000, Jilin, China
*Email: wjhjhhx@163.com

Abstract: As a kind of fundamental materials which mainly formed under the hypergenic geologic process, Ground substrate can support the formation of various natural resources. Ground substrate can be influenced by human activities to a certain extent. Ground substrate combined with water, air and biomass to form the ground substrate layer organically, and interacts with natural resources such as forests, grasslands and wetlands to maintain the normal operation of the Earth's surface ecosystem. As a new concept put forward according to the theory of Earth system science, Ground substrate effectively connects the hypergenic geologic process, human activities and the needs of ecological civilization construction, and provides a new path for the study of the relationship between geological processes and livable Earth. Black soil is a rare and precious natural resource and a special type of Ground substrate, which plays the production and ecological service function that cannot be ignored. There is great significance of Ground substrate survey for the protection and utilization of black soil. Important progress has been made in the research and application of Ground substrate, but there are still some research areas need scientists to explore.

Key words: Ground substrate, Earth's environment, Earth Critical Zone, black soil

INTRODUCTION

The Earth's environment is closely related to the existence and development of human beings. At present, the world is still faced with problems such as food shortage and degradation of land and water resources (Arantes *et al*., 2023; He *et al*., 2023; Amin *et al*., 2024; Saleem *et al*., 2024). It is urgent to have a thorough understanding of the current situation of the Earth's environment and its changing trend. Scientists have established the discipline system of Geoscience based on their long-term exploration of Earth. As a branch of Geoscience, the Earth system science plays more emphasis on the study of the operating mechanism among the various components of the Earth from a systematic perspective (Kump *et al*., 2014; Steffen *et al*., 2020; Wang *et al*., 2024). The near-surface spheres is the most direct and significant part of the interaction between the Earth's environment and human activities. In order to solve the problems of resource, environment and ecological, scientists are currently focusing more on the study of the Earth surface system (Zheng *et al*., 2024), and the Earth Critical Zone (NRC, 2001) is the operational framework of the Earth surface system research (Zhang *et al*., 2021). The Earth Critical Zone is based on the transformation of bedrock into regolith (including loose sediments such as weathered bedrock and sapropelic soil) and soil (Holbrook *et al*., 2019), which belong to Ground substrate. Therefore, Ground substrate is an important part of the Earth Critical Zone. Various materials in Ground substrate are mainly formed by geological processes, and their spatial distribution is controlled by geological background, geomorphic conditions, climatic characteristics and human activities (Hou *et al*., 2022; Zhu *et al*., 2024).

Previous studies on soil layer have been unable to satisfy the needs of food security and ecological environment protection, and there is an urgent need to understand the composition of matter in the deeper space and its evolution characteristics in time and space (Ge *et al*., 2020; Hou *et al*., 2021a; Ge *et al*., 2023; Hao *et al*., 2024). Ground substrate is an important complement to the study of the Earth Critical Zone. Since 2020, China has deployed Ground substrate surveys in major grain-producing areas and ecological functional areas, such as the black soil in northeast China, the red soil area in south China and mountainous plain transition area in north China, and identified the characteristics of Ground substrate in the those working areas (Hou *et al*., 2022; Wang *et al*., 2023).

Chinese scientists have also finished a lot of exploratory work in scientific research and application services (Shao *et al*., 2023; Yin *et al*., 2023; Ge *et al*., 2023; Yuan *et al*., 2023). In this paper, the concept and scientific connotation of Ground substrate are described systematically. Then the research actuality of Ground substrate is summarized. Finally, the application practice of Ground substrate survey in the black land of northeast China is summarized.

THE CONCEPT AND SCIENTIFIC CONNOTATION OF GROUND SUBSTRATE

The concept of Ground substrate was first proposed in 2020 by the *General Plan for the Construction of Natural Resources Survey and Monitoring System* (hereinafter referred to as the *General Plan*) of the Ministry of Natural Resources of China, which classifies Ground substrate as a part of natural resources (Hou *et al*., 2021a). According to the *Ground Substrate Classification Scheme* (hereinafter referred to as the *Classification Scheme*) issued by the Ministry of Natural Resources of China, Ground substrate refer to the basic materials that are currently exposed in the shallow surface of the Earth's land or the bottom of the water body, which are mainly formed by natural materials through natural process, and are or can be used to breed and support various natural resources such as forests, grasslands, water and wetlands (Hou *et al*., 2022). Ground substrate belong to natural resources and support other natural resources.

The concept of Ground substrate integrates the theoretical connotation of geology, geography, pedology, agronomy, ecology and other disciplines. Ground substrate has important scientific significance and research value and is an important part for the study of the Earth Critical Zone (Figure 1) (Chorover *et al*., 2007; Hou *et al*., 2022). For purpose of facilitate the survey and research of Ground substrate, according to the *Classification Scheme*, Ground substrate can be divided into four first classes: rock, gravel, soil and mud (Table 1; Figure 2). The secondary classes are divided into 14 secondary classes according to petrogenesis, particle composition, texture and origin. The tertiary classes are divided according to the existing division standards and naming principles of related subjects (Table 1). On this basis, four types of Ground substrate layer vertical configurations can be established, namely single-layer, double-layer, multi-layer configuration and weathering crust type configuration (Figure 2). The Ground substrate seamlessly cover the Earth's land surface or the bottom of the water body. Due to the complexity of geological processes and the diversity of geomorphic conditions, the types of Ground substrate and the depth of Ground substrate layer vary significantly in space (Zhu *et al*., 2024). From the perspective of investigative work, the depth of Ground substrate should comprehensively consider the types of natural resources supported by the Ground substrate layer and the maximum depth on which human activities can influence. Scholars generally divide the Ground substrate layer into surface layer, middle layer and deep layer. The surface layer is the production layer (0 ~ 2 m), which supports production activities. The middle layer is the ecological layer (2 ~ 10 m), which supports vegetation growth and biome activities. The deep layer is the sedimentary layer (10 ~ 20 m), which generally reveals the formation and evolution history of Ground substrate through the study of geological processes (Hou *et al*., 2022; Yin *et al*., 2023; Liu *et al*., 2024).

Ground substrate survey collects samples in the field, then obtain indicators and data through observation and laboratory analysis. The indicators of Ground substrate survey include spatial distribution characteristics, physical and chemical properties (such as structure, color, texture, bulk density, porosity, nutrient elements, heavy metals, pH value, pollutants concentration, etc.), mineral composition

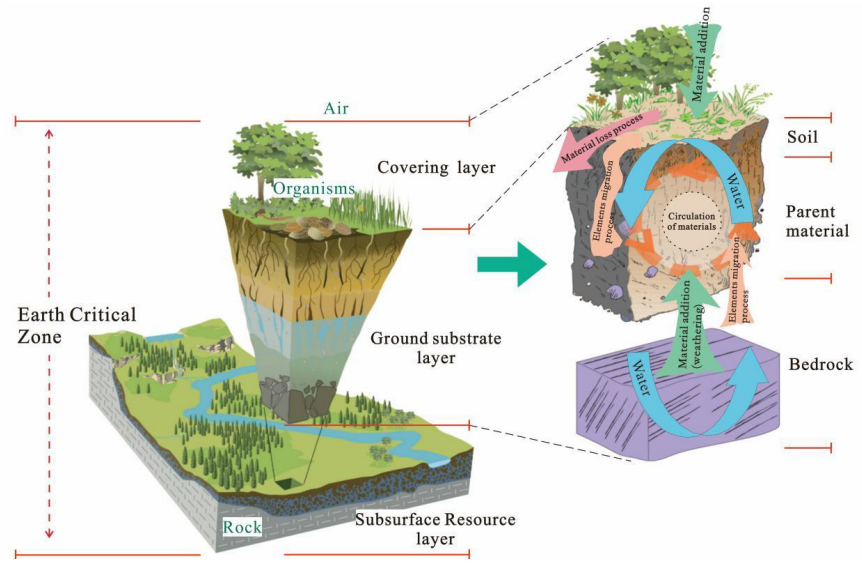

Figure 1: The position of Ground substrate in Earth Critical Zone (Chorover *et al*., 2011).

Table 1: The Ground Substrate Classification Scheme (Hou *et al*., 2021).

Number	First classes & its basis		Secondary classes & its basis		Tertiary classes & its basis	Description
1	According to the development process of the Ground substrate	(A) Rock				The naturally occurring mineral assemblage having a certain structural structure, a few consisting of natural glass, colloids or biological remains.
			Petrogenesis	(A1) Igneous Rock	Reference: Classification and nomenclature schemes of the rocks (GB/T17412.1/2/3-1998) (China national standard)	Formed by magma erupts to the surface or intrudes into the crust to cool and solidify.
				(A2) Sedimentary Rock		Under the conditions of the crust surface, the parent rock is the product of weathering, biological action, chemical action and some volcanic action, which is transported and deposited to form loose sediments in layers, and then consolidated into rocks.
				(A3) Metamorphic Rock		Under the condition of metamorphism, the rocks that already exist in the earth's crust (magmatic rocks, sedimentary rocks and previously formed metamorphic rocks) are transformed into rocks with new mineral assemblages and metamorphic structure characteristics.
2		(B) Gravel				It refers to the rock debris, mineral debris or a mixture of them formed by weathering, transport and deposition of the surface rocks, and the volume content of particles with size ≥2 mm is ≥75%.
			Particle composition	(B1) Boulder	Reference: Clastic grain classification of Quaternary sediments (Wentworth'classification).	The volume content of particles with size ≥256 mm is ≥75%.
				(B2) Coarse gravel		The volume content of particles with size 256 ~ 64 (include) mm is ≥75%.
				(B3) Medium gravel		The volume content of particles with size 64 ~ 4 (include) mm is ≥75%.
				(B4) Fine gravel		The volume content of particles with size 4 ~ 2 (include) mm is ≥75%.
3		(C) Soil				The loose sediments of the earth surface composed of different fractions of gravel (< 75% by volume), sand and clay in different proportions, which can grow plants under appropriate conditions.
			Texture	(C1) Regosols	Reference: Criteria for establishment of soil family and soil series in Chinese soil taxonomy (Zhang *et al*.,2013).	The volume content of gravel is 25% (include) ~ 75%.
				(C2) Sand		The volume content of gravel with different grades is < 25%, and the quality content of sand after screening gravel is ≥55%.
				(C3) Loam		The volume content of gravel with different grades is < 25%, after screening grave the quality content of sand is <55% and clay is <35%.
				(C4) Clay		The volume content of gravel with different grades is < 25%, after screening grave the quality content of clay is ≥ 35%.
4		(D) Mud				
			Origin	(D1) Silt	Reference: Classification and nomenclature of deep sea sediments (Zhang *et al*., 2006).	The modern sediments formed under the condition of microbial participation at the bottom of a lake, river, bay or offshore water body, rich in organic matter, with a natural water content greater than the liquid limit.
				(D2) Ooze		Deep-sea muddy sediments with a mass content of biological remains < 30%.
				(D3) Abyssal clay		A general term for fine pelagic sediment with a mass content of biological remains < 30%.

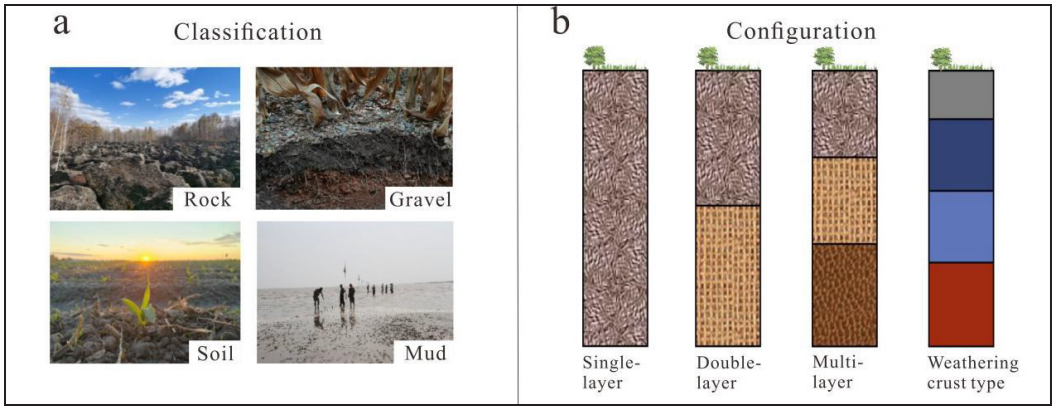

Figure 2: Ground substrate classification (a), and Ground substrate layer vertical configuration (b).

(such as major minerals, accessory minerals, clay minerals, etc.), biological characteristics (such as total biomass, microorganisms, fossils, etc.) of Ground substrate and water characteristics (such as water content, water body type, groundwater characteristics, water quality, etc.), landscape properties (such as geomorphic landscape, hydrological landscape, geological landscape, etc.) and ecological properties (such as vegetation type, ecological environmental issues, etc.) of the survey area. Each indicator has its own function. For example, nutrient elements are essential to the growth of vegetation, heavy metals can pollute arable land, texture is the most important physical property of the Ground substrate, clay minerals are used to study the material composition of the Ground substrate and the environment when the Ground substrate was forming, various landscape properties have important control on the spatial distribution and physical and chemical properties of the Ground substrate.

RESEARCH ACTUALITY OF GROUND SUBSTRATE

The research on Earth Critical Zone has experienced three stages: embryonic stage (2001-2006), initial stage (2007-2017) and rapid development stage (2018-2024) (Yang *et al*., 2024). Research emphases of Earth Critical Zone mainly focus on the classification, structure, process simulation, service and decision-making (Yang *et al*., 2024). The concept of Ground substrate provides a new idea for the study of Earth Critical Zone when the study of Earth Critical Zone is in a period of rapid development (Figure 3). The structure of Earth Critical Zone currently focuses on the subsurface structure and its formation mechanism (St Clair J *et al*., 2015; Yang *et al*., 2024), which is the main body of Ground substrate survey and research. Since the concept of Ground substrate was proposed, Ground substrate survey work has been carried out in important grain-producing areas and ecological functional areas in China, and related research work is also being carried out. At present, the research work on Ground substrate is in the initial stage, and has made important progress in many

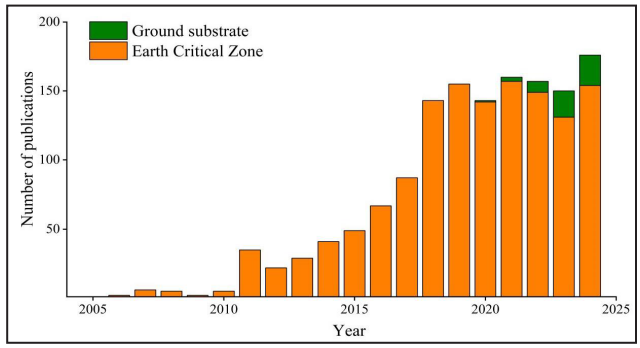

Figure 3: Literature publication of Ground substrate and Earth Critical Zone (from CNKI and Web of Science Core Collection).

aspects. In this paper, the key words “Earth Critical Zone” and “Ground substrate” were used to search the published articles, and the research directions of Ground substrate articles were sorted out. These directions mainly include the theoretical connotation, the technical method system of survey and research, scientific research and application of Ground substrate.

Theoretical connotation

At present, scholars mainly focus on four aspects of the theoretical connotation, including how to specify the bottom boundary of Ground substrate, the stratification principle and function of Ground substrate, the classification scheme of Ground substrate, and how to determine the properties of Ground substrate survey indicators system. The bottom boundary of the Ground substrate needs to be determined based on the function of the Ground substrate, which is affected by many factors, including the depth of plant roots, the position of underground variable temperate zone, weathering crust thickness, and the depth of water table (Hao *et al*., 2024). The depth of the Ground substrate layer is generally no more than 20 m, and the depth value will vary in special areas (Hao *et al*., 2024; Liu *et al*., 2024). The vertical range of Ground substrate is deeper than that of soil, which requires stratification research, and its functions are different at different levels (Hao *et al*., 2024;

Liu *et al*., 2024). Therefore, the stratification principle and bottom boundary of the Ground substrate are closely related to the function of the Ground substrate.

According to the *Classification Scheme*, the Ground substrate is divided into four primary classes: rock, gravel, soil and mud, and further divided into 14 secondary classes (Table 1). The tertiary classes refer to the existing disciplinary system and are further divided according to texture, particle size, physical and chemical properties and mineral composition. However, there is no clear and feasible tertiary classification method in the *Classification Scheme*. Since the area of sand in China exceeds 9×10^5 km^2, Hao *et al*. (2024) added "sand" to primary classes to highlight its importance. The tertiary classes of Ground substrate located in mountainous and plain areas were further divided in terms of the lithology, main mineral composition, weathering product, particle morphology and texture, pH, organic matter, etc. (Liu *et al*., 2023). Pei *et al*. (2024) puts forward a three-level system with high scientific and operability through scientific numbering in accordance with the practice of natural science terms being first, according to the existing research achievements and current technical standards. Liu *et al*. (2024) has explored the stratification of the Ground substrate survey and constructed the testing indicator system. The proposed vertical stratified testing indicator system for Ground substrate include 4 required indicators and N selected indicators (Liu *et al*., 2024).

Scientific research

In this part, scholars have explored the map compilation methods of Ground substrate, the significance of Ground substrate to geological environment, the constraint effect of Ground substrate on vegetation communities, and the genetic mechanism of ecological problems. Firstly, Ground substrate mapping is an important task of Ground substrate survey and research. For example, Shao *et al*. (2023) compiled the Ground substrate map of Ruyi River Basin in China, and divided Ground substrate into 9 types, including basalt, residual slope sand and gravel, eolian sand and bog silt etc. Meanwhile, the coupling relationship diagram between Ground substrate and covering layer was compiled, which supported the research on multi-layer interaction of Earth Critical Zone such as lithosphere, pedosphere, hydrophere and biosphere (Shao *et al*., 2023). Chen *et al*. (2024) has explored the classification standards and map compilation methods of Ground substrate in Inner Mongolia. Secondly, Ground substrate survey can reveal the characteristics of regional geological environment. Shao *et al*. (2024) studied the sedimentary characteristics and sedimentary environment of Ground substrate in Baiquan area, Songnen Plain, and clarified the sedimentary genetic types, paleoenvironment and formation times of the Ground substrate. Thirdly, the research of Yin *et al*. (2023) showed that under the same climate conditions, different Ground substrate types have obvious effects on vegetation types and their combinations, and the heterogeneity of Ground substrate can affect the type and spatial distribution pattern of vegetation. Fourthly, Ground substrate survey can make an important exploration into the formation mechanism of the ecological problems of black soil in northeast China. Ma *et al*. (2024) studied the causes of soil salinization and found that the presence of clay in this region hindered the migration of saltions. In addition, Ground substrate survey and research work on carbon storage (Chen *et al*., 2023) and the formation mechanism of black soil (Li *et al*., 2024) have also made useful explorations.

Working technique and method

Scholars have put forward a technical and methodological system of Ground substrate survey, which takes Earth system science and natural resource stereomodel as the guiding theory and takes demand-oriented, goal-oriented and problem-oriented as the basic principles. This system also fully absorbs the methods of previous related geological and soil surveys, which integrates collection, modification and utilization of data, remote sensing interpretation, comprehensive mapping, field survey, geochemical analysis and geophysical methods to study the types, physical and chemical properties, landscape attributes, formation process and change trend of Ground substrate (Figure 4).

Research achievements of Ground substrate focus on scientific problems and application services, which has practical significance and application value. This system provides a reference for the survey and research of Ground substrate (Hou *et al*., 2021; Ge *et al*., 2022). The application of the technical method system in black soil in northeast China has achieved great achievements: systematically identifying the spatial distribution of Ground substrate and the status quo of the quantity and quality of black soil resources (Hou *et al*., 2022; Liu *et al*., 2022; Wu *et al*., 2024). In addition, Chinese scholars have made meaningful scientific exploration in the Ground substrate survey in the drilling technology (Su *et al*., 2023; Li *et al*., 2024), sample analysis test method (Xie *et al*., 2024), remote sensing interpretation (Li *et al*., 2024), geophysics (Zhu, 2023) and other specific technical methods.

Application service

In respect of application service, scholars mainly discussed black soil protection and utilization, cultivated land suitability evaluation and high-standard farmland construction, etc. In northeast China, the fertile black soil with good properties is suitable for farming. However, due to the intensively use of black soil and the change of climate, the quality of black soil resources is deteriorating, such as the decrease of fertility, the deterioration of soil structure, the erosion of black soil resources, the salinization of soil and the desertification of soil. Ground substrate survey on black soil area identified the spatial structure characteristics of the Ground substrate and obtained important attribute

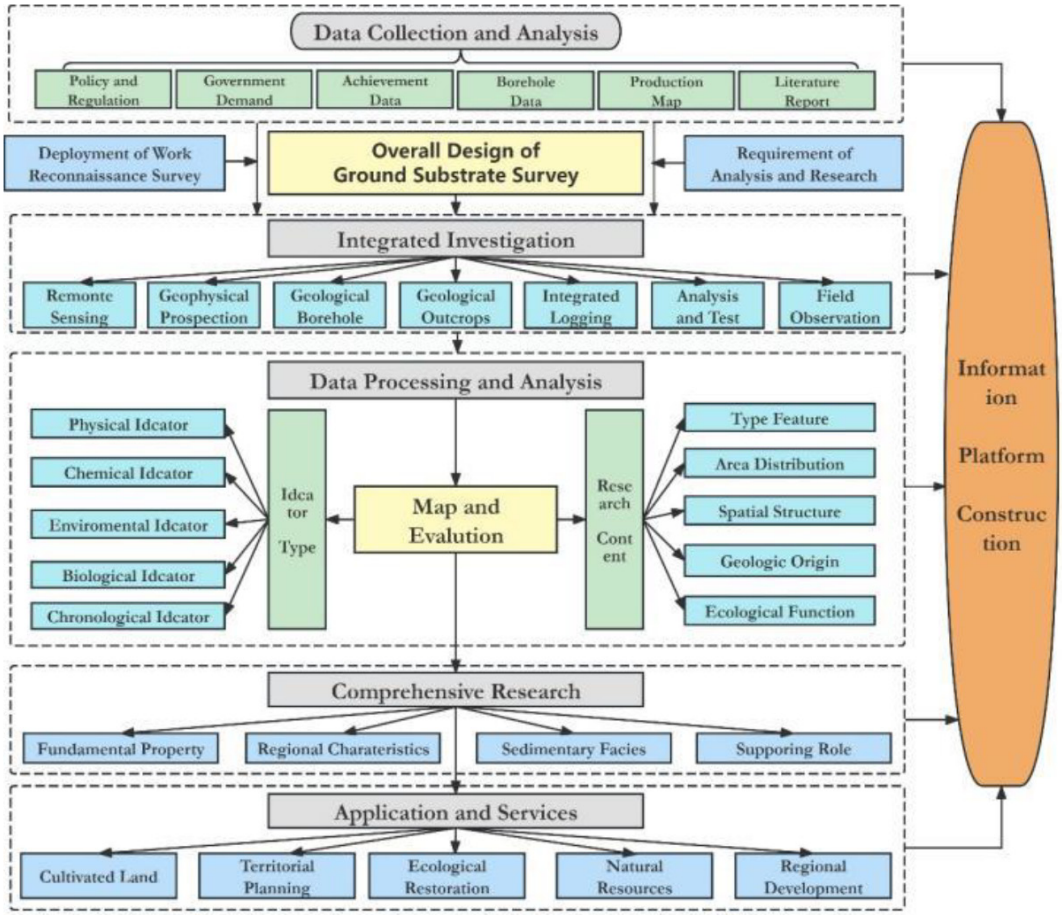

Figure 4: Technology roadmap of Ground substrate survey.

information such as physical and chemical properties of the black soil layer and its parent material layer, which can provide basic data support for the protection and utilization of black soil (Hou *et al*., 2022). The spatial distribution of Ground substrate are controlled by geological forces and geomorphic types. Ground substrate affects the change of regional land system components, such as water availability, solar energy acquisition and nutrient absorption, by influencing the direction and location of energy flow, and thus affects the cultivation suitability of land (Li *et al*., 2023). In 2005, China put forward the concept of high-standard farmland construction for the first time. High-standard farmland refers to "Cultivated land with flat plots, centralized contiguity, perfect facilities, efficient water saving, convenient operation, fertile soil, ecological friendliness, strong disaster resistance, and consistent with modern agricultural production and management mode, with guaranteed harvest and stable and high yield in drought and flood". Among them, important activities such as field regulation, disaster prevention and resistance, soil improvement, removal of obstacle layers, and soil fertilization are closely related to the content of Ground substrate survey (Ge *et al*., 2023).

In summary, important progress has been made in the research of existing literature. However, there are still some areas where the research is not enough: (1) Research on Ground substrate has not been able to effectively support the research on the Earth Critical Zone. (2) The stratified classification of Ground substrate and the indicator system of survey and research have not formed a unified standard. (3) Ground substrate map types, mapping methods and expression styles of map need to be optimized. (4) The level of Ground substrate survey techniques and methods should be improved. (5) The research on the formation and evolution of Ground substrate as well as the influence of Ground substrate on vegetation is not deep enough. (6) The practicability and operability of Ground substrate survey and research achievements need to be improved. In addition, according to the published articles, Ground substrate researchers are mainly from China, and their articles are mainly published in Chinese academic journals. In the future, we will continue to strengthen related research work, and actively disseminate the experience and results of Ground substrate survey and research abroad, so as to carry out international exchanges and cooperation.

PRACTICAL APPLICATION OF GROUND SUBSTRATE SURVEY AND RESEARCH - A CASE STUDY OF BLACK SOIL AREA IN NORTHEAST CHINA

Overview of the region

Since 2021, CGS has implemented Ground substrate survey on black soil in northeast China, with a total area of 41.17×10^4 km^2 (Figure 5). The black soil in northeast China is mainly distributed in Songliao Plain and Sanjiang Plain. Songliao Plain is surrounded by the Greater Khingan Mountains, Lesser Khingan Mountains and Changbai Mountains respectively, while Sanjiang Plain is surrounded by Lesser Khingan Mountains and Wanda Mountains respectively. The overall topographic and geomorphologic pattern of northeast China was basically formed in the early and middle Neogene, and the tectonic and geomorphologic patterns were further developed in the Quaternary period. Sanjiang Plain is a basin formed by Tertiary depression on the basement composed of pre-Paleozoic metamorphic rocks, Paleozoic and Mesozoic sedimentary rocks. The climatic conditions in northeast China are mainly characterized by the cold-temperate continental monsoon type.

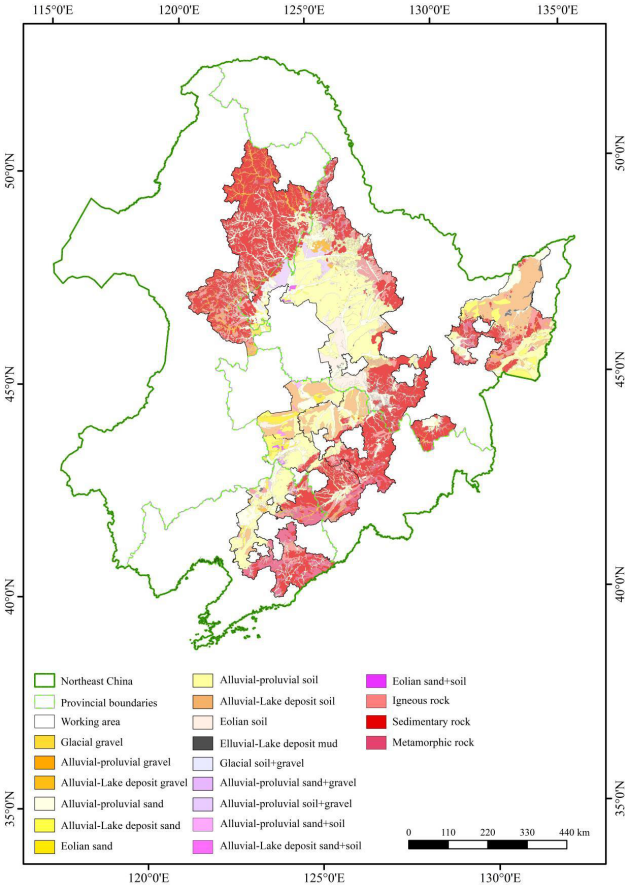

Figure 5: Spatial distribution map of Ground substrate layer configuration in northeast China.

Sample collection, analysis and testing

The drilling sample layout method mainly considers the layout density, uniformity, representativeness of the sample points and the depth setting of the drilling holes at the point, as well as the analysis and test indicators setting of the samples. The layout method of sample points is mainly aimed at scientifically revealing the spatial structure characteristics of the Ground substrate at a certain depth and the service functions of Ground substrate. Our work has obtained more than 30,000 survey points, a total of more than 1.2 million data. The analysis and testing indicators of the samples include texture, bulk density, pH value, organic carbon and total carbon, major elements, trace elements, rare earth elements, etc. Certain test indicators can be increased or decreased according to the actual situation of the specific survey area, the purpose of the survey, the direction of supporting services and the existing ecological problems.

Ground substrate characteristics and black soil resources

Genetic type characteristics

The formation of Ground substrate is mainly controlled by geological background and topographic features. The survey area of the Ground substrate on black soil in northeast China is divided into three levels: The first level is based on the large-scale geomorphic form formed by the crustal fluctuation which controls the geomorphic pattern; The second division is based on the specific geomorphic type; The third level is further refined, mainly reflecting the genetic of the Ground substrate. For example, "Songnen Plain subsidence zone (first level) low plain (second level) allustrine deposit (third level) Ground substrate area". According to this basic principle, the working area is divided into 8 first-level Ground substrate areas and 39 second-level Ground substrate areas. The genetic types of Ground substrate in the working area include alluvial, lacustrine, diluvial, eolian, glacial, residual and slope deposits. Each genetic type forms a certain Ground substrate layer configuration regularly.

Characteristics of spatial structure

The terrain of Songnen Plain is relatively gentle, the Ground substrate genetic types are mainly alluvial and lacustrine, and the Ground substrate configuration is mainly loam+clay or whole loam. The terraces and floodplains distributed along rivers are mainly alluvial and diluvial, mostly loam+sand or loam+fine gravel, which are affected by hydrodynamic action. In the eastern part of Liaohe Plain, aeolian sand is distributed. In Sanjiang Plain, the main Ground substrate type is whole loam, and the local soil is loam+sandy. In mountainous and hilly areas, it is dominated by residual and slope deposits. Due to the obvious relief and large slope of the terrain, the Ground substrate layer is often thin and covered on

top of rocks. The configuration of the Ground substrate is characterized by soil+rock, coarse bone soil+rock, and there is bare bedrock where the loose sediment is missing (Figure 5).

Distribution of black soil resources

The survey targets of black soil area not only find out the spatial structure of the Ground substrate, but also identified the distribution of black soil resources. With reference to the indicators of "black soil layer thickness ≥20 cm" of FAO International Black Soil Alliance and the domestic standard "organic matter content ≥15 g/kg", we delineated a total area of 387,500 square kilometers of black soil using nearly 30,000 boreholes and profile survey results. Spatially, the quality level of black soil resources has obvious spatial variability. The data show that the maximum thickness of the black soil layer is 610 cm, the average thickness is 56.85 cm, the maximum content of organic matter in the black soil layer is 583.75 g/kg, and the average is 37.05 g/kg. On the whole, the thickness and organic matter content of the black soil layer decrease with the latitude get lower, and the most fertile black soil was mainly distributed in the east of Songnen Plain (Figure 6).

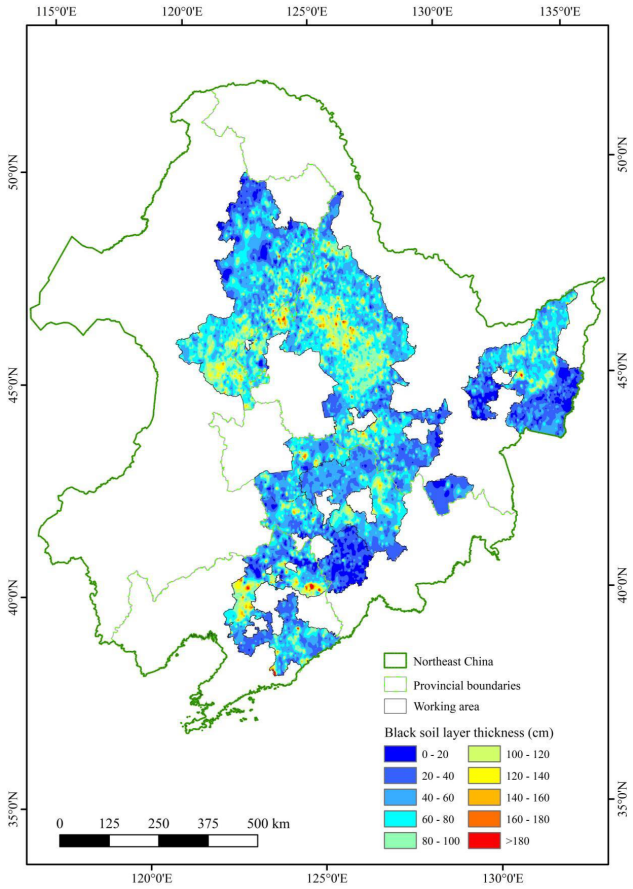

Figure 6: Spatial distribution map of black soil layer thickness in northeast China.

Control and influence of Ground substrate on black soil resources

Ground substrate and black soil resource distribution

According to the type of Ground substrate, the rock areas mainly distributed in hills and mountains, the average thickness of surface black soil is 39.06 cm, and the average content of organic matter is 47.52 g/kg. The gravel mainly distributed in the upper reaches of rivers and the piedmont transition zone. The average thickness of black soil is 60.59 cm, and the average content of organic matter is 54.56 g/kg. The sand mainly distributed in the plain area, where the average thickness of surface black soil is 61.78 cm and the average content of organic matter is 37.19 g/kg. The soil mainly distributed in the palaeo-lake and aeolian soil areas, where the average thickness of surface black soil is 59.63 cm, and the average content of organic matter is 32.67 g/kg. The mud mainly distributed in lakes and marshes, where the average thickness of black soil is 70.03 cm, and the average content of organic matter is 57.33 g/kg. From the perspective of Ground substrate layer configuration, alluvial soil, aeolic soil and other single layer configuration areas, the Ground substrate layer has stable structure, as well as strong water and fertilizer retention ability, which is conducive to the development of black soil. The average thickness of surface black soil is 53.89 cm, and the average content of organic matter is 29.84 g/kg in those areas. Alluvial soil+sand, soil+gravel and other double-layer structure area with good permeability and water permeability, which is also conducive to the development of black soil. The average thickness of black soil is 55.33 cm, the average content of organic matter is 24.35 g/kg in those areas. In the weathering crust type configuration areas such as bare rock and soil+rock, the surface process is dominated by weathering and denudation. The average thickness of surface black soil is 39.06 cm, and the average content of organic matter is 47.52 g/kg in those areas.

Ground substrate and degradation of black soil

Influenced by natural conditions and human activities, the ecological problems of black soil in northeast China includes: water and soil loss, land desertification, land salinization, etc. In soil and water loss areas, the Ground substrate layer configuration mainly consists of soil+rock, soil+sand and soil+gravel, etc. In these areas, the support stability of sand and gravel under the soil is poor, hence the black soil is prone to loss. The structure of the Ground substrate layer configuration in the desertification area is mainly sand and soil+sand. The soil in these areas is susceptible to erosion, then the sand layer will expose to the surface. The Ground substrate layer configuration in salinized area is predominantly clay and clay+silt, and the Ground substrate texture in these areas is dense, easy to accumulate salts. The Ground substrate layer in the "broken gravel" area is sand and gravel, and the Ground substrate layer in these areas has a loose structure and poor stability.

Therefore, to solve the problem of black soil degradation, we should deeply understand the type and configuration of the Ground substrate, and the corresponding measures and suggestions for management and protection should duly proposed.

CONCLUSIONS

The proposal of the Ground substrate provides a new path for the study of the mutual relationship between geological processes and habitable Earth, and is a new direction and part of Earth system science research.

Scientists have made important explorations in the theoretical connotation, scientific research, working technology methods and application services of Ground substrate. The results of Ground substrate research can make important contributions to food security and ecological environment protection. In the future, it is necessary to continue to carry out Ground substrate survey work in typical areas and continue to explore the key research areas of Ground substrate.

Except for human activities and other natural environment conditions, the types and layer configuration of Ground substrate are the main controlling factors for different black soil degradation problems.

ACKNOWLEDGEMENTS

The authors would like to thank for the support and funding of the project (1:250,000 Ground Substrate Survey in North Jiangsu Plain/DD20242041) and for that we would like to express our appreciation to China Geological Survey of the Ministry of Natural Resources of China. We would like to thank the staff of the Ground substrate survey team for the collection and analysis of samples from the black soil Ground substrate survey. In addition, many thanks to editorial office and anonymous reviewers for their valuable comments that have improved the quality of this manuscript. Their time and efforts dedicated to this review are greatly appreciated.

AUTHORS CONTRIBUTION

Hong Xing Hou: manuscript draft, literature review, analysis, and interpretation; Hui Qin: manuscript draft, guidance, analysis, and interpretation; Junhua Li: analysis, editing, and review; Bingzhang Ren, Peng Chen, Pengfei Shi: analysis, editing, and review; Guigang Zhang, Ming Li, Li Qi, Xin Du: analysis, editing, and review.

DECLARATION OF COMPETING INTEREST

The authors declare that there is no conflict of interest in relation to this article.

REFERENCES

Amin, M., & Romshoo, S.A., 2024. Assessment and monitoring of land degradation indicators and processes using a geospatial approach. Modeling Earth Systems and Environment, 11(1), 1-19.

Arantes, L.T., Arantes, B.H.T., Sacramento, B.H., Costa, H.F.D., Oliveira, R.A.D., Simonetti, V.C., Silva, D.C.D.C., & Lourenco, R.W., 2023. Application of spatial environmental indicators in the assessment of degradation potential of water resources in water basins. Environmental Monitoring and Assessment, 1-34.

Chen, L., Guo, H.Q., Shang, X.Y., Li, F., Zhang, C., Liu, Z., & Dong, S., 2023. Change Trend and Determinants of Organic Carbon Storage in Ground Substrate of Xinle City. Heilongjiang Agricultural Sciences, 2023(3), 34-40.

Chen, P., Hou, H.X., Ma, J.C., Sun, H., & Jing, Y., 2024. Exploration of classification standards and map compilation methods for ground substrate: A case study of Yalu River Basin in Inner Mongolia. Geological Survey of China, 11(2), 51-61.

Chorover, J., Kretzschmar, R., Garcia-Pichel, F., & Sparks, D.L., 2007. Soil biogeochemical processes within the critical zone. Elements, 3(5), 321-326.

Daniel, deB. Richter Jr., & Megan, L.Mobley, 2009. Monitoring Earth's Critical Zone. Science, 326(5956), 1067-1068.

Hao, A.B., Yin, Z.Q., Li, H.Y., Lu, Q.Y., Peng, L., Shao, H., Jiang, Q.D., Zhao, X.F., Liu, J.F., Pang, J.M., Yang, K., Chen, P., Kong, F.P., Hou, H.X., & Lu, M., 2024. The scientific connotation and theoretical framework of ground substrate. Acta Geolofica Scnica, 98, 1-13. https://doi.org/10.19762/j.cnki.dizhixuebao.2024439.

Ge, L.S., & Yang, G.C., 2020. New Field of Natural Resources Survey and Monitoring: Ground Substrate Survey. Natural Resource Economics of China, 33(9), 4-11+67.

Ge, L.S., Hou, H.X., & Xia, R., 2022. Construction of Technical System for Ground Substrate Survey of Natural Resources. Geomatics World, 29(5), 20-27.

Ge, L.S., & Xia, R., 2023. High-Standard Farmland Construction: Ground Substrate Survey-Based Solutions. Natural Resource Economics of China, 36(5), 4-13.

Holbrook, W.S., Marcon, V., Bacon, A.R., Brantley, S.L., Carr, B.J., Flinchum, B.A., Richter, D.D., & Riebe, C.S., 2019. Links between physical and chemical weathering inferred from a 65-m-deep borehole through Earth's critical zone. Scientific Reports, 9(1), 1-11.

Hou, H.X., Ge, L.S., Sun, X., Kong, X.B., Lu, W.H., Qin, T., Kong, F.P., Yang, B.H., & Yang, K., 2022. A study on the application of ground substrate in the survey and evaluation of China's black soil resources: Based on ground substrate survey in Baoqing, Heilongjiang province. Journal of Natural Resources, 37(09), 2264-2276.

Hou, H.X., Zhang, S.J., Lu, M., Zhang, Z.Y., Sun, X., Qin, T., Wang, X., Zhang, J.L., Shao, X.K., & Wang, W., 2021a. Technology and Method of the ground substrate layer survey of natural resources: Taking Baoding area as an Example. Northwest Geology, 54(3), 277-288.

Hou, H.X., Ge, L.S., Sun, X., Lu, W.H., Lu, M., Qin, T., Yang, B.H., Yang, K., & Kong, F.P., 2021b. Discussion on the contents of ground gubstrate survey and the index system of elements and attributes. Open Journal of Natural Science, 9(4), 433-442.

He, F., Mohamadzadeh, N., Sadeghnejad, M., Ingram, B., & Ostovari, Y., 2023. Fractal Features of Soil Particles as an Index of Land Degradation under Different Land-Use Patterns and Slope-Aspects. Land, 12(3), 1-14.

Kump, L.R., Kasting, J. F., & Crane, R.G., 2014. The Earth System. Pearson Education Limited, London. 462 p.

Li, J.H., Hou, H.X., Wang, W., Ren, B.Z., Zhang, G.G., Li, M., Qi,

L., Du, X., Shi, L.F., Zhan, Z.D., & Xi, G.Y., 2024. Geochemical Characteristics of the Ground Substrate Layer in the Black Soil Area of the Northern Songnen Plain and Its Implications for the Provenance of Black Soil. Acta Geoscientica Sinica, 1-14. https://link.cnki.net/urlid/11.3474.P.20241206.1401.004.

Li, Z.Y., Li, L., Liu, N., Tang, X.H., & Wang, J.J., 2024. Remote sensing interpretation of surface substrates using multi-source data and image segmentation:a case study in the northern area of Dianjiang. Bulletin of Surveying and Mapping, 2024(S1), 166-171.

Liu, J.F., Zhao, X.F., Hou, H.X., Qin, T., Chen, Z.S., Xu, L.M., Yang, K., Kong, F.P., Liu, X.H., Lu, B., Li, Z.Q., Liu, J., Bao, R., & Hao, A.B., 2024. Exploration on the Stratification of the Ground Substrate Survey and the Design and Construction of Its Testing Indicator System. Rock and Mineral Analysis, 43(1), 16-29.

Liu, Q.J., Liu, Y.X., Wang, Y., Wang, L.F., & Yan, G.X., 2023. A proposed scheme for third-level classification of ground substrate. Urban Geology, 18(01), 1-8.

Liu, H.B., Kong, F.P., Zhao, J., He, J.B., & Liu, B.W., 2022. Exploration and Experiment of Surface Substrate Investigation Technique: A Case Study of Black Soil Investigation in Baoqing County, Heilongjiang Province. Geomatics World, 29(6), 1-5.

Li, X.L., 2023. Study on Land Type Classification and Cultivated Land Suitability Evaluation in China. China University of Geosciences(Beijing), Beijing, China. 176 p.

Li, Y.Z., Wu, J., Sun, X., Su, J.X., Guo, G.P., Han, T., Yang, Y.Q., & Zhang, Q., 2024. Application research of backpack drill in the black soil surface matrix survey. Drilling Engineering, 51(S1), 307-312.

Ma, M., Zuo, Z., Han, Y.D., Qiu, Y., & Qiao, M.D., 2024. A research on soil salinization - alkalization genesis of its ground-substrate characters in Songnen Plain. Remote Sensing For Natural Resources, 1-12. https://link.cnki.net/urlid/10.1759.P.20241112.0834.008.

National Research Council (NRC), 2001. Basic research opportunities in earth science. National Academy Press, Washington DC, USA.

Saleem, A., Anwar, S., Nawaz, T., Fahad, S., Saud, S., Rahman, T.U., Khan, M.N.R., & Nawaz, T., 2024. Securing a sustainable future: the climate change threat to agriculture, food security, and sustainable development goals. J.Umm. Al-Qura Univ. Appll. Sci., 1-17. https://doi.org/10.1007/s43994-024-00177-3.

St Clair, J., Moon, S., & Holbrook, W.S., 2015. Geophysical imaging reveals topographic stress control of bedrock weathering. Science, 350(6260), 534-538.

Su, X.T., Ran, L.J., Zhu, Q., Feng, Y.W., Zhang, Y.X., Zhang, S.Y., & Sun, X.Y., 2023. Method and application research on drilling sampling techniques of surface substrate. Geological Review, 69(6), 2039-2046.

Shao, H., Wang, Y.N., Yin, Z.Q., Xing, B., Jin, A.F., Pang, J.M., & Wang, R.F., 2023. An exploration on survey and mapping of ground substrate in Ruyi River Basin, Bashang Plateau, Chengde City. Hydrogeology & Engineering Geology, 50(2), 150-159.

Shao, X.K., Hou, H.X., Ren, B.Z., Shi, L.F., Zhan, Z.D., Xi, G.Y., Li, J.H., Cao, L.Y., & Gao, Y., 2024. Sedimentary characteristics analysis and paleoenvironmental restoration of the ground substrate in Baiquan County, Qiqihar area, Songnen Plain. Geological Bulletin of China, 43(9), 1498-1514.

Steffen, W., Richardson, K., Rockström, J., Schellnhuber, H.J., Dube, O.P., Dutreuil, S., Lenton, T.M., & Lubchenco, J., 2020. The emergence and evolution of Earth System Science. Nat. Rev. Earth Environ., 1, 54-63.

Wang, X., Lu, M., Hou, H.X., Sun, X., Wang, H.H., Qiao, Y.Y., & Liu, Y., 2023. Analysis of spatial heterogeneity of soil substrate in mountainous plain transition area: A case study of Eastern Yi County of Hebei Province. Geological Survey of China, 10(3), 60-66.

Wu, P., Yuan, Y.J., Zhang, M.S., & Han, X., 2024. Practice and Investigation of the Technical Procedure for Surface Matrix Survey-Utillzing the Surface Survey of Weinan Municipality in Shananxi Province as an Illustrative Eample. Geology Of Shaanxi, 42(1), 7-12.

Xie, X., Lu, B., Zhao, W.Z., Lv Cheng, He, T., Zhang, Y., & Han, C.H., 2024. Determination of Iodine in Black Soil Surface Matrix Survey Samples by Inductively Coupled Plasma Mass Spectrometry(ICP-MS) with Microwave Digestion. Chinese Journal of Inorganic Analytical Chemistry, 14(7), 980-985.

Yang, S.H., Song, X.D., Wu, H.Y., Wu, K.N., & Zhang, G.L., 2024. A Review and Discussion on the Earth's Critical Zone Research & Status Quo and Prospect. Acta Pedologica Sinica, 61(2), 308-318.

Yin, Z.Q., Chen, Z.R., Li, X., Wei, X.F., & Shao, H., 2023. Connotation, layering, mapping and supporting objectives of the integrated survey of ground substrates. Hydrogeology & Engineering Geology, 50(1), 144-151.

Yuan, G.L., Hou, H.X., Liu, J.Y., Wang, Q., Guo, X.Y., & Jia, Y.H., 2023. Introduction to the Methods of Ecology−Geological Survey for Servicing Ecological Civilization: Example from Ecology−Supporting Sphere Survey. Northwestern Geology, 56(3), 30-38.

Zhang, F.Y., Li, A.C., Lin, Z.H., Zhang, W.Y., Zhang, Z.Y., & Zhang, J., 2006 Classification and nomenclature of deep sea sediments. Oceanologia et Limnologia Sinica, 37(6), 517-523.

Zhang, G.L., Wang, Q.B., Zhang, F.R., Wu, K.N., Cai, C.F., Zhang, M.K., Li, D.C., Zhao, Y.G., & Yang, J.L., 2013. Criteria for establishment of soil family and soil series in Chinese soil toxonomy. Acta Pedologica Sinica, 50(4), 826-834.

Zhang, G.L., Zhu, Y.G., & Shao, M.A., 2019. Understanding sustainability of soil and water resources in a critical zone perspective. Sci. China Earth Sci., 62, 1716-1718.

Zhang, G.L., Song, X.D. & Wu, K.N., 2021. A classification scheme for Earth's Critical Zones and its application in China. Science China Earth Sciences, 64 (10), 1709-1720.

Zhen, Y.F., Guo, Z.T., Jiao, N.Z., Mu, M., Piao, S.L., Fu, S.Y., Yang, D.H., & Zhu, M.Y., 2024. A holistic perspective on Earth system science. Science China Earth Sciences, 67(10), 3013-3040.

Zhu, C.G., 2023. Application Research of Joint Inversion of Vertical Electric Sounding Data and Rayleigh-wave Dispersion Data in the Ground Substrate Layer Survey. Chang'an University, Xi'an, China. 74 p.

Zhu, X.S., Pei, X.L., Wang, W., Zhang, Z.Y., Sun, W.T., Ni, S.B., & Gong, W.X., 2024. Spatial heterogeneity characteristics of ground substrate in hilly area and its impact on vegetation ecology. Geological Bulletin of China, 43(9), 1544−1554.

Geochemical characterization of Surat Thani hot springs: Implications for health and geotourism development

Jakratorn Kaewpradit*, Jitisak Premmanee

Geological Conservation and Management Division, Department of Mineral Resources, Bangkok, Thailand
* Email: Jakratorn@dmr.mail.go.th

Abstract: Approximately 114 hot springs have been documented throughout Thailand. The geochemical properties are needed to support tourism and public health initiatives. This study focuses on Surat Thani, where hot springs are famous for spa activities. Hot spring bathing, also known as balneotherapy, has health and cultural significance, leading to the critical research question: Which hot springs in Surat Thani possess the ideal geochemical properties for spa development, and how do these properties align with health-related concerns?

The hypothesis emerged that hot springs with specific geochemical compositions may offer more significant health benefits, thus holding potential for tourism development. The study collected and analysed 14 water samples from 9 hot springs, measuring essential ions (Ca^{2+}, K^{+}, Mg^{2+}, Na^{+}, CO_3^{2-}, HCO_3^{-}, Cl^{-}, SO_4^{2-}) and total dissolved solids (TDS). The geochemical facies were identified using Piper's diagram, while Gibbs' diagram helped trace the origin of the waters.

The results indicated four distinct geochemical facies. Saline springs like Siam Hot Spring Chaiya, Pak Dan, and Rattana Kosai were influenced by seawater, while others were derived from precipitation and rock formations. These profiles were compared to ideal chemical properties for spa use, identifying specific springs suitable for further development.

The findings will be reported to local authorities to guide future actions, such as engaging local communities in sustainable tourism development. Further studies should explore the health impacts of these geochemical properties to enhance public health and geotourism.

Keywords: Geochemical characteristic, hot springs, saline hot springs, Surat Thani

INTRODUCTION

Hot springs are geological phenomenon indicating high thermal energy under the earth's surface (Raksaskulwong, 2008). Most hot springs in Thailand are considered to be tourist spots and often used for recreational proposes such as bathing, massaging or cooking (boiling eggs). Only one at Fang district, Chiangmai province, northern Thailand has been developed for power generation by the Electricity Generating Authority of Thailand since 1988 (iEnergyGuru, 2023), through a cooperation works with the Department of Mineral Resources (DMR) and Chiangmai University (EGAT, 1997; Subtavewung, P. *et al*., 2005).

Through cooperative works of many international organizations and the focal organization, DMR of Thailand during 1977 to 1989 (Raksasakulwongs, 2013) lead to document more than 114 hot springs throughout Thailand (Subtavewung, P. *et al*., 2005; Raksaskulwong, 2008). Results show that hot springs in the northern Thailand display higher surface temperature than in the south, ranging from 40ºC to 100ºC in the north while from 40ºC to 80ºC in the south (Lund *et al*., 2021; Ngansom, W. & Dürrast, H., 2021).

Surat Thani is a province in the central part of southern Thailand and has many attractions such as Kho Samui, Koh Phangan, Koh Tao, Rajjaprabha Dam/Lake, Wat Suan Mokkhaphalaram or Rattana Kosai saline hot spring. Moreover, Surat Thani hosts 9 hot springs, the highest number in southern Thailand (Ngansom, W. *et al*., 2019) and consisting of both saline and fresh water hot springs. So, it is interesting to map or classify those hot springs through chemical components in which may help to properly promote the utilization's. Furthermore, Division of Mineral Resource Analysis and Identification of the DMR used to analyse and report some chemical components of those hot springs in the past (Charaj, W., 2003; Raksaskulwong, M., 2003), and wish to update the assays with current analytical technologies and methodology.

GEOLOGICAL BACKGROUND OF THE STUDY AREA

Surat Thani covers approximately 3,830 km^2 with 160 kilometers eastern shoreline to the Gulf of Thailand (Figure 1). It's topography composes of 3 terrains: (1) western mountain range adjacent to Ranong and Phangnga

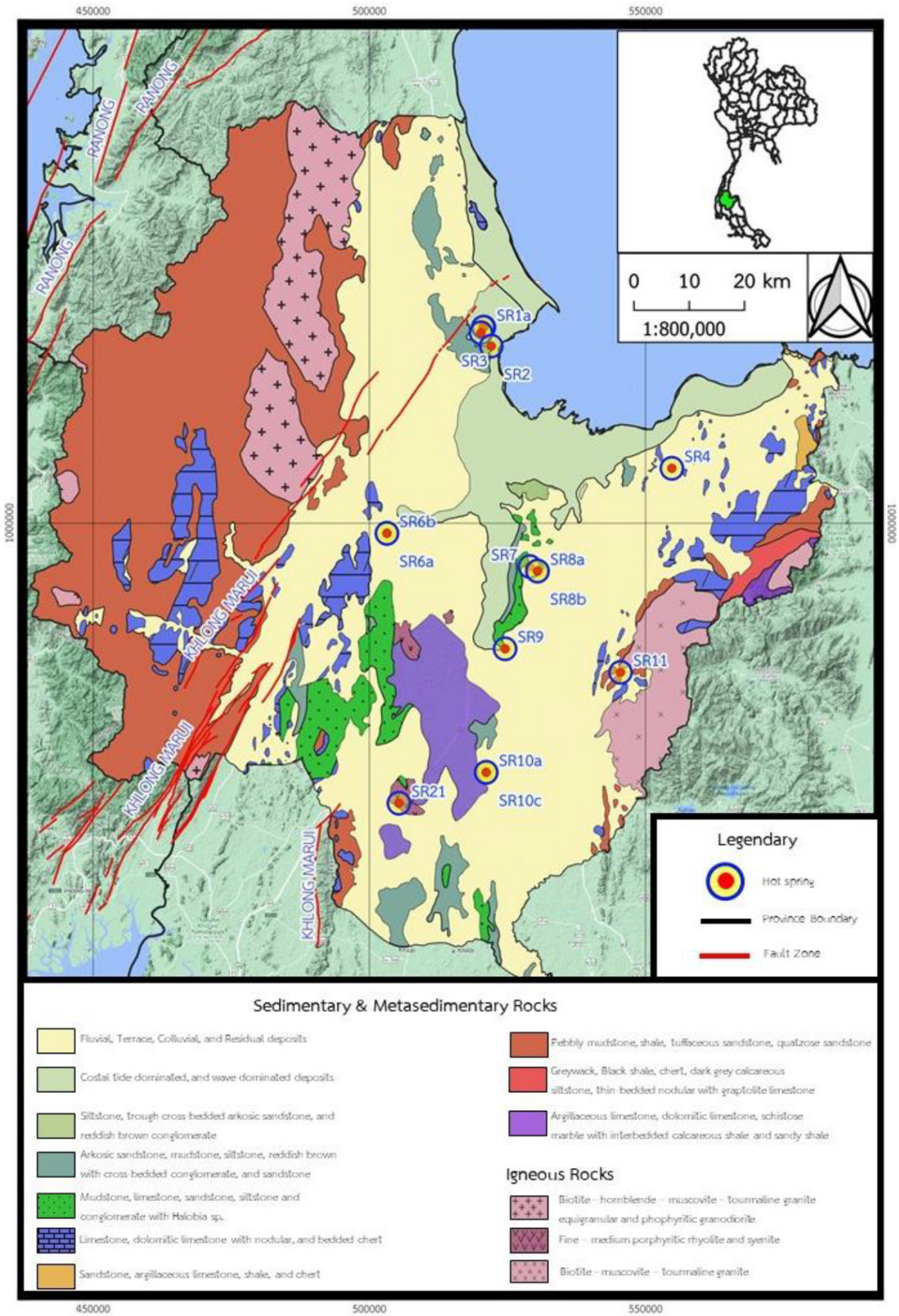

Figure 1: The study area and geological mapping of Surat Thani province, Southern Thailand, shows geological strata that can be recognized.

provinces, (2) relatively flat area in the central part with Tapi and Khiri Rat rivers where draining to the gulf of Thailand in the east, and (3) eastern mountain range (Khao Louang) adjacent to Nakorn Sri Thammarat province.

Based on published geological map (DMR, 2023), Surat Thani comprise of rocks range from Ordovician to Recent sedimentary and metamorphic rock intruded by Triassic and Cretaceous granite. A widespread sedimentary units are Kaeng Krachan Group of Carboniferous-Permian Period, including pebbly mudstone, shale, siltstone, chert, tuffaceous sandstone, quartzose sandstone, and dark grey, greenish gray, and brown limestone with brachiopods, bryozoans, corals, and crinoid. Quaternary–Holocene terrestrial and flood sediment always cover those units.

Two main fault zones control structural geology of the province, the NNE-SSW direction Ranong and Khlong Marui faults. They are considered to be active strike slip fault (Watkinson *et al*., 2008*).* It is presumed that these 2 fault zones control most of the hot springs in this area as well as provide conduits for circulation of water from both precipitation and sea water.

GEOLOGY OF HOT SPRING

Hot springs are natural springs heated by geothermal energy. Erfurt, P. (2021) has classified hot springs into 2 origins: volcanic and non-volcanic related. The volcanic ones usually occur near active volcanic areas and the heat derives from magma chamber nearby. Fumarole often seen nearby and the surface water temperature is very high (>180ºC). The non-volcanic ones occur away from the active volcanic area and the surface water temperature is lower (25 - >100ºC). The heat may derive either from heat remaining within the intrusive body or radioactive decay from the rock formation. Geothermal gradient under the continental crust may contribute some heat into the water also.

Most of the hot spring water originate from surface water either from precipitation or sea water, small portion may squeeze from the rock formation. The water seeps through voids and cracks within the rock formation, picks up the heat from sources, and moves upward to the surface as hot springs water. Depth of this circulation processes may be about 2-3 kilometers depend on pressure and thermal gradient. In Thailand where absence of volcanic activities, Geothermica Italicana Slr. (1984) has classified hot springs into 2 groups, first group found on granitic outcrop and the other on sediments outcrop with granitic body at depth. The first group exhibits high pressure and surface temperature with less amount of water quantity vice versa for the second group.

Many studies of Surat Thani hot springs on physical and chemical characteristics (Charaj, W., 2003; Raksaskulwong, M., 2003; Ngansom, W. *et al.*, 2019; Ngansom, W. *et al*., 2020; Ngansom, W. & Dürrast, H., 2021, Klamthim, P. & Dürrast, H, 2022) indicated that hot springs water exhibit low enthalpy (low water quantity and pressure) and sea water from the Gulf of Thailand has assimilate with precipitated fresh water on land forming the hot spring water.

MATERIAL AND METHODS

Based on Charaj (2003), there are 9 hot springs in Surat Thani province, designated SR1 to SR9. Eight of them were re-sampled in 2023 but the SR4. However, a new hot spring was found during the field trip (SR10), so, total 9 hot springs were sampled. Furthermore, some of the hot springs were collected more than 1 sample. Table 1 shows details of those samplings and the field measurements. In addition, a spring water, SR21, was sampled, but it is not considered as hot spring due to the surface temperature is less than 40 degree.

Sampling methods follow the National Environment Board No. 8 (B.E. 2537) on the determination of water quality standards in surface water. The 1,000 mL polypropylene bottles cleaned and rinsed with deionized water were used for sampling. Always, each sampling, the bottle will be rinsed with the hot spring water prior collection and collect 2 bottles of a sample. The first bottle will be use for field measurement of pH, conductivity and Total Dissolve Solids (TDS) without additive substance. The second bottle will be filled with 5 ml of 1:1 nitric acid to preserve metal content in the water. Then the samples will sent to laboratory in Bangkok for further analysis.

Table 2 and 3 shows the analysis methods and results for all of the samples by the Division of Mineral Resources Analysis and Identification, DMR. The methods follow standards set up by the United States Environmental Protection Agency (US.EPA) and the American Water Works Association (AWWA).

RESULTS AND DISCUSSION

Chemical composition

Surface temperature range from 40-70°C average at 51.3°C while pH range 6.4-7.2 average at 6.9 (Table 1). These parameters ranges are suitable for simple utilization, such as mixing with local water supply making temperature less than 40°C, which can be use to hot bathing. Local residents widely apply public and private bathing for their therapeutic benefits, particularly for relieving muscle tension, enhancing blood circulation, and overall relaxation.

The 4 cations used for characterization hot spring water are Ca^{2+}, Mg^{2+}, K^{+} and Na^{+}. The Ca^{2+} varies from 14.9 to 616.4 mg/L, with 288.4 average. The average K^{+} present at 30.9 mg/L with range 4 to 115 mg/L. SR7 shows the highest K^{+} concentration at 115 mg/L, but SR9, SR10a, SR10b, and SR10c are low K^{+} at 4 mg/L. The mean value of Mg^{2+} is 40.9 mg/L, varies from 0.6 to 85.9 mg/L. The Na^{+} content ranges from 2,733 to 6 mg/L with 694.1 average, SR1a and SR1b show very high values at 2,733 and 2,567 mg/L, respectively.

There is no detection of CO_3^{2-} in terms of $CaCO_3$ concentration, but there are presented in HCO_3^{-} in $CaCO_3$

Table 1: The hot spring location and physical properties of Surat Thani, Southern Thailand. TDS refers to total dissolve solids.

Hot Spring Code	Hot Spring Name	Location (WGS-84)		Surface Temperature (°C)	pH	Conductivity (ms/cm)	TDS (mg/L)
		East (m)	North (m)				
SR1a	Siam hot spring Chai Ya	520758	1035187	40.6	6.74	20.74	10,145
SR1b		520623	1035164	67.8	6.43	18.93	9,275
SR2	Tarn Nam Ron saline hot spring	522086	1031789	40.0	6.76	2.118	1,039
SR3	Pak Dan hot spring	520223	1034173	43.0	7.15	12.77	6,258
SR6a	Tham Sing Khon hot spring	503178	998215	51.3	7.02	0.97	477
SR6b		503203	998194	42.8	7.11	0.98	480
SR7	Rattana Kosai hot spring	529070	992236	70.0	6.84	18.98	9,301
SR8a	Ban Khao Plu hot spring	530446	991417	61.0	6.85	2.11	1,035
SR8b		530465	991436	61.7	6.90	2.11	1,032
SR9	Khao Tork hot spring	524585	977493	58.4	6.86	1.62	794
SR10a	Song Pee Nong hot spring	521170	955333	49.8	6.95	0.57	279
SR10b		521170	955333	44.2	7.08	0.57	279
SR10c		521170	955333	46.3	7.10	0.57	277
SR11	Plum Phun Sarb hot spring	545486	973266	41.4	7.24	0.38	189
SR21	Sai Sopha hot reservoir	505355	949795	33.2	6.77	0.61	794
SRS	Seawater (Klamthim, P. & Dürrast, H., 2022)	522993	1058851	29.2	7.88	-	-
			Minimum	33.2	6.43	0.38	189
			Maximum	70.0	7.24	20.74	10,145
			Average	50.1	6.92	5.60	2,743

concentration, ranging 246 to 83 mg/L of $CaCO_3$ and averaging at 173 mg/L of $CaCO_3$. The Cl^- content shows 2 distinct groups, 2 to 19 mg/L (10 samples: average 7.9) and 4,266 to 7,243 mg/L (4 samples: average 6,156). Fluoride contents vary from 8.3 to 1.8 mg/L with 3.5 average, SR4 shows the highest value of 8.3 mg/L.

Hot spring chemical classification

Surat Thani hot springs are classified by the relationship of cation concentrations (Ca^{2+}, K^+, Mg^{2+}, Na^+), anion concentrations (CO_3^{2-}, HCO^{3-}, Cl^-, F^-), namely Piper's diagram (Piper, A.M., 1944) as displayed in Figure 2. There are four geochemical facies based on the following diagram;

(1) Sodium – potassium chloride – sulfate type, predominantly composed of sodium, potassium, chloride, and sulfate in hot spring water. This hot spring can be called non-carbonate alkaline water, comprising SR1a, SR1b, SR3, and SR7.

(2) Calcium-magnesium chloride-sulfate type or non-carbonate hardness water, including SR2, SR6a, SR6b, SR8a, SR8b, and SR9, combines the main components of calcium and sulfate.

(3) Calcium – magnesium bicarbonate type consists of SR10a, SR10b, SR10c, and SR21. Calcium and bicarbonate ions are the primary components in hot spring water. These can be named carbonate-hardness water.

(4) Sodium – potassium bicarbonate type comprises SR11, representing the sodium, potassium, and bicarbonate concentrations that are the main components of hot spring water, namely carbonate alkali water.

VARIATION DIAGRAM

The variation diagram (Figure 3) shows the relationships between major elements (Na^+, K^+, Mg^{2+}, Ca^{2+}) and chloride (Cl^-), which highlight the influence of seawater on several hot springs. Specifically, SR1a, SR1b, SR3, and SR7 are indicated by higher Na^+ and Cl^- concentrations, indicating

Table 2: The standard methods and detection limits of geochemical analysis at the Division of Mineral Resources Analysis and Identification, DMR, Thailand.

Parameter	Methods	Analyzer	Detection limit (mg/L)
Ca^{2+}	US.EPA 3050B	Inductively Couple Plasma - Optical Emission Spectrometer (ICP-OES)	0.5
K^{+}			2
Mg^{2+}			0.1
Na^{+}			1
Cl^{-}	APHA/AWWA/WEF. Standard Method for the Examination of Water and Wastewater. 23rd ed.2017.part 4500-ClB.	Titration	-
F^{-}	US.EPA 9214	Ion - Selective Electrode analyzer	0.2
pH, Conductivity, TDS, Salinity	-	Ion Selective Electrode (ISE)	-
SO_4^{2-}	AWWA 4500-SO_4^{2-} D	UV - visible Spectrophotometer	20
HCO_3^{-} , CO_3^{2-} concentration as $CaCO_3$	Standard Methods for the Examination of Water and Wastewater 2320: Alkalinity	Titration	-

Table 3: The chemical concentration of Surat Thani hot spring samples. ND refers to non-detect and DL refers to detection limit.

Hot Spring Code	Ca^{2+} (mg/L)	K^{+} (mg/L)	Mg^{2+} (mg/L)	Na^{+} (mg/L)	CO_3^{2-} (mg/L $CaCO_3$)	HCO_3^{-} (mg/L $CaCO_3$)	Cl^{-} (mg/L)	F^{-} (mg/L)	SO_4^{2-} (mg/L)
SR1a	616.4	99	85.9	2,733	ND	109	7,243	2.9	1,095
SR1b	595.3	92	81.4	2,567	ND	122	6,846	2.9	971
SR2	296.5	12	48.8	32	ND	83	13	3.5	1,169
SR3	467.6	60	64.3	1,721	ND	172	4,266	2.0	575
SR6a	184.6	5	20.3	13	ND	244	6	1.8	294
SR6b	176.5	5	20.1	13	ND	246	6	1.8	393
SR7	418.0	115	65.9	2,495	ND	104	6,267	3.2	738
SR8a	384.2	12	52.0	31	ND	166	19	3.5	1,591
SR8b	397.4	12	51.2	31	ND	165	18	3.4	1,657
SR9	251.2	4	31.2	10	ND	156	4	3.4	1,252
SR10a	84.0	4	17.3	7	ND	215	2	4.0	96
SR10b	74.7	4	16.9	7	ND	213	2	3.9	120
SR10c	73.3	4	16.7	6	ND	216	2	4.0	112
SR11	14.9	5	0.6	52	ND	158	7	8.3	ND
SR21	77.6	DL	20.0	6	ND	230	4	0.5	120
SRS	149.9	122.2	383.8	3219	-	91.5	5,611	*NA*	816.1
Minimum	14.9	4	0.6	6	-	83	2	0.5	96
Maximum	616.4	115	85.9	2,733	-	246	7,243	8.3	1,657
Average	274.1	31	39.5	648	-	173	1,647	3.3	733

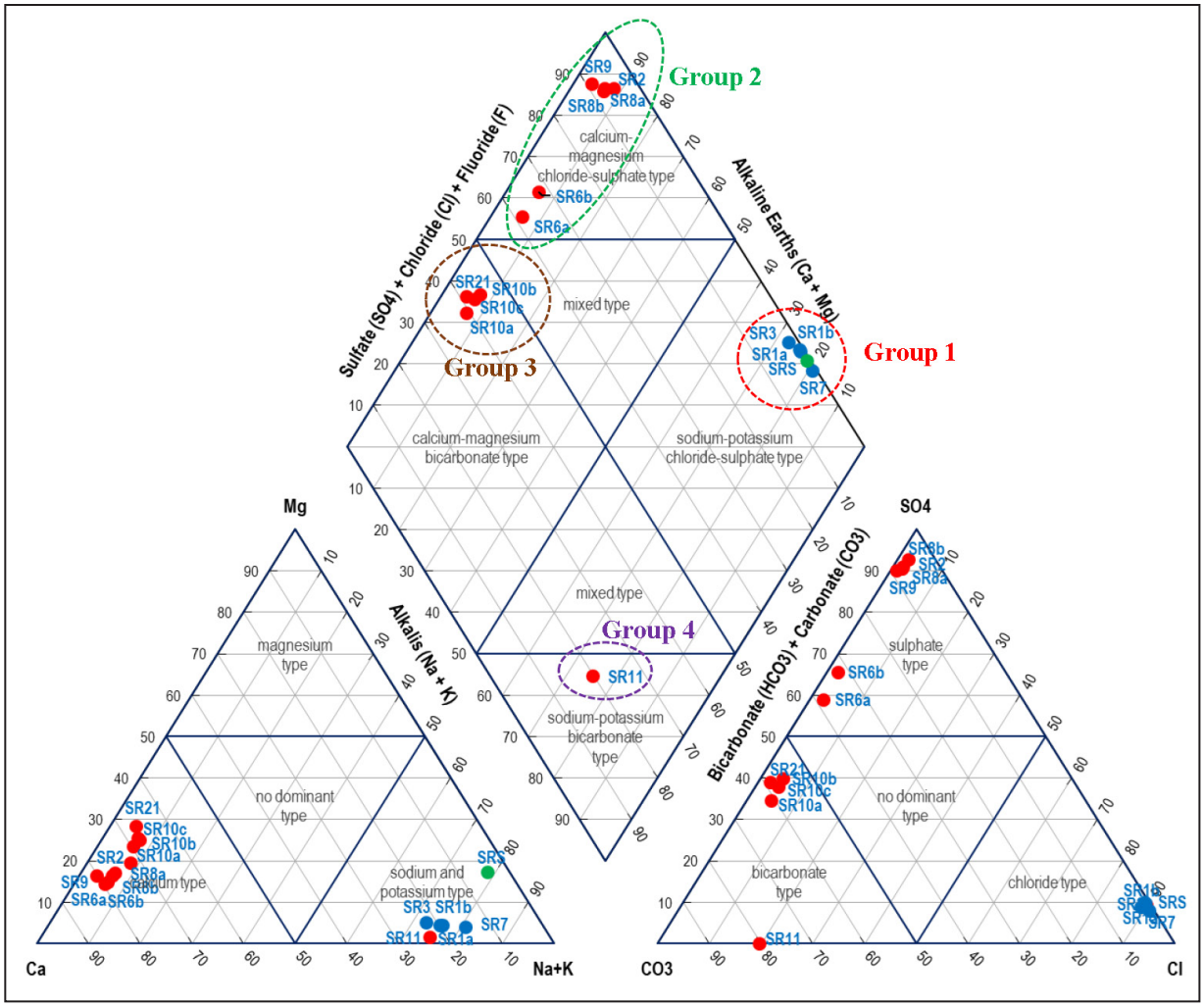

Figure 2: Surat Thani hot springs are classified by Piper's diagram (Piper, A.M., 1944).

significant seawater intrusion into the hot spring system. The K^+, Mg^{2+} and Ca^{2+} diagrams further confirm the seawater intrusion, as these ions are typically abundant in seawater and tend to increase proportionally with Cl^- concentrations when seawater is present.

In contrast, non-saline springs in the region exhibit lower Cl^- and Na^+ levels and are primarily influenced by water-rock interactions rather than seawater mixing. These springs are enriched with Ca^{2+} and HCO_3^-, reflective of carbonate mineral dissolution within local geological formations, and suggest a precipitation-dominated recharge source.

Water–rock interaction

The water-rock interaction is described by the primary mechanisms and factors that control the chemical composition of the elements. The diagram was suggested by Gibbs, J.R., 1970 (Figure 4), which used the chemical concentration that can be defined as atmospheric precipitation, rock dominance, and evaporation-crystallization processes. The Surat Thani hot springs are classified into two groups based on chemical origin. The dominance of evaporation precipitation is remarkable because of the influence of seawater mixing, which is SR1a, SR1b, SR3, and SR7. Other samples are rock-dominated chemical mixing.

CONCLUSION

The study of Surat Thani's hot springs based on 14 hot water samples collected from 9 hot springs were assaying for Ca^{2+}, K^+, Mg^{2+}, Na^+, CO_3^{2-}, HCO^{3-}, Cl^- and SO_4^{2-} and TDS (total dissolved solid) to signify geochemical characteristics. The hot springs can be classified into two geochemical facies driven by different sources of mineralization and chemical composition.

(1) The saline group, categorized as non-carbonate alkaline water, suggests potential for leveraging therapeutic applications. The mineral content derived from seawater influence that sodium – potassium chloride – sulfate are dominant from the seawater intrusion, which is Siam Hot Spring Chaiya (SR1a, SR1b), Pak Dan (SR3), and Rattana Kosai hot springs (SR7) that can be called non-carbonate alkaline water.

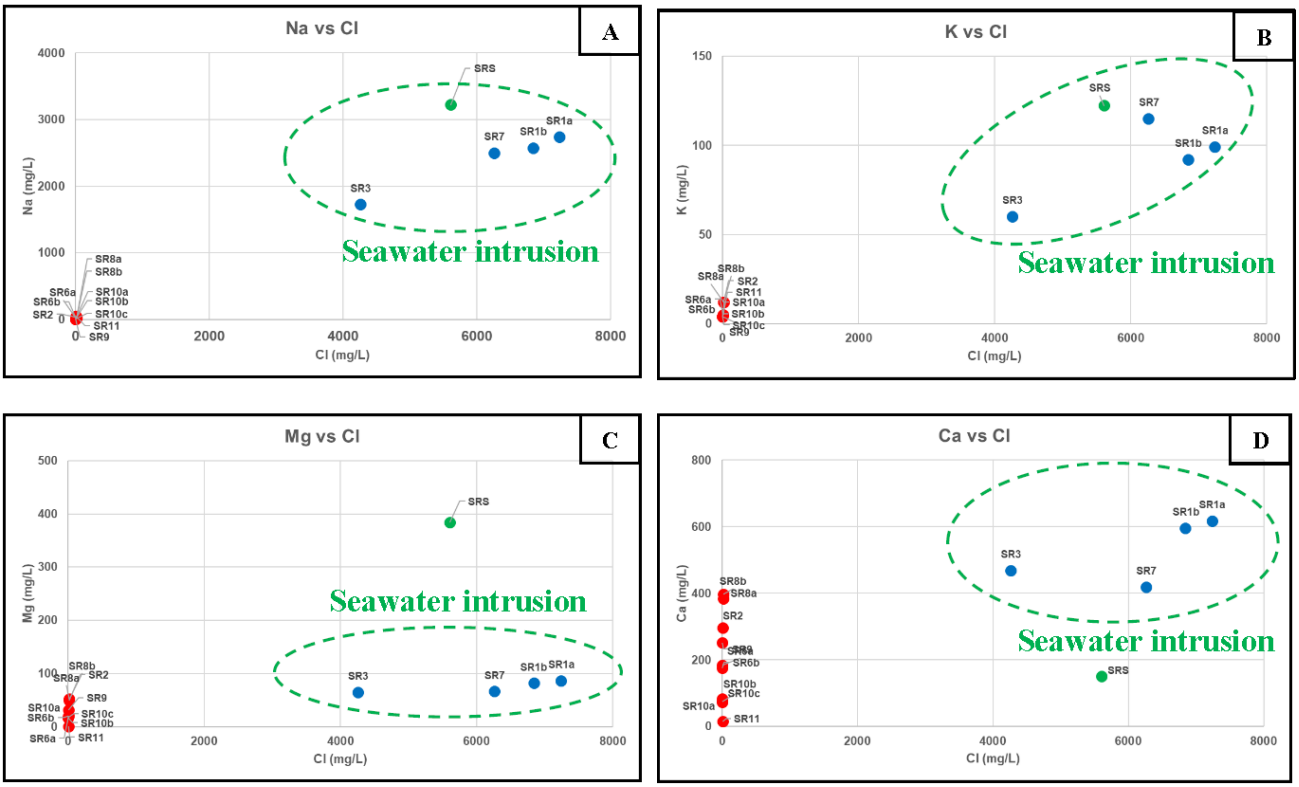

Figure 3: The variation diagram of the concentration of cation plots against Cl^- in mg/L (A.) Na^+ (B.) K^+, (C.) Mg^{2+}, and (D.) Ca^{2+}.

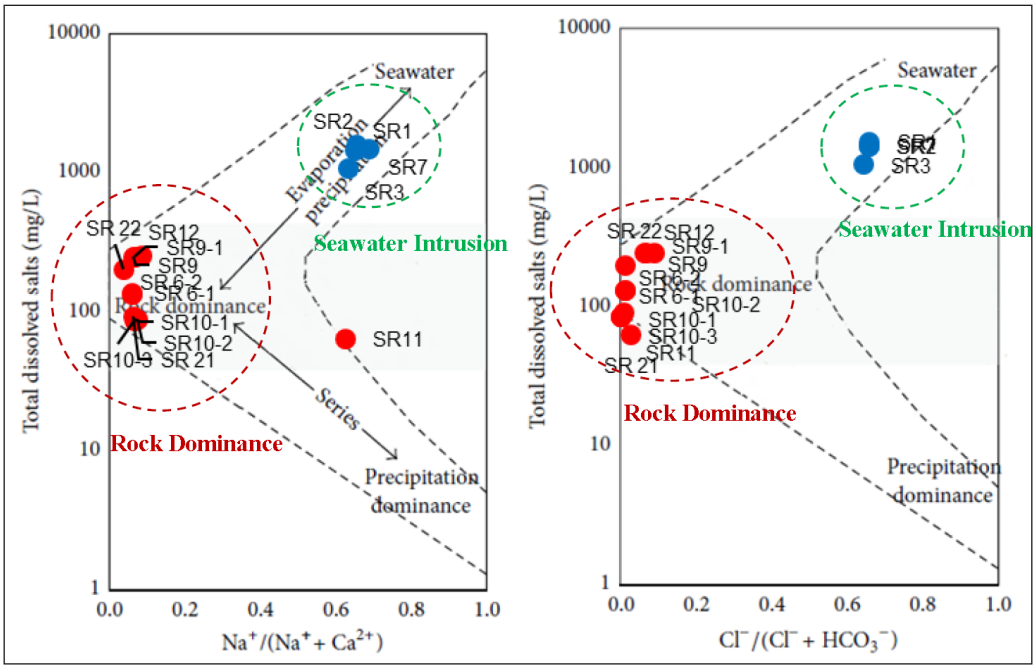

Figure 4: Gibb's diagram shows the chemical of water-rock influence with the hot spring (Gibbs, J.R., 1970).

(2) The non-saline hot spring group exhibits a more varied ionic composition, where calcium and bicarbonate ions dominate. It aligns with non-saline water profiles, making it suitable for a broader range of wellness applications. The variable of major concentration is the dominance of element mixing from the rock formation in the hot spring system, comprising of Tarn Nam Ron (SR2), Tham Sing Khon (SR6a, SR6b), Ban Khao Plu (SR8a, SR8b), Khao Tok (SR9), Song Phi Nong (SR10a, SR10b, SR10c), Pherm Phun Sab (SR11) and Sai Sopha (SR21) hot springs.

This characterization underscores the potential of Surat Thani's hot springs for geotourism development, particularly in health and wellness geotourism. Seawater-influenced springs offer a unique therapeutic appeal due to their mineral content, while non-saline springs provide diverse options for spa and balneotherapy applications. Further research into the specific health impacts of these mineral properties can enhance the public health benefits of these natural resources and support sustainable tourism initiatives involving local communities.

REFERENCES

Charaj, W., 2003. Chemical properties of hot springs in Thailand, Division of Mineral Resources Analysis and Identification, Department of Mineral Resources. 80 p.

Electric Generating Authority of Thailand (EGAT), 1997. Update on Geothermal development in Thailand. 12th meeting on geothermal power development, ASEAN Power Utilities/ Authorities. Chiang Mai, Thailand, 4 p.

Erfurt, P., 2019. Geoheritage, Geoparks and Geotourism Conservation and Management Series. Springer.

Erfurt, P., 2021. The Geoheritage of Hot Springs. Springer.

Geotermica Italiana Slr., 1984. Geothermal Reconnaissance Survey of Northern Thailand, Department of Mineral Resources, Thailand.

Giggenbach, W.F., 1988. Geothermal solute equilibria. Derivation of Na-K-Mg-Ca geoindicators. Geochimica et Cosmochimica Acta, 52, 2749–2765. https://doi.org/10.1016/0016-7037(88)90143-3.

Gibbs, J.R., 1970. Mechanisms controlling world water chemistry. Science (80-)170, 1088–1090.

Greene, A.C., Wright, M.H., & Aldosary, H.A., 2016. Bacterial diversity and metal reducing bacteria in Australian thermal environments. In: Méndez-Vilas A. (Ed.), Microbes in the spotlight: recent progress in the understanding of beneficial and harmful microorganisms. BrownWalker Press, Boca Raton.

Klamthim, P. & Duerrast, H., 2022. Geochemical Signatures of Hot Springs in Southern Thailand. The 3rd International Conference On Natural Sciences, Mathematics, Applications, Research, and Technology (ICON SMART 2022), Bali, 3-4 June.

Lund, J.W., & Toth, A.N., 2021. Direct utilization of geothermal energy 2020 worldwide review. Geothermics 2021, 90, 101915.

Ngansom, W. & Dürrast, H., 2019. Assessment and Ranking of Hot Springs Site Representing Geothermal Resources in Southern Thailand using Positive Attitude Factors. Chiang Mai Journal of Science, 46(3), 592 – 608.

Ngansom, W., Pirarai, K., & Dürrast, H., 2020. Geological setting and hydrogeothermal characteristic of the Kapong non-volcanic hot spring area in Southern Thailand. Geothermics 2020, 85, 101746.

Ngansom, W. & Dürrast, H., 2021. Geochemical Characterization of Hot Spring Waters from Southern Thailand as the Base for Geothermal Energy Utilization. Environment Asia, 14(3), 37 – 49.

Piper, A.M., 1994. A graphic procedure in the geochemical interpretation of water – analyses. Transactions American Geophysical Union, 25, 914-928.

Premmanee, J., 2023. Compilation of hot springs chemical assays in Krabi, Phangnga and Surat Thani Provinces. Division of Mineral Resources Analysis and Identification, Department of Mineral Resources.

Pollution Control Department, Ministry of Natural Resources and Environment, 1994. Announcement of the National Environment Board No. 8 (B.E. 2537) on the determination of water quality standards in surface water sources.

Raksaskulwong, M., 2003. Geothermal distribution and development in southern Thailand. In: Exploration and Exploitation of geothermal resources as dispersive type energy. The 5th Asian Geothermal Symposium (AGS5), 79 - 85.

Raksaskulwong, M., 2008. Thailand Geothermal Energy: Development History and Current Status. 8th Asian Geothermal Symposium (AGS8), 39 – 46.

Subtavewung, P., Raksaskulwong, M., & Tulyatid, J., 2005. The Characteristic and Classification of Hot Spring in Thailand. World Geothermal Congress 2005 (WGC2005). 7 p.

Walkinson, I., Elder, C., & Hall, R., 2008. The kinematic history of the khlong marui and Ranong Faults, southern Thailand. Journal of Structural Geology 2008, 30(12), 1554 – 1571.

Wright, M.H., Patel, B.K.C., & Greene, A.C., 2012. Thermophilic bacteria from paralana hot springs in the northern flinders ranges of South Australia. Conference paper 10.13140/ RG.2.1.2765.5525.

Accumulated phosphate in calcareous sediment is an effective indicator of terrestrial load, linked to coral density and bleaching: A case study from Sekisei Lagoon, Japan

Mariko Iijima[1,*], Jun Yasumoto[2], Takashi Nakamura[3], Akira Iguchi[1], Shugo Watabe[4], Ko Yasumoto[4]

[1] Geological Survey of Japan, National Institute of Advanced Industrial Science and Technology (AIST) , Ibaraki, Japan
[2] Faculty of Agriculture, University of the Ryukyus, Okinawa, Japan
[3] Faculty of Science, University of the Ryukyus, Okinawa, Japan
[4] School of Marine Biosciences, Kitasato University, Kanagawa, Japan
*Email: m.iijima@aist.go.jp

Abstract: In recent years, coral reefs have been experiencing a significant decline on a global scale, with widespread coral bleaching becoming increasingly prominent. One of the primary factors contributing to the diminished resilience of corals is the damage caused by excessive nutrient runoff, particularly from agricultural activities. This nutrient pollution accelerates coral degradation, impacts biodiversity, increases water turbidity, and promotes bacterial growth, which in turn can lead to coral diseases. While the effects of nitrogen on coral health have been extensively studied, the role of phosphorus—often overlooked due to its low concentration in seawater—remains poorly understood. It has been observed that coral reefs accumulate terrestrial phosphates within their calcareous sediments. We propose using this accumulated phosphate as a novel indicator to assess the terrestrial influence on coral reef ecosystems. In the Sekisei Lagoon, located between Ishigaki and Iriomote Islands, a coral monitoring project under the Ministry of the Environment has been established. This project has set up 31 fixed monitoring points where annual surveys are conducted to evaluate coral coverage and other biological factors. The objective of this study is to explore the relationship between the levels of accumulated phosphate and the biological data obtained from these monitoring efforts.

Sediment samples were collected three times between 2021 and 2023 from fixed observation points within Sekisei Lagoon. The concentration of phosphate leached from the calcareous sediments was measured. The phosphate concentration per gram of sediment (μg/g) was calculated as the accumulated phosphate value, and its relationship with biological data, such as genus-specific coral density (both adult and juvenile corals), the proportion of bleached corals, and the coverage of major algae, was investigated.

The results showed no significant annual variations at the observation points. However, high accumulated phosphate levels were consistently observed at observation points along the coasts of several islands, suggesting a possible influence from effluent from aquaculture facilities on these islands. In contrast, observation points outside the reef tended to show lower accumulated phosphate values. In several coral genera, a significant negative correlation was found between the accumulated phosphate value and genus-specific coral cover. For juvenile corals, a significant negative correlation was observed in three genera, but no positive correlation was identified. Significant positive correlations were found with non-bleached corals and certain algae species. Along the southeastern coast of Kuroshima Island, consistently high accumulated phosphate values were observed over the three years. Kuroshima is known for its thriving livestock farming, and concerns have been raised about the potential impact of livestock waste, as phosphate concentrations in the groundwater are also high.

Keywords: Calcareous sediments, adsorbed phosphorus, phosphate load, coral reef

INTRODUCTION

Coral reefs are essential for supporting biodiversity and providing ecosystem services such as fisheries, coastal protection, and tourism. However, recent years have seen an increase in coral bleaching events, largely due to rising seawater temperatures and other environmental stressors, which have weakened reef resilience (Wiedenmann *et al*., 2013; Raj *et al*., 2021). Terrestrial runoff, including nutrients and toxins, negatively impacts coral reefs even at distances of up to 10 km from river mouths (Richmond *et al*., 2019). As climate change worsens, reducing local stressors is key to mitigating bleaching and related issues like ocean acidification.

Nutrient runoff, particularly from agricultural and urban sources, can exacerbate reef degradation by promoting eutrophication and algal blooms, though the specific

mechanisms are not fully understood (Morimoto *et al*., 2010). Despite low nitrate and phosphate levels in areas like Sekisei Lagoon, coral juvenile populations, especially Acropora, have been steadily declining (Duprey *et al*., 2016; Muko *et al*., 2019). Phosphate, in particular, is known to inhibit coral skeletal formation at concentrations above 5 µM (Iijima *et al*., 2019).

Our research revealed that phosphate, originating from terrestrial sources, accumulates in the calcareous sediments typical of coral reef environments. This "accumulated phosphate" is gradually released into the seawater, posing a risk to coral juvenile growth (Iijima *et al*., 2021; Iijima *et al*., 2022). Sediments near urban areas and river mouths were found to release over 10 µM of phosphate, a level that significantly inhibits coral skeletal formation. In this study, we examined the relationship between accumulated phosphate and coral health in Sekisei Lagoon, Okinawa, by analyzing sediment samples from 117 sites, including government-monitored locations.

We determined that accumulated phosphate levels of 0.62 µg/g are a critical threshold for the survival of Acropora juveniles. These findings help clarify the link between terrestrial nutrient loads and coral reef decline, offering valuable insights for conservation efforts. They also emphasize the need to reduce phosphate use to protect coral ecosystems and address the broader issue of phosphate resource depletion (Demay *et al.*, 2023).

MATERIALS AND METHODS

Monitoring in Sekisei Lagoon and sample collection

Sekisei Lagoon, a national park in Japan, spans 20 km wide and 15 km long, surrounded by a semi-barrier reef (Figure 1). The lagoon's reef, with a maximum depth of 20 m, consists largely of calcareous sediment. In 2003, the Ministry of the Environment initiated the Sekisei Lagoon Nature Restoration Project, establishing 31 monitoring sites to track changes in coral cover, bleaching, and algal types.

Annual surveys are conducted from August to December, with researchers snorkeling for 15 minutes in 50 × 50 m areas at depths of 2–10 m. Coral juveniles, including Acropora and Pocillopora, are counted using quadrats at each site. Sampling locations were also set near Kuroshima and Taketomi Islands. In September 2021, calcareous sediments and seawater were collected at the 31 sites. Sediments were frozen, and seawater samples refrigerated for analysis.

Sample preparation and phosphate analysis

Sediments were dried, sieved, and mixed with seawater to elute phosphate, which was then analyzed using the molybdenum blue method. The released phosphate (µg/g) was defined as "accumulated phosphate." Dissolved inorganic phosphate (DIP) levels in seawater were also measured.

Correlation and threshold analysis of accumulated phosphate impact

Spearman's correlation analysis in R software was used to explore the relationship between accumulated phosphate and coral health indicators. TITAN analysis determined the phosphate threshold levels linked to coral bleaching, juvenile density reduction, and algal coverage at the 31 sites. The threshold marks significant changes, while "purity" and "reliability" reflect the consistency and accuracy of these relationships.

RESULTS

Accumulated phosphate levels in Sekisei Lagoon

We measured the accumulated phosphate levels at 31 monitoring sites in Sekisei Lagoon. These levels represent

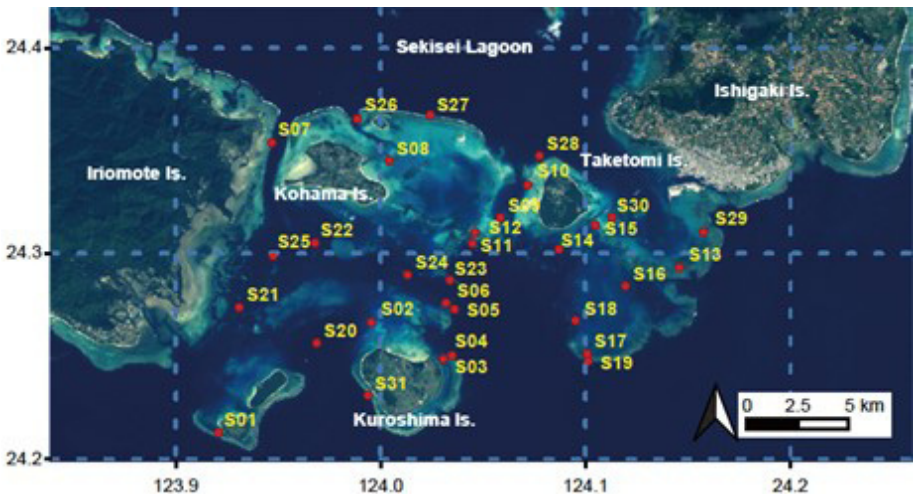

Figure 1: Research sites in the Sekisei Lagoon, located between Ishigaki and Iriomote islands in southern Japan and the accumulated phosphate levels in the sediments at the 31 monitoring sites in the Sekisei Lagoon.

the amount of phosphate (µg/g) desorbed from calcareous sediments into seawater. The highest phosphate levels were observed at sites S3, S12, and S13, with values of 0.94 ± 0.32 µg/g, 1.12 ± 0.66 µg/g, and 1.22 ± 0.32 µg/g, respectively. Sites S5, S6, S17, S19, S26, S27, and S28 showed relatively low phosphate levels of around 0.2 µg/g. Dissolved inorganic phosphate (DIP) in seawater was mostly below the detection limit (<0.006 mg/L).

Significant correlations were found between accumulated phosphate and coral health indicators. "Healthy" coral was negatively correlated with phosphate levels (rho = -0.57, $p < 0.001$), with a threshold of 0.62 µg/g. Beyond this level, healthy coral was limited to 10%. *Acropora* and *Pocillopora* juvenile densities also showed negative correlations with phosphate (rho = -0.34, $p = 0.06$), with thresholds of 0.62 µg/g and 0.51 µg/g, respectively. In contrast, "overall light-colored" coral and *Dictyota* algal cover were positively correlated with phosphate levels (rho = 0.62, $p < 0.001$ and rho = 0.43, $p < 0.05$), with thresholds of 0.38 µg/g and 0.53 µg/g.

Kuroshima and Taketomi Islands, areas with livestock and shrimp farming. The highest phosphate levels reached 14.0 µg/g near Kuroshima and 18.8 µg/g near shrimp farms on Taketomi Island.

DISCUSSION

The impact of excessive nutrients from terrestrial sources on coral reef ecosystems has long been a concern. Despite low nitrate and phosphate concentrations in surface seawater at Sekisei Lagoon, coral juveniles, particularly Acropora, have continued to decline. Previous studies revealed that phosphate strongly adsorbs onto calcium carbonate in seawater sediments, inhibiting coral juvenile skeletal formation. The release of phosphate from sediments varies by location, making it a useful indicator of land-based nutrient loading on corals.

Phosphate is known to adsorb onto calcium carbonate in the presence of calcium ions and easily desorb into oligotrophic seawater. This process suggests that areas with continuous phosphate input from land show high levels of "accumulated phosphate." Our findings show a clear correlation between high accumulated phosphate levels and decreased coral health, particularly bleaching. Algal cover was also high in these areas, competing with corals for resources and inhibiting coral photosynthesis. Direct effects of phosphate, like skeletal formation inhibition, further contribute to coral health decline.

TITAN analysis identified phosphate thresholds critical for coral reef health, suggesting that keeping phosphate levels below 0.62 µg/g is essential for maintaining healthy coral populations. Areas near shrimp farms and livestock industries, like Taketomi and Kuroshima islands, showed significantly higher phosphate levels. These results indicate human activity as a significant source of phosphate and underscore the importance of reducing terrestrial inputs to protect coral reefs. Incorporating accumulated phosphate as an indicator could improve our understanding of human impacts on reef ecosystems.

REFERENCES

Demay, J., Ringeval, B., Pellerin, S., & Nesme, T., 2023. Half of global agricultural soil phosphorus fertility derived from anthropogenic sources. Nat. Geosci. 16, 69–74.

Duprey, N.N., Yasuhara, M., & Baker, D.M., 2016. Reefs of tomorrow: Eutrophication reduces coral biodiversity in an urbanized seascape. Glob. Chang. Biol., 22, 3550–3565.

Iijima, M., Yasumoto, J., Iguchi, A., Koiso, K., Ushigome, S., Nakajima, N., Kunieda, Y., Nakamura, T., Sakai, K., Yasumoto-Hirose, M., Mori-Yasumoto, K., Mizusawa, N., Amano, H., Suzuki, A., Jimbo, M., Watabe, S., & Yasumoto, K., 2021. Phosphate bound to calcareous sediments hampers skeletal development of juvenile coral. R. Soc. Open Sci., 8, 201214.

Iijima, M., Yasumoto, J., Mori-Yasumoto, K., Yasumoto-Hirose, M., Iguchi, A., Suzuki, A., Mizusawa, N., Jimbo, M., Watabe, S., & Yasumoto, K., 2022. Visualisation of Phosphate in Subcalicoblastic Extracellular Calcifying Medium and on a Skeleton of Coral by Using a Novel Probe, Fluorescein-4-Isothiocyanate-Labelled Alendronic Acid. Mar. Biotechnol., 24, 524–530.

Iijima, M., Yasumoto, K., Yasumoto, J., Yasumoto-Hirose, M., Kuniya, N., Takeuchi, R., Nozaki, M., Nanba, N., Nakamura, T., Jimbo, M., & Watabe, S., 2019. Phosphate enrichment hampers development of juvenile Acropora digitifera coral by inhibiting skeleton formation. Mar. Biotechnol., 21, 291–300.

Morimoto, N., Furushima, Y., Nagao, M., Irie, T., Iguchi, A., Suzuki, A., & Sakai, K., 2010. Water-quality variables across sekisei reef, A large reef complex in Southwestern Japan. Pac. Sci., 64, 113–123.

Muko, S., Suzuki, G., Saito, M., Nakamura, T., & Nadaoka, K., 2019. Transitions in coral communities over 17 years in the Sekisei Lagoon and adjacent reef areas in Okinawa, Japan. Ecol. Res., 34, 524–534.

Raj, K.D., Aeby, G.S., Mathews, G., Williams, G.J., Caldwell, J.M., Laju, R.L., Bharath, M.S., Kumar, P.D., Arasamuthu, A., Asir, N.G.G., Wedding, L.M., Davies, A.J., Moritsch, M.M., & Edward, J.K.P., 2021. Coral reef resilience differs among islands within the Gulf of Mannar, southeast India, following successive coral bleaching events. Coral Reefs, 40, 1029–1044.

Richmond, R.H., Golbuu, Y., & Shelton, A.J., 2019. In: E. Wolanski, J.W. Day, M. Elliott, & R. Ramachandran (Eds.). Coasts and estuaries (pp. 445–459). Elsevier.

Wiedenmann, J., D'Angelo, C., Smith, E.G., Hunt, A.N., Legiret, F., Postle, A.D., & Achterberg, E.P., 2013. Nutrient enrichment can increase the susceptibility of reef corals to bleaching. Nature Clim. Change, 3, 160–164.

Standardization of performance evaluation tests for adsorbents used in the remediation of geogenic contaminated soils

Miu Nishikata*, Kazuya Morimoto, Yukari Imoto, Tetsuo Yasutaka

Institute for Geo-Resources and Environment, Geological Survey of Japan (GSJ), National Institute of Advanced Industrial Science and Technology (AIST), 305-8567, Tsukuba, Ibaraki, Japan
*Email: m.nishikata@aist.go.jp

Abstract: Excavated soil and rocks from construction works such as tunnels contain naturally occurring heavy metals, and in some cases heavy metal concentrations are above the standard. One of the low cost and environmental impact countermeasures is the attenuation layer method. To prevent the infiltration of toxic elements, the attenuation layer is installed on the embankment foundation. Adsorbents used in the attenuation layer method must be able to adsorb heavy metals over a long period of time, but performance evaluation methods are not standardised. In this research, we introduced an example of a study on the standardization of performance evaluation tests for adsorbents for attenuation layer method. In the standardization process, we conducted studies on the types of reagents used in adsorption tests, room temperature, and contact between water and adsorbent, as well as inter-room precision evaluation tests. The results of this study were reflected in the standardized method.

Keywords: Attenuation layer method, batch adsorption tests, standardization

INTRODUCTION

Excavated soil and rocks from construction works such as tunnels contain naturally occurring heavy metals, and in some cases heavy metal concentrations are above the standard. One of the low-cost, low-environmental-impact method for handling these soils is the attenuation layer method (See Figure 1). In the attenuation layer method, an attenuation layer is laid at the bottom of the contaminated soil to prevent the diffusion of heavy metals. The attenuation layer is a layer made up of an adsorbent and highly permeable soil. The adsorbent used in the attenuation layer method is required to maintain its performance over a long period of time. However, there were issues regarding the suitability of the adsorption performance test method for assessing long-term adsorption performance, and also the issue that the test method had not been standardized.

The first problem is that the impact of the contact between water and the adsorbent on the adsorption performance has not been taken into account. In the case of natural soil, where the adsorption mechanism of heavy metals is mainly due to a pure adsorption reaction, it is thought that performance evaluation is possible even with a single batch adsorption test. On the other hand, in the case of the attenuated layer method, which uses various types of adsorbents, the adsorption mechanism is also diverse. For example, in the attenuation layer method, it is expected that the adsorption performance will be maintained for several decades or more. However, if the main immobilization mechanism of heavy metals is a hydration reaction of the adsorbent, etc., there is a possibility that the adsorption performance will be lost with a single contact with water, making it unsuitable as a material for the attenuation layer method, but it is difficult to evaluate this in a single batch adsorption test.

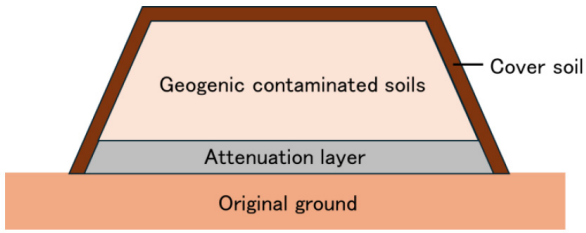

Figure 1: Concept of attenuation layer.

The second issue is due to the lack of standardization of the testing methods. Because the method for batch adsorption testing is not standardized, different methods are used not only for test conditions such as shaking time, liquid-solid ratio, and concentration of naturally occurring heavy metals in the solution used, but also for the calculation method for the distribution coefficient based on the results obtained. These differences not only affect the distribution coefficient obtained, but also make it difficult to compare test results.

To solve this issue, we conducted several researched and standardized the adsorption performance test of adsorbent

since 2019 and published "Report of the Standardization Study Committee for Testing Methods for Adsorbent Used in Attenuation Layer Methods (Committee for Testing Methods for Adsorbent Used in Attenuation Layer Methods, 2022)". This paper introduced a research related to the contact between water and adsorbents. Please note that this content is already published (Nishikata *et al*., 2022).

METHOD

Adsorbent: We conducted adsorption tests targeting fluorine using four adsorbents containing magnesium oxide (Mg-type), iron hydroxide (HFO-type), layered double hydroxide (LDH-type) and zero-valent iron (ZVI-type).

Preparation of test solution: A standard solution of 1000 mg/L fluoride was diluted to prepare a 24 mg/L solution, which was used in the adsorption test. The pH was not adjusted.

Immersion treatment: In order to investigate the differences in the effects of the contact time between the water and the adsorbent on the adsorption performance, the materials were immersed in water before the adsorption test. The water and the adsorbent were sealed in a tube so that the liquid-solid ratio was 4, and then left to stand for 14, 28, or 180 days. After that, the adsorption test was conducted using the materials that had undergone immersion treatment.

Serial batch adsorption test: Serial batch test is a method that is often used in leaching tests. In this test, the material and water are sealed in a bottle, and then shaken for a certain period of time. After solid-liquid separation, the material is shaken again with water added, and the process is repeated. In this study, the adsorbent and fluoride solution were sealed in a tube so that the liquid-solid ratio was 100, and shaken for 16 hours. After shaking, the supernatant liquid was removed by centrifugation, and then the remaining adsorbent was again added to the fluoride solution and shaken and solid-liquid separation was carried out under the same conditions. This procedure was repeated four times for each adsorbent. The solution after each centrifugation was filtered through a membrane filter and the concentration of fluoride was measured.

RESULTS AND DISCUSSION

Figure 2 shows the removal rate of fluorine for each number of adsorption cycles for the Mg-type and LDH-type materials in the tests with no immersion treatment, and with 14, 28 and 180 days of immersion treatment. In the tests with no immersion treatment, there was no difference in the removal rate for either material, even after repeated shaking. When immersion treatment was carried out, a decrease in the removal rate was confirmed for the Mg-type material. The removal rate decreased the longer the immersion treatment time was. In addition, when immersion treatment was carried out, the removal rate decreased with each repeated shaking. On the other hand, no change in the removal rate was observed for the LDH-type material, even when immersion treatment was carried out. This is thought to be due to the difference in the removal mechanism of fluorine for each material. LDH has a layered structure and the anions between the layers have the property of being exchanged (Miyata, S., 1983). Therefore, it is thought that fluoride ions were also removed by being taken up between the layers. For magnesium oxide, it is thought that the removal mechanism of fluoride ions is the coprecipitation of fluoride ions associated with hydration and adsorption to the generated magnesium hydroxide (Yoshiyuki, K. *et al*., 2012; Shinichiro, W. *et al*., 2013). It has been reported that coprecipitation of fluoride ions contributes more to the removal of fluoride ions than adsorption to magnesium hydroxide. In this study, it is thought that the cause of the decrease in the removal rate was the fact that the hydration of magnesium oxide progressed due to the immersion treatment with water. In actual sites, the LDH-type has little effect on the contact between the adsorbent and water, but there is a concern that the performance of Mg-type materials will decrease when they come into contact with water.

CONCLUSION

The results of the immersion treatment and serial batch adsorption tests showed a decrease in the removal rate of fluoride ions in the tests using Mg-type materials. This is thought to be due to the hydration reaction of the adsorbent

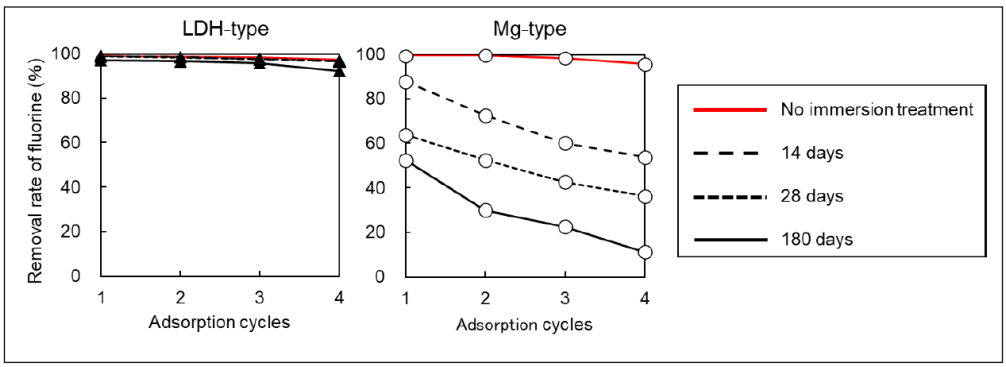

Figure 2: The removal rate of fluorine for each number of shaking cycles (Nishikata *et al*., 2022).

being promoted by contact with water. Since it is assumed that the performance of the adsorbent will change due to contact with water in real environments, promoting the reaction between water and the adsorbent through immersion treatment could be an effective method for evaluating performance.

The adsorbents used in attenuation layer methods vary, and each has a different mechanism. For example, as in this study, the effect on performance due to contact between water and the adsorbent differs for each material. However, without standardized testing methods, it is difficult to select materials that are suitable for actual sites. Standardization of testing methods for evaluating the performance of adsorbents is important for the low-cost, sustainable management of construction soil. In addition to this study, we also conducted research on the types of reagents used in adsorption tests, the room temperature, and inter-laboratory precision evaluation tests. The standardized test has not yet been released, but the test method devised for standardization has been released on the AIST website. It is hoped that the standardization of testing methods that can be applied to various materials will make it possible to select materials that are suitable for actual sites.

REFERENCES

Kojima, Y., Oshima, F., Matsuyama, Y., & Moriya, M., 2012. Elucidation of the mechanism of heavy metal ion immobilization by magnesium oxide. Journal of the Society of Inorganic Materials, 19, 15-22.

Miyata, S., 1983. Anion-exchange properties of hydrotalcite-like components. Clays and Clay Minerals, 31(4), 305-311.

Nishikata, M., Yasutaka, T., Morimoto, K., & Imoto. Y., 2022. Evaluation of water contact influence on adsorbents by water immersion pretreatment and serial batch tests. Journal of Geotechnical Engineering, 17(2), 195-204.

Research Institute for Geo-Resources and Environment National Institute of Advanced Industrial Science and Technology, 2022. Report of the Committee on Standardization of Test Methods for Materials, https://unit.aist.go.jp/georesenv/geoevaluation/adsorption-layer/.

Wada, S., & Morishita, T.,2013, Immobilization of heavy metal-contaminated soil by magnesium oxide and mineralogical reactions in soil. Clay Science, 51(3), 107-117.

Evaluating pilot-scale passive treatment of manganese and zinc at a legacy mine: Implications for sustainable mine practices

Sereyroith Tum[1], Taiki Katayama[1], Naoyuki Miyata[2], Miho Watanabe[2], Takaya Hamai[3], Yuki Semoto[3], Miu Nishikata[1], Tetsuo Yasutaka[1,*]

[1]Institute for Geo-Resources and Environment, Geological Survey of Japan (GSJ), National Institute of Advanced Industrial Science and Technology (AIST), 305-8567, Tsukuba, Ibaraki, Japan
[2]Department of Biological Environment, Akita Prefectural University, 241- 438, Shimoshinjo-Nakano, 010-0195, Akita, Japan
[3] Metals Environment Management Department, Japan Oil, Gas, and Metals National Corporation (JOGMEC), 105-0001, Minato, Tokyo, Japan
*Email: t.yasutaka@aist.go.jp

Abstract: Mine drainage, characterized by the release of toxic metals and acidic water from mining sites, is commonly treated using active treatment methods. While these methods are effective, they are costly and result in significant CO_2 emissions. For sustainable mining management, nature-based solutions, known as passive treatment, are considered a viable alternative method. However, they are not always applicable to all mine sites. In this study, we evaluate the effectiveness of a pilot-scale passive treatment system for reducing manganese (Mn) and zinc (Zn) concentrations at a legacy mine.
A continuous-flow bioreactor was constructed in an underground tunnel, utilizing two water tanks containing limestone (unit A-1) and polypropylene-vinylon fibers (unit A-2) to promote metal precipitation and microbial activity. Water samples from the treatment units, and sludge precipitated on the media, were collected for detailed analysis, including water chemistry, mineralogical composition, and microbial community characterization. Geochemical modeling was conducted using PHREEQC with the WATEQ4F database to simulate water chemistry and predict mineral saturation indices during treatment.
The system achieved Mn and Zn removal efficiencies of 97% and 89%, respectively, with a total hydraulic retention time of 6 days at the initial state. Remarkably, the Mn-oxidizing bacteria were active without the addition of organic material, facilitating the oxidation of Mn(II) to Mn(IV) and leading to birnessite formation. Additionally, analytical data and geochemical modeling indicated that Zn removal occurred through co-precipitation with MnO_2 (forming woodruffite) and adsorption onto the birnessite surface. These results suggest that passive treatment systems driven by Mn-oxidizing bacteria can efficiently remove Mn and Zn concentrations, providing an environmentally friendly solution for managing mine drainage at legacy sites. This study underscores the potential for scaling this approach to broader applications in sustainable mine water management.

Keywords: Mine drainage, passive-treatment, Mn-oxidizing bacteria, legacy mine, sustainable mining

INTRODUCTION

Mine drainage treatment has become one of the major challenges for environmental risks and aquatic life due to the high concentrations of heavy metals, including iron (Fe), aluminum (Al), and manganese (Mn), zinc (Zn), lead (Pb), arsenic (As), and other element (Sánchez-España *et al*., 2011; Barboza *et al*., 2017; Tum *et al*., 2023). Active treatment is commonly used to mitigate these issues, but it is not considered a sustainable method for long-term implementation. Therefore, an alternative method known as passive treatment, which utilizes nature-based solutions, is suggested. However, this method is designed based on site-specific conditions, which requires a detailed investigation before being applied to an actual mine site (Skousen *et al*., 2017). Our research team has been operating a pilot-scale passive treatment plant using a manganese-oxidizing bacteria reactor in the underground tunnel of a legacy mine site to evaluate the removal efficiency of Mn and Zn since 2020. Our aim is to determine the treatment mechanisms for Mn and Zn in the pilot-scale project, with future implications for full-scale passive treatment systems. An overview of the research results, which have been published in various papers and other publications, be provided in this paper.

MATERIALS AND METHODS

Pilot scale treatment installation

The pilot-scale plant consisted of three 700 L tanks, A-0, A-1 and A-2. Mine drainage was pumped from a small drainage ditch (MD) at mine X into A-0, which then fed into A-1 (porosity: 45%), a tank filled with limestone. The

treated water from A-1 flowed into A-2 (porosity: 92%), a tank equipped with polypropylene-vinylon fibers (Figure 1). Approximately 2L of sediment from the MD, containing Mn-oxidizing bacteria (Miyata *et al*., 2024), was spread in the A-1 and A-2 tanks. Air agitators were installed in both A-1 and A-2 to supply oxygen. The pilot-scale passive treatment was conducted at a pH of 6.5–7.5. A detailed description of the passive treatment system can be found in Watanabe *et al*. (2024).

Analytical methods

The water sample was collected at MD and each treatment tank (A-0, A-1, and A-2) to characterize the water chemistry. Particularly, MD and A-0 had the same water quality. Sediment that naturally precipitated in the small stream (MD) and sludge from the passive treatment system (A-1) were collected for analysis. The sludge precipitated on in A-1 and A-2 were collected for mineralogy and chemical composition by X-ray diffraction (XRD), X-ray fluorescence, and scanning electron microscopy with energy-dispersive X-ray spectroscopy (SEM-EDS).

Geochemical modelling

The PHREEQC computer code, using the WATEQ4F.dat database (Parkhurst & Appelo, 2013) was employed to simulate water chemistry, predict mineral saturation indices, and model Zn adsorption on birnessite during treatment. The Zn adsorption database for birnessite was taken from Tonkin *et al*. (2004).

Microorganism analysis in the passive treatment plan

The microbial community structure and metagenomic analysis, along with a cultivation-based evaluation of manganese-oxidizing bacteria, were conducted as described in Watanabe *et al*. (2024). The discussion includes DNA sequence data deposition related to manganese deposits. The microbial analysis is not addressed in this paper; those interested in this aspect are referred to Watanabe *et al*. (2024).

RESULT AND DISCUSSION

Mn and Zn treatment efficiency

The water quality of the pilot-scale passive treatment plant from summer 2022 to winter 2023 is summarized in Figure 2 and Table 1. The average Mn and Zn concentrations in A-0 were 15-25 mg/L and 6-9.8 mg/L, respectively. However, after passing through A-1 and A-2, the Mn and Zn concentrations decreased to under 1 mg/L and 2 mg/L, respectively until autumn. The treatment efficiency reached up to 98%, although the removal rate varied depending on the hydraulic retention time (HRT) of the mine drainage as it flowed through A-1 and A-2. Mn and Zn concentrations were monitored over a 152-day period in the pilot-scale passive treatment under different HRTs of 2 days, 0.5 days, and 0.3

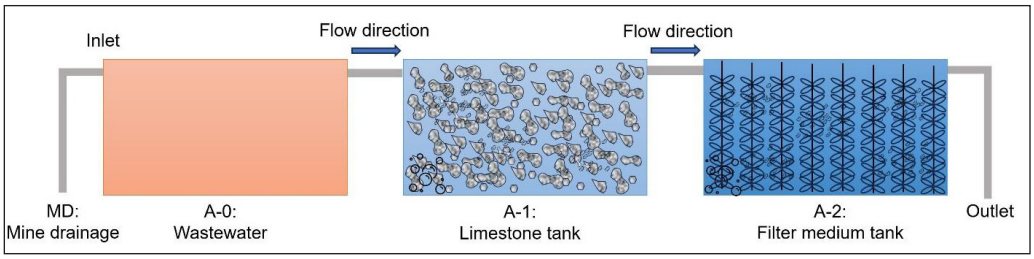

Figure 1: The schematic of the pilot-scale passive treatment system; the wastewater in A-0 was pumped from the mine drainage (MD) and discharged into A-1 before being directed A-2. Air agitators were installed in A-1 and A-2 to allow oxygen saturation in the treatment plant (Tum *et al*., 2024).

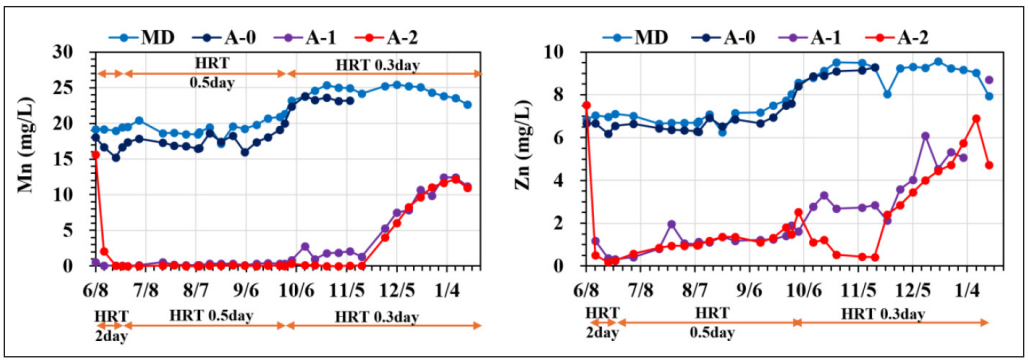

Figure 2: The changes in Mn and Zn concentrations in the pilot-scale passive treatment plant. This field investigation obtained by a joint research involving AIST, Akita Prefectural University, and JOGMEC (JOGMEC *et al*., 2022).

Table 1: The average water quality in the treatment system (Tum *et at*., 2024).

	Unit	A-0 (wastewater)	A-1	A-2
Mn	mg/L	19.19	0.72	0.72
Zn	mg/L	6.99	0.35	2.11
pH		6.8	7.1	7.0
OPR	mV	178	161	177
DO	mg/L	7.3	9.2	9.5
EC	µS/cm	1138	1101	1096

days (in A-1). Changing the HRT did not significantly affect Mn removal; however, Zn removal efficiency decreased to 80% when the HRT was reduced to 0.3 days. In addition, after temperature decrease in November, the removal efficiency rapidly decreased.

Mn and Zn removal mechanisms

The XRD pattern of the sludge sample shown in Figure 3 reveals that the primary mineral present in the MD (drainage ditch), A-1, and A-2 is birnessite (MnO_2) (Watanabe *et al*., 2024), which formed under biotic conditions at circumneutral pH (Bruins *et al*., 2015). Liang *et al*. (2016) reported that Mn-oxidizing bacteria were the main factor controlling the Mn removal rate, due to their role in catalyzing Mn oxidation in the pilot-scale passive treatment plant (Morgan, 2005; Liang *et al*., 2016). Additionally, woodruffite ($ZnMn_3O_7 \cdot 2H_2O$), a mineral with a structure similar to todorokite (Tajima *et al*., 2022), was also detected in the XRD analysis of the sludge samples from A-1 and A-2. The co-existence of Mn and Zn allows birnessite to co-precipitate and adsorb Zn from the mine drainage, as Zn(II) can bind to Mn(IV) vacancy sites within the hexagonal birnessite structure,

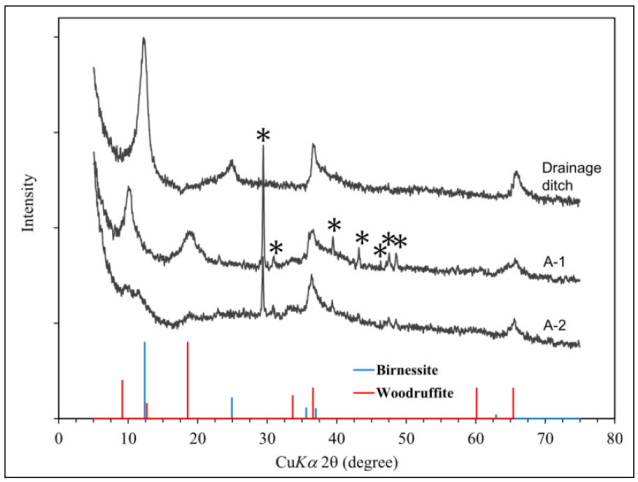

Figure 3: XRD patterns of Mn deposits collected from drainage ditches (MD) and bioreactors A-1 and A-2 at 120 days (Watanabe *et al*., 2024).

forming inner-sphere surface complexes through triple-corner sharing (Kwon *et al*., 2009). Geochemical models reveal that, under equilibrium conditions, the Zn adsorption capacity on birnessite surfaces can reach up to 99% at neutral pH. However, since the pilot-scale passive treatment was implemented under continuous flow conditions, the physical flow rate and Zn sorption kinetics may influence the reduction of Zn removal efficiency.

CONCLUSIONS

The pilot-scale passive treatment conducted at the X mine demonstrated the potential to transition from the current active treatment plant to a full-scale passive treatment system. Mn and Zn were treated biologically from the mine drainage using an assisted limestone tank within the passive treatment system, without the need for additional organic substrates. The presence of limestone facilitated the growth of Mn-oxidizing bacteria, which catalyzed Mn oxidation, leading to the rapid formation of birnessite and woodruffite. Zn were primarily removed through co-precipitation with birnessite, adsorption, and ion exchange on the birnessite surface.

ACKNOWLEDGEMENTS

The authors express their sincere gratitude to all individuals, both directly and indirectly involved, who have made valuable contributions to this research project. This study was partly funded by METI (Ministry of Economy, Trade, and Industry).

REFERENCES

Barboza, N.R., Morais, M.M.C.A., Queiroz, P.S., Amorim, S.S., Guerra-Sá, R., & Leão, V.A., 2017. High Manganese Tolerance and Biooxidation Ability of Serratia marcescens Isolated from Manganese Mine Water in Minas Gerais, Brazil. Front. Microbiol., 8, 1946. https://doi.org/10.3389/fmicb.2017.01946.

Bruins, J.H., Petrusevski, B., Slokar, Y.M., Huysman, K., Joris, K., Kruithof, J.C., & Kennedy, M.D., 2015. Biological and physico-chemical formation of Birnessite during the ripening of manganese removal filters. Water Research, 69, 154–161. https://doi.org/10.1016/j.watres.2014.11.019.

JOGMEC, AIST, Akita Prefectural University, 2022. 2022 Investigation Project on Advanced Technology for Treating Mine Wastewater at Discontinued Mines. Japan Energy, Metals & Minerals National Corporation (JOGMEC).
https://www.meti.go.jp/policy/safety_security/industrial_safety/sangyo/mine/portal/report/R4koudokareport.pdf.

Liang, J., Bai, Y., Hu, C., & Qu, J., 2016. Cooperative Mn(II) oxidation between two bacterial strains in an aquatic environment. Water Research, 89, 252–260. https://doi.org/10.1016/j.watres.2015.11.062.

Miyata, N., Suganuma, R., Sunouchi, K., Okano, K., Fuchida, S., Watanabe, M., Fujibayashi, M., Sato, Y., & Tokoro, C., 2024. Biological Mn(II) oxidation under organic substrate-limited conditions and its application in mine drainage remediation. Biochemical Engineering Journal, 203, 109187. https://doi.org/10.1016/j.bej.2023.109187.

Morgan, J.J., 2005. Kinetics of reaction between O_2 and Mn(II) species in aqueous solutions. Geochimica et Cosmochimica Acta, 69, 35–48. https://doi.org/10.1016/j.gca.2004.06.013.

Parkhurst, D.L., & Appelo, C.A.J., 2013. Description of Input and Examples for PHREEQC Version 3—A Computer Program for Speciation, Batch-Reaction, One-Dimensional Transport, and Inverse Geochemical Calculations. Techniques and Methods.

Sánchez-España, J., Yusta, I., & Diez-Ercilla, M., 2011. Schwertmannite and hydrobasaluminite: A re-evaluation of their solubility and control on the iron and aluminium concentration in acidic pit lakes. Applied Geochemistry, 26, 1752–1774. https://doi.org/10.1016/j.apgeochem.2011.06.020.

Skousen, J., Zipper, C.E., Rose, A., Ziemkiewicz, P.F., Nairn, R., McDonald, L.M., & Kleinmann, R.L., 2017. Review of Passive Systems for Acid Mine Drainage Treatment. Mine Water Environ., 36, 133–153. https://doi.org/10.1007/s10230-016-0417-1.

Tajima, S., Fuchida, S., & Tokoro, C., 2022. Coprecipitation mechanisms of Zn by birnessite formation and its mineralogy under neutral pH conditions. Journal of Environmental Sciences, 121, 136–147. https://doi.org/10.1016/j.jes.2021.09.019.

Tonkin, J.W., Balistrieri, L.S., & Murray, J.W., 2004. Modeling sorption of divalent metal cations on hydrous manganese oxide using the diffuse double layer model. Applied Geochemistry, 19, 29–53. https://doi.org/10.1016/S0883-2927(03)00115-X.

Tum, S., Katayama, T., Miyata, N., Watanabe, M., Hashimoto, Y., & Yasutaka, T., 2024. Understanding a passive treatment mechanism of manganese and zinc at a legacy mine in northern Japan using geochemical modelling. Presented at the West Virginia Mine Drainage Task Force Symposium & 15th International Mine Water Association Congress 2024, IMWA, pp. 611–612.

Tum, S., Matsumoto, S., Nishikata, M., & Yasutaka, T., 2023. Assessment of seasonal changes in groundwater quality of waste rock dump in temperate continental climate, northern Japan. Chemosphere, 138482. https://doi.org/10.1016/j.chemosphere.2023.138482.

Watanabe, M., Tum, S., Katayama, T., Gotore, O., Okano, K., Matsumoto, S., Yasutaka, T., & Miyata, N., 2024. Accelerated manganese(II) removal by in situ mine drainage treatment system without organic substrate amendment: Metagenomic insights into chemolithoautotrophic manganese oxidation via extracellular electron transfer. Journal of Environmental Chemical Engineering, 12, 113314. https://doi.org/10.1016/j.jece.2024.113314.

Effects of natural factors on wetland treatment system for the purification of mining-influenced water

Shinji Matsumoto

Geological Survey of Japan, National Institute of Advanced Industrial Science and Technology (AIST),
Central 7, 1-1-1 Higashi, Tsukuba, Ibaraki, 305-8567, Japan
Email: shin.matsumoto@aist.go.jp

Abstract: Mining activities have historically been conducted worldwide to extract resources such as metals and coal. The development of mines exposes subsurface sulfide minerals to the atmosphere and water, resulting in the formation of mine-influenced water (MIW), also known as acid mine drainage (AMD), which contains heavy metals. If released untreated into the environment, MIW can have significant detrimental effects on the surrounding environment. Therefore, to mitigate these effects, the neutralization of MIW through the addition of limestone is commonly implemented. However, MIW will continue to be generated indefinitely, requiring substantial costs and efforts for its treatment as long as sulfide minerals are present. To reduce treatment costs and labor, constructed wetlands have been used as a method for treating MIW. While the neutralization of MIW through the addition of limestone is classified as active system, the use of constructed wetlands falls under the category of passive system. This system utilizes the natural purification capabilities of water, soil, and vegetation in wetlands, making it low-cost and energy-efficient. Wetland systems are typically installed in natural outdoor environments, making them highly susceptible to the influence of unpredictable weather and surrounding flora and fauna, collectively referred to as "natural factors". More information is needed on the effects of these natural factors for optimizing the design and functionality of wetland treatment systems.
This paper introduces fundamental insights into strategies for addressing MIW issues and presents case studies that examine the impact of natural factors on wetland treatment system for MIW. The focus is on aerobic constructed wetlands implemented at legacy mine in Japan. Field investigations suggest that wildlife intrusion and uneven water flow within the wetlands can potentially reduce MIW treatment capacity. When implementing constructed wetlands in the field, it is essential to address these issues to maximize MIW treatment efficiency by constructed wetland.

Keywords: Mine, mining-influenced water, wastewater, natural factors, wetland, passive treatment

INTRODUCTION

Mining-influenced water (MIW) is generated when underground sulfide minerals are exposed to atmospheric oxygen and water sources such as precipitation and groundwater due to mining activities. This MIW often exhibits strong acidity and contains heavy metals, adversely affecting the surrounding environment. It is recognized worldwide as a serious water pollution problem caused by mining development (Glover, 1983; Younger, 1997; Acharya & Kharel, 2020). In many cases, MIW originates from underground tunnels where mining has occurred and/or from waste dumping site where excavated rocks and tailings accumulate. Furthermore, MIW continues to be generated semi-permanently even after mining operations have ceased, unless all sulfide minerals are consumed or contact between sulfide minerals and water or oxygen is completely blocked, requiring enormous costs and time for mitigation and treatment. Strategies for addressing MIW include "source control" and "migration control" (Johnson & Hallberg, 2005). The former involves methods such as submerging underground tunnels or covering waste dumping site with impermeable materials to block contact between minerals and atmospheric oxygen, thereby preventing the generation of MIW itself. Ideally, source control should be implemented in parallel with mining operations, as it is generally desirable to prevent the formation of MIW at the earliest stage. The latter strategy focuses on reducing environmental impact by treating the generated MIW. This includes active technologies, which involve neutralizing MIW by adding limestone or chemicals, and passive systems, where MIW is passively treated by flowing through artificially constructed wetlands or drainage channels built with limestone. Compared to active systems, passive systems are recognized as requiring less cost and effort for MIW treatment. In the latter half of the 20th century, it was discovered in the United States that natural MIW was purified as it flowed through wetlands. This led to initiatives utilizing artificial wetlands for MIW treatment to reduce treatment costs and maintenance expenses of treatment facilities (Mitsch & Wise, 1998). In recent years,

the use of artificial wetlands for MIW treatment has become widespread globally.

There are two types of constructed wetlands: aerobic and anaerobic systems. Aerobic constructed wetlands treat MIW by flowing it over the wetland surface, exposing it to air, which oxidizes metals such as iron and manganese contained in the wastewater, causing them to precipitate and be removed (Batty & Younger, 2002). This system requires securing a large area and ensuring uniform water flow within the wetland to provide sufficient retention time for the MIW. In contrast, anaerobic constructed wetlands have layers of organic matter and limestone (or mixed layers) installed in the lower strata of the wetland. In the surface layer, metal oxidation and hydrolysis are promoted under aerobic conditions. Meanwhile, in the lower layers, the MIW is treated through various reactions under anaerobic conditions, such as the formation and precipitation of metal sulfides and the generation of alkalinity by microorganisms and limestone (RoyChowdhury *et al*., 2015). It has been reported that effective treatment can be achieved in the anaerobic wetland system when the concentration of heavy metals in the MIW is not particularly high and the flow rate is low. As described above, different systems exist for wetland treatment of MIW. It is necessary to select an appropriate wetland system depending on the pH, net alkalinity of the MIW, and the target metals to be removed. It is also known that combining different wetland systems can improve the treatment efficiency of MIW; thus, treatment is sometimes carried out by integrating multiple wetland systems (Johnson & Hallberg, 2005).

In the aerobic wetland systems as described, securing a large wetland area and ensuring uniform water flow within the wetland are key factors in achieving effective wastewater treatment. However, wetland systems are usually installed in natural outdoor environments, where unpredictable weather such as heavy rain and snowfall, as well as surrounding flora and fauna, may cause a loss of wetland functionality. Such natural factors vary depending on the surrounding environment where the wetland is installed, the size and location of the wetland system, and other site-specific conditions. Therefore, accumulating information and expertise on dealing with these natural factors is crucial when considering the development of more effective wetland systems. In this study, we conducted water quality measurements and visual observations within an aerobic constructed wetland system implemented at a legacy mine in Japan to identify the impact of natural factors on the MIW treatment system. Based on these results, we examined design considerations for constructing a sustainable wetland system.

MATERIAL AND METHODS

Site description

The study area is the legacy mine, located in northern Japan. Discovered in 1936, the mine primarily extracted copper, lead, and zinc through underground mining methods. Mining operations were suspended in March 1967 due to a decline in ore quantity and grade. After relinquishment of mining rights in 1978, the mine was officially closed. Underground mine voids exist within the mountain mass upstream of a stream that flows through the former mine site, and five mine entrances remain along the stream. The MIW targeted for treatment originates from these mine entrances and from a waste dumping site in the midstream area where excavated rocks were backfilled. This MIW is conveyed to an artificial wetland downstream. After being treated to meet discharge standards—specifically targeting Fe, Zn, Pb, As, and pH—through the artificial wetland and the addition of limestone, the water is discharged into surrounding rivers.

The artificial wetland at this mine is designed as an integrated system combining aerobic and anaerobic processes. The initial section comprises a limestone channel and an aerobic wetland, where Fe and As are primarily removed. A settling pond designed to precipitate and remove sand is installed in the 10-meter section upstream of the aerobic wetland. In the subsequent anaerobic wetland, heavy metals such as Zn and Pb are mainly removed, and ultimately the pH is adjusted to meet regulatory standards (Fuchida *et al*., 2020). This study focuses on the aerobic wetland. The aerobic wetland measures approximately 20 m in width and 100 m in length, covering an area of about 2,000 m². The wetland has a depth of 0.9 m, consisting of 0.7 m of topsoil overlain by approximately 0.2 m of water. Figure 1 presents a schematic diagram of the aerobic wetland; the MIW entering the aerobic wetland after passing through the limestone channel is labeled “Inlet,” and the MIW exiting after passing through the wetland is labeled “Outlet.” Light blue arrows indicate the flow direction of MIW within the wetland, and the areas shown in green represent the spatial distribution of vegetation observed visually. At locations indicated by lines on the Inlet side and midstream area of the wetland (Figure 1), there is a slight elevation where

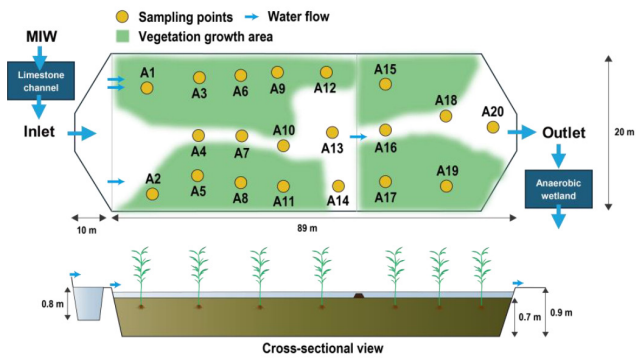

Figure 1: Schematic diagram of the aerobic wetland. The yellow circles represent the measurement points, and the green areas indicate regions where vegetation was visually confirmed at the site. Light blue arrows depict the water flow within the wetland.

the wetland bottom is raised, serving as pathways for maintenance. *Phragmites australis* were transplanted into the wetland during construction and continue to thrive. Currently, the wetland's vegetation is predominantly composed of *Phragmites australis*, but other plant species are also present. Since the aerobic wetland was constructed in 2013, as of 2024, it has been in operation for 11 years.

Field investigation

Visual observations of vegetation growth within the wetland were conducted to record spatial distribution and growth status by measuring the height of plants above the water surface. Additionally, water quality measurements of the MIW flowing through the wetland were performed at 20 locations (A1–A20 in Figure 1). pH and electrical conductivity (EC) were measured using a D-210PC meter (Horiba, Japan) equipped with a 9652-10D pH sensor and a 9383-10D EC sensor, respectively. Oxidation-reduction potential (ORP) and dissolved oxygen (DO) were measured using a D-200PD meter (Horiba, Japan) equipped with a 9300-10D ORP sensor and a 9552-20D sensor with a 5402 DO sensor chip. Principal component analysis (PCA) was performed using R (R Core Team, 2021) on the water quality data measured on-site.

RESULTS AND DISCUSSION

The spatial distribution of vegetation in the aerobic wetland at this mine was uneven. As shown in Figure 1, areas without vegetation were observed near the inlet, as well as just before the step in the midstream area. Near the outlet around point A20, there is very little vegetation, with only small patches of *Phragmites australis* present in some areas. Additionally, a flow path approximately 40 cm wide without vegetation exists in the center of the wetland, connecting these unvegetated areas. As indicated by the light blue arrows in Figure 1, the MIW primarily flowed through these unvegetated areas and channels, following preferential pathways from upstream to downstream within the wetland. This pathway of MIW could reduce its retention time within the wetland and potentially decrease the treatment efficiency of the aerobic system. Therefore, it is desirable to have uniform vegetation throughout the wetland. Within this wetland, areas near the inlet and outlet, as well as around the midstream step, serve as channels where large volumes of MIW can easily flow. This may influence the spatial heterogeneity of vegetation.

During observations, the water level within the wetland was almost the same level as the outlet area and the midstream step. As illustrated by the light blue arrows in Figure 1, MIW was flowing over specific points of the step. While the biased flow of MIW due to the wetland's structure could affect vegetation distribution, this cannot be conclusively determined from the current survey results alone. Additionally, numerous deer droppings were observed in the unvegetated central channel of the wetland. Given that deer tend to repeatedly use specific migration routes (Sawyer *et al*., 2019), it is possible that this wetland has become a pathway for them. The formation of an unvegetated animal trail in the central area due to wildlife movement may contribute to the preferential flow of MIW within the wetland.

Regarding water quality within the wetland, the ORP and DO of the MIW at the inlet were 111 mV and 9.9 mg/L, respectively. In contrast, at points A8, A11, A12, and A15, the ORP was below 100 mV and the DO was below 2.0 mg/L, indicating a reductive environment with lower dissolved oxygen compared to other locations. Approximately 11 years have passed since the construction of this wetland, during which organic matter such as fallen leaves and roots of *Phragmites australis*, as well as iron precipitates, are likely to have accumulated. Oxygen is consumed during the microbial decomposition of these organic materials. Furthermore, sediment accumulation was observed near A8, A11, A12, and A15, with minimal water flow in these areas. Consequently, spatial biases in water flow and inadequate distribution of oxygen-rich water throughout the wetland may have led to zones with low dissolved oxygen and reductive conditions. It is inferred that the purification function of the aerobic wetland may not be fully operational in these locations.

Figure 2 presents the results of the PCA using water quality data from the aerobic wetland. Principal components

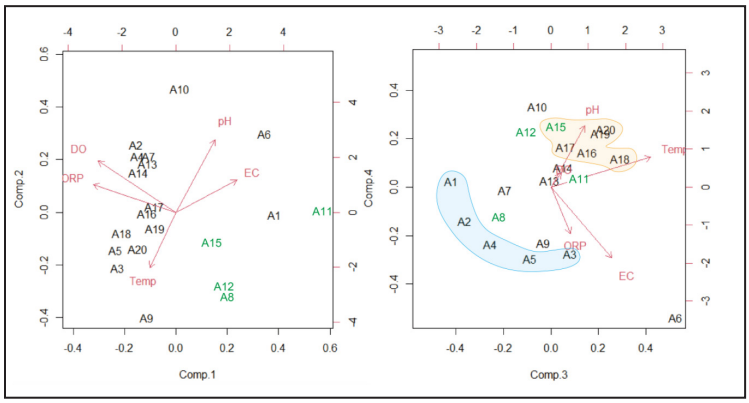

Figure 2: Results of principal component analysis (PCA) for water parameters reported at the aerobic wetland. The left figure shows the relationship between PC1 and PC2, while the right figure depicts the relationship between PC3 and PC4. In the left figure, locations with an ORP below 100 mV are labeled in green, as shown in Figure 2. In the right figure, the upstream section of the wetland (locations A1 to A5) and the downstream section (locations A15 to A20) are grouped and highlighted with blue and yellow color.

PC1 and PC2 explain approximately 67% of the data variance. Points A8, A11, A12, and A15, highlighted in green, are plotted in regions distinct from other locations. This indicates that as ORP and DO decrease, electrical conductivity (EC) increases, and environments with higher water temperatures and lower pH and DO levels emerge. These findings suggest that at these points, decreased dissolved oxygen and the development of reductive environments, along with slow water flow, have resulted in increased water temperatures due to solar heating. Moreover, these locations exhibit different water conditions compared to other points and may not be benefiting fully from the MIW purification function of the aerobic wetland. Principal components PC1 through PC4 explain about 98% of the data variance. There is a tendency for separation between the inlet side of the wetland, indicated by blue areas in Figure 2, and the outlet side, indicated by yellow areas. Compared to the upstream inlet area, water temperature and pH tend to be higher from the midstream to downstream sections. This reflects the warming of MIW due to solar heating as it moves downstream—owing to a certain retention time within the wetland—and a slight increase in pH during passage through the aerobic wetland (Skousen & Ziemkiewicz, 2005). The primary purposes of the vegetation within the wetland are to ensure adequate retention time by preventing MIW rapid flow and to filter precipitates. The results suggest that while there is some retention time across the wetland, partial MIW stagnation and preferential flow of MIW occur, indicating areas where MIW purification is not effectively functioning. Previous studies have reported that Fe and As are sufficiently removed in this aerobic wetland (Fuchida *et al*., 2020). However, necessary maintenance could further enhance the MIW treatment function of the aerobic wetland. Currently, from the perspective of water quality standards, the wetland adequately treats MIW. Nevertheless, addressing these issues is crucial for the sustainable future use of the aerobic wetland within this mine.

CONCLUSIONS

Focusing on an aerobic constructed wetland employed for MIW treatment at a legacy mine in northern Japan, we conducted visual observations of vegetation growth conditions and water quality surveys within the wetland. As a result, we observed that the spatial distribution of vegetation within the wetland was uneven and that reducing environments had formed in parts of the wetland. These conditions suggest that the purification function of the aerobic wetland for treating MIW may not be fully operational. Furthermore, these conditions may have arisen due to spatial biases in MIW flow and vegetation growth within the wetland, caused by the wetland's structure and the influence of surrounding wildlife. Our results highlight the impact of aerobic constructed wetland design and surrounding natural factors on the MIW purification system. Additionally, we compiled information on maintenance necessary to resolve issues affecting the wetland's treatment performance, providing insights useful for achieving long-term maintenance and management of aerobic artificial wetlands. Since some hypotheses cannot be conclusively determined based solely on the results obtained in this study, we plan to conduct more detailed investigations into the influence of surrounding flora, fauna, and climate through geochemical analysis of collected water samples, fixed-point observations using thermal imaging cameras, and surveys utilizing environmental DNA within the wetland.

ACKNOWLEDGEMENTS

This research was financially supported by the Research Laboratory on Environmentally Conscious Developments and Technologies (E-code) at the National Institute of Advanced Industrial Science and Technology (AIST). We also express our gratitude to the mining personnel and researchers who cooperated with this study.

REFERENCES

Acharya, B.S., & Kharel, G., 2020. Acid mine drainage from coal mining in the United States—An overview. Journal of Hydrology, 588, 125061.

Batty, L.C., & Younger, P.L., 2002. Critical role of macrophytes in achieving low iron concentrations in mine water treatment wetlands. Environmental Science & Technology, 36(18), 3997–4002.

Fuchida, S., Suzuki, K., Kato, T., *et al*., 2020. Understanding the biogeochemical mechanisms of metal removal from acid mine drainage with a subsurface limestone bed at the Motokura Mine, Japan. Scientific Reports, 10, 20889.

Glover, H.G., 1983. Mine water pollution—an overview of problems and control strategies in the United Kingdom. Water Science and Technology, 15, 59–70.

Johnson, D.B., & Hallberg, K.B., 2005. Acid mine drainage remediation options: a review. Science of the Total Environment, 338(1–2), 3–14.

Mitsch, W.J., & Wise, K.M., 1998. Water quality, fate of metals, and predictive model validation of a constructed wetland treating acid mine drainage. Water Research, 32(6), 1888–1900.

R. Core Team, 2021. R: A language and environment for statistical computing. R Foundation for Statistical Computing, Vienna. https://www.r-project.org.

RoyChowdhury, A., Sarkar, D., & Datta, R., 2015. Remediation of acid mine drainage-impacted water. Current Pollution Reports, 1, 131–141.

Sawyer, H., LeBeau, C.W., McDonald, T.L., Xu, W., & Middleton, A.D., 2019. All routes are not created equal: an ungulate's choice of migration route can influence its survival. Journal of Applied Ecology, 56(8), 1860–1869.

Skousen, J., & Ziemkiewicz, P.F., 2005. Performance of 116 passive treatment systems for acid mine drainage. In: Proceedings of the 22nd ASMR, Breckenridge, CO, pp. 1100–1133.

Younger, P.L., 1997. The longevity of minewater pollution: a basis for decision-making. Science of the Total Environment, 194/195, 457–466.

Fortifying geoscience data through establishment of National Geoscience Data Discovery Centre (NGDDC) strategic programs

Siti Suzila binti M Radzi

PETROLIAM NASIONAL BERHAD, Kuala Lumpur, Malaysia
Email: suzila.mradzi@petronas.com.my

Abstract: A strategic roadmap has been developed for the National Geoscience Data Discovery Centre (NGDDC), a Centre of Excellence dedicated to fortifying geoscience data and knowledge for a sustainable future. The establishment of NGDDC is pivotal in enhancing the complexity of geoscience data management on an operational scale, particularly transitioning from traditional access operations to an autonomous mode. This shift is essential for fostering collaboration within the national geoscience community. Addressing the prolonged analysis time due to reliance on physical data, limited access to restricted data areas, and underutilization of geoscientist capabilities is imperative. These challenges have hindered timely insights generation and decision-making, leading to business opportunity losses and suboptimal utilization of geoscientist capabilities. NGDDC's strategic programs aim to establish a one-stop center for geoscience data, ensure excellent geoscience data operations, and create a synergistic geoscience data collaboration hub.

NGDDC aims to enhance the quality, comprehensiveness, and trustworthiness of geoscience data through data digitization and the creation of a unified geoscience data platform. The demand from businesses can significantly aid in the basin to prospect maturation workflow and business decision-making for new geoscience data, including data beyond the oil and gas sector. This includes geoscience collaboration projects for data enhancement, enrichment, and augmentation.

The establishment of a Geoscience Data Discovery Hub in Malaysia, equipped with state-of-the-art facilities, aims to boost innovation and efficiency through autonomous data operations, machine learning, and artificial intelligence applications. The NGDDC, as a modern experience center, will accelerate future value creation, enhancing Malaysia's attractiveness as an investment destination by leveraging renowned geoscience capabilities.

NGDDC is positioned as a unique collaboration center, expanding its roles on a national scale to foster new collaborative partnerships that encourage ideation and innovation, and enhance geoscience data management and utilization capabilities. NGDDC supports business excellence and acts as a key enabler for health, safety, and environment (HSE), sustainability, and digital and technology initiatives. This underscores the importance of collaboration with solution partners to enrich lives and achieve the aspiration of transforming the upstream business into a digitally enabled organization for a sustainable future. Overall, NGDDC provides a comprehensive plan for establishing a Centre of Excellence for Geoscience Data, leveraging advanced technologies and fostering collaboration to enhance data utilization and support sustainable development.

Keywords: Geology, SE Asia, CCOP, Thematic Session

A comprehensive strategic roadmap has been developed for the National Geoscience Data Discovery Centre (NGDDC), with the vision to establish it as a Centre of Excellence dedicated to fortifying geoscience data and knowledge for a sustainable future. The creation of NGDDC signifies a significant advancement in geoscience data management. The core mission of NGDDC is to transition from traditional access operations to an autonomous mode, thus enhancing the complexity and efficiency of geoscience data management on an operational scale. This transformation is essential for fostering collaboration within the national geoscience community.

Current geoscience data management practices face numerous challenges, including reliance on physical data that prolongs analysis times, limited access to restricted data areas, and the underutilization of geoscientists' capabilities, all of which lead to missed business opportunities and suboptimal decision-making. NGDDC aims to address these issues by establishing a unique collaboration center designed to create a geoscience data discovery hub for Malaysia. This hub will be equipped with cutting-edge facilities that ensure operational excellence and strengthen synergistic collaboration within the geoscience fraternity, fostering innovation in geoscience data to deliver value creation.

The strategic programs of NGDDC are crafted to tackle these challenges through three key initiatives which are the establishment of a one-stop center for geoscience data, ensuring excellent geoscience data operations, and creating a synergistic geoscience data collaboration hub. The core strengths of this center lie in the comprehensive

availability of geoscience information, data, and knowledge of Malaysia, outfitted with advanced technologies and refined work processes. Together, these elements will create a hub that fosters collaborative work among experts within the geoscience fraternity.

The implementation of a one-stop center for geoscience data is vital for improving the quality, comprehensiveness, and trustworthiness of geoscience data. This initiative supports the agenda to maximize business value creation through digitization, simplification of data exchange, centralization of requests, and the establishment of a unified geoscience data platform. The availability of high-quality, comprehensive geoscience data is substantial for the basin-to-prospect maturation workflow, business decision-making for new geoscience data (including sectors beyond oil and gas), and collaborative projects focused on data enhancement, enrichment, and augmentation initiatives.

Furthermore, NGDDC is instrumental in advancing the complexity of geoscience data management at an operational scale, particularly in transitioning from traditional access operations to an autonomous mode. It also plays a crucial role in establishing collaboration within the geoscience fraternity. Through these efforts, NGDDC aims to become a beacon of innovation and excellence in geoscience data management, supporting sustainable development and enhancing Malaysia's appeal as an investment destination.

In a world where the demand for accurate, comprehensive, and timely data is ever-increasing, the establishment of the Geoscience Data Discovery Hub (NGDDC) in Malaysia represents a significant milestone. This hub is poised to revolutionize the field of geoscience data management, equipping it with state-of-the-art facilities designed to boost innovation and efficiency. By integrating autonomous data operations, machine learning, and artificial intelligence (AI) applications, the NGDDC aims to accelerate future value creation and enhance Malaysia's attractiveness as an investment destination.

At the heart of the NGDDC's success lies its cutting-edge facilities. These facilities are crucial for advancing the complexity and efficiency of geoscience data management on an operational scale. Autonomous data operations will reduce the reliance on manual processes, allowing for more accurate and timely data analysis. Machine learning and AI applications will further enhance this process by providing advanced analytical capabilities that can uncover insights and patterns that would be impossible to detect manually.

The success of the National Geoscience Data Discovery Centre (NGDDC) hinges on several critical factors that will ensure its effectiveness and excellence in advancing geoscience data management. Efficient geoscience data operation management is paramount to become an effective management of data operations ensuring that high standards of data accuracy and accessibility are maintained. This involves the streamlined handling and storage of data, as well as the implementation of robust processes and protocols that govern data usage. Efficient data management is crucial for timely insights and decision-making, which are essential for the success of any geoscience research and studies.

Accelerating the aspiration through advanced preservation technologies and the digitization of geo-samples will streamline data handling and preservation processes, ensuring that valuable geological samples are maintained in optimal conditions. This digital transformation will enable easier access to data and improve the overall efficiency of geoscience operations. This includes investing in high-speed networks, robust data storage solutions, and advanced analytical tools, which are vital for handling the complex and voluminous data involved in geoscience projects.

Another critical success factor is through comprehensive benchmarking of other NDR facilities. By conducting thorough benchmarking against other National Data Repository (NDR) facilities, the NGDDC can identify best practices and areas for improvement. Learning from the exemplary NDRs worldwide and its successes and challenges faced will enable the NGDDC to optimize its operations and enhance its effectiveness.

The geoscience data discovery hub in Malaysia is poised to revolutionize geoscience data management. By equipping the hub with cutting-edge facilities and focusing on key success factors, it will set a new standard for efficiency and innovation in the field. The anticipated outcomes of the hub's initiatives highlight its potential to significantly enhance Malaysia's geoscience capabilities and solidify its position as a leading investment destination. Through these efforts, the NGDDC aims to become a beacon of innovation and excellence in geoscience data management, supporting sustainable development.

The initiatives undertaken by the NGDDC are expected to yield several impactful outcomes that will revolutionize geoscience data management. Firstly, the shift to autonomous data operations will enhance efficiency and reduce the reliance on manual processes. Autonomous operations will lead to faster and more accurate data analysis, enabling quicker decision-making and response times. This will significantly improve the overall efficiency of geoscience projects.

Secondly, process cycle efficiency (PCE) improvement by over 30% is anticipated through process simplification. Simplifying processes will result in tasks being completed more quickly and with fewer resources, leading to cost savings and increased productivity. This improvement in efficiency will enable the NGDDC to handle more projects and deliver better results in a shorter timeframe.

The NGDDC will feature a modern facility building in compliance with authority requirements. this facility will be a state-of-the-art building that complies with all relevant authority requirements, ensuring that it meets the highest standards of safety and environmental performance. This will not only provide a safe and efficient working environment but also enhance the NGDDC's reputation as a leading geoscience facility.

Furthermore, the technology-driven facility will be equipped with intelligent building capabilities and leading-edge technologies, driving better efficiency in geoscience data operations. The use of smart systems for energy management, security, and environmental monitoring will enhance the overall operational efficiency and sustainability of the facility.

Lastly, the amplification of value through innovation will be a significant outcome of the NGDDC initiatives. By leveraging new geoscience approaches and techniques, the NGDDC will support business decision-making and amplify value creation through innovation. This includes developing new methods for data analysis, creating more accurate geological models, and identifying new opportunities for exploration and development. The innovative approaches developed at the NGDDC will contribute to the advancement of the geoscience field and support sustainable development.

The establishment of the NGDDC marks a significant advancement in geoscience data management. Positioned as a unique collaboration center, the NGDDC aims to expand its role on a national scale, fostering new collaborative partnerships, encouraging ideation and innovation, enhancing geoscience data management and utilization capabilities, and supporting business excellence as a key enabler for health, safety, and environment (HSE), sustainability, and digital and technology initiatives.

Several critical success factors underpin the NGDDC's mission to enhance geoscience data management and foster innovation. The foundation of the NGDDC's success lies in forging strong partnership agreements and facilitating synergistic collaboration through sustainable programs with PETRONAS, the government, industry, and academia at the national level. These partnerships are essential for pooling resources, sharing expertise, and driving forward collaborative geoscience projects. These programs will also contribute in upskilling and reskilling geoscientists, ensuring they are equipped with the latest knowledge and skills to handle advanced geoscience data technologies and methodologies. Continuous learning and professional development will enhance the overall capability and efficiency of geoscientists, inspiring the next generation of geoscientists and stakeholders through advanced technology and innovations.

In conclusion, the critical success factors and expected outcomes of the NGDDC highlight its potential to significantly enhance geoscience data management in Malaysia. By focusing on efficient data operation management, advanced core preservation technologies, comprehensive benchmarking, enhanced digital infrastructure, and fostering innovation, the NGDDC will set a new standard for excellence in the field. The anticipated outcomes of autonomous data operations, improved process efficiency, modern facilities, and innovative value creation will boost the NGDDC's capabilities. The anticipated outcomes of enriched geoscience data, upskilled geoscientist capabilities, and enhanced innovation and collaboration highlight the NGDDC's potential to revolutionize the field of geoscience. Through these efforts, the NGDDC aims to become a beacon of innovation and excellence, supporting sustainable development and advancing the geoscience field in Malaysia and beyond. NGDDC aims to enhance data utilization and support sustainable development, thereby transforming the upstream business into a digitally enabled organization for a sustainable future.

Optimizing industrial waste for sustainable mineral production: A geoscientific approach for precipitated calcium carbonate in Malaysia

Zawawi Mahim*, Rohaya Othman, Emee Marina Salleh,
Siti Noorzidah Mohd Sabri

Mineral Research Centre, Department of Mineral and Geoscience Malaysia, Ipoh,
Jalan Sultan Azlan Shah, 31450 Ipoh, Perak, Malaysia
*Email: zawawi@jmg.gov.my

Abstract: The growing global emphasis on sustainability has driven numerous industries to explore innovative ways of reducing waste and minimizing environmental impacts. This paper reports the potential of utilizing industrial waste specifically carbide lime waste from acetylene production to produce precipitated calcium carbonate (PCC) in Malaysia. PCC plays a crucial role in industries including plastics, paints, and paper. Recycling industrial waste, such as carbide lime, into high-grade products like PCC demonstrates the capability of transforming by-products into valuable resources. PCC produced from waste offers high purity and quality, making it suitable for demanding industrial applications. This process also reduces the environmental footprint associated with the extraction and processing of virgin materials. Limestone is a key raw material in PCC production, and Malaysia has a well-established limestone mining sector. In 2022, the production of limestone in Malaysia reached 25.3 million metric tons, an increase of 12.4% from the previous year. As a major non-metallic mineral, limestone serves as the backbone of industries like cement and construction, but its extraction comes with environmental challenges. By focusing on waste-derived PCC, Malaysia can reduce its reliance on limestone quarrying, contributing to more sustainable mineral practices. Case studies and collective data from Malaysia's mineral sector, coupled with insights into the regulatory framework, provide a comprehensive view of the environmental and economic benefits of waste-derived PCC production.

Keywords: Geology, SE Asia, CCOP, thematic session, precipitated calcium carbonate (PCC), industrial waste recycling, sustainable mineral production, carbide lime, circular economy

INTRODUCTION

The concept of sustainability has gained prominence within the mineral sector as global demand for raw materials grows. Malaysia, with its rich mineral resources, faces the challenge of balancing economic growth with environmental sustainability. In 2022, Malaysia's mineral industry contributed RM10.49 billion to the national gross domestic product (GDP), representing 0.6% of the overall Malaysian economy (2022 Malaysian Mining and Sustainability). According to annual mineral report, production of limestone-based product so-call precipitated calcium carbonate (PCC) plays a significant role in Malaysia's mineral economy. This type of mineral is used in various industries including plastic, paint, and paper (2022 Malaysian Mining and Sustainability).

Traditional PCC production involves mining limestone; however, this condition comes with high environmental cost, including habitat destruction and greenhouse gas emission. Therefore, this paper explores the use of acetylene waste, specifically calcium hydroxide [$Ca(OH)_2$], as an alternative feedstock for PCC production. By repurposing industrial waste, Malaysia can enhance its resource efficiency while contributing to sustainability goals.

MALAYSIAN MINERAL INDUSTRY

Mineral production in 2022

According to 2022 Malaysian Mining and Sustainability, Malaysia's mineral production increased by 12.3% in 2022, with the number of active mines rising from 169 in 2021

Table 1: Key mineral statistics (2022).

Mineral Type	2021 Production (MT)	2022 Production (MT)	Change (%)
Limestone	22.5 million	25.3 million	+12.4
Silica Sand	1.5 million	1.7 million	+13.3
Kaolin	0.6 million	0.65 million	+8.3

to 188 in 2022. The non-metallic mineral sector, including limestone and calcium carbonate, remains a key contributor to this mineral growth. However, the industry is under increasing pressure to adopt more sustainable practices.

The transition towards sustainability in mineral extraction is crucial for aligning with Malaysia's "TIM 2021-2030" transformation goals, which aims to increase the mineral sector's GDP contribution up to 1% by 2030 (2022 Malaysian Mining and Sustainability). PCC production from industrial waste represents an opportunity to meet this target by reducing reliance on virgin resources.

UTILIZING INDUSTRIAL WASTE FOR PCC PRODUCTION

Acetylene waste as a resource

The production of acetylene gas generates calcium hydroxide as a byproduct, often regarded as waste. This material, however, can be transformed into PCC through carbonation due to its high calcium content. This process involves reacting calcium hydroxide with carbon dioxide (CO_2) gas, which results in a formation of high-purity calcium carbonate, i.e PCC. By utilizing industrial waste, PCC production can shift from a resource-intensive practice to a more sustainable route.

This approach can potentially support Malaysia's goals in order to reduce its carbon footprint and promotes the circular economy. As reported in 2021 study, it was estimated that recycling industrial waste could reduce CO_2 emissions due to its efficient usage in PCC production by up to 40%.

Economic and environmental benefits

The environmental benefits of repurposing acetylene waste for PCC production are substantial. Traditional mining for limestone and the subsequent processing into PCC is energy-intensive and contributes significantly to CO_2 emissions. By contrast, using mineral waste as a main raw material not only reduces the need for mining, but it may also divert the abundant waste from landfills.

According to the Malaysian Minerals Yearbook 2022, Malaysia's PCC production reached a value of RM943.6 million in 2022, with further growth expected as industries seek sustainable solutions. The adoption of waste-based PCC production can reduce costs for manufacturers while improving their environmental footprint.

Table 2: PCC production value (2018-2022).

Year	Production Value (RM Million)
2018	780.5
2019	810.2
2020	856.3
2021	900.1
2022	943.6

Case study: Omya Malaysia Sdn. Bhd.

Omya Malaysia Sdn. Bhd., a Malaysian leader in calcium carbonate production, has started integrating waste-derived PCC into its product line. The company's efforts reflect broader industry trends towards sustainability and are in line with Malaysia's mineral industry transformation plans. As more companies adopt these practices, the industry can achieve its dual goals of economic growth and environmental preservation.

Recycling hydrated lime from the acetylene gas industry into PCC

Hydrated lime (calcium hydroxide), a byproduct of the acetylene gas industry, is an important material that can be transformed into PCC through a relatively simple chemical process known as carbonation. This process not only adds economic value to what would otherwise be considered waste but also has significant environmental benefits by minimizing the need for traditional limestone mining and reducing carbon emissions.

Carbonation process

The reaction to convert hydrated lime into PCC involves introducing carbon dioxide (CO_2) into a solution containing calcium hydroxide [$Ca(OH)_2$]. The reaction produces calcium carbonate ($CaCO_3$) and water (H_2O):

$$Ca(OH)_2 + CO_2 \longrightarrow CaCO_3 + H_2O$$

This process forms high-purity PCC, which can then be used in various industrial applications. The purity and particle size of the PCC can be controlled by adjusting reaction conditions, making it a versatile material with applications in industries such as paper, plastics, paints, and pharmaceuticals (2022 Malaysian Mining and Sustainability).

Environmental and economic benefits

By recycling hydrated lime from acetylene production into PCC, manufacturers can significantly reduce their reliance on raw limestone, which is typically extracted through environmentally mining practices. Traditional limestone mining contributes to deforestation, loss of biodiversity, and significant CO_2 emissions due to transportation and processing. In contrast, the use of acetylene byproduct may help in reducing these aforesaid impacts, as the waste material is repurposed directly at the production site, thus minimizing transport-related emissions.

A 2021 study on waste recycling in the calcium carbonate industry found that PCC production using industrial byproducts like hydrated lime could reduce energy consumption by up to 30% compared to traditional mining and processing methods. This scenario does not only reduce operational costs for manufacturers but also may support the global shift towards more sustainable production practices.

Case example: Hydrated lime to PCC in Europe

A similar method of recycling industrial byproducts into PCC has been implemented successfully in Europe, where the hydrated lime from acetylene production is transformed into PCC for use in the paper and plastics industries. This process has led up to 40% reduction in CO_2 emissions across several production sites and helped companies meet stringent environmental regulations. Malaysia could benefit from adopting these best practices, particularly as the country looks to strengthen its sustainability credentials under initiatives like the TIM 2021-2030 and the United Nations Sustainable Development Goals (SDGs).

REGULATORY AND POLICY FRAMEWORK

Malaysia's regulatory framework supports the sustainable development of its mineral resources. The National Mineral Policy 2 and the TIM 2021-2030 both emphasize responsible mineral extraction and the importance of transitioning towards sustainable practices.

Additionally, Malaysia has committed to the United Nations Sustainable Development Goals (SDGs), particularly Goal 12, which focuses on responsible consumption and production. Government incentives, such as tax reductions for companies adopting green technologies, have further encouraged the recycling of industrial waste into valuable products like PCC.

CHALLENGES AND OPPORTUNITIES IN ALIGNING MALAYSIA'S MINERAL INDUSTRY WITH GLOBAL SUSTAINABILITY GOALS

Global commitments and the role of Malaysia

Malaysia, as other developing countries, is under increasing pressure to align its industrial activities with global sustainability goals. The United Nations Sustainable Development Goals (SDGs), particularly Goal 12, emphasize responsible consumption and production, urging nations to reduce waste generation, increase recycling initiative, and promote sustainable industries. For Malaysia, meeting these targets requires balancing economic development with environmental stewardship, a challenge that is particularly relevant in the mineral industry.

One area where Malaysia is making strides is in the transition to a circular economy—a concept that aims at minimizing waste and maximizing resource efficiency by recycling and reusing materials. The production of PCC from acetylene waste is a case in point of on how Malaysia can contribute to a circular economy while reducing its reliance on virgin raw materials (2022 Malaysian Mining and Sustainability). By utilizing the industrial byproducts, Malaysia is demonstrating its commitment towards more sustainable production processes, which could serve as a pioneer model for other developing nations.

Malaysia's unique challenges

Despite these advancements, Malaysia faces several challenges in achieving sustainability in its mineral industry:

i. Infrastructure Gaps: While larger companies like Omya Malaysia Sdn. Bhd. have adopted sustainable practices such as utilizing waste-derived PCC (2022 Malaysian Mining and Sustainability), lower-scaled mining and processing operations may lack the infrastructure and resources needed to integrate that type of technologies. This gap in technological capacity can downtrend the overall adoption of greener practices in the industry.
ii. Environmental Degradation: The continued reliance on traditional mining methods for raw materials such as limestone poses a significant environmental risk. Malaysia's rich biodiversity, especially in limestone hill areas that are frequently targeted for quarrying, faces threats from deforestation and habitat destruction. Environmental activists and organizations like the Malaysian Nature Society have raised concerns about the long-term impacts of quarrying on ecosystems, emphasizing the need for stricter regulations and incentives for sustainable practices.
iii. Global Market Pressures: Malaysia's mineral industry is subjected to global market demands, particularly from high-growth industries such as construction, electronics, and automotive manufacturing. As global demand for PCC and other minerals increases, Malaysia may face the challenge of scaling up production while adhering to sustainability principles. Balancing economic competitiveness with environmental preservation will require durable governmental policies and industry collaboration.
iv. Policy and Regulatory Enforcement: Malaysia has robust policies, such as the TIM 2021-2030 plan and National Mineral Policy 2, that support sustainable mining and mineral processing (2022 Malaysian Mining and Sustainability). However, ensuring effective implementation and enforcement of these policies remains a challenge. For example, illegal mining activities, particularly for valuable minerals like rare earth elements (REE), continue to pose environmental threats and undermine Malaysia's sustainability efforts.

Opportunities for global leadership

By overcoming these challenges, Malaysia has the potential to position itself as a global first-step maker in sustainable mineral production. Leveraging technologies for recycling industrial waste, such as the hydrated lime to PCC process, can place Malaysia at the forefront of innovative green technologies that contribute to both environmental and economic goals. Further investment in research and development (R&D), coupled with public-private

partnerships, could help Malaysia to profitably export these sustainable technologies to the other developing nations.

Malaysia's ability to meet global sustainability goals will also depend on international collaboration. Partnerships with countries that are leaders in circular economy practices such as Germany and the Netherlands, that could provide Malaysia with the technological expertise needed in scaling up its waste-recycling efforts.

CONCLUSIONS

Malaysia's mineral industry is at a crossroads as it seeks to balance economic growth with environmental sustainability. The production of PCC from acetylene waste offers a promising resolution to the industry's environmental challenges, allowing Malaysia to reduce its reliance on raw limestone, decrease carbon emissions, and contribute to a circular economy. While the country has made progress through policies like the TIM 2021-2030 plan and sustainable initiatives by key industry players, significant challenges remain. Infrastructural gaps, environmental degradation, and global market pressures must be addressed to a complete transition to sustainable mineral production.

However, these challenges also present many opportunities. By effectively investing in technological innovations, strengthening recycling practices, and fostering international partnerships, Malaysia can become a global leader in sustainable mineral production. The integration of waste-derived PCC production does not only support Malaysia's sustainability goals but also strengthens its position in global markets increasingly driven by environmental regulations and responsible consumption practices. With the right policy enforcement, industry collaboration, and commitment to innovation, Malaysia can pave the way for a more sustainable future in the mineral sector, contributing significantly to global efforts to combat the climate change and resource depletion.

REFERENCES

Malaysian Mineral Statistics 2022. (Malaysia Minerals Yearbook 2022).

Jabatan Mineral dan Geosains Malaysia. (Malaysian Mining and Sustainability 2022).

Omya International. "Sustainability Report 2021: Waste Reduction in Calcium Carbonate Production."

United Nations. "Sustainable Development Goal 12: Responsible Consumption and Production."

Smith, R. & Chen, H., 2021. Industrial Waste Recycling for PCC: Environmental and Economic Benefits. Journal of Sustainable Engineering.

Sahu, A. *et al*., 2021. Carbonation Process Optimization for PCC Production from Industrial Byproducts. Journal of Environmental Management, 296, 113-128.

Carus, M. & Dammer, L., 2020. Recycling of Industrial Byproducts for High-Value Applications in the Calcium Carbonate Industry. Circular Economy Journal, 15(3), 42-54.

Malaysian Nature Society, 2021. Conservation of Limestone Hills in Malaysia: Environmental and Biodiversity Considerations. MNS Report (2021).

Geological CO2 storage potential in Indonesia: The case of Java Island

Andy S. Wibowo*, Joko Wahyudiono, Indra Nurdiana

Geological Survey Centre, Geological Agency, Ministry Of Energy And Mineral Resources Republic Of Indonesia
*Email: asw8513@gmail.com

Abstract: Although reducing the amount of CO2 emissions as a means of tackling climate change has become a major issue in the development and implementation of carbon capture and storage (CCS), but actually this applied technology is very strategic during the energy transition period. Some countries realize that the continued need for fossil fuels while that clean energy growth is slow. Artificial CCS is still the most effective ways to maintain that environmental balance. Key success of implementing CCS technology today is not in the CO2 capture method but in the availability of large storage that are able to restrain the CO2 release to the surface.

Indonesia's geological history allows for sedimentary basins to be ideal CO2 storage. Geological formations that have the ability to store, can be injected and conventional trapping systems are the majority of its components. Unproduced coal formations, depleted oil and gas reservoirs, and geological formations saturated with salt water that are not suitable for consumption are potential CO2 storage resources in Indonesia's sedimentary basins.

Oil and gas fields found in many sedimentary basins in Indonesia have even been produced for more than 300 years, which is part of the evidence of Indonesia's carbon storage potential. Some others are still hidden in unproduction sedimentary basins. This study was conducted to find hidden potential storage through a comprehensive G&G survey including detailed geology descriptions, petrophysical and rock mechanics laboratory measurements. Formation evaluation is carried out based on these data to characterize the components of the CO2 storage system. Meanwhile, pore volume of geological formations modeling is formed by applying gravity inversion. Storage capacity is calculated by considering physical properties and regional pressure-temperature gradients.

Java Island as the fastest industrially developed in Indonesia is the area of this investigation, especially the southern part. Four intermountain basins and one back-arc basin have been identified as having the potential for geological formation CO2 storage resources of up to 1225 Giga Tons of CO2, that is East Java of 392 Giga Tons of CO2, Central Java of 278 Giga Tons of CO2, and West Java of 555 Giga Tons of CO2. Ultimate CO2 storage capacity which fully fill the pore volume of rock informs the enormous potential of geological carbon storage resources.

Keywords: CO2 storage resources, formation evaluation, G&G survey, Java Island Indonesia

INTRODUCTION

Carbon storage in subsurface geological formations has been widely stated by researchers before as the most efficient alternative technology to reduce carbon emissions in the atmosphere. Along with the application of this alternative technology to prevent world climate change, the role of this technology is very strategic in supporting the transition from fossil energy to clean energy in Indonesia.

Indonesia as part of the world is committed to reducing carbon emissions by targeting an *Enhanced Nationally Determined Contribution* (E-NDC) of 32% or equivalent to 912 million tons of CO2 by 2030. At the same time, Indonesia is developing in all fields of industries that require very large energy, while the development of clean energy and renewable energy is still slow. The high carbon content in fossil energy often hampers the operation of Indonesia's oil and gas fields. Thus, effective efforts to handle carbon emissions in most of Indonesia's oil and gas fields are needed to achieve national energy security.

Carbon reinjection into reservoirs has been carried out by many oil and gas operators for *Enhanced Oil Recovery* (EOR) and has been proven to be able to temporarily store carbon emissions before they come back to the surface with hydrocarbon production. Injecting carbon into reservoirs that have lost pressure has become Indonesia's strategy in storing carbon emissions more permanently to control the amount of greenhouse gas emissions in the atmosphere. Carbon storage in coal and cavern formations has begun to be developed even in shale and basalt formations that are still in the research stage. The geological formation of saline aquifers as a carbon sink is a topic especially in this paper. Its wide distribution with an even thickness and tends to form in each sedimentary basin becomes a very potential carbon storage geological resource. Although the lack of geological data and information and the difficulty

of obtaining geological analogies for the characterization of saline aquifer geological formations are challenges in this study.

This study is intended to identify the characteristics of the rocks that make up geological formations as components of carbon storage systems (reservoirs, seal rocks, trapping) to map the potential of carbon storage saline aquifer geological resources in Indonesian sediment basins that have not yet been produced. Detailed and comprehensive analysis of data on rock physics, structural geology and geomorphology as well as sedimentology and stratigraphy were carried out systematically on more than 100 outcrops representing the geological formations of carbon storage system components. Gravity data taken with a space of 2000 m can provide subsurface model information including the dynamics of the bedrock and the vertical and lateral distribution of sedimentary rock formations and alluvium as components of the sedimentary basin. The dynamics of the sediment basin can be mapped, the analogy of the characteristics of the geological formation of the sedimentary basin components can be quantified and the characteristics of the fluid can be assumed based on the pressure gradient, regional temperature and type curve then the theoretical capacity of the geological resources of carbon storage can be calculated.

REGIONAL GEOLOGY OF JAVA ISLAND

Java Island is a young geosynchronous and organic path with a strong influence of volcanism, has an elongated and narrow formation with an area of 127,000 km^2. Geologically, Java Island is a historical complex of basin subsidence, displacement, folding and volcanism under the influence of different stress regimes from time to time influenced by tectonic activity of the Eurasian Plate and the Indo-Australian Plate. The geological structure on the island of Java has regular patterns. Sunda Strait pattern which is North-South, the Meratus pattern which is Northeast Southwest, and the Javanese pattern is West-East (Figure 1). The first and second patterns are likely to be produced by pre-Tertiary tectonics which then undergo reactivation in younger tectonic activities. The third pattern, the Javanese pattern, is caused by Neogene tectonics and is the most developed pattern on the island of Java (Bachri, 2014).

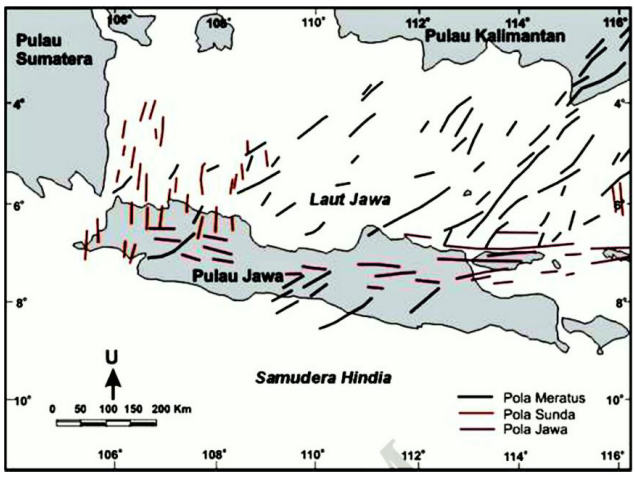

Figure 1: Pattern of geological structure in Java Island.

The geological process takes place endlessly and arranges various morphology of the Java Island time by time. The first deposits themselves are estimated to have occurred between 54 and 36 million years ago (Eocene) due to plate stretching. The revelation of conglomerates, limestone, sandstone, and coal showed the characteristics of shallow river-sea deposition at that time.

Then Java Island was exposed to compressive pressure from the south which caused the Indo-Australian oceanic plate moving northward to hit the Eurasian continental plate from the south side. Oceanic plates that have a higher specific period undergo subduction and produce subduction pathways. Due to subduction, sea troughs, new mountains, and volcanic activity are formed. There was also a melting of material from the Indo-Australian Ocean plate which became magma and created a volcanic path parallel to the long axis of Java Island.

After the formation of an ancient fire cluster as a volcanic path, from the Late Oligocene – Early Miocene period, a series of extremely powerful volcanic events occurred. This is evidenced by the discovery of many pyroclastic outcrops and volcanic sediments. From the outcrop, at least 2 ancient volcanoes are recognized, namely Semilir and Nglanggeran.

During the Middle Miocene, the slope of the Indo-Australian Ocean plate subduction also began to decline, so that the melting process that produced magma also shifted to the north. This process continued into the Pleistocene and is still going on today. The shift in the volcanic path inactivates all ancient volcanoes because the supply of molten magma beneath the earth's surface shifts northward. Therefore, magmatism activity began to decrease and there was continuous precipitation until now.

After that, there was a deposition of deltas, rivers, and shallow marine over the island of Java. Sea level decline occurs slowly. At the same time, the Indo-Australian oceanic plate continues to move, pressing on the Eurasian Plate, causing orogen's, and other uplift.

EVOLUTION OF SEDIMENTARY BASINS OF JAVA ISLAND

A sedimentary basin is a depression where sedimentary deposits accumulate and acts as a container for the sedimentation and maturation of sediments containing hydrocarbons (Boggs, 2006). The structure of the basin can be identified based on geological and geophysical analysis. Geological analysis estimates the existence of basins based on tectonics, physiology and regional geological order of an area. Geophysical analysis uses geophysical data based on certain physical parameters to be interpreted for subsurface geological modeling (Setiadi & Pratama, 2018).

The evolution of sedimentary basins in Java is a multifaceted process influenced by tectonic dynamics, sedimentation patterns, and volcanic activity. Java's geological history is marked by significant tectonic events, particularly the interactions between the Indo-Australian Plate and the Eurasian Plate, which have shaped the sedimentary landscape of the region. This paper aims to provide a comprehensive overview of the evolution of Java's sedimentary basins, focusing on critical basins such as the East Java Basin, West Java Basin, and Banyumas Basin.

The tectonic development of the island of Java which is studied from geological structure patterns over time shows the fact that there are basins with certain patterns on the island of Java. In general, there are two basin groups, that is the western North Java Basin and the eastern North Java Basin which are separated by the Karimun Java height. The western North Java basin group has a geometric shape extending relatively north-south with basin boundaries in the form of faults in the north-South and East-West directions. Meanwhile, the basins in the Eastern - North Java basin group generally have an East - West longitudinal geometry with a more dominant east-west structural role (Kusumadinata, 1975; Pulunggono, 1994).

During the Eocene period until the end of the Late Oligocene, there was uplift of the subduction path of the Eurasian Plate with the Indian Ocean plate separating the northern part of Java with its deep depression from the southern part characterized by a terrestrial deposition, exposure and shallow environment (Sonearth, 2010). Along the southern coast of Java, there is a group of volcanic rocks called the "old andesite formation" which is of early Oligocene age. The characteristics of the rock are gravitational flow deposits such as lava which is mostly composed of igneous rock fragments and sediments, such as andesite, tuff and limestone. The thickness reaches 7000m. The western North Java Basin is characterized by an exposed deposition pattern, generally consisting of limestone, clay and quartz sand deposits and a shallow sedimentation environment. Its depth reaches more than 5000m.

The region's volcanic activity further complicates the evolution of sedimentary basins in Java. The Cenozoic volcanic arc in southern Java has played a crucial role in shaping the sedimentary landscape, with volcanic eruptions contributing to ash deposition and pyroclastic materials (Smyth *et al*., 2008; Clements *et al*., 2009). The interaction between volcanic and sedimentary processes has led to the formation of unique sedimentary structures, such as turbidites and lahar deposits, indicative of the dynamic geological environment in Java (Clements *et al*., 2009; Riza *et al*., 2019).

Moreover, the sedimentary basins in Java have been subject to various sedimentation processes influenced by paleogeographical changes. For instance, the East Java Basin has undergone significant sedimentation influenced by volcanic activity and tectonic uplift, accumulating diverse sedimentary facies (Ningsih, 2023). The analysis of sedimentary structures and ichnofacies in regions like West Java further elucidates the evolved complex depositional environments (Muljana *et al*., 2021).

DISCUSSION

The sedimentary basin in the southern part of Java Island is located in the transition area which is an area of interaction between plates at this time. This transition area with volcanic and seismic activities is still active. The volcanic arc extends from East to West with a relatively constant position limiting the northern and southern sedimentary basins. The southern part of Java Island has five sedimentary basins: South-East Java Basin, Wonosari Basin, South-Central Java Basin, the Banyumas Basin, South West Java Basin. The sedimentary basin in the southern part of Java Island has an average depth of 3500 m.

Pyroclastic sedimentary rocks and volcanic sediments dominate the stratigraphic stratigraphy of the sedimentary basin in the southern part of Java Island from the Late Oligocene to the Early Miocene. From the sedimentary rock outcrops, at least two ancient volcanic products are recognized: Semilir Formation and the Nglanggeran Formation which are deposited in conformity and spread widely. The first deposition itself is thought to have occurred during the Eocene due to plate stretching. The revelation of conglomerates, limestone, sandstone, and coal showed the characteristics of shallow river-sea deposition at that time. During the Middle Miocene to the Late Pliocene, magmatism activity began to decrease and there was continuous precipitation until now.

South East Java has five sub-basins: Ponorogo Sub-Basin, Kediri Sub-Basin, Blitar Sub-Basin, Malang Sub-Basin, and Lumajang Sub-Basin. Central Java has three basins: Banyumas Basin, South Central Java Basin and Wonosari Basin. The Banyumas Basin can be divided into six sedimentary Sub-Basins: Citandui Sub-Basin in Cilacap district, Majenang Sub-Basin in Brebes district, Purbalingga Sub-Basin in three districts: Banyumas, Purbalingga and Banjarnegara, Wonosobo Sub-Basin in Wonosobo district and the Karangkobar Sub-Basin in Banjarnegara district. The South-Central Java Basin consists of Kedu Sub-Basin which is located in Purworejo district, Ambarawa Sub-Basin, and the Sragen Sub-Basin. The southern part of West Java has been identified two Basin: Bogor Basin and South-West Java Basin. Ciamis Sub-Basin, Tasikmalaya Sub-Basin, Garut Sub-Basin, Cianjur Sub-Basin, Sukabumi Sub-Basin and Pelabuhan Ratu Sub-Basin part of South-West Java Basin.

Modeling of sediment basin dynamics is carried out using gravity data through the process of inversion into the density magnitude. The rock components that make up the sedimentary basin can be modeled well when there is a large difference in rock density. As empirically understood that the density of bedrock, sedimentary rock and alluvium rock has a significant density difference so that the modeling of

basin dynamics can be well described by the inversion of gravity data. The sedimentary basin in Southern Java has a depth of up to 3500 m, which is top basement and bottom sediment at a density greater than 2.9 gr/cc. The density of alluvium deposits is formed in conformity overlay the sedimentary rocks at a density of 1.67 gr/cc – 2.00 gr/cc (Figure 2). Thus, the bulk volume of sedimentary rocks formed in South-East Java Basin is 12,548 Km^3, South-Central Java Basin is 5602 Km^3, Banyumas Basin is 15,273 Km^3, and South-West Java and Bogor Basin is 20,754 Km^3.

The CO2 storage system in the Southern Sedimentary Basin of Java Island consists of reservoir: sandstone, reef limestone and clastic volcanic rocks, seal rock: platform carbonate rocks, breccia and clay. The average reservoir thickness of more than 2000 meters is porous and permeable, which is 20% pu and 25.2 mD. Impermeable caprocks have an average thickness of 1470 m.

One of the physical properties of rocks that greatly affects the process of water change by CO2 in the pores of the rock is irreducible water saturation, which is the volume of water in the pore volume in a porous medium that is immobile. As it is understood that CO2 can only replace the mobile fluid in the pores. Irreducible water saturation greatly affects the ability of fluids to flow through a reservoir rock pore with an inverse correlation and has a reciprocal relationship. Thus, the greater the permeability of the reservoir rock, the smaller the irreducible water saturation so that the amount of irreducible water saturation can be estimated. Timur (1968) empirically describes the relationship through the following equations:

$$K = (0{,}316\ \Phi^{4.4})/Sw_{irr}$$

Naturally, the mutual relationship of the physical properties of the rock is unique, influenced by lithology, geometry and structural pore especially the distribution of grain size and depositional environment respectively. Therefore, the prediction of the physical properties of rocks will be better when measured in the laboratory.

The southern part of Java Island has a relatively normal regional geothermal gradient of 30°C/Km, although in some parts it is higher due to the influence of subduction zones that have a transverse axis along the island of Java. At a high salinity of >10000 ppm formation water, the density of carbon dioxide will increase relative to depth compared to areas with lower geothermal gradients. Therefore, the mobility of carbon dioxide to the formation water will be higher and the potential for mixing between the two fluids will be higher in the sedimentary basin of Southern Java Island.

Earthquakes caused by volcanic and tectonic activities greatly affect the quality of carbon dioxide storage in subsurface geological formations. The island of Java, especially the southern part, has a geological history that experiences a lot of tectonic and volcanic activity. The displacement of the volcanic axis to the North of Java Island

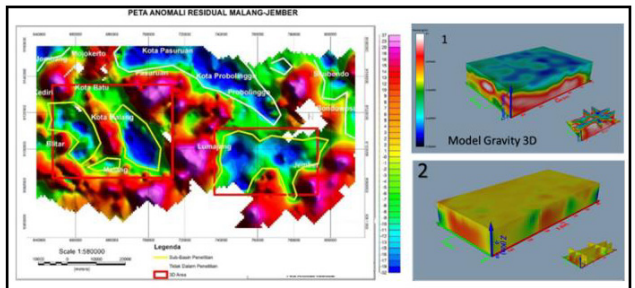

Geology Formation	Lithology	Component	Thickness (m)	Porosity (frac)	Permeability (mD)
Wonosari	Limestone & Clay	Capsrock	800	< 0.01	< 0.001
Oyo	Sandstone	Reservoir	200	0.18	50
Wuni	Breccia & Sandstone	Reservoir	800	0.1	20
Campurdarat	Clastics Carbonate	Reservoir	300	0.05	5
Jaten	Conglomerate & Sandstone	Reservoir	100	0.15	15
Nampol	Siltstone & Sandstone	Reservoir	100	0.1	38
Arjosari	Breccia	Capsrock	500	<0.01	< 0.001
Dayakan	Sand-shale lamination	Reservoir	600	0.13	13

(a)

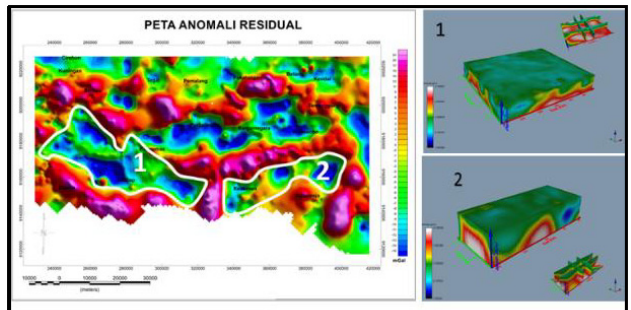

Geology Formation	Lithology	Component	Thickness (m)	Porosity (frac)	Permeability (mD)
Peniron	Breccia	Capsrock	400	<0.01	< 0.001
Sentolo	Limestone	Reservoir	350	0.2	17
Kepek	Napal	Capsrock	350	<0.01	< 0.001
Penosogan	Sandstone	Reservoir	400	0.1	8
Halang	Sandstone	Reservoir	700	0.27	75
Wonosari	Limestone	Capsrock	800	<0.01	< 0.001
Jonggrangan	Conglomerate	Reservoir	200	0.13	11
Sambipitu	Sandstone	Reservoir	230	0.23	45
Kebobutak	Sandstone	Reservoir	650	0.15	21
Nanggulan	Sandstone	Reservoir	270	0.17	25

(b)

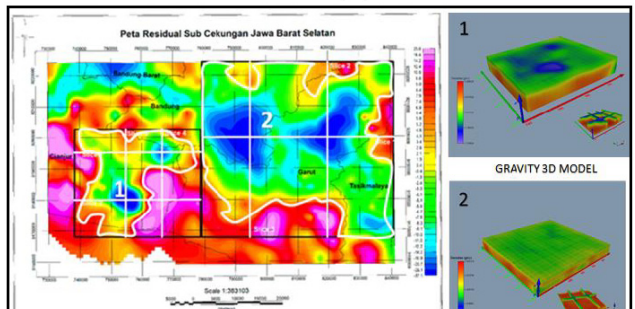

Geology Formation	Lithology	Component	Thickness (m)	Porosity (frac)	Permeability (mD)
Bentang	Sandstone	Reservoir	800	-	-
Cibodas	Limestone	Reservoir	250	-	-
Jampang	Limestone	Capsrock	5000	<0.01	< 0.001
Koleberes	Sandstone	Reservoir	550	0.19	26
Kalipucang	Limestone	Reservoir	450	0.1	18

(c)

Figure 2: Sedimentary basin dynamics: (a) Southern East Java Island, (b) Southern Central Java Island, (c) Southern West Java Island.

due to the flattening of the Ocean crust in its subduction zone provides a downward trend of volcanic activity in the southern part of Java Island, but tectonic activity due to the movement of continental plates and the Ocean still produces earthquakes along the southern part of Java Island. Based on earthquake data and information in 2023, the level of earthquake vulnerability in South Java can be mapped (Figure 3).

The integration of sedimentological and stratigraphic information, structural geology and geomorphology, geophysics and formation evaluation showed that the CO2 storage potential in the saline Aquifer formation in the sedimentary basin of Southern Java Island was very large, which was around 1225 Gton CO2e with medium to high geological risk (Figure 4).

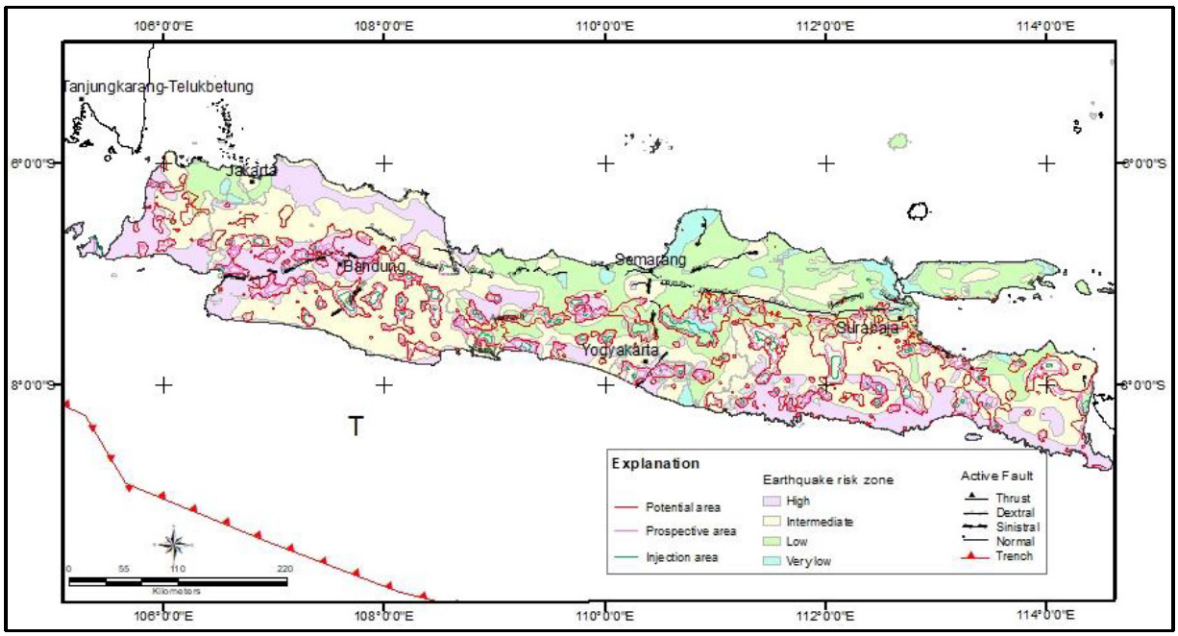

Figure 3: Carbon capture and storage (CCS) potential across Java Island, Indonesia.

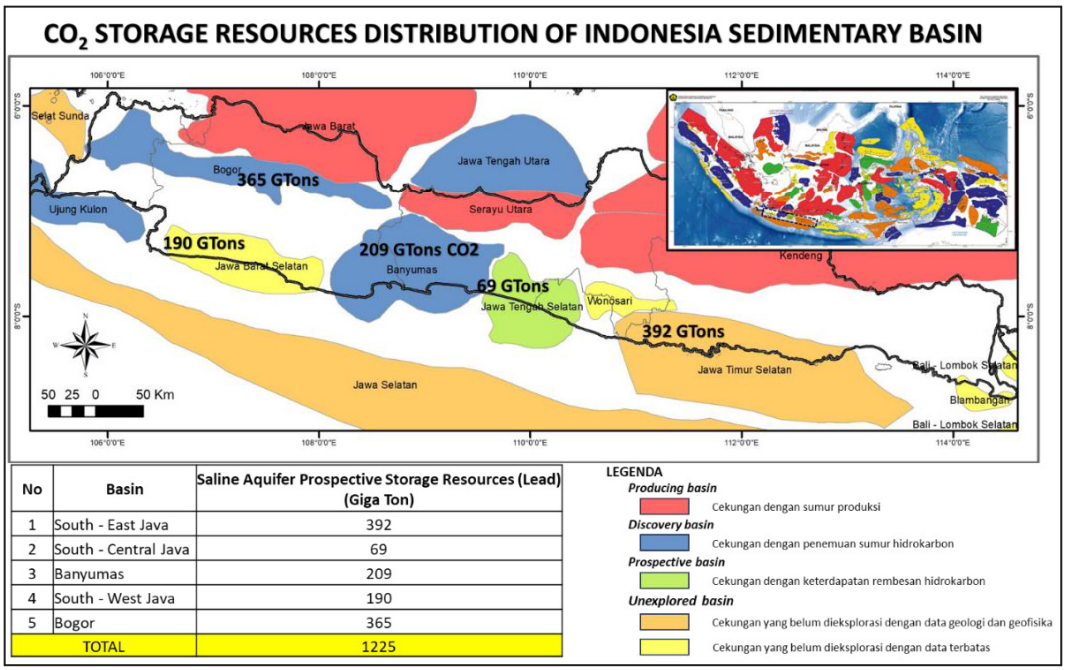

No	Basin	Saline Aquifer Prospective Storage Resources (Lead) (Giga Ton)
1	South - East Java	392
2	South - Central Java	69
3	Banyumas	209
4	South - West Java	190
5	Bogor	365
TOTAL		1225

LEGENDA
Producing basin
Cekungan dengan sumur produksi
Discovery basin
Cekungan dengan penemuan sumur hidrokarbon
Prospective basin
Cekungan dengan keterdapatan rembesan hidrokarbon
Unexplored basin
Cekungan yang belum dieksplorasi dengan data geologi dan geofisika
Cekungan yang belum dieksplorasi dengan data terbatas

Figure 4: Carbon dioxide storage capacity of Southern Java Island, Indonesia.

CONCLUSIONS

Investigation of geological carbon dioxide storage resources based on basin-scale and geological criteria on the Java Island which reaches 1225 Giga Ton CO2 with the following details:

1. The South-East Java Basin is an intermountain basin (Intermontane basin) located in the Southern East Java Province. Sedimentary basins with depths up to 3500 m, saline aquifer reservoir thickness up to 1200 m and theoretical geological resources carbon dioxide storages 392 Giga Tons with low to medium geological risk
2. The South-Central Java Basin is located in the Southern Central Java Province. This intermountain basin (Intermontane basin) has a sediment thickness of up to 3000 m with an average saline aquifer reservoir thickness of 1000 m and theoretical geological resources of carbon dioxide storages of 69 Giga Tons with medium to high geological risk
3. The Banyumas Basin is an intermountain basin (Intermontane basin) located in Banyumas Regency, Central Java Province. Sedimentary basins with a depth of up to 3640 m, saline aquifer reservoir thickness of up to 1600 m and theoretical geological resources of carbon dioxide storages of 209 Giga Tons with low to medium geological risk
4. The South-West Java Basin is located in the Southern part of West Java Province. This intermontane basin has a saline aquifer reservoir thickness of 2400 m and a theoretical geological resource of carbon dioxide storages of 190 Giga Tons with medium to high geological risk.
5. The Bogor Basin is located in the provinces of West Java and Banten. This Back-Arc basin has a saline aquifer reservoir thickness of 1200 m and a theoretical geological resource of carbon dioxide storages of 365 Giga Tons with medium to high geological risk.

REFERENCES

Amyx, J.W., Bass JR, D.M & Whiting, R.L., 1960. Petroleum reservoir engineering: Physical properties. McGraw-Hill Book Co., New York, 80 p.

Bachri, S., 2014. The Effect Of Regional Tectonics To The Structural Pattern And Tectonics Of Java Island. J.G.S.M., 15, 215 – 221.

Bachu, S., 2003. Screening and ranking of sedimentary basins for sequestration of CO2 in geological media in response to climate change. DOI: 10.1007/s00254-003-0762-9, Environmental Geology, 44, 277-289.

Setiadi, I., & Pratama, A.W., 2017. Structural Pattern and Subsurface Geological Configuration of North West Java Basin Based on Gravity Analysis. J.G.S.M., 19, 59–72.

Timur, A., 1968. An Investigation of Permeability, Porosity, and Residual Water Saturation Relation for Sandstone Reservoirs. Log Analysts, 9, 4.

Wave energy potential assessment in the sea of Southern Bali, Indonesia

Irwan H. Suherman[1,*], Sunindyo Herdadi[1], Luli Gustiantini[1], Susilohadi[2], Nina Konitat[3]

[1]Marine Geological Institute (MGI), Geology Agency, Ministry of Energy and Mineral Resources (MEMR) Republic of Indonesia, Bandung, West Java, Indonesia
[2]National Research and Innovation Agency of Indonesia (BRIN), Bandung, Indonesia
[3]National Research and Innovation Agency of Indonesia (BRIN), South Tangerang City, Indonesia
*Email: irwan.suherman@esdm.go.id

Abstract: The 2021-2030 Electricity Supply Business Plan targets a renewable energy 23% in 2025 and a decarbonization program in 2060. That's the main concern of the MEMR pursuing national electrification ratio increase. One of the outermost areas that has new renewable energy (NRE) potential is Nusa Penida District, Klungkung Regency, Bali Province, Indonesia. According to the Bali Provincial Electricity Roadmap, the site will be a pilot location for the NRE project in 2030, with Nusa Penida Island as 100% renewable source utilization, one of which is from sustainable marine, specifically wave energy. According to Cornett (2008), the Southern Bali Sea has a wave potential of 20-25 kW/m. Similar modelling results were made by Rizal & Ningsih (2020), which revealed that the same location has a wave potential of 20-25 kW/m. A potential simulation as well was carried out by MGI, revealing that Southern Bali produces a yearly mean power of around 22.62 kW/m. Significant wave height (SWH) is in the range of 1.5-2.5 m (occurrence frequency of 63.83%), wave period (Ts) 10-15 s (occurrence frequency of 73.83%) and wave power potential (occurrence frequency of 55.82%) in the range of 4-20 kW/m and 20-40 kW/m (occurrence frequency of 32.73%) taking into account monthly and seasonal variability index calculation in the interest area. Various mean power (kW/m) of the Nusa Penida (NSP) model simulation in January, February, March, April, May, June, July, August, September, October, November, and December are 18.64, 23.66, 13.52, 23.47, 21.55, 22.44, 35.97, 33.04, 34.04, 20.19, 10.60, and 14.39, respectively. While the maximum power (kW/m) are 46.85, 46.83, 31.06, 56.93, 42.97, 63.96, 74.55, 77.34, 79.01, 81.05, 26.86, and 29.50, respectively. The average value of the potential power density shall produce an annual mean energy potential of 190.97 MWh/m in southern Bali (west-southwest Nusa Penida Island). From several districts that produce annually potential power (kW/m), including Jungut Batu, Devil's Tear Beach, Tanglad, Ped, Bunga Mekar, Lembongan, and Ceningan are 1.75, 11.97, 17.85, 1.37, 17.19, 11.25, and 11.63, respectively. The Levelized Cost of Energy (LCOE) of the wave power plant in Nusa Lembongan is around $0.12/kWh minimum with various appropriate types of Wave Energy Converter (WEC) are Fixed Oscillating Water Column and Heaving Device Turbine Generator.

Keywords: Wave energy, Nusa Penida, Southern Bali, marine renewable, NSP Power Density Model (kW/m), Significant Wave Height (SWH), LCOE, Wave Energy Converter (WEC)

INTRODUCTION

To support sustainable national development and energy security, renewable energy is one of the most important sources of driving economic growth because it is very much needed by every element of society (Indonesia Constitution No.30 of 2007). Therefore, limited energy resources will be an obstacle that could hinder the pace of economic growth in the future. The steps taken by the government to anticipate an energy crisis in Indonesia include the National Energy Policy, Constitution Number No. 30 Year 2009, and the National Marine Exploitation Policy, which emphasises energy sustainability through the creation and utilisation of renewable sources. In Government Regulatory National Energy Regulation 2014, the composition of renewable is expected to be 23% in 2025 (Figure 1).

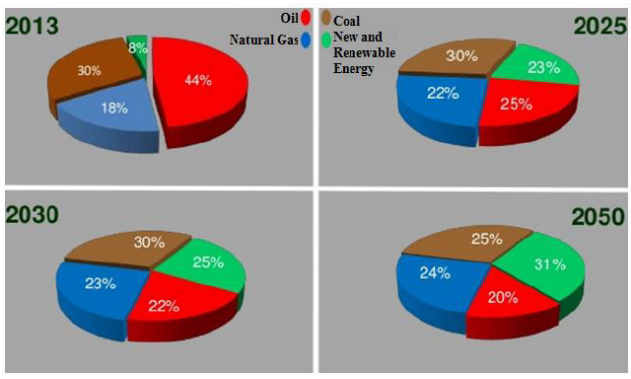

Figure 1: Energy mix achievement targets in 2025.

One of the renewable sources that is currently developing is marine energy. Several technologies are currently in the development stage to improve the performance of power plants sourced from wave energy (Lopez *et al*., 2013). The policy of MEMR Indonesia in responding to national issues regarding energy diversification is to diversify supply and use of various renewable sources, one of which is marine energy that's able to be utilised as power plants based on wave energy. From this perspective, in the next few decades, wave energy is expected to generate at least 10% of global energy demand (Silva *et al*., 2016). The study site was selected as one of the areas that have wave power potential along the south coast of Bali, with a mean power flux reaching up to 20–30 kW/m (Figure 2).

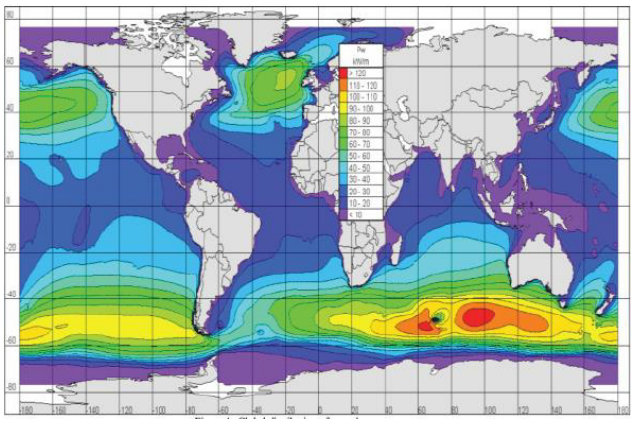

Figure 2: Global distribution of annual mean wave power (Cornett A. *et al.*, 2008).

One of the locations that has a large number of wave resources is Nusa Penida Island, Province Bali, Indonesia. Nusa Penida is one of the outermost islands located in the Indian Ocean (Figure 3). Administratively, Nusa Penida Island is located in South Bali Island, 37 km away from the centre of the provincial capital. It is necessary to have the main supporting supply of electrical energy from renewable at Nusa Penida Island. Nusa Penida Island enters category 3, where locations that are potentially and practically suitable but for the accessible stage still need to be reviewed because there are no regulations on marine spatial planning, and dominantly SWH 1-1.5 m with period 5-7 s, able to generate 17-160 kW of electricity produce from several turbines (Setyawan, 2018). Capital Cost around $0.17/kWh, meanwhile feed in tariff around $0.08/kWh (assumption $1= Rp.15.474,34).

MATERIALS AND METHOD

Study description

The parameters were SWH (Hs), maximum wave height (Hmax), period (Tp), direction (θ_0) and spectrum energy (E). These parameters are used as input for calculating wave power potential. Waters between Asia-Australia and Pacific-Indian Oceans are a geographically specific structure (Wrytki, 1961). The Nusa Penida Islands waters are used for the domain area. Secondary bathymetric data was obtained from GEBCO (Global Bathymetric Chart of Oceans) with 1 mnt resolution (Figure 4), and wind data from ECMWF (European Centre for Medium-Range Weather Forecasts).

Figure 3: Site study location Nusa Lembongan, Nusa Penida Island, Bali, Indonesia.

Model setup

The model area is discretised with varying grid sizes, thus the largest grid being 1000 m^2, consisting of 2645 nodes and 4297 elements with a distance of 28-33 km coastline to offshore with a domain area of 115.08 – 115.53 E and 8.63 – 8.91 S (Figure 5).

At the open boundary, wave data is obtained from wind data processing (2023) that's used as elevation input, including Hs, H_{max}, Tp, and θ_0. Open boundaries of model consisted of 8 (northwest, west, southwest, south, southeast, east, northeast, and north). The simulation was carried out with converting into annual average data where both (Hs) and (Tp) were needed. The bathymetry input for the Southern Bali region, including Nusa Penida, and the basic friction coefficient used are the Manning coefficient of 32 m$^{1/3}$/s, the Smagorinsky horizontal diffusivity of 0.28, and the quadraplet wave coefficient of 0.25.

Calculation of wave energy potential

Electrical power estimation of wave energy conversion is undertaken using the following equation (Holthuijsen *et al*., 2007):

$$P = \frac{\rho g^2}{64\pi} H_{m0}^2 T_e \approx \left(0.5 \frac{kW}{m^3.s}\right) H_{m0}^2 T_e ,$$

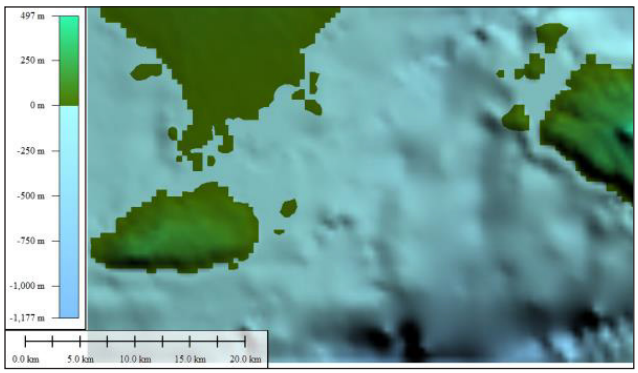

Figure 4: Bathymetry of the Nusa Penida in Southern Bali waters (Source: GEBCO).

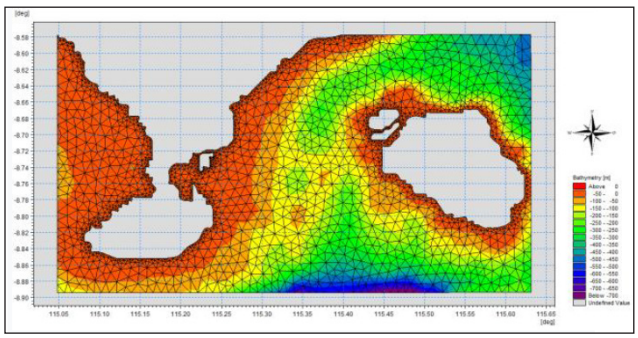

Figure 5: Unstructured mesh in the regional model of Southern Bali waters.

where:
P = Electrical power per unit wavelength (W/m)
ρ = Water density (1025 kg/m^3)
g = Gravitational acceleration (m/s^2)
H_{m0} = Significant wave height (m)
T_e = Wave periode (s)

In the model, calculation is used at each node of the grid domain area so as to produce a lateral distribution of wave power (P). Calculation of wave energy potential is the basis for planning the use of wave converter technology design (Falcao, 2009).

RESULT AND DISCUSSION

Comparison with point data

The comparison between the model simulation and the ECMWF was quite good, as seen in the SWH comparison graph, which has a correlation of 82.73% (Figure 6). The validation results show that the SWH model is greater than the altimetry. According to Muliati, Y. *et al*. (2016), analyzing the comparison of observed significant heights (Hs) to altimetry data is 1.959. While in this study, the comparison of coefficient value is more emphasized on comparative data per season. In several conditions (season), west (1.032), transition-I (1.006), east (1.003), and transition-II (1.007). From the validation graph, it was still below the permitted value (<1.959).

Local wave power analysis and regional

The model is discretised with elevation inputs (Hs,Tp, θ_0 & θ). The wind generation factor uses ECMWF (6 hourly) with resolution 0.25° by considering fetch length calculations. Open boundaries consist of three (East, West, and South).

The power flux equation explains that the variation in power produced (P) is a function of significant height (Hs) and peak period (Tp). The power flux varies following the period and significant height pattern because the relationship is a linear function, and the greater Hs and Tp, the greater P (Figure 8). From the results, power density is a function of SWH and Tp, so mean energy produced around 22.61

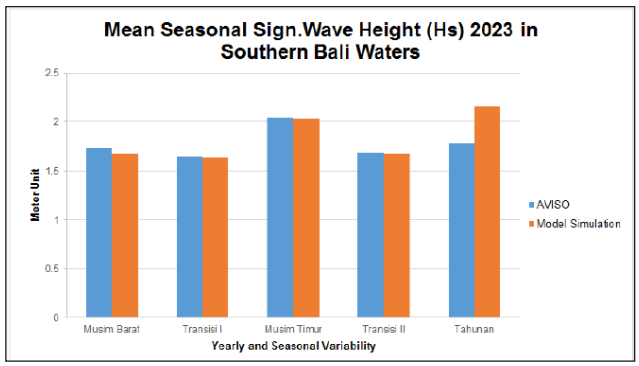

Figure 6: Comparison graph of SWH simulation model against altimetry data based on the representative seasonality of the year.

kW/m throughout the seasonal representative. The maximum electrical power generated was 81.05 kW/m on 4 October 2023 at 18:00 Middle Indonesia Time with SWH of 3.14 m and Tp 16.68 s (Suherman, 2024).

Inter-annual, monthly variability and inter-seasonal variabilities

Seasonal patterns include four seasons, namely the west monsoon, transition-1, eastsoutheast monsoon, and transition-2. The annual average of Hs and Tp modelling in the south-west (180° – 270°) of Nusa Penida has SWH ranging from 1-2.5 m, within a peak period about 10 s, and the dominant direction around south-southwest direction (180° – 225°), with an average power (P) of 8-24 kW/m. As a comparison, waves with a height of (0.5-1.5 m) produce 28% of events throughout the year with a period of 6% with range (5–10 s), a power 4-20 kW/m (55.82% frequency of occurrence).

The wave energy pattern in the southern Bali waters, including Nusa Penida Island, is shown in yearly average wave power (Figure 9). This becomes a reference for calculating time and space variability, and wave climate. From June – October, SWH around 1.65 – 2.22 m within power potential is ranging from 20 - 36 kW/m, and the largest value reaching 36 kW/m in July. In the quiet month period, the values were below 15 kW/m (March and November). The energy flux experiences a dominant annual variation throughout the month and changes in wave power in the southwest Nusa Penida (Tanglad – Bunga Mekar) of indication a difference between energy during both monsoons. The greatest wave power occurs in Tanglad, which is 35.97 kW/m that occured

Figure 7: Domain Area Nusa Penida (Source: Google Earth).

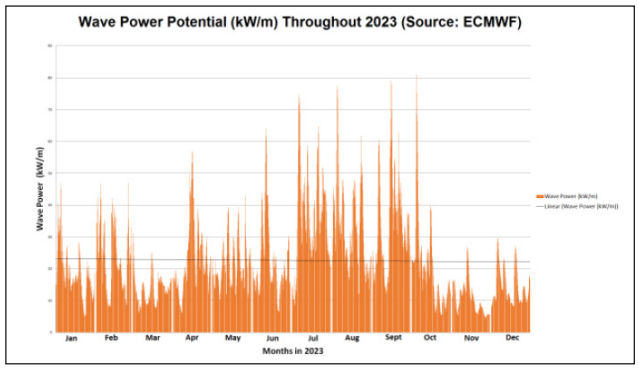

Figure 8: Relationship functioned of power produce at the model.

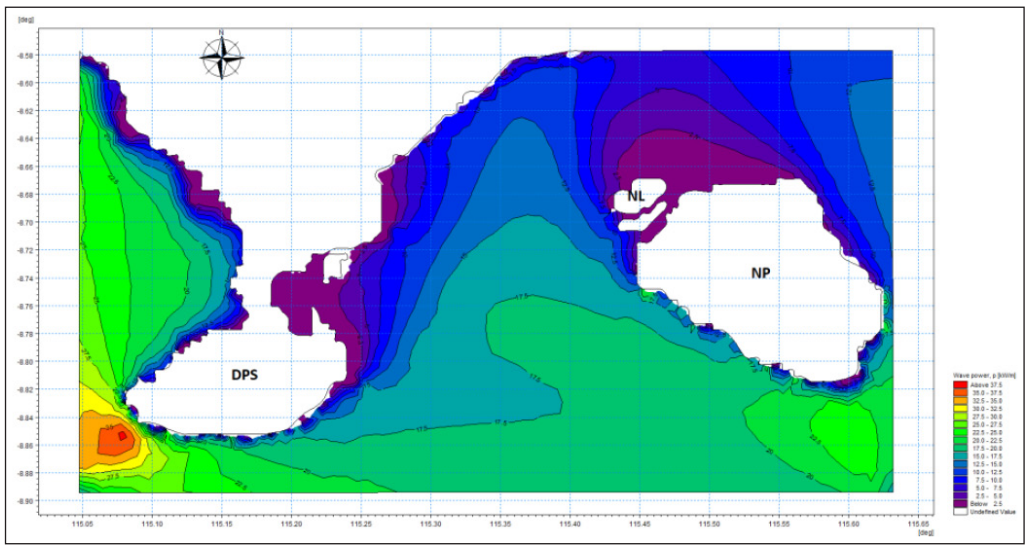

Figure 9: Annual Wave Power Potential (kW/m) in Southern Bali (Suherman, 2024).

at Eastern – Transition II Monsoon or June-October. The average power decreased from a high value in deep water and when entering the shallow waters of the west coast to the lowest value (around 7-12 kW/m). The spatial variability dissipation results in 8-15 kW/m in shallow water, while a decrease below 10 kW/m in the area of Tembeling. In the west monsoon, there are Hs 1.73 m, Tp 12.36 s, θ_0 221°, and P 18.90 kW/m. In the transition-I, Hs 1.65 m, Tp 13.90 s, θ_0 199.22°, and P 19.51 kW/m. In the east monsoon, Hs 2.04 m, Tp 14.02 s, and θ_0 189° and P 30.48 kW/m. In the transition-II, Hs 1.69 m, Tp 13.49 s, θ_0 203°, and P 21.61 kW/m. October has the greatest power potential reaching up to 80 kW/m. In the quiet month period, P <15 kW/m occur in March and November throughout the year (Figure 10). Maximum power is generated from the southwestsouth, exceeding 16-20 kW/m. Meanwhile, minimum wave power occurs in the shallow waters of Nusa Penida, which results in increased energy dissipation by bottom friction. At this location, around 13% of the power intensity only produces less than 10 kW/m. This area is formed by an intermediate density of energy with the direction arrival more than 15 kW/m (67% of events). In these two seasons, the wave energy flux is concentrated for waves in two directions, west and southwest. The choice of technology is expected to produce maximum efficiency in the range of significant heights and directions with a fairly constant period.

Wave energy characterization, prominent potential sites for wave energy utilization, and recommendation & proposed pilot projects by Installing Wave Energy Converter (WEC) in Nusa Penida

Nusa Penida has power potential ranging from 16-22.5 kW/m, so that if accumulated, the yearly average energy potential reaches up to 197.1 MWh/m (Figure 11). The south coast of Java-Bali has an average wave energy flux in the range 20-30 kW/m based on a global scale model (Mark *et al*., 2010) with a period of 10 years (1997-2006). The same thing was stated by Magagna & Andreas (2014), that the same

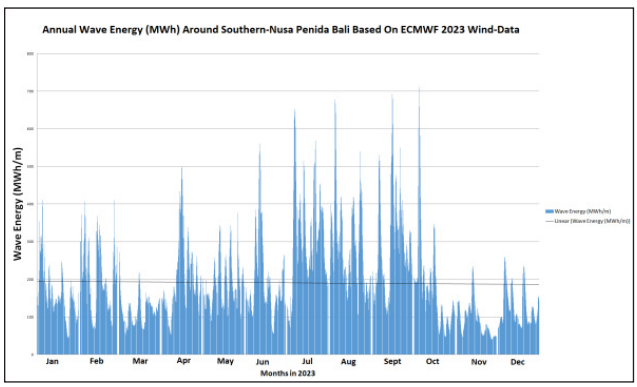

Figure 10: Annual time series predictions of overall wave power in the west-southwestsouthern waters of the Nusa Penida.

location has a power potential ranging from 20-30 kW/m. However, their consideration is essential in the investigation of WECs reliability and survivability (Carballo, 2012). The performance of a WEC is often evaluated in terms of the yearly mean of power output, energy production, or the ratio between energy production and the rated power of the WEC, the so called capacity factor (Bozzi, 2014). Referring to the morphology of the site, it is not recommended for northern part of Nusa Penida (Jungutbatu, Ped, Devil's Tear, north Lembongan, and Ceningan).Geographically, the area does not have a significant power potential. In the west-southwest region of Tanglad-Bunga Mekar is relatively high with a SWH, just 6,9% not more than 2.5 m, and out of period ranging 10-15 s (probability 26%). Thus, mean power is estimated reach up to 15-22.5 kW/m because that area is in direct contact with the open waters of the Indian Ocean. However, the area is close to the Indonesia Electricity Ltd. (PLN) Nusa Penida grid, with a distance of about 12 km to prominent site on the southwest coast. This area is the same as the previous location, with the minimum number of local residents living far from the coast and a considerable distance to the PLN Nusa Penida grid. There are 4 seasons that represent the distribution of wave power. The wave height between 1.5 – 2.5 m is more than 63% of the number of events with a fairly constant period between 10 – 15 s (occurance 73%) during the year, so it affects the maximum value of the wave flux power (Figure 12). Maximum energy is generated from the west, southwest, and south directions, with wave power exceeding 21-30 kW/m. At this location, about 11.50% of the wave energy produces more than 40 kW/m throughout the year. From the NSP simulation results in Table 1 below, the exact coordinates for installing a wave power plant are in the following simulation (Site-3 & Site-5) at the Tanglad & Bunga Mekar location, with an average power of around 17 kW/m and the distance to the coastline was just less than 4 km. In comparison, waves with a height between (0.5 – 1.5 m) able to produce 29% of occurrences throughout the year with rated power (5 – 10 kW/m).

This area is formed by the intermediate density of wave energy with the direction of the wave incident producing values in excess of 14-25 kW/m for more than 41% of occurrences (Type of Heaving Device Turbine). Thus, a similiar site produces power in excess of 25-32 kW/m for 12.64% of occurrences (Type of Oscillating Water Column Turbine) in accordance with Cruz, 2008. The power model is calculated based on the relationship between the significant height variable function and the wave period.

The average power generated in the NSP model in the western, transition I, southeast, and transition II seasons is 18.89, 19.51, 30.48, and 21.61 (kW/m) respectively.

Levellized cost of energy (LCOE) of Wave Energy Converter (WEC) in Nusa Penida

Financial analysis aims to calculate the costs required to build an energy installation by considering the interest

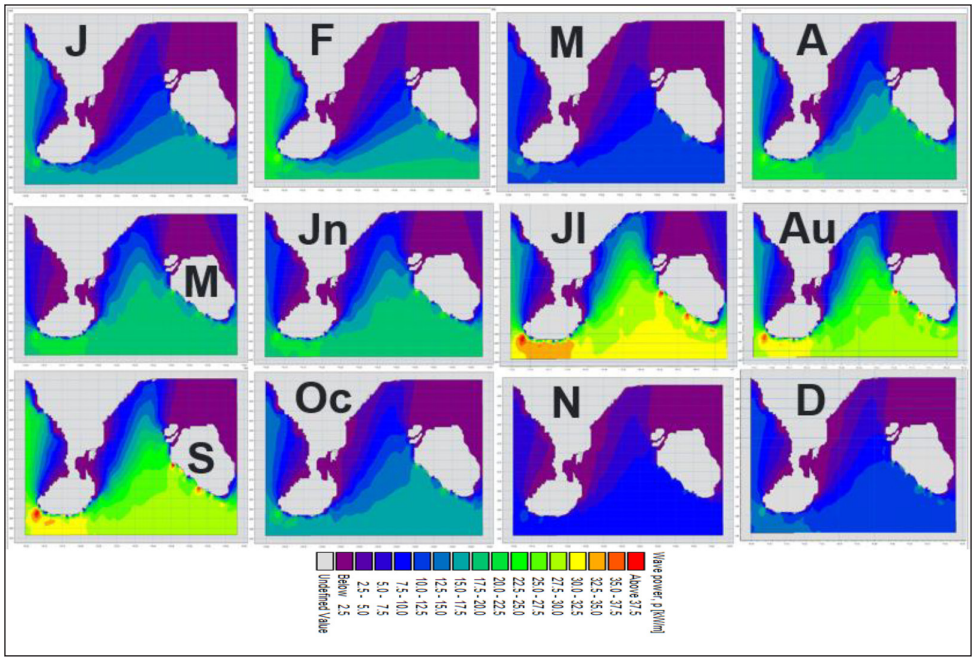

Figure 11: Monthly average of Wave Power Variability Potential NSP Model along the south coast of Bali Island, specific site study at Nusa Penida, several districts have wave potential power that were assessed (Marine Geology Institute, MEMR, 2024).

Table 1: Location, depth, distance to shoreline and annual average wave energy flux calculated.

Sites	Area/ District	Latitude	Longitude	Depth (m)	Distance to coastline (km)	P mean (kW/m)
#1	Jungutbatu	-8.6676	115.4377	5	1.8	1.75
#2	Devil's Tear	-8.7025	115.416	28	2	11.97
#3	Tanglad	-8.8031	115.6224	45	2.11	17.85
#4	Ped	-8.6582	115.5147	53	1.98	1.37
#5	Bunga Mekar	-8.774	115.4567	50	3.07	17.19
#6	Lembongan	-8.7027	115.4217	6	2.21	11.25
#7	Ceningan	-8.734	115.4331	2	0.65	11.63

rate, capital costs, capacity factors, and investment costs which are dependent on the interest rate and economic life. All of these factors must be paid by taking into account the age of the generator with the formula so that the amount of costs incurred to produce per kWh of electricity is visible (Azis, 2010). Capital expenditure of a marine renewable project for 1 MW is depicted on the following graph below by Andres, 2017 (Figure 13).

Based on financial analysis of marine power plant development, it is considered to have the opportunity to develop ocean waves. It was indicated by the large electricity tariff each 1 kWh produced, which is considered to be able to compete with the non-subsidised (conventional energy) tariff sold by PLN for $0.07/kWh, namely $0.12/kWh for 15 years of lifetime, and around $0.81 M/kW investment in wave energy (Luhur *et al*., 2013).

CONCLUSIONS

The Nusa Penida is able to produce energy with a mean power up to 22.62 kW/m for a certain period. Wave prediction produces annual and seasonal variability of wave power in a particular season, which is analysed in monthly variables. On the west-southwest coast, Nusa Penida represents mean energy (>15 kW/m) with around 67% probability of occurrence. The NSP model gives good results for power fluxes with a potential of up to 20 kW/m.

ACKNOWLEDGEMENT

The authors'd like to thank the Head of MGI, Geology Agency, MEMR Indonesia for his permission to conduct this study of wave energy potential assessment in Nusa Penida, Bali. This study was carried out in collaboration

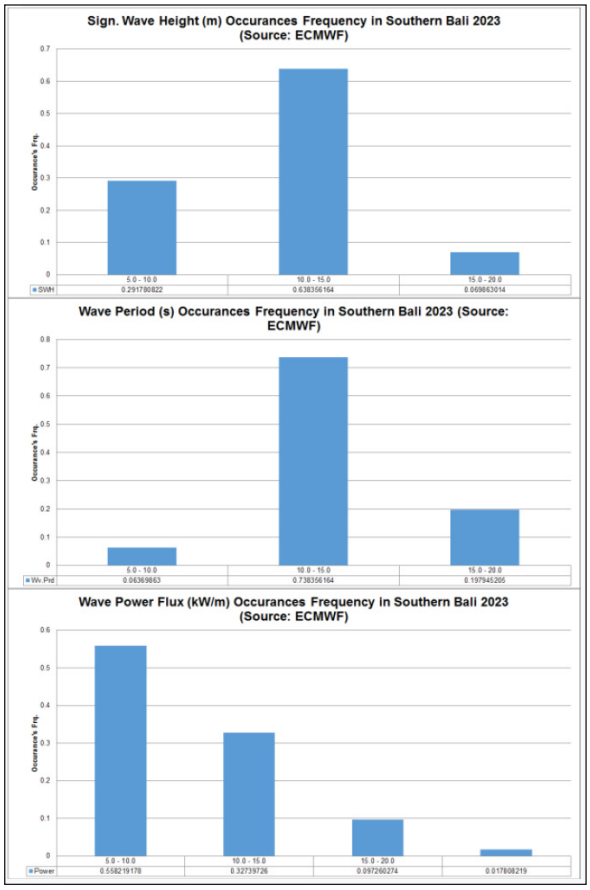

Figure 12: Predicted percentage: (Top) SWH (Hs), (Middle) Peak Wave Period (T), and (Bottom) Mean Power Density (P) at NSP model locations.

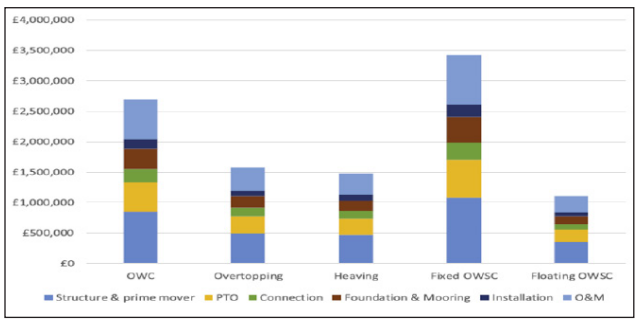

Figure 13: Cummulative CAPEX average AEP per device (1 MW Project).

with MGI and other institutions that have undertaken any marine renewable projects, around the Indonesia Sea's area, as well as all parties who have assisted in writing this paper and marine energy map (inclosed below). And last, we want to thank GEBCO for the bathymetric and wind data from ECMWF.

REFERENCES

A. de Andres, etc, 2017. On the reversed LCOE calculation: Design constraints for wave energy commercialization. International Journal of Marine Energy, 18(2017), 88–108.

Azis, A., 2010. Study of Utilization of Electrical Energy Ocean Current Power in Alas Strait, Lombok Regency, NTB. Sepuluh Nopember Institut of Technology, Department of Electrical Engineering, Surabaya.

Bozzi, S., Archetti, R., & Passoni, G., 2014. Wave electricity production in Italian offshore: A preliminary investigation. Renew. Energy, 62, 407–416.

Carballo, R., & Iglesias, G., 2012. A methodology to determine the power performance of wave energy converters at a particular coastal location. Energy Convers. Manag., 61, 8–18.

Cornett, A.M., 2008. A Global Wave Energi Resource Assesement. Proceeding of the 18th International Offshore and Polar Engineering Conference. Vancouver.

Cruz, J, 2008. Ocean Wave Energy, Current Status and Future Prepective. Springer.

Falcao, A.F.O., 2009. Wave energy utilisation: a review of the technologies. Renewable and Sustainable Energi Reviews, 14, 901.

Holthuijsen, L.H., 2007. Waves in Oceanic and Coatal Waters. Cambridge University Press, Cambridge.

Lopez, I., Andreu, J., Ceballos, S., Alegria, I. M., & Kortabaria, I., 2013. Review of Wave Energy Technologies and The Necessary Power Equipment. Renewable and Sustainable Energy Reviews, 27, 413-433.

Luhur, E.S., Muhartono, R., & Suryawati, S.,H., 2013. Financial Analysis of Developing Ocean Energy in Indonesia. J. Sosek KP, 8(1), Year 2013.

Magagna & Andreas, 2014. JRC Ocean Energi Status Report - Technology, market and economic aspects of ocean energy in Europe. Report EUR 26983 EN, European Commission.

Mark, G., Bartsow, S., Kabuth, A., & Pontes, T., 2010. Assessing the Global Wave Energi Potential. Paper presented at the 29th International Conference on Ocean, Offshore mechanics and Artics Engineering, Shanghai.

Muliati, Y., Wurjanto, A., & Pranowo, W., 2016. Validation Of Altimeter Significant Wave Height Using Wave Gauge Measurement In Pacitan Coastal Waters, East Java, Indonesia. International Journal of Advance In Engineering Research, 12(IV), 25-33.

Setyawan, F.O., 2018. Identification And Mapping Of Potential Locations Ocean Wave Energy In Indonesian Waters. Sepuluh November Technology Institute. Thesis- MO142528, Surabaya, Indonesia, 68 p.

Silva, D., Rusu, E., & Soares, C.G., 2016. High Resolution Wave Energy Assessment in Shallow Water Accounting for Tides. Energies MDPI Journal, 1.

Wyrtki, K., 1961. The flow of water into the deep sea of the western south Pasific Ocean. Aust. J. Mar. Freshw. Res., 12(1), 1 - 16.

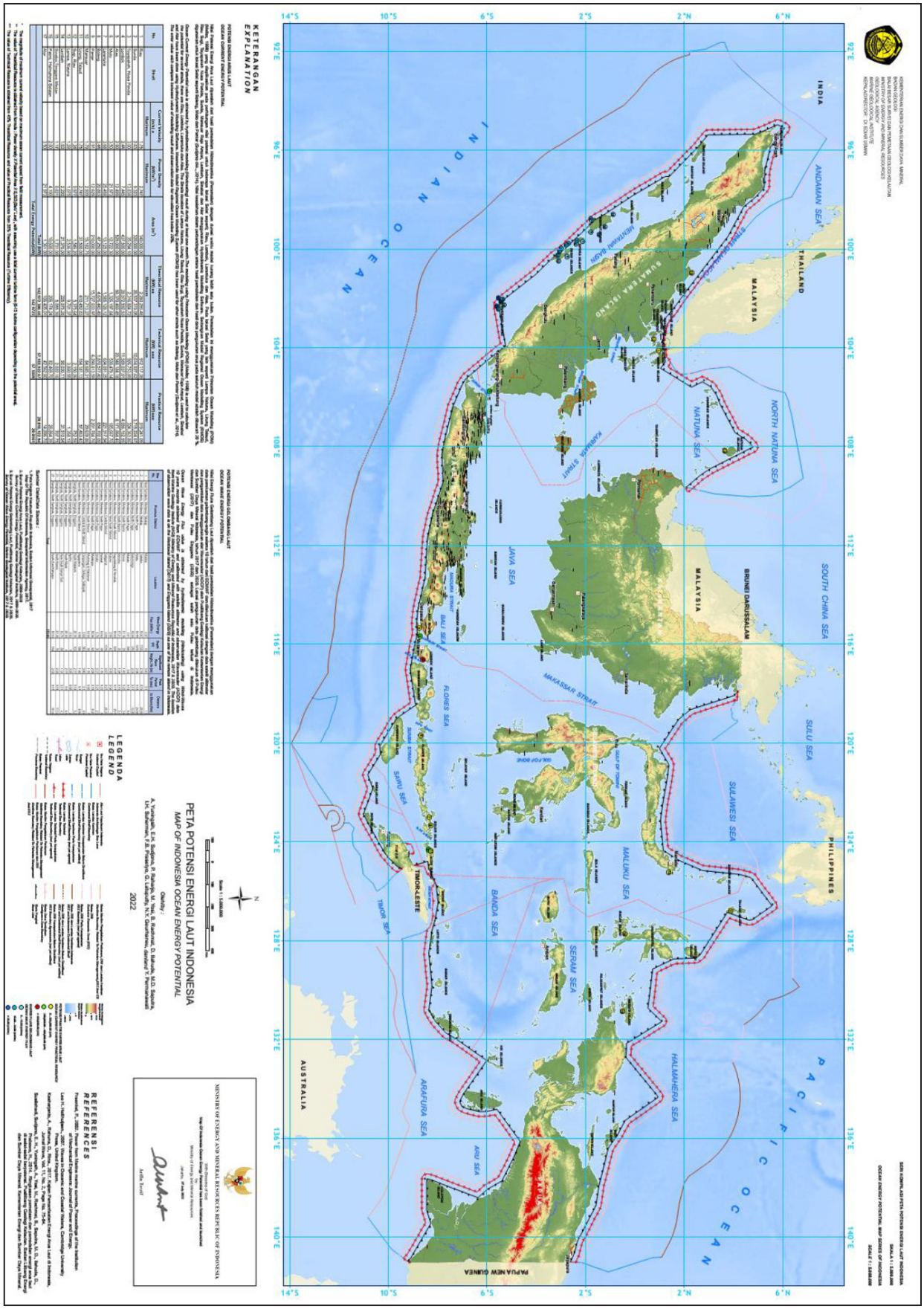

Map of Ocean Energy Potential Around in Indonesia Waters (Marine Geology Institute, Ministry of Energy and Mineral Resources Republic of Indonesia, 2022).

The future of coal: Advanced material extracted from coal A preliminary study

Rahmat Hidayat[1,*], Eko Budi Cahyono[1], Penny Oktaviani[1], Fatimah[1], Vivi Purwandari[2]

[1] Center for Mineral, Coal, and Geothermal Resources - Indonesia
[2] Faculty of Science, Technology and Information, Sari Mutiara University – Indonesia
* Email: rahmatkahidayat@gmail.com

Abstract: Advanced materials are materials that are specifically engineered to exhibit new properties or have improved characteristics so that they can provide superior performance compared to conventional materials (Kennedy *et al*., 2019). There are various types of advanced materials, one of which is advanced carbon materials (advanced carbon-based materials) such as graphene, fullerenes, hierarchical carbon and carbon nanotubes.
Coal has the potential to produce advanced carbon-based materials considering that carbon is the largest component in coal. This study was carried out to determine the possibility of extracting advanced materials from selected Tertiary Indonesian coal and to identify its characteristics.
Graphene and its derivatives extraction was carried out on 32 coal samples from Musi Banyuasin, Muaraenim, Lahat, East Kotawaringin and Paser districts using the ultrasonication method. The extraction process produces graphene (G), reduced graphene oxide (rGO), and graphene quantum dots (GQDs). Identification of coal quality using proximate, ultimate and coal ash analysis shows that the samples analyzed have varying qualities with calories ranging from low to very high calories.
G/rGO recoveries ranged from 80% to 97%. Meanwhile, the yield of GQDs ranged from 201 ppm to 635 ppm. The graphene produced can be categorized into few - multi layer graphene.

Keywords: Coal, graphene, reduced graphene oxide, graphene quantum dots

INTRODUCTION

Advanced materials are engineered substances designed to have superior properties compared to conventional materials. Currently, there are many examples of advanced materials, including advanced carbon material (advanced carbon-based material) which has carbon components in it. Advanced carbon materials are a diverse group of materials that leverage the unique properties of carbon to achieve exceptional performance in various applications. According to Ikram *et al*., (2021), advanced carbon-based materials include graphene, fullerenes, hierarchical carbon and carbon nano tubes. Coal is a sedimentary rock with carbon as the largest component. Therefore, coal has great potential to produce advanced carbon-based materials.

The government is currently encouraging coal downstream activities to increase coal added value, among others is extracting coal into advanced materials. There are various types of advanced carbon-based materials as mentioned above. This study will focus on graphene from coal. The objective of this study is to identify various possible graphene groups that can be produced from coal.

Graphene, graphite and diamond, are materials that are made from carbon in common, but have different structures

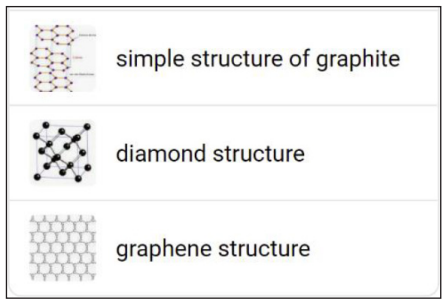

Figure 1: The difference between graphite, diamond, and graphene structure (Wikipedia).

as can be seen in Figure 1. Graphene has a two-dimensional structure while graphite has a three-dimensional structure. A graphite is composed of layers of graphene. 1 mm thick graphite contains about 3 million layers of graphene.

As an advanced material, graphene has unique characteristics that are rarely found in other materials. Graphene has excellent thermal conductivity (higher than diamond), low electrical resistivity (lower than copper), and very high electron mobility (better than silicon). Apart from that, graphene is also currently believed to be the strongest material in the world which is very thin, transparent and

impermeable (Balandin *et al*., 2008; Chen *et al*., 2008; Lee *et al*., 2008; Sheehy & Schmalian, 2009; Berry, 2013; Liu *et al*., 2017).

Indonesia has quite large coal potential, namely 97.3 billion tons of resources and 31.7 billion tons of reserves (PSDMBP, 2023), some of this potential can be utilized to be developed into advanced materials in the form of graphene. This evaluation activity was carried out to determine the possibility for advanced materials that can be extracted from selected Indonesian coal.

DATA AND METHODOLOGY

Graphene extraction was carried out on 32 (thirty-two) coal samples of various quality, consisting of 14 coal samples from Musi Banyuasin Regency, 11 samples from Muara Enim and Lahat Regency (South Sumatra), 5 samples from East Kotawaringin Regency (Central Kalimantan), and 2 samples from Paser Regency (South Kalimantan). The extraction process was carried out at the Chemical Engineering Laboratory, Sari Mutiara Indonesia University, which has a patent registration for extracting graphene from coal using the ultrasonication method.

Ultrasonic technology is often used to synthesize nanomaterials. Ultrasonic treatment forms thousands of small bubbles in the liquid producing mechanical force that can destroy the C-C carbon bonds, thus forming graphene (G) and graphene quantum dot's (GQDs) as illustrated in Figure 2. This study is using multi-phase ultrasonication method to extract G and GQDs from coal. This method is environmentally friendly and effective for extracting graphene from coal.

RESULTS AND DISCUSSION

The extraction process produces graphene (G), reduced graphene oxide (rGO) and graphene quantum dots (GQDs). The yield of G, rGO and GQDs for each sample is presented in Table 1. The resulted G and rGO ranges from 80% to 97%. Meanwhile, the resulted GQDs ranges from 201 ppm to 635 ppm. G, rGO and GQDs were then characterized using Raman Spectroscopy, X-Ray Diffraction (XRD) and photoluminescence to identify their properties.

The ultrasonication method which is carried out repeatedly can change the morphology of the coal surface so that the resulting graphene has a larger surface area. Graphene that has a stack of 2-10 layers is called few layers graphene. Above 10 layers is called multi-layer graphene.

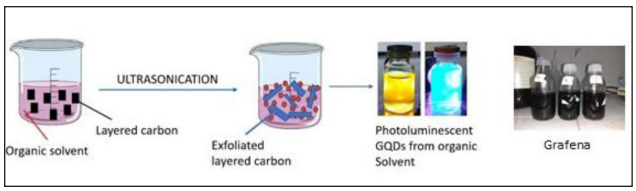

Figure 2: Illustration of G and GQDs extraction using ultrasonication method.

Raman spectroscopy analysis shows that the graphene extracted from this coal is graphene with the characteristics of few layers and multi layers based on 2D peak appearance (Figure 4).

XRD analysis shows that the maximum particle diameter size of the entire sample is 28.3 nm in the BRN 02 sample, and the minimum diameter size is 1.80 nm in the PNSC 02 sample. It can be concluded that low rank coal has a larger particle diameter than high rank coal.

Light excitation tests under UV light and photoluminescence tests show that GQDs from coal have different colors depending on the quality of the coal. The color of the GQDs represents the energy level and particle size of each GQDS as shown in Figure 5.

Figure 3: Graphene extracted from coal; graphene from Musi Banyuasin coal samples (top), graphene from Muara Enim and Lahat coal samples (bottom left) and graphene from East Kotawaringin coal samples (bottom right)

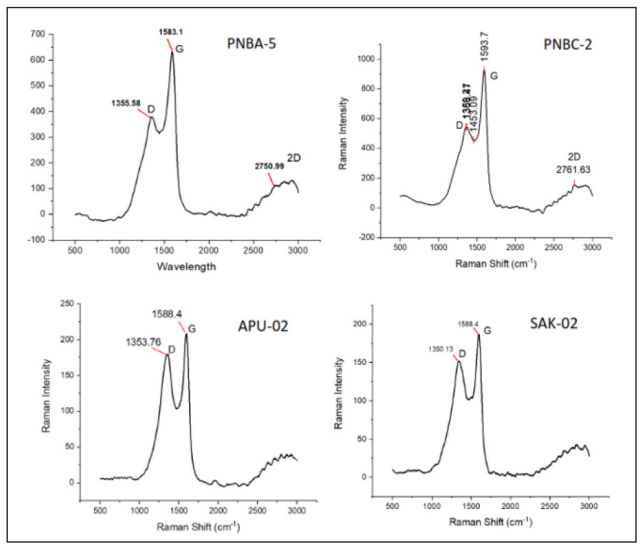

Figure 4: Raman spectra of PNBA 05, PNSC 02, APU 02, and SAK 02.

Table 1: Extraction yield.

No	Sample Code	Location	CV (kal/gr, GAR)	Yield		Layers	GQDs (ppm)
				G (%)	rGO (%)		
1	ASD-01	Muba	4.763		84	9 *(few)*	587
2	ASD-02	Muba	4.655		89	-	549
3	ASD-03	Muba	2.715		81	13 *(multi)*	303
4	CK-01	Muba	3.614		81	-	558
5	CK-03	Muba	2.645		89	-	563
6	API-01	Muba	3.110		85	6 *(few)*	568
7	APU-02	Muba	3.050		84	-	589
8	APU-03	Muba	3.312		84	-	502
9	BRN-01	Muba	3.235		86	10 *(multi)*	602
10	BRN-02	Muba	4.768		86	-	576
11	SR-01	Muba	3.349		82	8 *(few)*	312
12	SR-02	Muba	3.676		80	-	478
13	SAK-01	Muba	3.454		83	-	201
14	SAK-02	Muba	2.904		83	4 *(few)*	237
15	PNBA-01	Muaraenim	4.492	96		3 *(few)*	474
16	PNBA-02	Muaraenim	4.918	94		-	467
17	PNBA-03	Muaraenim	6.114	95		-	447
18	PNBA-04	Muaraenim	7.732	93		-	465
19	PNBA-05	Muaraenim	8.277	97		3 *(few)*	479
20	PNBA-06	Muaraenim	4.706	96		-	427
21	PNBA-07	Muaraenim	3.993	97		-	432
22	PNBA-08	Muaraenim	3.868	96		-	435
23	PNBA-09	Muaraenim	5.053	94		-	422
24	PNSC-01	Lahat	6.363	91		-	327
25	PNSC-02	Lahat	7.726	92		3 *(few)*	435
26	STK-01	Kotim	2.788		82	-	413
27	STK-02	Kotim	2.719		85	-	583
28	STK-03	Kotim	2.769		85	15 *(multi)*	568
29	STK-04	Kotim	2.942		87	-	402
30	STK 04 SB	Kotim	2.270		80	-	635
31	MS 01	Paser	4.006		84	5 *(few)*	313
32	MS 02	Paser	4.296		88	-	346

The GQDs derived from the PNBA and PNSC samples glow a light blue color under an ultraviolet lamp and with an ultraviolet laser a yellow absorption is visible except for PNBA-5 which displays a green color. From the color spectrum of quantum dots, the blue color shows the wavelength absorbed by PNBA and PNSC GQDs is 450-495 nm and the photon energy is 2.50-2.75 eV, the yellow line resulting from UV laser light on the sample shows the particle size of the GQDs which is around 4 nm. Meanwhile, the green line on PNBA-5 shows the particle size of these GQDs is around 3 nm. Samples MS 01 and MS 02 provide a green laser light line, the GQDs particles of this sample are approximately 3 nm in size. The average sample particle size is around 4 nm based on the laser light

Figure 5: Light excitation of some samples tested under ultraviolet lamp and ultraviolet laser.

line which shows a yellow color, except for APU-02 which shows a red line. The particle size of the GQDs from APU-02 is larger, namely around 7 nm.

From the utilization side, all the produced G and GQDs have their own uses. Musi Banyuasin, East Kotawaringin and Paser coal samples generally produce GQDs with yellow light excitation which are very suitable for use as biomedical materials, opto-electronics and various applications related to the environment and energy. Meanwhile, for high and very high calorie coal (Muara Enim and Lahat samples), utilization is more focused on the resulted graphene, considering that the quality of the resulted GQDs is not as good as GQDs from low calorie coal.

CONCLUSIONS

Extraction of advanced materials in the form of graphene (G), reduced graphene oxide (rGO) and graphene quantum dots (GQDs) has been proven to be possible on every type of coal, from low calorie coal to very high calorie coal with quite promising results.

Advanced materials extraction from coal is also enable to increase the economic value of coal which is in line with the Coal Added Value program.

ACKNOWLEDGEMENT

We gratefully thank Centre for Mineral Coal and Geothermal resources who funded this study. Big thanks are also delivered to the Head of CMCGR and Head of Coal Division who supported this study.

REFERENCES

Balandin, A.A., Ghosh, S., Bao, W., Calizo, I., Teweldebrhan, D., Miao, F., & Lau, C.N., 2008. Superior Thermal Conductivity of Single-Layer Graphene. American Chemical Society Publications.

Berry, V., 2013. Impermeability of Graphene and its Applications. Carbon Journal, 62, 1 – 10.

Chen, H., Muller, M.B., Gilmore, K.J., Wallace, G.G., & Li, D., 2008. Mechanically Strong, Electrically Conductive, and Biocompatible Graphene Paper, 2008. Advanced Materials, 10, 3557 – 3561.

https://id.wikipedia.org/wiki/Grafena

Ikram, M., Raza, A., Shahzad, K., Haider, A., Haider, J., Durrani, A.K., Rizvi, A.H., Maqsood, A.,& Ikram, M., 2021. Advanced Carbon Materials: Base of 21st Century Scientific Innovations in Chemical, Polymer, Sensing and Energy Engineering. doi: 10.5772/intechopen.95869.

Kennedy, A., Brame, J., Rycroft, T., Wood, M., Zemba, V., Weiss Jr, C., Hull, M., Hill, C., Geraci, C., & Linkov, I., 2019. A definition and categorization system for advanced materials: The foundation for risk-informed environmental health and safety testing. Wiley.com.

Lee, C., Wei, X., Kysar, J.W., & Hone, J., 2008. Measurement of the Elastic Properties and Intrinsic Strength of Monolayer Graphene. Science, 321, 385.

Liu, L., Chen, J., Zhou, Z., Yi, Z., & Ye, X., 2018. Tunable Absoption Enhancement in Electric Split-Ring Resonators-Shaped Graphene Arrays. Material Research Express, Volume 5.

PSDMBP (Pusat Sumber Daya Mineral Batubara dan Panas Bumi), 2023. Neraca Sumber Daya dan Cadangan Mineral dan Batubara Indonesia Tahun 2023. Badan Geologi, Bandung.

Sheehy, D.E., & Schmalian, J., 2009. Optical Trnasparency of Graphene as Determined by the Fine-Structure Constant. American Physical Society Journals.

Carbon sink of natural resources and its capacity enhancement

Huaju Yang[1,2], Liankai Zhang[1,2,*], Canfeng Li[1,2], Can Xu[1,2], Keqiang Shan[1,2]

[1]Kunming General Survey for Natural Resources Center, China Geological Survey, Kunming, Chian, 650100
[2]Technology Innovation Center for Natural Ecosystem Carbon Sink, Ministry of Natural Resources, Kunming, Chian, 650100
* Email: zhang_liankai@126.com

Abstract: Natural resources are closely related to the global carbon cycle. Natural carbon sinks can neutralize about 50% of carbon dioxide emissions every year, which is one of the important ways to achieve global carbon neutrality. Forest, grassland, wetland, lake, soil, rock and other natural elements all participate in the carbon cycle process to varying degrees. It is an important content to discover the global carbon balance and make up for the global carbon loss to systematically master the carbon cycle process and carbon sinks of different natural resource elements. However, at present, the systematic evaluation methods of carbon sinks of natural resources are not perfect and the standards are not uniform, which leads to great differences in the estimation structure of carbon sinks, which is not conducive to carbon balance research and government decision-making. At the same time, with human activities and global warming, the carbon sink of natural resources is undergoing profound changes. Therefore, it is of great significance to study the present situation and future trend of carbon sequestration of natural resources and discuss how to consolidate and enhance the capacity of carbon sequestration. This paper summarizes the research status, existing problems and investigation methods of carbon sequestration of natural resources, and puts forward technical methods to consolidate and improve the carbon sequestration capacity of natural resources in southwest China. The article aims to provide technical support for global carbon cycle investigation and carbon sequestration trading.

Keywords: Natural resources, Carbon sink, carbon cycle, carbon sequestration, sink enhancement

INTRODUCTION

Global change, marked by global warming, continues to affect the survival and development of mankind (IPCC, 2014) and has become a major political, economic and diplomatic issue of concern to all countries and social circles in the world (Liu, L.Y. *et al*., 2021). In order to cope with climate change, the United Nations adopted the United Nations Framework Convention on Climate Change (UNFCCC) in 1992, which requires the parties to share the greenhouse gas emission reduction targets (Quéré, C.L. *et al*., 2016) (Figure 1). Many countries, regions and organizations have successively carried out research on coping with climate change, and found that natural ecosystems such as forests, grasslands, wetlands and oceans have strong carbon sequestration capacity (Dixon, R.K. *et al*., 1994). According to the research results of Canadell and others in 2007, about 55% of man-made carbon emissions are eliminated by nature, thus changing the concentration of greenhouse gases in the atmosphere and slowing down climate warming (Canadell, J.G., 2007; Le Quéré *et al*., 2013; Piao *et al*., 2022). Therefore, studying the carbon sequestration process of natural resources system and developing technical measures to enhance the carbon sequestration capacity of natural resources have become an important content for all parties to formulate goals and plans to deal with climate change.

THE IMPORTANT ROLE OF CARBON SINKS IN NATURAL RESOURCES

Natural ecosystem is an important part of the earth's surface system and deeply participates in the global carbon cycle. CO_2 in the atmosphere enters the biosphere, lithosphere, PEDOSPHERE and hydrosphere after being absorbed by land and ocean, and part of it is fixed in natural ecosystem under biogeochemistry (Huang, H. *et al*., 2022; Cai, W. *et al*., 2022; Wu, Y. *et al*., 2022) (Figure 2).The average annual carbon sequestration in terrestrial ecosystems and marine ecosystems offset about 30% and 23% of anthropogenic carbon emissions, respectively, indicating the important role of natural carbon sinks in coping with climate change (Xu, E.Y. *et al*., 2020; Xie, L. *et al*., 2022). As one of the key ways to deal with climate change, the research progress of natural resource carbon sink at home and abroad is deepening. At the international level, Nature-based Solutions (NbS) are widely recognized and applied to the holistic approach to climate change, biodiversity loss and other issues. It is estimated that by 2030, the implementation of NbS in all ecosystems can achieve at least 5-11.7 billion tons of carbon dioxide equivalent emission reduction and removal every year (Lu, F. *et al*., 2018; Lu, N. *et al*.,

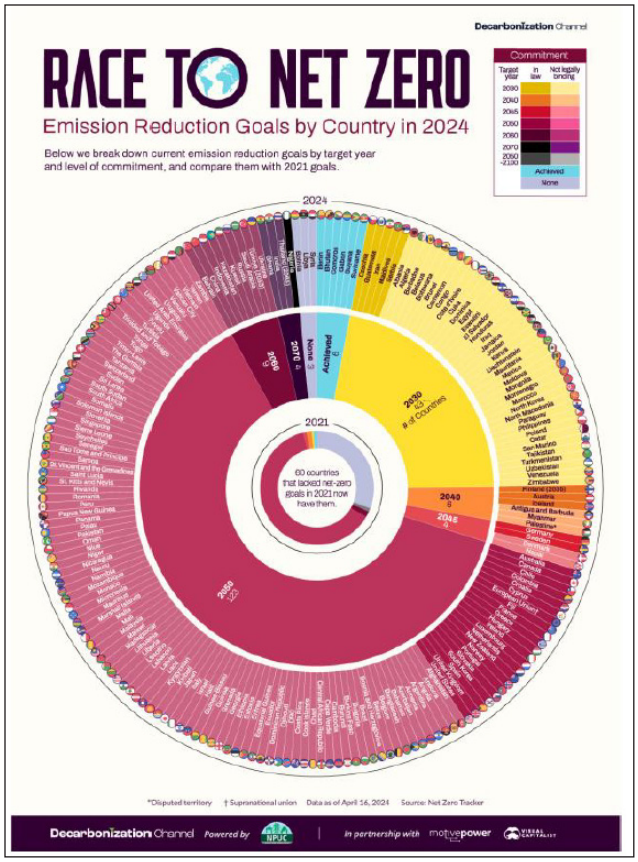

Figure 1: Timeline of achieving net zero emission (carbon neutrality) in different countries and regions.

2022). Developed countries have formulated a series of management measures to play the carbon sink function of ecosystems. At the same time, multinational companies are also active in NbS investment, and the trading quota of the global voluntary carbon credit market continues to grow (Yu, X. & Y. Alex, 2014; Zhou, K. & Li, Y.W., 2019). In China, remarkable progress has been made in improving the function of ecological carbon sink. By increasing forest area, reducing losses and improving forest quality, the continuous "double growth" of forest area and accumulation has been realized, making it one of the fastest growing countries in the world (Chloe, W. *et al*., 2024). The total area of woodland, grassland and wetland in China is 6.05 billion hectares, the coverage rate of forest and grass is 55.11%, the total carbon storage of forest and grass is 11.443 billion tons, and the annual carbon sink is 1.28 billion tons (Zhang, Y. *et al*., 2022; Yang, Y.H. *et al*., 2022). China has promoted the integrated protection and restoration of mountains, rivers, fields, lakes, grass and sand, created a good practice with ecological, economic and social benefits, transformed green mountains and green hills into Jinshan Yinshan, and promoted the synergy in coping with climate change, biodiversity protection and economic and social development (Li, Z. *et al*., 2020; Zhu, X.J., *et al*., 2022) (Figure 3).

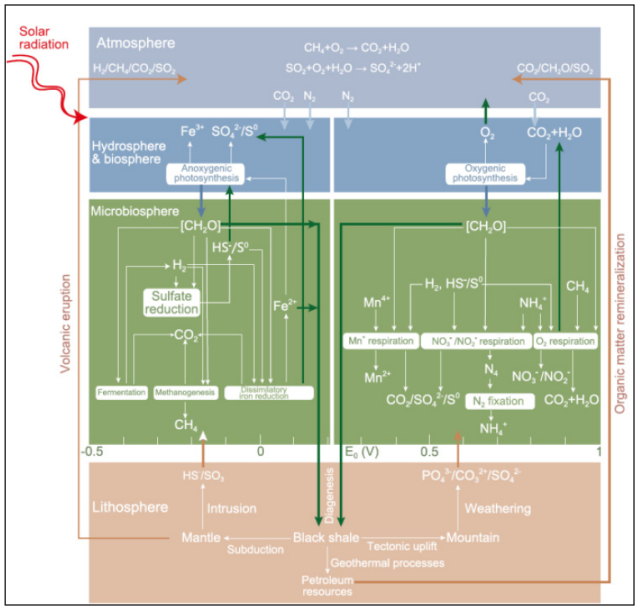

Figure 2: A generalized model showing the cycling of carbon and related elements in the Earth system, (Falkowski, P.G., 2008).

THE MAIN PROBLEMS IN THE STUDY OF NATURAL RESOURCES CARBON SEQUESTRATION

Carbon sinks of natural resources play an important role in coping with climate change and achieving the goal of carbon neutrality. It should be pointed out that there is great spatial heterogeneity in natural ecosystems, and the investigation, accounting and evaluation of carbon sinks also face some challenges and problems, such as: (1) Uncertainty of carbon sink estimation: due to the strong heterogeneity of natural processes, there is great uncertainty in carbon sink estimation. At present, the survey indicators mainly focus on single factors such as forest, grass, wetland and soil, and lack of investigation and monitoring of the coupling relationship between systems. The investigation and monitoring system of carbon cycle between different natural resources elements has not yet been established. (2) Data fusion and standard unification: there is a lack of data fusion mechanism between different departments and survey and monitoring methods, and the survey and evaluation standards are not unified, which leads to great differences in evaluation results. (3) Omission and repetition in the calculation of carbon pools: There are problems of omission and repetition in the calculation of different carbon pools, and the transformation process of carbon cycle cannot be accurately grasped. Therefore, in order to make better use of natural carbon sink resources, it is necessary to strengthen the investigation and study of natural carbon sink process, build a systematic and comprehensive carbon sink investigation and monitoring system, and improve the management and utilization efficiency of natural carbon sink.

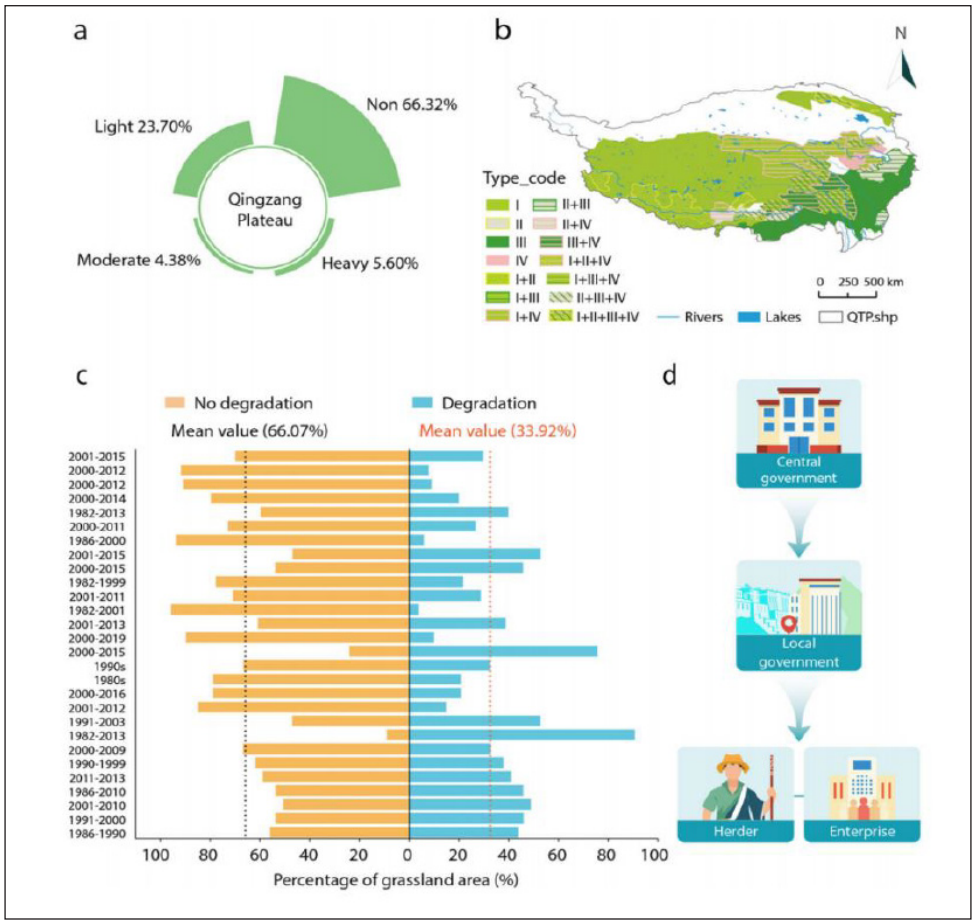

Figure 3: The basis and urgency of implementing NbS to improve carbon sequestration through remediation projects. Proportion of grassland degradation in Qinghai-Tibet Plateau (a). Distribution and location of ecological restoration projects in Qinghai-Tibet Plateau (b). The figure shows the locations of grassland ecological project (I), sand source control project (II), forest ecological project (III) and soil erosion control project (IV). Almost all restoration projects have adopted the top-down design and method (c). Percentage of degraded grassland area in Qinghai-Tibet Plateau in the past decades obtained from different studies (d) (Sun, J., 2024).

INVESTIGATION METHODS OF CARBON SINKS IN NATURAL RESOURCES

The investigation of carbon sinks in natural resources is a key work, which helps us to understand and evaluate the mitigation effect of natural ecosystems on climate change. This survey covers a variety of ecosystems, including rocks, forests, grasslands, farmland, lakes and wetlands and hydrology. Mainly includes:

1. Field measurement method: It is suitable for setting up sample plots in forests, grasslands, farmland and soil, and directly measuring the corresponding vegetation factors and related indicators of soil, so as to estimate the carbon content and carbon storage of vegetation and soil. This method is suitable for detailed investigation in a small area or a specific area.
2. Biomass estimation method: estimate the biomass of forest, grassland, farmland and other ecosystems by combining remote sensing technology and measured data on the ground, and then calculate the carbon storage. This method is suitable for large-scale rapid evaluation.
3. Remote sensing estimation method: Using sensors carried by satellites or aircraft to monitor vegetation coverage and biomass on the surface, and then estimate carbon storage. This method is suitable for remote areas that are difficult to reach or situations that require large-scale investigation.
4. Model simulation method: Using ecosystem model or process model, combined with climate, soil, vegetation and other data, simulate the carbon cycle process of the ecosystem and evaluate the carbon sink function.

STRATEGIES TO CONSOLIDATE AND ENHANCE THE CARBON SINK CAPACITY OF NATURAL RESOURCES SYSTEM

Clear natural ecological security boundary

Protecting the existing ecosystem is the basis for consolidating and enhancing the carbon sink capacity. By strengthening the protection of forests, grasslands, wetlands, oceans and other ecosystems and preventing ecosystem degradation, its carbon sink capacity can be effectively

maintained and enhanced. For example, by implementing natural forest protection projects to prevent deforestation and deforestation, the carbon storage capacity of forests can be maintained. At the same time, strengthening grassland protection and preventing overgrazing and grassland degradation can enhance the carbon absorption capacity of grassland.

Promote the management of grass and sand system in landscape forest, field and lake

Overall layout and implementation of major ecological protection and restoration projects are the key to enhance the increment of carbon sinks in ecosystems. By implementing projects such as returning farmland to forest and grassland, building shelter forest system and protecting and restoring wetlands, the area of ecosystem can be increased and its carbon storage and absorption capacity can be improved. For example, by restoring wetland vegetation, the carbon storage of wetland ecosystem can be increased. At the same time, strengthening the ecological restoration of rivers and coastal zones can increase vegetation coverage, reduce soil erosion and help enhance carbon sink capacity.

Establish an ecosystem carbon sink monitoring and accounting system

Constructing a perfect monitoring and accounting system of carbon sequestration in ecosystem is an important guarantee to enhance carbon sequestration capacity. By constructing the monitoring and evaluation system of ecosystem carbon sequestration and perfecting the measurement system of ecosystem carbon sequestration, the accurate evaluation of ecosystem carbon sequestration capacity can be realized. At the same time, strengthening scientific and technological support and international cooperation and introducing advanced technology and experience can improve the monitoring and evaluation level of carbon sequestration capacity of ecosystems in China. For example, by means of remote sensing technology and model simulation, real-time monitoring and dynamic evaluation of carbon sequestration capacity of ecosystems can be realized.

Improve the relevant laws and policies on carbon sequestration in ecosystems

Perfecting the relevant laws and regulations on carbon sequestration in ecosystems is the institutional guarantee for enhancing carbon sequestration capacity. By formulating and perfecting relevant laws, regulations, policies and measures, we can clarify the ownership and trading rules of carbon sinks in ecosystems, and promote the implementation of carbon sink projects and the development of carbon sink trading. At the same time, by establishing and improving the compensation mechanism for ecological protection that reflects the value of carbon sinks, promoting the trading of carbon sinks in ecosystems, and improving the diversified investment mechanism for ecological protection and restoration, we can stimulate the enthusiasm of all sectors of society to participate in the protection of carbon sinks in ecosystems. For example, through carbon trading, resources can be transformed into assets and the value of ecological products can be realized.

OUTLOOK

The comprehensive investigation of natural resources carbon sinks belongs to a new field, and it is an interdisciplinary subject, covering earth system science, geology, geochemistry, ecology, botany, remote sensing technology and other related knowledge. It is necessary to further improve the reliability of the comprehensive investigation method of natural resources carbon sinks, and at the same time, develop efficient and scalable carbon sequestration and sink enhancement technologies and carry out interdisciplinary comprehensive research. “Measurable, reportable and verifiable” of carbon sinks in natural ecosystems is an important scientific basis for formulating policies to reduce emissions and increase sinks in China (Piao, S.L. *et al*., 2022). How to meet this decision-making demand timely and effectively is both a challenge and an opportunity for the scientific community. At present, the investigation method of carbon sinks in natural resources mentioned above is still an important means to quantitatively study carbon sinks in natural ecosystems and their temporal and spatial changes, and it is being further improved. At the same time, because different methods involve multiple time and space scales, and their sources of uncertainty are different, it is also a big problem to quantitatively evaluate their uncertainty.

To build a unified regional scale natural resources carbon sink observation system standards

In recent years, many experts and scholars have carried out a lot of monitoring and research work on the carbon storage/sink of natural ecosystems in China, laying a solid foundation for finding out the carbon storage background and carbon sink potential of natural resources in China. However, due to the rich types and wide distribution of natural ecosystems in China, the observation of key areas of natural resources carbon sinks is still insufficient. Strengthen the observation of underground carbon pools, especially soil carbon pools. At present, the observation of aboveground vegetation carbon pool in China is sufficient, and it can be combined with remote sensing observation to reflect the changes of vegetation carbon pool at different time and space scales. However, the regular observation of soil carbon pool with unified national standards is still insufficient, especially in the central and western regions, where the uncertainty of soil carbon storage estimation is still large. For example, the estimation of carbon pool in 0~3m permafrost in Qinghai-Tibet Plateau is more than twice as different as the results of different studies (Ding

et al., 2019; Wang, T.H. *et al*., 2020).In order to accurately estimate the soil carbon pool and its changes in China, it is necessary to carry out a unified and comprehensive inventory of soil carbon pool on a regular basis. Strengthen the observation of carbon sinks in climate change sensitive areas such as wetlands and deserts. In the past, the carbon sink observation of terrestrial ecosystem mainly focused on forest, grassland and other ecosystem types. However, the carbon sinks of non-forest and grass ecosystem types, such as wetlands and deserts, can not be ignored when accurately estimating land carbon sinks at regional scale. For example, since the Holocene, the soil carbon accumulation rate of Zoige wetland has reached 5 ~ 48gC $m^{-2}a^{-1}$, which has obvious carbon sink potential (Chen *et al*., 2014). Because there is no unified observation of terrestrial carbon sinks in desert areas on the national scale and the data are scarce, it is urgent to increase the research in this direction in the future.

Research and development of natural-human coupling terrestrial ecosystem carbon cycle process model

The carbon cycle model based on natural ecosystem is an important tool to predict the future changes of land carbon sink. At present, there are more than ten different carbon cycle models widely used in the global carbon plan and IPCC's global terrestrial ecosystem carbon budget dynamic change assessment. After more than 30 years of development, the mainstream international carbon cycle model has been able to simulate the response of carbon cycle process of natural ecosystems to climate change (Fisher & Koven, 2020; Friedlingstein *et al*., 2020), but it is generally unable to describe the impact of human activities on ecosystems (Bonan & Doney, 2018). For example, only a few models can describe the impact of forest management on carbon sources and sinks of ecosystems (Pugh *et al*., 2019); Most models do not consider the lateral transport process of organic carbon in terrestrial ecosystems (Ciais *et al*., 2021), agricultural ecosystem management (Le Quéré *et al*., 2018) and the influence of forest age on carbon sinks (Yao *et al*., 2018b). Models that can simulate these processes at the same time have not been reported. Therefore, it is still a great challenge to accurately quantify the contribution of each component of natural and human activities to the potential of natural ecosystem to increase foreign exchange. Considering that the carbon sinks of terrestrial ecosystems in China have largely benefited from ecological projects such as returning farmland to forests and afforestation in the past few decades (Lu *et al*., 2018), it is very important to develop a model of ecosystem carbon cycle process coupled with nature and humanity to accurately predict the carbon sinks potential of terrestrial ecosystems in China and quantitatively distinguish the contributions of natural and human factors.

Strengthen the research, development and demonstration of carbon sequestration and sink enhancement technologies in different natural ecosystems

According to different climate change and atmospheric subsidence scenarios, combined with major ecological projects and various human management measures in China, this paper discusses the potential of increasing foreign exchange in different periods and different emission scenarios, quantifies the contribution of climate change and human activities to the potential of increasing foreign exchange in natural resource carbon pools, and puts forward an optimized scheme for systematic management of increasing foreign exchange in natural resource carbon pools on the basis of fully considering the carbon fixation rate (dynamic characteristics), stability and sustainability. Based on the comprehensive investigation and analysis of natural resources, we will optimize the allocation of resources, develop ecological restoration technology based on the consolidation and improvement of carbon sink capacity, implement monitoring and evaluation of the effectiveness of ecological protection and carbon sink restoration, and explore the model of "ecological restoration+carbon sequestration and sink enhancement" in typical fragile ecological areas.

REFERENCES

Bonan, G.B., & Doney, S.C., 2018. Climate, ecosystems, and planetary futures: The challenge to predict life in Earth system models. Science, 359, 6375.

Cai, W., He, N., Li, M., Xu, L., Wang, L., Zhu, J., Zeng, N., Yan, P., Si, G., & Zhang, X., 2022. Carbon sequestration of Chinese forests from 2010 to 2060: Spatiotemporal dynamics and its regulatory strategies. Sci. Bull., 67, 836–843.

Canadell, J.G., Le Quéré, C., Raupach, M.R., Field, C.B., Buitenhuis, E.T., Ciais, P., Conway, T.J., Gillett, N.P., Houghton R.A., & Marland G., 2007. Contributions to accelerating atmospheric CO_2 growth from economic activity, carbon intensity, and efficiency of natural sinks. Proc. Natl. Acad. Sci. USA Nov. 20, 104(47), 18866-70.

Chen, H., Yang, G., Peng, C., Zhang, Y., Zhu, D., Zhu, Q., Hu, J., Wang, M., Zhan, W., Zhu, E., Bai, Z., Li, W., Wu, N., Wang, Y., Gao, Y., Tian, J., Kang, X., Zhao, X., & Wu J., 2014. The carbon stock of alpine peatlands on the Qinghai-Tibetan Plateau during the Holocene and their future fate. Quat. Sci., 95, 151–158.

Ciais, P., Borges, A.V., Abril, G., Meybeck, M., Folberth, G., Hauglustaine, D., & Janssens, I.A., 2006. The impact of lateral carbon fluxes on the European carbon balance. Biogeosciences, 5, 1259–1271.

Ding, J.Z., Wang, T., Piao, S.L., Smith, P., Zhang, G.L., Yan, Z.J., Ren, S., Liu, D., Wang, S.P., Chen, S.Y., Dai, F.Q., He, J.S., Li, Y.N., Liu, Y.W., Mao, J.F., Arain, A., Tian, H.Q., Shi, X. Y., Yang, Y.H., Zeng, N., & Zhao L., 2019. The paleoclimatic footprint in the soil carbon stock of the Tibetan permafrost region. Nat. Commun., 10, 4195.

Dixon, R.K., Solomon, A.M., Brown, S., Houghton, R.A., Trexier, M.C., & Wisniewski, J. , 1994. Carbon Pools and Flux of Global Forest Ecosystems. Science, 263, 185–190.

Falkowski, P.G., Fenchel, T., & Delong, E.F., 2008. The microbial

engines that drive Earth's biogeochemical cycles. Science. May 23, 320(5879), 1034-9.

Fisher, R.A., & Koven, C.D.,2020. Perspectives on the future of land surface models and the challenges of representing complex terrestrial systems. J. Adv. Model. Earth Syst., 12, e2018MS001453.

Friedlingstein, P., O'Sullivan, M., Jones, M.W., Andrew, R.M., Hauck, J., Olsen, A., Peters, G.P., Peters, W., Pongratz, J., Sitch, S., Le Quéré, C., Canadell, J.G., Ciais, P., Jackson, R. B., Alin, S., Aragão, L E O C, Arneth, A., Arora, V,. Bates, N.R., Becker, M., Benoit-Cattin, A., Bittig, H.C., Bopp, L., Bultan, S., Chandra, N., Chevallier, F., Chini, L.P., Evans, W., Florentie, L., Forster, P.M., Gasser, T., Gehlen, M., Gilfillan,D., Gkritzalis, T., Gregor, L., Gruber, N., Harris, I., Hartung, K., Haverd, V., Houghton, R.A., Ilyina, T., Jain, A. K., Joetzjer, E., Kadono, K., Kato, E., Kitidis, V., Korsbakken, J.I., Landschützer, P., Lefèvre, N., Lenton, A., Lienert, S., Liu, Z., Lombardozzi, D., Marland, G., Metzl, N., Munro, D.R., Nabel, J E M S, Nakaoka, S.I., Niwa, Y., O'Brien, K., Ono, T., Palmer, P. I., Pierrot, D., Poulter, B., Resplandy, L., Robertson, E., Rödenbeck, C., Schwinger, J., Séférian, R., Skjelvan, I., Smith, A J P, Sutton, A.J., Tanhua, T., Tans, P.P., Tian, H., Tilbrook, B., van der Werf, G., Vuichard, N., Walker, A.P., Wanninkhof, R., Watson, A.J., Willis, D., Wiltshire, A.J., Yuan, W., Yue, X., & Zaehle, S., 2020. Global carbon budget 2020. Earth Syst. Sci. Data, 12, 3269–3340.

Huang, H., & Zhou, J., 2022, Study on the Spatial and Temporal Differentiation Pattern of Carbon Emission and Carbon Compensation in China's Provincial Areas. Sustainability, 14, 7627.

IPCC, 2013. Climate Change 2013：The Physical Science Basis［M］. Cambridge University Press, Cambridge.

Le Quéré, C., Andres, R.J., & Boden, T., 2013. The global carbon budget 1959—2011. Earth Syst. Sci. Data, 5(1), 165-185.

Le Quéré, C., Andrew, R.M., Friedlingstein, P., Sitch, S., Pongratz, J., Manning, A.C., Ivar Korsbakken, J., Peters, G.P., Canadell, J.G., Jackson, R.B., Boden, T.A., Tans, P.P., Andrews, O.D., Arora, V.K., Bakker, D C E., Barbero, L., Becker, M., Betts ,R. A., Bopp, L., Chevallier, F., Chini, L.P., Ciais, P., Cosca, C.E., Cross, J., Currie, K., Gasser, T., Harris, I., Hauck, J., Haverd, V., Houghton, R.A., Hunt, C.W., Hurtt, G., Ilyina, T., Jain, A.K., Kato, E., Kautz, M., Keeling, R.F., Klein Goldewijk, K., Körtzinger, A., Landschützer, P., Lefèvre, N., Lenton, A., Lienert, S., Lima, I., Lombardozzi, D., Metzl, N., Millero, F., Monteiro, P.M.S, Munro, D.R., Nabel, JE M. S., Nakaoka, S.I., Nojiri, Y., Antonio Padin, X., Peregon, A., Pfeil, B., Pierrot, D., Poulter, B., Rehder, G., Reimer, J., Rödenbeck, C., Schwinger, J., Séférian, R., Skjelvan, I., Stocker, B.D., Tian, H., Tilbrook, B., Tubiello, F.N., Laan-Luijkx, I T. V., Werf, G.R.V., Van Heuven, S., Viovy, N., Vuichard, N., Walker, A.P., Watson, A. J., Wiltshire, A.J., Zaehle, S., & Zhu, D., 2018. Global carbon budget 2017. Earth Syst. Sci. Data,10, 405–448.

Li, Z., Cheng, X., & Han, H., 2020. Future Impacts of Land Use Change on Ecosystem Services under Different Scenarios in the Ecological Conservation Area, Beijing, China. Forests, 11, 584.

Liu, L.Y., Bai, Y., Sun, R., & Niu, Z.G., 2021. Overview and research progress of the project: Stereoscopic observation and inversion of key parameters of global ecosystem carbon cycle. Remote sensing technology and application, 36(01),11-24.

Liu, Z.H., Macpherson, G.L., Groves, C., Martin, J.B., Yuan, D.X., & Zeng, S.B., 2018.Large and active CO_2 uptake by coupled carbonateweathering. Earth Sci. Rev., 182, 42–49.

Lu, F., Hu, H.F., & Sun, W. J., 2018. Effects of National Ecological Restoration Projects on Carbon Sequestration in China from 2001 to 2010. Proceedings of the National Academy of Sciences, 115(16), 4039−4044.

Lu, N., Tian, H.Q., & Fu, B.J., 2022. Biophysical and Economic Constraints on China's Natural Climate Solutions. Nature Climate Change, 12(9), 847−853.

Piao, S.L., He, Y., & Wang, X.H., 2022. Estimation of China's terrestrial ecosystem carbon sink: methods,progress and prospects. Sci. China Earth Sci., 65(4) , 641-651.

Piao, S.L., He, Y., Wang, X.H., & Chen, F.H., 2022. Carbon sequestration estimation of terrestrial ecosystem in China: method, progress and prospect. China Science: Earth Science, 52(06), 1010-1020.

Pugh, T.A.M., Lindeskog, M., Smith, B., Poulter, B., Arneth, A., Haverd, V., & Calle L., 2019. Role of forest regrowth in global carbon sink dynamics. Proc. Natl. Acad. Sci. USA, 116, 4382–4387.

Quéré, C.L., Andrew, R.M., & Canadell, J.G., 2016. Global Carbon Budget. Earth System Science Data, 8(2), 605-649.

Sun, J., Wang,Y.X., Lee,T.M., Nie,X.W., Wang,T., Liang, E.Y., Wang,Y.F., Zhang, L., Wang, J., Piao, S.L., Chen, F.H. & Fu,B. J.,2024. Nature-based Solutions can help restore degraded grasslands and increase carbon sequestration in the Tibetan Plateau. Commun. Earth Environ., 5, 154.

Wang, L., Gao, Y., & Shen, Z., 2024. Research progress on evaluation methods of farmland soil carbon storage under the background of climate change. Journal of Agricultural Engineering, 40(16),1-11.

Wang, T.H., Yang, D.W., Yang, Y.T., Piao, S.L., Li, X., Cheng, G. D., & Fu, B.J., 2020. Permafrost thawing puts the frozen carbon at risk over the Tibetan Plateau. Sci. Adv., 6, eaaz3513.

Xie, L., Bai, Z., Yang, B., Chen, M.G., Fu, S., & Mao, Y., 2022. Domestic and foreign lands in the context of carbon neutrality Research progress on assessment methods of terrestrial ecosystem carbon sink. Geosci. Front.

Xu, L., He, N., Li, M., Cai, W., & Yu, G.,2024. Spatiotemporal dynamics of carbon sinks in China's terrestrial ecosystems from 2010 to 2060. Resources, Conservation and Recycling, 203, 107457.

Xu, E.Y., Wang, W.F., Nie, Y., & Yang, H., 2020. Regional distribution and potential prediction of forestry carbon contribution in China. China Popul. Resour. Environ., 30, 36–45.

Yang, Y.H., Shi, Y., Sun, W.J.,Chang, J.F., Zhu, J.W., Chen, L.Y., Xin, W., Guo, Y.P., Zhang, H.T., Yu, L.F., Zhao, S.Q., Xu, W., Zhu, J.L., Shen, H.H., Wang, Y.Y., Peng, Y.F., Zhao, X., Wang, Y.P., Hu, H.F, Chen, S.P., Huang, M., Wen, X.F., Wang, S.P., Zhu, B., Niu, S.L., Tang, Z.Y., Liu, L.L., & Fang, J.Y.,2022. Characteristics of carbon sources and sinks of terrestrial ecosystems in China and the world and their contribution to carbon neutrality. China Science: Life Science, 52(04), 534-574.

Yao, Y.T., Piao, S.L., & Wang, T., 2018b. Future biomass carbon sequestration capacity of Chinese forests. Sci. Bull., 63, 1108–1117.

Yu, X., & Y., Alex, 2014. Carbon finance and the carbon market in China. Nature Climate Change, 5(1), 15-16.

Zhang, Y., Li, X.G., & Wen, Y.L., 2022. Analysis of forest carbon sequestration potential in China under the background of carbon neutrality in peak carbon dioxide emissions. Journal of Beijing Forestry University, 44(01), 38-47.

Zhou, K., & Li, Y.W., 2019. Carbon finance and carbon market in China: Progress and challenges. Journal of Cleaner Production, 214, 536-549.

Zhu, X.J., 2022. Effects of ecosystem types on the spatial variations in annual gross primary productivity over terrestrial ecosystems of China. Science of The Total Environment.

Web services and machine learning algorithm for mapping disaster areas using satellite images

Joel Bandibas*, Shinji Takarada

Geological Survey of Japan (GSJ), Tsukuba City, Japan
*Email: joel.bandibas@aist.go.jp

Abstract: Mapping areas affected by natural disasters is crucial for an effective rescue and relief response. Land cover change detection using satellite images before and after the event is the most efficient method for mapping large areas affected by natural disasters. The conventional method for detecting changes using satellite images involves detecting changes in the land cover spectral and spatial patterns before and after the occurrence of the event. Satellite images covering disaster areas have high spectral frequency, and pixel values belonging to a spectral class are often not normally distributed. This makes the change detection methods using parametric statistics less accurate. This paper presents a change detection method using Artificial Neural Network (ANN). ANN computing is an implementation of a machine learning algorithm inspired by how the brain's neurons process information. Using ANN to detect land cover change is independent of an assumed data distribution, making it more accurate. The study presents a change detection method using ANN consisting of three major steps. First, the satellite image taken before the occurrence of the event is segmented into several spectral classes or clusters using a simple moving average clustering algorithm; second, a 3-layered ANN is trained to identify spatial signature of each cluster using its neighboring pixels within a defined window in the first image and, third, the final change detection process is implemented by feeding the trained ANN with pixel values from the same location of the images taken before and after the event, generating two ANN outputs. The difference between the two outputs higher than a set threshold signifies change. The third step is implemented for all pixel locations in the satellite images, producing a change map.
WebGIS is an efficient and cost-effective platform for viewing and processing geospatial data using web services. It is linked with Web Map Service (WMS) and Web Processing Service (WPS) for rendering and processing remotely sensed data online, respectively. In this study, a WebGIS is developed and WPS are formulated to sample satellite images, train ANN, and detect land cover changes. WMS is also formulated on the fly to make the mapped disaster areas instantaneously viewable online. The developed system successfully maps damaged areas in Wajima City, Ishikawa Prefecture, Japan, after the January 1, 2024 earthquake using Sentinel 1 Synthetic Aperture Radar (SAR) images. It is also used to map areas affected by landslides in Maco, Davao de Oro, Philippines, in February 2024, using Sentinel 2 visible and infrared images.

Keywords: Disaster area mapping, satellite images, machine learning, ANN, WebGIS, WPS, WMS

INTRODUCTION

Timely identification of areas affected by natural disasters is very important for a successful and effective emergency relief efforts. The use of satellite images to delineate areas damaged by natural disasters is very cost-effective and efficient. Satellite images can cover huge areas and cheaper to obtain compared to aerial photographs and information obtained from drones and field surveys. Change detection is a process that observes the differences of an object or phenomenon at different times (Singh, 1989). The identification of damaged areas using remotely changed data involves the determination of the spectral and spatial changes in satellite images taken before and after the occurrence of the disaster. Areas that sustained significant damage show significant changes in spectral and spatial characteristics.

There are several classification methods for detecting land cover change from multi-temporal remote sensing data sets. Image differencing is the most common and straightforward method for change detection. It is simply the subtraction of the pixel digital values of an image recorded at one date from the corresponding pixel values of the second date (Hayes & Sader, 2001). Image differencing involves the processing of one band of the digital images at a time. Other methods use multiple bands of data for change detection. These include image differencing using bands ratios like vegetation indices and principal component analysis (PCA). In the temporal change detection using PCA, both the surface proportion and the magnitude of the changed area in an image determine which principal component images will contain change information. It is the relative amount of variance between the change area

and the unchanged part in an image that determine which particular PCs contain change information (Sing, 1989).

The conventional unsupervised change detection algorithms are primarily pixel by pixel- based method of identifying changes of land cover using multi-temporal remotely sensed data sets. However, changes in pixel values between two images are sometimes not good indication of land cover change, like areas damaged by natural disasters. Indeed, in many instances, a particular pixel's brightness covering a damaged area does not change. The indications that it covers a damaged area are the changes in the brightness of the surrounding pixels, the change in image texture. More often, changes in texture are more important in identifying damaged areas than the changes in brightness in images. Delineating damaged areas often involves identifying regions in the image whose texture significantly change in the multi-temporal data sets. Texture change detection is also termed spatial signature change detection in satellite images.

Several algorithms were developed to determine the spatial signature of pixels in satellite images like the contextual identification of pixels or spatial correlation (Alonso & Soria, 1991; Lira & Maletti, 2002). A similar method developed by Peddle & Franklin (1989) termed this spatial correlation procedure as gray level-spatial dependency co-occurrence. Gong & Howarth (1992) formulated the frequency based contextual classifier wherein the identity of a pixel is defined by the frequency of occurrence of the different spectral classes of its surrounding pixels. These methods use parametric statistics in determining change. However, remotely sensed data in areas affected by natural disasters are often high frequency images and pixel values can be more random and not normally distributed. These make change detection using parametric statistics less accurate.

One of the most widely used machine learning algorithms for pattern recognition is Artificial Neural Networks (ANN). ANN computing is an implementation of a machine learning algorithm inspired by how the brain's neurons process information. It is the study of networks of adaptable nodes which, through a process of learning from task examples, store experiential knowledge and make it available for use (Alexander & Morton, 1990). It has been used for many kinds of applications like recognizing speech (Dede & Sazli, 2012) and face (Aitkenhead & McDonald, 2003). ANN has been used for pattern recognition in satellite images (Civco, 1993; Atkinson & Tatnall, 1997, Bandibas & Kohyama, 2001; Rai *et al.*, 2020). ANNs do not require an assumption for the data to follow certain distribution models, making them useful for identifying changes in satellite images covering areas affected by natural disasters. This study presents an unsupervised method to detect changes in satellite images using trained ANN to map areas affected by natural disasters. The method is implemented through the formulation of web services, which can be accessed and executed from a web-based Geographic Information System (WebGIS).

METHODS

ANN & Error Back-Propagation Neural Network Computing

ANN computing is inspired by the structure and functions of neurons and their connections in the human brain. ANN gains experience, through training, to build a new model of the data generating process so that it can generalize and predict outputs from inputs (Atkinson & Tatnall, 1997). One of the most important neural computing methodologies is the Error Back-Propagation Neural Network (EBPNN) computing. This is a feed forward method wherein neurons are organized as sequential layers, each composed of one or more neurons: the input layer, middle layer(s) and output layer, like the one shown in Figure 1. The relationship between neurons from adjacent layers, the connection paths, is defined by the weights assigned to them. The weight values and their distribution within the ANN determine its information processing behavior.

Given a network with N_i, N_j and N_k as the nodes of the input, middle and output layers, respectively. For the *pth* presentation of the input/output pair for training, the output O_{pj} of node N_j in the middle layer is defined by the sigmoid function (Rumelhart *et al*., 1986) :

$$O_{pj} = \frac{1}{1+e^{-A_{pj}}}, \quad (1)$$

where A_{pj} is the activation value of node N_j as expressed in the form:

$$A_{pj} = \sum (for\ all\ i) O_{pi} W_{ji} + U_j, \quad (2)$$

where O_{pi} is the training input value entering the *ith* input node from the *pth* input training set while W_{ij} is the connection weight between nodes N_i and N_j. U_j is the threshold value of node N_j. The network's output, the output of node N_k , is defined by the equation:

$$O_{pk} = \frac{1}{1+e^{-A_{pk}}}, \quad (3)$$

where the activation value of node N_k is in the form:

$$A_{pk} = \sum (for\ all\ j) O_{pj} W_{kj} + U_k, \quad (4)$$

where W_{kj} is the connection weight between the *jth* and the *kth* nodes of the middle and the output layers, respectively. U_k is the threshold value of node N_k.

ANN is initialized by the assignment of random values for the connection weights between the neurons of adjacent layers and the threshold values for the neurons in the middle and output layers. Training starts after initialization

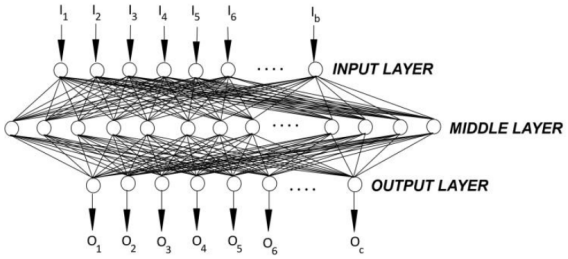

Figure 1: A 3-layered feed forward Artificial Neural Network with b and c number of neurons in the input and output layers, respectively.

by entering training inputs into the network. The resulting output Opk is compared to the desired training output Tpk to compute the error, which is proportional to the difference |Opk−Tpk|. The error is then back-propagated to the network and weights are altered proportional to the scale of the error, to minimized it during the next iteration. After several iterations, the actual outputs will gradually converge towards the desired outputs. The number of iterations to reach convergence depends on the complexity and the size of the data used for training. The mathematics behind the computations for the changes of the connection weights between neurons during training is describe in detail by Bandibas (1996) and Kawabata & Bandibas (2009).

Spectral and spatial signatures of land cover

Spectral signature of a land cover is the amount of radiation that it reflects. Spectral signature is what we perceive as color, corresponding to the reflected radiation covering the visible spectral frequency range from blue to red. In remote sensing, spectral signature is the radiance, measured in pixel values, for each frequency range called band. Most pixels covering a land cover type have unique spectral signatures. On the other hand, we can visually sense the spatial signature of a land cover type based on its shape, size and texture. In remote sensing, a land cover spatial signature can be defined by the distribution pattern of different pixel spectral classes covering it. In this study, we setup an ANN structure and training scheme to capture land cover spatial signatures in satellite images. Determining their changes before and after the occurrence of natural disasters is the basis for the generation of maps identifying areas damaged by natural disasters.

The change detection process is implemented in three major steps:

- First, the satellite image taken before the occurrence of the event is segmented into several spectral classes or clusters using a simple moving average clustering algorithm.
- Second, a 3-layered ANN is trained to identify spatial signature of each cluster using its neighboring pixels within a defined pixel window in the first image.
- Third, the final change detection process is implemented by feeding the trained ANN with pixel values from the same location of the satellite images taken before and after the event, generating two ANN outputs. The difference between the two outputs higher than a set threshold signifies change. The third step is implemented for all pixel locations in the satellite images, producing a change map.

Satellite image spectral class segmentation and sampling

In this study, the satellite image taken before the occurrence of the disaster is classified into a maximum of 30 spectral classes using a simple moving averages clustering algorithm (Richards, 1987). Each of these spectral classes is called cluster and its spatial signature is defined by the distribution pattern of its neighboring pixels, within a set pixel window size. Figure 2 shows the spatial signature of clusters for each band, as defined by the distribution of pixel values within the defined 3 by 3 pixel window. In this study, 15 samples are taken for each cluster.

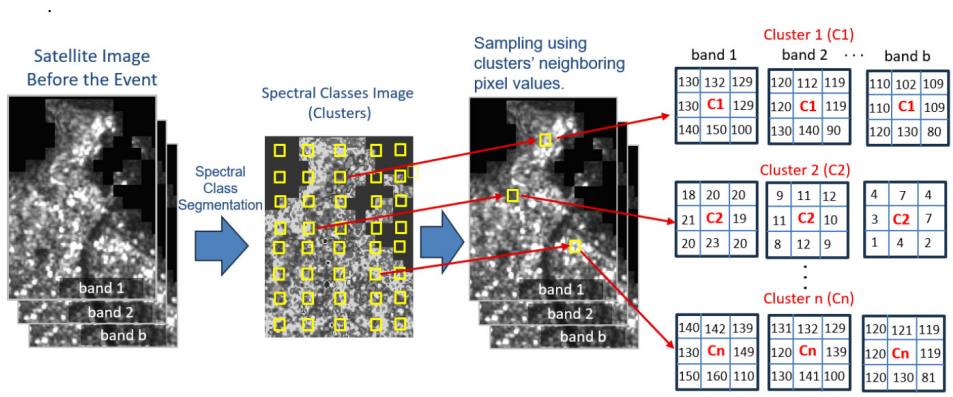

Figure 2: Segmentation of satellite image before the event and spatial signature sampling using cluster neighboring pixel distribution pattern within a 3 by 3 pixel window.

ANN structure and input - Output training pairs

The ANN used in this study has three layers: the input, middle and output layers. The number of neurons in the input layer is equal to the square of the used pixel window size times the number of bands used. For a 3 by 3 pixel window using 3 bands, the number of neurons in the input layer is 27. The number of neurons in the output layer is equal to the number of clusters used. The default number of neurons in the middle layer is set at 25. This number is increased or decreased depending on the complexity of the training data, reflected on the learning speed of ANN during training. The ANN input training pattern consists of the sample pixel values for each cluster. The input pixel values are all recalculated to the range between 0 to 1. The training output value for each neuron can either be 0 and 1. Figure 3 and Figure 4 show the ANN structure and training scheme used in this study, respectively.

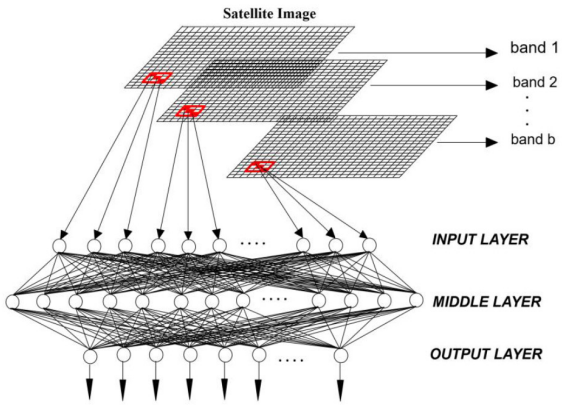

Figure 3: The ANN structure used in this study.

Change determination using trained ANN

Change determination using the trained ANN is done by running a pixel window, pixel by pixel, over the entire satellite images before and after the occurrence of the event. The center pixel of the pixel window is determined to have changed or not, by determining the distance of the ANN output with inputs from satellite images before and after the event. The distance, D, between the two outputs is expressed as:

$$D = \frac{1}{n}\sum_{i=1}^{n}(x1_i - x2_i)^2 \quad , \qquad 5$$

where n is the total number of pixels in a pixel window times the number of bands. The x1 and x2 are the window pixel values of the satellite image before and after the event, respectively. Figure 5 shows the change detection scheme to generate a land cover change map using the trained ANN and the satellite images before and after the event. In this study, the system is tested to map areas damaged by the January 1, 2024 Noto Peninsula earthquake in Wajima City, Ishikawa Prefecture, Japan, using Sentinel 1 satellite images. It is also used to identify areas affected by the February 2024 landslides in Maco, Davao de Oro, Philippines, using Sentinel 2 data.

WebGIS and web services

WegGIS has recently been the preferred platform for processing geospatial information. It deals with geographic information, including geospatial analysis, within the online environment (Netek *et al*., 2023). Most WebGIS are developed using Free and Open-Source Software (FOSS), making them highly accessible and cost-efficient. It provides spatial information processing capabilities through its access to web services. These web services include the Web

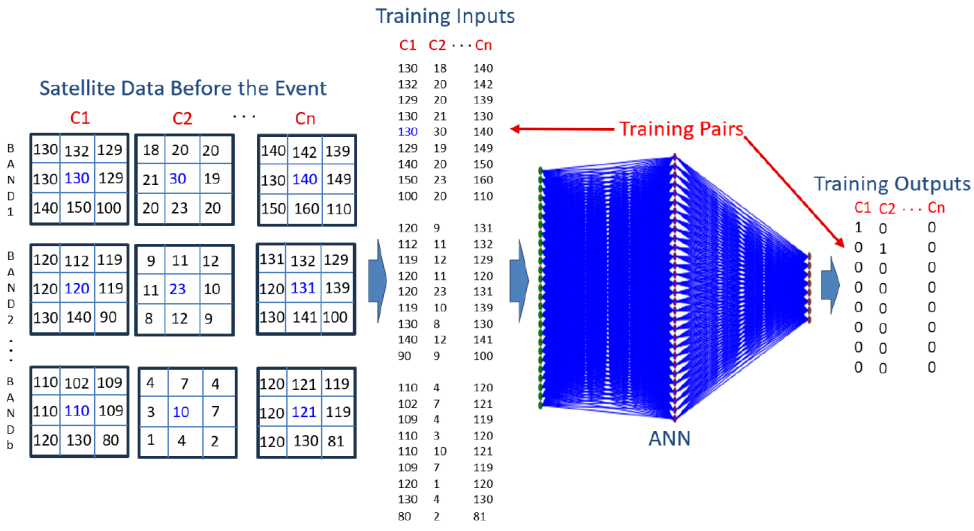

Figure 4: The ANN training scheme using clusters pixel samples and the formulated outputs as the training inputs–outputs pairs.

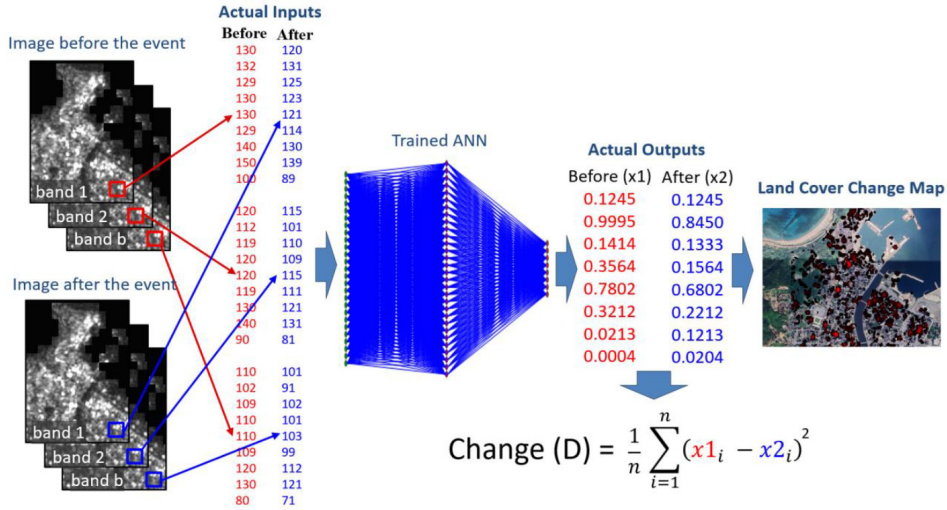

Figure 5: Mapping areas damaged by natural disaster using trained ANN and satellite images taken before and after the event.

Map Service (WMS) and Web Processing Service (WPS), following the Open Geospatial Consortium (OGC) standards. WMS provides a simple Hypertext Transfer Protocol (HTTP) interface for requesting geo-registered map images from one or more distributed databases (OGC, 2019a). WebGIS renders maps by sending requests to WMS servers, which are set up to accept requests to query online databases and return map images. WebGIS also processes spatial information by sending requests to WPS servers. WPS provides a robust, interoperable, and versatile protocol for process execution of web services (OGC, 2019b). It is a service interface through which information processing can be done over the Internet (Tripathi *et al*., 2019). The service can provide simple task like sampling satellite images for classification or more complex processing like Normalized Difference Vegetation Index (NDVI) computation. These web-based computing capabilities recently made WebGIS the preferred system for storing, distributing, and processing geographically referenced information. In this study, a WebGIS system is developed with access to WMS and WPS for rendering and processing of remotely sensed data to detect land cover change using ANN. An interface is developed to upload satellite images, formulate color composite for multi-band image processing and formulate WMS to display satellite images and land cover change maps in the WebGIS main page. WPS is also formulated to classify satellite images into spectral classes and the sampling of pixels needed for training the ANN. The interface for training ANN and the generation of land cover change map is also developed.

RESULTS AND DISCUSSION

The methods for satellite image spectral class segmentation and sampling pixels for land cover spatial signature identification using ANN computing are successfully developed. These are implemented using the formulated WMS and WPS, executed through the developed WebGIS. The system is successfully used for the mapping of disaster areas using satellite images and trained ANN. The system is used to map areas affected by the January 1, 2024 Noto Peninsula earthquake in Wajima City, Ishikawa Prefecture, Japan. Sentinel 1 Synthetic Aperture RADAR (SAR) VH images taken on December 30, 2023 and January 11, 2024 are used for ANN training and mapping. Figure 6 shows the change detection interface, trained ANN, and the areas identified by ANN to have been damaged by the earthquake in Wajima city. The identified damaged areas are confirmed by aerial photographs taken after the occurrence of the earthquake.

The system is also used to map areas affected by the February 2024 landslides in Maco, Davao de Oro, Philippines. Sentinel 2 images with bands 3,4 and 8, taken on November, 14, 2023 and March 3, 2024 are used for ANN training and the identification of landslide areas. Figure 7 shows the landslide areas identified by the trained ANN, which are confirmed using aerial photographs taken after the landslide events. The generated disaster area map, being served as a WMS, can be viewed online instantaneously using web browsers on PCs and mobile devices. The determination of optimal ANN training learning rate, training time, number of nodes at the middle layer and pixel window size for a more efficient and accurate mapping of disaster areas is still ongoing.

CONCLUSIONS

The ANN training procedure is formulated for the identification of spatial signatures of land cover types in satellite images. WMS and WPS are also successfully setup for displaying satellite images and training ANN, respectively. A WebGIS linked to these web services is developed and successfully used for the mapping of areas

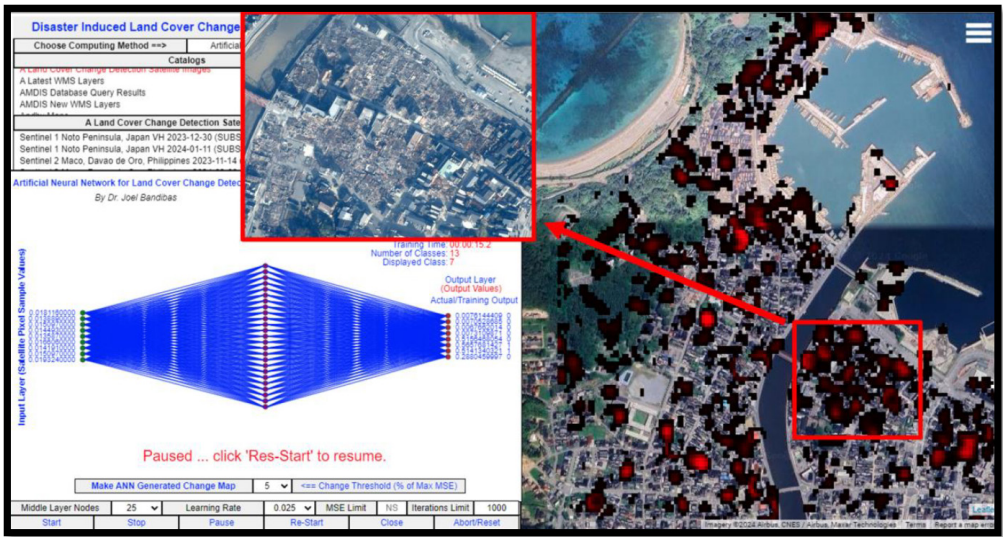

Figure 6: Areas identified by the trained ANN to have been damaged by the January 1, 2024 earthquake in Wajima City, Ishikawa Prefecture, Japan.

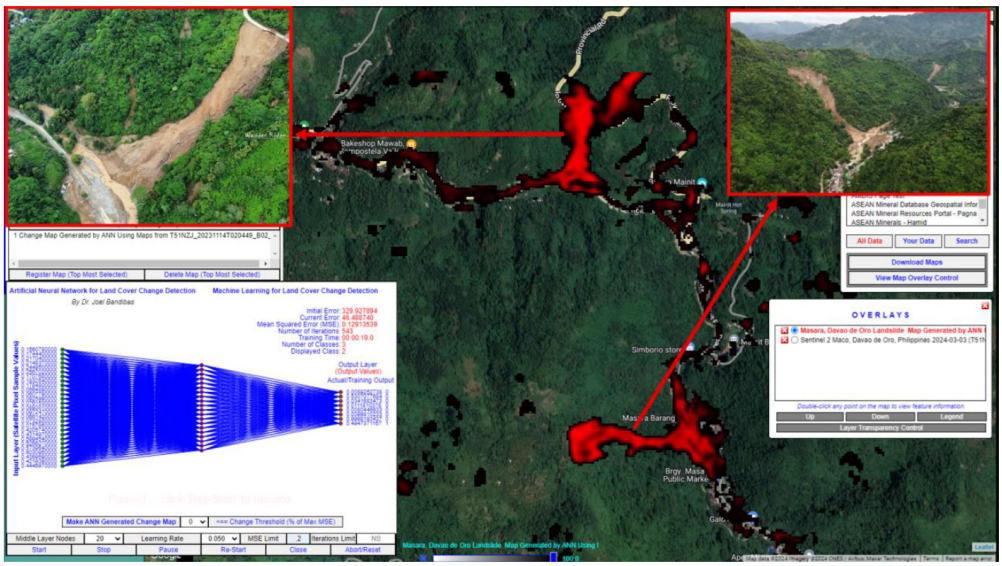

Figure 7: Areas identified by the trained ANN as areas affected by the February 2024 landslides in Maco, Davao de Oro, Philippines.

affected by natural disasters using satellite images and trained ANN. The initial results of the study indicate that the system can accurately identify areas affected by natural disasters using Sentinel 1 and 2 satellite images. The study is still ongoing but the initial results show that the developed system could be a highly accessible, cost-efficient and useful tool for disaster response.

REFERENCES

Aitkenhead, M.J., & McDonald, A.J.S., 2003. A neural network face recognition system. Engineering Applications of Artificial Intelligence, 16, 167–176.

Alexander, I., & Morton, H., 1990. An Introduction to Neural Computing. Chapman and Hall, London, 468 p.

Alonso, F.G., & Soria, S.L., 1991. Using contextual information to improve land use classification of satellite images in central Spain. International Journal of Remote Sensing, 12(11), 2227-2235.

Atkinson, P.M., & Tatnall, A.R.L., 1997. Neural networks in remote sensing. International Journal of Remote Sensing, 18, 699–709.

Bandibas, J.C., 1996. The Automated Land Evaluation Using Artificial Neural Network Based Expert's Knowledge, GIS and Remotely Sensed Data: Spatial and Spectral Signatures for Satellite Image Classification. Ghent University. Faculty of Sciences, Ghent, Belgium. 201 p.

Bandibas, J., & Kohyama, K., 2001. An efficient artificial neural network training method through induced learning retardation: inhibited brain learning. Asian Journal of Geoinformatics, 1(4), 45–55.

Civco, D.L., 1993. Artificial neural networks for land-cover classification and mapping. International Journal of Geographical Information Systems, 7, 173–186.

Dede, G., & Sazli, M.H., 2009. Speech recognition with artificial neural networks. Digital Signal Processing, 20, 763–768.

Franklin, S.E., & Peddle, D.R., 1989. Spectral texture for improved class discrimination in complex terrain. International Journal of Remote Sensing, 10(8), 1437-1443.

Gong, P., & Howarth, P.J., 1992. Frequency-based contextual classification and gray-level vector reduction for land-use identification. Photogrammetric Engineering & Remote Sensing, 58(4), 423-437.

Hayes, D.J., & Sader, S.A., 2001. Comparison of change-detection techniques for monitoring tropical forest clearing and vegetation regrowth in a time series. Photogrammetric Engineering & Remote Sensing, 67(9), 1067-1075.

Kawabata, D., & Bandibas, J., 2009. Landslide susceptibility mapping using geological data, a DEM from ASTER images and an Artificial Neural Network (ANN). Geomorphology, 113, 97–109.

Lira, J., & Maletti., G., 2002. A supervised contextual classifier based on a region-growth algorithm. Computers and Geosciences, 28, 951-959.

Netek, R., Pohankova, T., Bittner, O., & Urban, D., 2023. Geospatial analysis in web browsers - Comparison study on WebGIS process-based applications. ISPRS Int. J. Geo-Inf., 2023, 12, 374.

Open Geospatial Consortium, 2019a. Web Map Service. http://www.opengeospatial.org/wms. Accessed 10 September 2019.

Open Geospatial Consortium, 2019b. Web Processing Service. http://www.opengeospatial.org/wps. Accessed 10 September 2019.

Rai, A.K., Mandal, N., Singh, A., & Singh, K.K., 2020. Landsat 8 OLI satellite image classification using convolutional neural network. International Conference on Computational Intelligence and Data Science (ICCIDS 2019), Procedia Computer Science, 167, 987–993.

Singh, A., 1986. Change detection in the tropical forest environment of northeastern India using Landsat. In: M.J. Eden & J.T. Parry (Eds.), Remote Sensing and Tropical Land Management. John Wiley & Sons, London, pp. 237-254.

Singh, A., 1989. Review Article: Digital change detection techniques using remotely-sensed data. International Journal of Remote Sensing, 10(6), 989-1003.

Tripathi, A.K., Agrawal, S., & Gupta, R.D., 2019. WPS enabled SDI: An open source approach to provide geoprocessing in web environment. ISPRS Annals of the Photogrammetry, Remote Sensing and Spatial Information Sciences Volume IV-5/W2, 2019.

Landslide mapping and susceptibility analysis for the determination of Early Warning System (EWS) installation location in Taman Eko-Rimba Chemerong (TER), Dungun, Malaysia

Pemetaan inventori tanah runtuh dan analisis kerentanan bagi penentuan lokasi pemasangan alat Sistem Amaran Awal (EWS) di Taman Eko-Rimba Chemerong (TER), Dungun, Malaysia

Ahmad Nor Zaimie Roslan[1,*], Ferdaus Ahmad[1], Farouk Md Aripin[2], Muhammad Afiq Ariff Mohd Hellmy[2], Wan Salmi Wan Harun[1], Mazlan Mohamad Zain[1], Habibah Tahir[1]

[1]Jabatan Mineral dan Geosains Malaysia, Terengganu
[2]Geomapping Technology Sdn Bhd (GMT)
*Email: zaimie@jmg.gov.my

Abstract: Taman Eko-Rimba Chemerong (TER) is situated in Dungun District, Terengganu, Malaysia, and serves as a prominent ecotourism destination that attracts a substantial number of visitors each year. In light of the frequent geological disaster events, such as debris flows and water surges in the region, this landslide mapping initiative aims to enhance the effectiveness of geological disaster management strategies. Geological disasters can have detrimental effects on both the environment and the socio-economic conditions of a country, often leading to loss of life and significant property damage. This study was undertaken to map landslide occurrences within the Chemerong River watershed, assessing their susceptibility and hazard levels to identify optimal locations for the installation of an Early Warning System (EWS). A total of 82 landslide events were identified and inventoried, classified based on attributes such as type, depth, distribution, pattern, and physical condition. The findings from this inventory were employed as input for the Analytic Hierarchy Process (AHP) model, which facilitated the generation of a landslide susceptibility map. The AHP model yielded an Area Under Curve (AUC) value of 78%, demonstrating satisfactory accuracy in forecasting landslide occurrences. Further analysis involved the use of Rapid Mass Movement Simulation (RAMMS) to develop a geological disaster management map. Two potential sites for EWS installation were identified as a result of this study. It is recommended that early mitigation measures be implemented to mitigate the impacts of disasters in high-risk areas.

Keywords: Landslide, debris flow, Analytic Hierarchy Process (AHP), Geographic Information System (GIS), geological disaster management, simulation, Rapid Mass Movement Simulation (RAMMS)

Abstrak: Taman Eko-Rimba Chemerong (TER) terletak di Daerah Dungun, Terengganu, Malaysia, dan merupakan destinasi ekopelancongan yang menarik sejumlah besar pengunjung setiap tahun. Memandangkan kejadian bencana geologi yang kerap, seperti aliran puing dan kepala air di kawasan ini, inisiatif pemetaan tanah runtuh ini bertujuan untuk meningkatkan keberkesanan strategi pengurusan bencana geologi. Bencana geologi boleh memberi kesan buruk terhadap alam sekitar dan keadaan sosioekonomi sesebuah negara, seringkali mengakibatkan kehilangan nyawa dan kerosakan harta benda yang ketara. Kajian ini dijalankan untuk memetakan kejadian tanah runtuh dalam kawasan tadahan Sungai Chemerong, menilai kerentanan dan tahap bahaya bagi mengenal pasti lokasi yang optimum untuk pemasangan Sistem Amaran Awal (EWS). Sebanyak 82 kejadian tanah runtuh telah dikenal pasti dan diinventori, ia diklasifikasikan berdasarkan ciri-ciri seperti jenis, kedalaman, taburan, corak, dan keadaan fizikal tanah runtuh. Penemuan dari inventori ini digunakan sebagai input untuk model Analisis Hierarki Beranalitik (AHP), yang memudahkan penghasilan peta kerentanan tanah runtuh. Model AHP menunjukkan nilai *Area Under Curve* (AUC) sebanyak 78%, yang membuktikan ketepatan yang memuaskan dalam meramal kejadian tanah runtuh. Analisis lanjut melibatkan penggunaan *Rapid Mass Movement Simulation* (RAMMS) untuk membangunkan peta pengurusan bencana geologi. Dua lokasi berpotensi untuk pemasangan EWS dikenalpasti hasil daripada kajian ini. Pihak berkuasa perlu merangka langkah-langkah mitigasi awal untuk dilaksanakan bagi mengurangkan impak bencana di kawasan berisiko tinggi.

Kata kunci: Tanah runtuh, aliran puing, Analisis Hierarki Beranalitik (AHP), Sistem Maklumat Geografi (GIS), pengurusan bencana geologi, simulasi, *Rapid Mass Movement Simulation* (RAMMS)

INTRODUCTION

Landslide hazards

Landslides are natural hazard that involves the movement of rock, debris, or earth down a slope due to gravity. These phenomena are triggered by a variety of factors, including heavy rainfall, seismic activity, volcanic eruptions, and human activities (Varnes, 1978). Landslides can result in catastrophic consequences, including loss of life, destruction of property, and environmental degradation, making them a significant concern in mountainous and hilly regions. Human activities, such as deforestation, mining, road construction, and improper land use, can exacerbate the risk of landslides by destabilizing slopes and reducing natural vegetation cover, which plays a critical role in slope stability (Glade, 2003).

Landslides cause significant economic losses, environmental damage, and human fatalities globally. According to the United Nations Office for Disaster Risk Reduction (UNDRR, 2019), landslides affect an average of 4.8 million people each year, with significant impacts in regions with rugged terrain and heavy rainfall. The frequency and severity of landslides are expected to increase due to climate change, which leads to more intense and unpredictable weather patterns, particularly in tropical and subtropical regions (Froude & Petley, 2018).

Malaysia, situated in a tropical climate zone, is particularly vulnerable to landslides, especially during the monsoon season when heavy rainfall saturates the soil, weakening slopes and leading to slope failure (Pradhan & Lee, 2010). The combination of steep topography, dense vegetation, and significant annual rainfall makes areas like Taman Eko-Rimba Chemerong (TER) prone to frequent landslides. Landslides in Malaysia have caused substantial damage to infrastructure, disrupted transportation, and posed serious threats to public safety, especially in mountainous and hilly areas (Chowdhury & Flentje, 2007). Figure 1 show the landslide classification illustration based on (Cruden & Varnes, 1996), modified by the British Geological Society. In order to mitigate landslide-related risks, there is a critical need for accurate landslide susceptibility mapping and the implementation of an Early Warning System (EWS).

Early Warning System (EWS)

An Early Warning System (EWS) is designed to detect the likelihood of natural hazards like landslides, allowing authorities and individuals to take preventive action before a disaster strikes. A well-functioning EWS includes four main components: risk knowledge, monitoring and forecasting, dissemination of alerts, and response capacity (UNISDR, 2009). EWS installations in landslide-prone areas are crucial for reducing the loss of life and minimizing damage. Effective EWS requires accurate hazard mapping and vulnerability assessments, which help in identifying optimal locations for the system's installation.

In regions prone to landslides, such as TER, an effective EWS involves real-time monitoring of rainfall, soil moisture, and slope movements to assess the stability of the terrain. A range of technologies can be utilized, including remote sensing, in-situ sensors, GPS systems, and hydrological models, which together provide comprehensive data for hazard assessment (Nadim *et al*., 2006). However, the success of EWS depends on accurate hazard mapping and susceptibility analysis, which identify high-risk areas where warning systems should be strategically placed (Guzzetti *et al*., 2005).

In Malaysia, various initiatives have been undertaken to install EWS in landslide-prone areas, particularly in urban and tourist zones. For example, EWS installed in the Cameron Highlands has proven effective in reducing landslide risks by monitoring weather conditions and providing early warnings to the public and authorities (Puja & Haigh, 2012). The findings from this research on TER aim to further contribute to such initiatives by identifying optimal locations for EWS installations based on landslide susceptibility analysis. Figure 2 shows example of EWS that was installed at one of the TER in Malaysia.

METHODOLOGY

Study area

The study area, Taman Eko Rimba (TER) Chemerong, is located within the Pasir Raja Forest Reserve in the district of Dungun, Terengganu. Taman Eko Rimba (TER) Chemerong covers an area of 292 hectares and is situated approximately 30 km from Bandar Al-Muktafi Billah Shah and 100 km from Kuala Terengganu. With an elevation of over 1000 meters above sea level, TER Chemerong is also well-known as a popular recreational hiking spot, featuring a trail known as the Chemerong Berembun Langsir (CBL) trail. Figure 3 shows the location of the study area and the Chemerong Waterfall. The terrain is characterized by steep slopes and dense forest cover, with significant rainfall throughout the year, particularly during the monsoon season. The area's topography, coupled with high rainfall, makes it susceptible to landslides. Several rivers traverse the region, contributing to the area's vulnerability to both surface and deep-seated landslides.

Landslide inventory mapping

Landslide inventory mapping is the foundation of susceptibility analysis. A total of 82 landslides were identified through field observations and photogrammetric analysis, with landslide types classified based on the methods of Varnes (1978) and Zaruba & Mencl (1969). Field data were recorded using the proforma (Figure 4) provided by the Department of Minerals and Geosciences Malaysia (JMG), which included information on landslide types, depths, physical conditions, and the extent of failure.

The landslide inventory mapping in the Chemerong River Basin area is presented in the form of a landslide

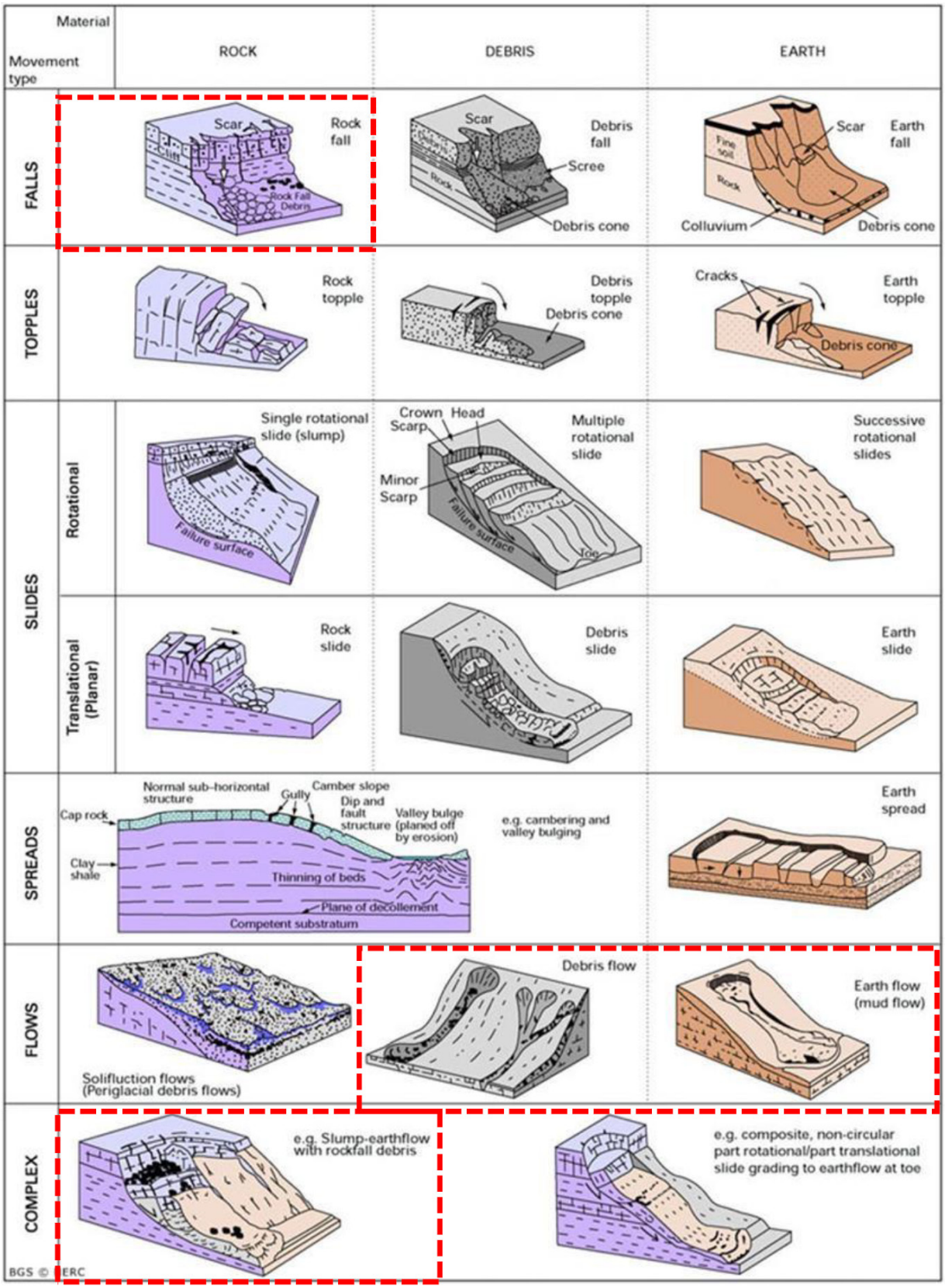

Figure 1: Landslide classification illustration based on (Cruden & Varnes, 1996), modified by the British Geological Society. The most common types of landslides in Malaysia are marked in red lines.

distribution map. This map indicates areas where landslides have occurred within the study area. The following features and elements were recorded during the mapping; 1) Type of landslide, 2) Depth of landslide, 3) Physical condition of the landslide, 4) Distribution of landslides and 5) Pattern of landslide. Table 1,2,3, and 4 show Classification of landslides by depth, physical conditions of landslides, landslide patterns and distribution of landslides.

GIS-based susceptibility analysis

The GIS-based susceptibility analysis involved generating factor maps to represent

Figure 2: Figure shows EWS installed at one of the TER in Malaysia.

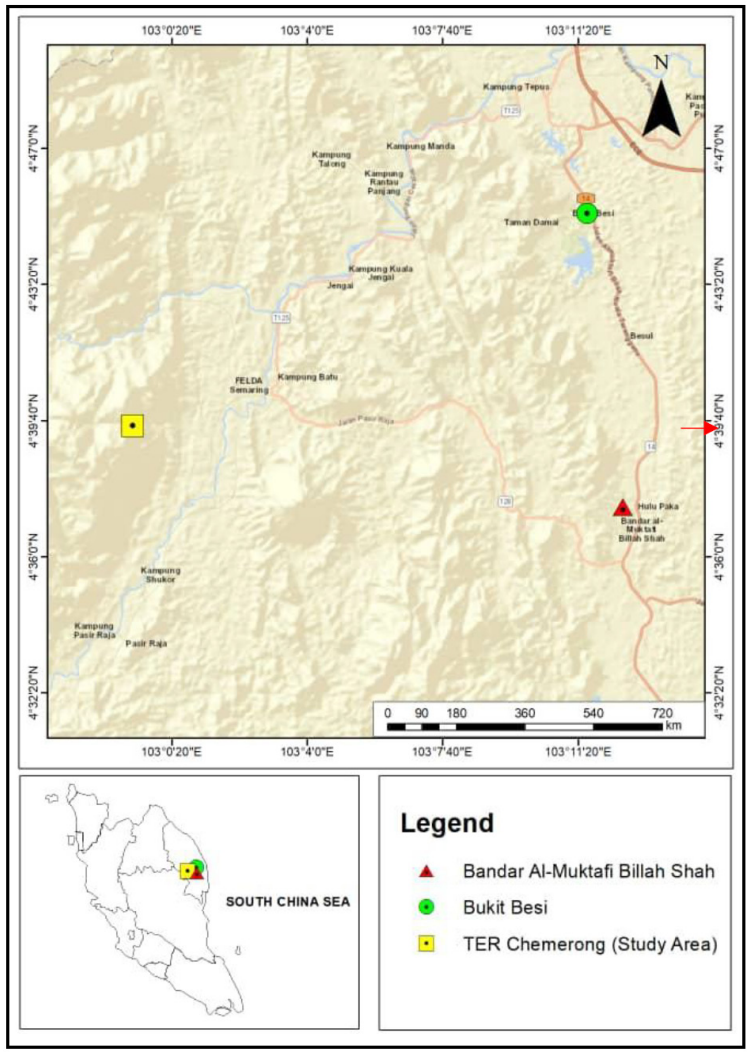

Figure 3: Figure show geological map of Dungun district which show TER Chemerong and the nearest town Bukit Besi and Bandar Al-Muktafi Billah Shah.

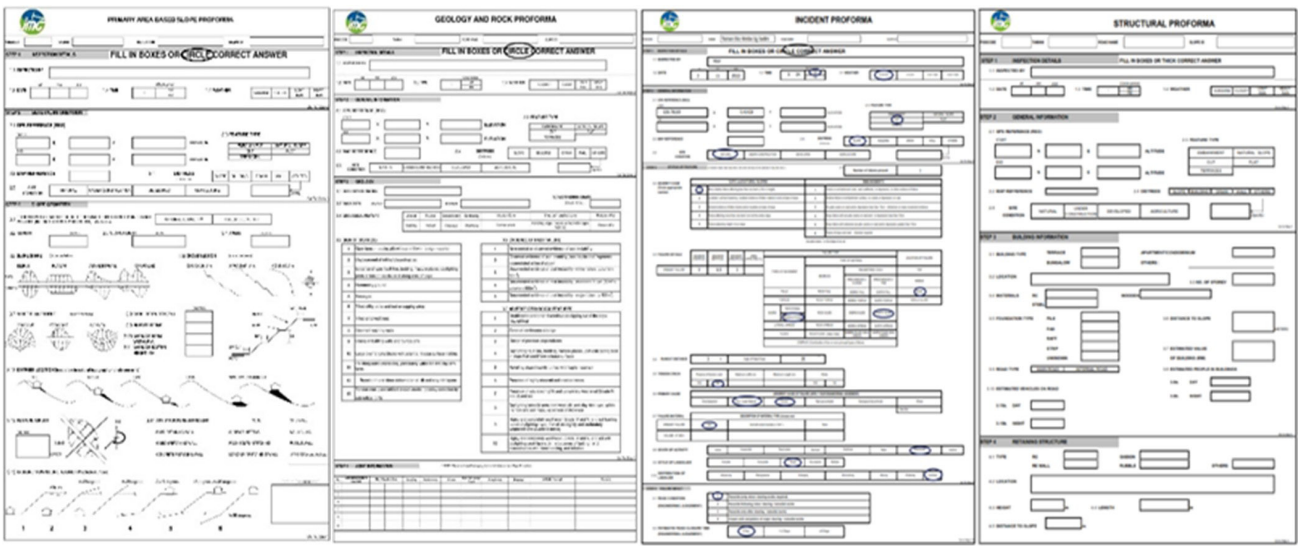

Figure 4: Profoma provided by JMG record all information landslide types, depths, physical conditions, and the extent of failure.

Table 1 : Classification of landslides by depth (modified from Broms & Wong, 1991, and Zaruba & Mencl, 1969).

Landslide Type	Maximum Depth (m)
Surface sliding	<1.5
Shallow sliding	1.5 to 5.0
Deep sliding	5.0 to 20.0
Very deep sliding	>20.0

Table 2: Physical conditions of landslides.

Physical Condition	Description
Active	The landslide is currently moving.
Suspended	The landslide moved within the last 12 months but is not currently active.
Reactivated	A previously active landslide that has become active again.
Inactive	The landslide has not moved in the last 12 months and can be categorized into Dormant, Abandoned, Stabilized, and Relict conditions.

Table 3: Landslide patterns.

Pattern	Description
Complex	Shows at least two types of movements (falling, sliding, spreading, and flowing) in sequence.
Composite	Displays at least two types of movements occurring simultaneously.
Successive	Similar to earlier landslides nearby but does not share the same displaced material or rupture surface.
Single	Displays one single movement of displaced material.
Multiple	Shows repetition of the same type of movement.

Table 4: Distribution of landslides.

Distribution	Description
Forward	The rupture surface expands in the same direction as the movement.
Retrogressive	The rupture surface expands opposite to the direction of displaced material.
Expanding	The rupture surface expands in two or more different directions.
Constricting	The volume of displaced material decreases.
Confined	There is a cliff, but no visible rupture surface at the base of the displaced mass.
Moving	The displaced material continues to move without any visible change in the rupture surface or the volume of displaced material.
Widening	The rupture surface expands on one or both sides of the landslide.

various environmental conditions influencing landslides. Eleven factors were considered in this study:

1. Geology – reflecting soil and rock composition
2. Geomorphology – describing surface features and landscape form
3. Hydrology – highlighting areas with water influence
4. Lithology – depicting rock types and their durability
5. Lineament density – showing the concentration of structural features
6. Distance to lineaments – measuring proximity to faults or fracture
7. Slope curvature (plan and profile) – representing slope geometry
8. Slope steepness – evaluating slope angles
9. Terrain Roughness Index (TRI) – indicating surface variability
10. Elevation – highlighting changes in altitude
11. Terrain Wetness Index (TWI) – represents moisture levels

These factors were assigned weights using the Analytical Hierarchy Process (AHP), a multi-criteria decision-making method that assigns relative importance to each factor

(Saaty, 2008). Each factor was rated on a scale from 1 to 9, where 1 represents equal importance and 9 represents extreme importance as shown in Table 5.

Photogrammetry and remote sensing

High-resolution aerial images were used to complement field data, particularly for areas that were inaccessible. These images were analyzed to identify landslide-prone areas that were previously undetected in the field. Landslide polygons were created and overlaid onto the GIS platform for further analysis.

Determination of EWS locations

Based on the results of the susceptibility analysis, zones with high and very high landslide susceptibility were identified as priority areas for EWS installation. These areas were further examined for their proximity to human settlements, roads, and critical infrastructure, as these factors determine the need for early warnings in terms of protecting lives and properties.

RESULTS AND DISCUSSION

Landslide inventory and distribution

A total of 82 landslides were mapped within the study area. Most of the landslides were classified as translational or rotational types, with varying dimensions and depths. A significant number of landslides were observed near riverbanks and hiking trails, where slope failure often results in debris flow into rivers, potentially creating natural dams. Figure 5 shows the distribution of landslides, with most occurring in the northern and southern parts of the catchment area. The inventory mapping revealed that landslides in these regions are primarily triggered by heavy rainfall and riverbank erosion.

Susceptibility analysis

The landslide susceptibility map produced from the AHP analysis (Figure 6) indicates that approximately 40% of the study area falls under high or very high susceptibility zones. These zones are concentrated in areas with steep slopes, high rainfall, and proximity to rivers, confirming the findings from the field observations. The Terrain Wetness Index (TWI) and lineament density were the most influential factors in determining landslide susceptibility, with TWI showing the highest weight (0.14). Table 6 shows the weighted values for each factor.

The high accuracy of the susceptibility map suggests that it can be used effectively to predict future landslide events and guide mitigation efforts.

Determining EWS installation locations

Based on susceptibility analysis, areas near rivers, steep slopes, and hiking trails were identified as priority zones for EWS installation. The high-susceptibility zones correspond to locations with frequent human activity, such as hiking routes and recreational spots, making them critical for early warning to prevent potential casualties. Figure 7 shows the proposed EWS installation locations, ensuring that the system covers high-risk areas while being strategically placed for effective monitoring.

Table 5: Point scale for pairwise comparison (Saaty, 2008).

Dominant values	Description	Explanation
1	Equal importance	Two factors contribute equally
3	Moderate importance	Activity slightly favours one factor over another
5	High prevalence	Activity highly favours one factor over another
7	Very high prevalence	Activity is very highly favoured over another
9	Extremely high prevalence	Activity is of highest possible degree favoured over another
2, 4, 6, 8	Intermediate values	Used when compromise is needed

Table 6: Weighted values for each factor.

Lithology	0.02
Terrain Roughness Index (TRI)	0.05
Slope Steepness	0.07
Lineament Density	0.13
Distance to River	0.06
Distance to Lineaments	0.11
Terrain Wetness Index (TWI)	0.14
Slope Aspect	0.07
Plan Curvature	0.15
Profile Curvature	0.12
Elevation	0.09

CONCLUSION AND RECOMMENDATIONS

This study provides a comprehensive analysis of landslide susceptibility in Taman Eko-Rimba Chemerong (TER) using GIS-based modeling and field observations. The identification of 82 landslide-prone areas and the creation of a high-resolution susceptibility map highlights the significant risk posed by landslides in this region. The

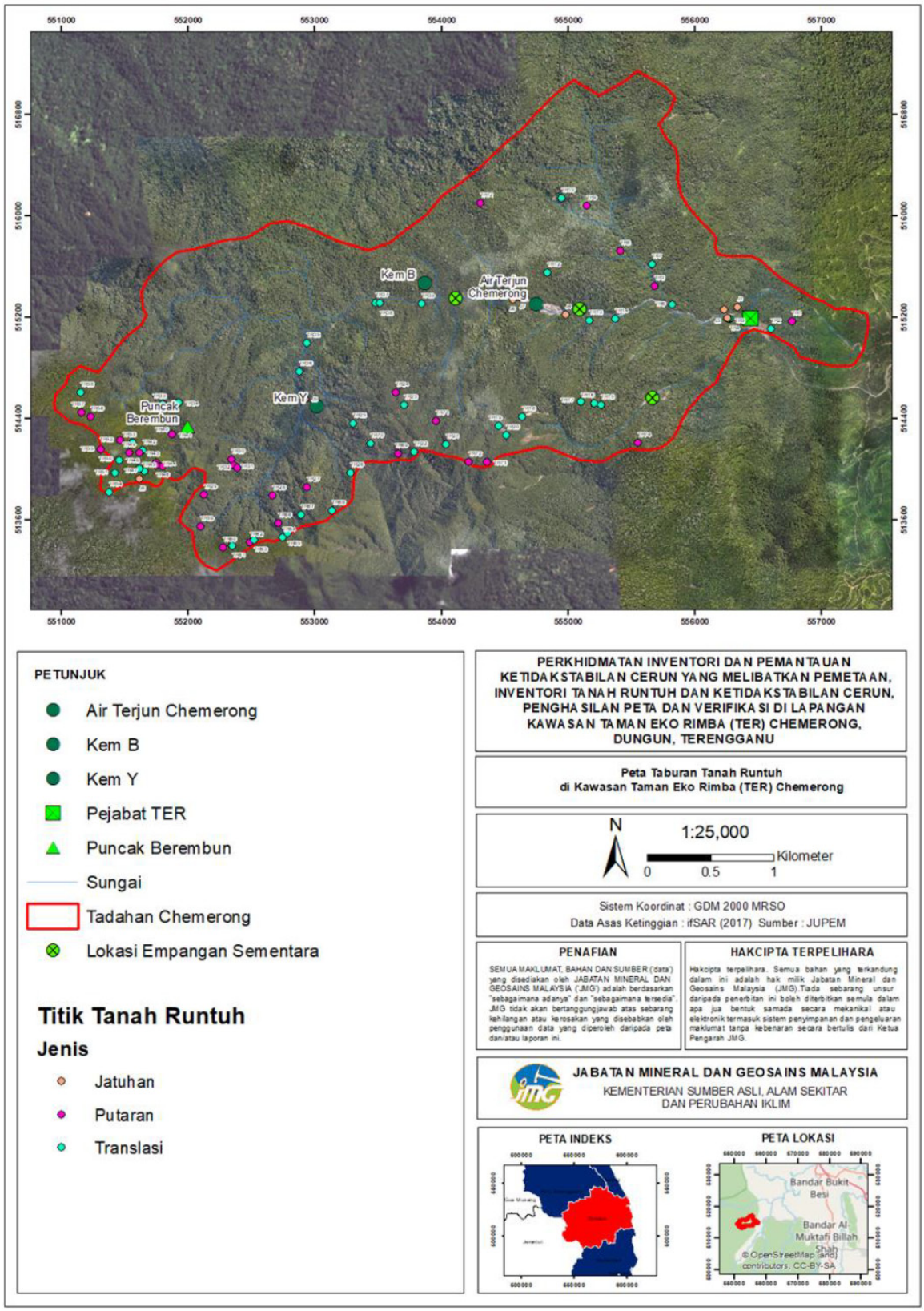

Figure 5: Figure shows the map of landslides distribution at TER Chemerong.

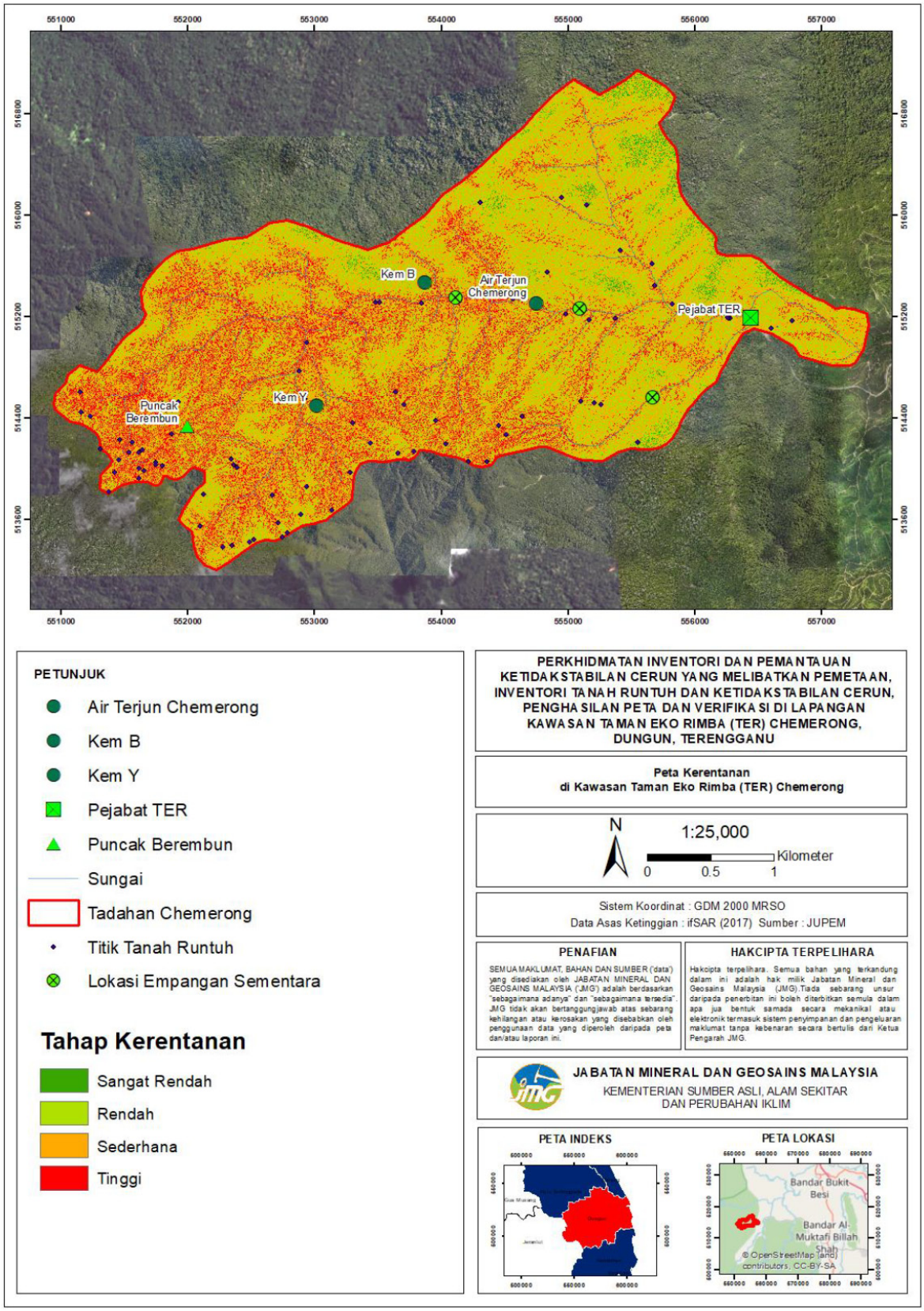

Figure 6: Figure shows Landslide Susceptibility Map in the TER Chemerong Catchment Area.

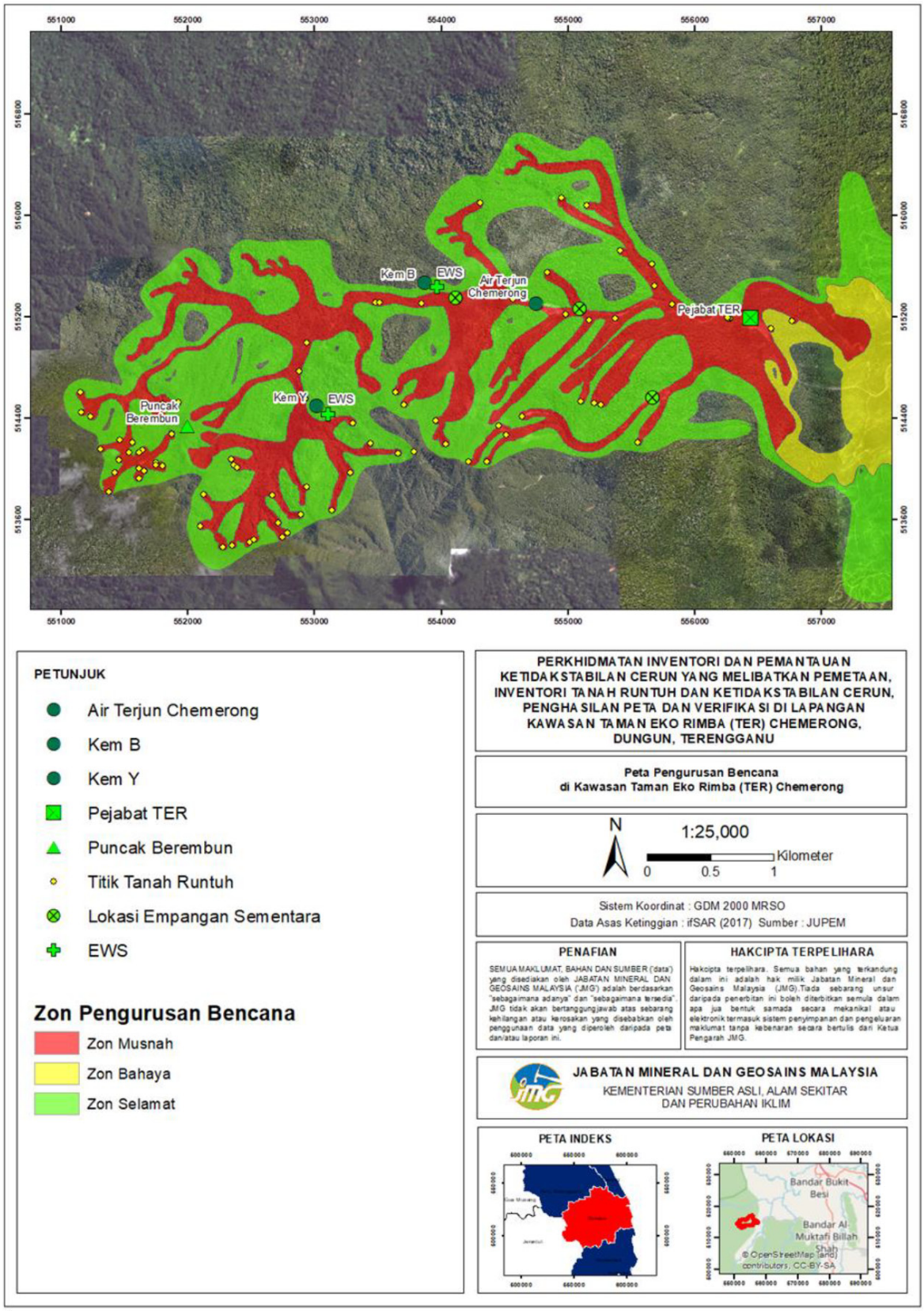

Figure 7: Figure shows two proposed EWS installation location map at TER Chemerong.

use of the AHP method allowed for the systematic weighting of factors influencing landslide occurrences, with TWI and lineament density emerging as key contributors. The study identifies several high-risk zones suitable for the installation of an Early Warning System (EWS), particularly along rivers and hiking trails where human activity is frequent. It is recommended that these areas be prioritized for EWS implementation to minimize risks and improve landslide preparedness.

Future research should focus on improving the accuracy of remote sensing technologies and integrating real-time monitoring systems into EWS for continuous updates on landslide conditions. Collaboration between local authorities, researchers, and stakeholders is crucial to ensure the success of EWS deployment in high-risk areas.

REFERENCES

Broms, B.B., & Wong, K.S., 1991. Landslides. Foundation engineering handbook, Second edition. 410-446.

Chowdhury, R., & Flentje, P., 2007. Geotechnical Slope Analysis. CRC Press.

Cruden, D.M., & Varnes, D.J., 1996. Landslide Types and Processes, Transportation Research Board, U.S. National Academy of Science, Special Report, 247, 36-75. https://www.researchgate.net/publication/269710331.

Froude, M.J., & Petley, D.N., 2018. Global fatal landslide occurrence from 2004 to 2016. Natural Hazards and Earth System Sciences, 18(8), 2161-2181. https://doi.org/10.5194/nhess-18-2161-2018.

Glade, T., 2003. Landslide occurrence as a response to land use change: a review of evidence from New Zealand. CATENA, 51(3-4), 297-314. https://doi.org/10.1016/S0341-8162(02)00170-4.

Guzzetti, F., Reichenbach, P., Cardinali, M., Galli, M., & Ardizzone, F., 2005. Landslide hazard assessment and risk evaluation: Limitations and prospects. Landslides, 2(1), 3-15. https://doi.org/10.1007/s10346-004-0032-y.

Nadim, F., Kjekstad, O., Peduzzi, P., Herold, C., & Jaedicke, C., 2006. Global landslide and avalanche hotspots. Landslides, 3(2), 159-173. https://doi.org/10.1007/s10346-006-0036-1.

Pradhan, B., & Lee, S., 2010. Landslide susceptibility assessment and factor effect analysis: Backpropagation artificial neural networks and their comparison with frequency ratio and logistic regression modelling. Environmental Modelling & Software, 25 (1), 747-759. https://doi.org/10.1016/j.envsoft.2009.10.016.

Puja, P.C., & Haigh, M.J., 2012. Monitoring and mitigation of landslide hazards in tropical mountain environments. International Journal of Landslide and Environment, 5(1), 27-39.

Saaty, T.L., 2008. Decision making with the analytic hierarchy process. International Journal of Services Sciences, 1(1), 83–98.

UNDRR, 2019. Global Assessment Report on Disaster Risk Reduction. United Nations Office for Disaster Risk Reduction.

UNISDR, 2009. Terminology on disaster risk reduction. United Nations International Strategy for Disaster Reduction. https://www.unisdr.org/we/inform/terminology.

Varnes, D.J., 1978. Slope movement types and processes. In R. L. Schuster & R.J. Krizek (Eds.), Landslides: Analysis and control , 11-33. National Research Council.

Zaruba, Q. & Mencl, V., 1969. Landslides and Their Control. Environmental Science, Geology. DOI:10.1016/c2009-0-09618-4.j

Vulnerability analysis of North Bengkalis Beach, Bengkalis Regency, Riau Province

Agus Setyanto[1,*], S.S. Herdadi[1], R. Rahardiawan[1], D. Setiady[1], Irwan H. Suherman[1], W.D. Kirana[2]

[1]Marine Geological Institute of Indonesia, Dr. Junjunan 236 Bandung-40174
[2]Marine Science and Technology Studies, IPB University, IPB Dramaga Bogor Campus, West Java, 16680
*Email: agussetyanto170865@gmail.com

Abstract: Coastal areas have an important role for the people living around them but are prone to damage. Damage to coastal areas requires mitigation efforts so that the impact can be minimized or eliminated. Before carrying out countermeasures, it is necessary to carry out a vulnerability analysis by determining coastal vulnerability. This research was conducted along the north coast of Bengkalis Island which directly borders the Malacca Strait. The coastal vulnerability index is calculated using physical variable values such as changes in coastline, visual observations, length and width of damage, width of green belt, lithology, wave height, tidal distance, land use and beach slope. The data required for research is satellite imagery, hydro oceanography, bathymetry and visual observations of damage. The analysis results show that Tanggang Beach, Teluk Papal Beach, Bantan Air Beach, Teluk Pambang Beach have very high coastal vulnerability. Jangkang Beach has high coastal vulnerability. The area that has moderate coastal vulnerability is Selat Baru Beach which has a low level of vulnerability.

Keywords: Coastal vulnerability, beach identification, Central Bantan District

INTRODUCTION

Coastal areas are transitional areas between terrestrial and marine ecosystems that are influenced by changes on land and at sea (Guntur, 2017). The sea and land areas are limited by the coastline. Changes in the coastline can cause coastal damage and changes in the area of coastal land (Kusumaningtyas, 2020). The coast of North Bengkalis Island which directly faces the Malacca Strait is affected by waves that cause abrasion. In addition, abrasion in this area occurs because several beaches do not have coastal protection (Putra, 2019). The level of damage to the length of the coast reaches ± 40 km, with a critical area length of 11 km and an average abrasion rate of 3-5 meters / year.

This study was conducted along the north coast of Bengkalis Island which directly borders the Malacca Strait. Coastal vulnerability is calculated using physical variable values such as coastal characteristics, visual observations, wave height, and tides. The data needed for the study are bathymetry and visual observations of coastal damage. The results of the analysis show that Bantan Air Beach, Teluk Papal Beach, Mentayan Beach, Selat Baru Beach, Deluk Beach and Jangkang Beach have very high coastal vulnerability. Anjang Beach has high coastal vulnerability. The area with moderate coastal vulnerability is Selat Baru Beach which has a low level of vulnerability.

MATERIALS AND METHODS

Time and place

The research area is located around the Malacca Strait, precisely around the North Bengkalis Waters which are administratively part of the Riau Mainland Province. Geographically located °00 - 1°37'22" North Latitude and 101°26'4" - 102°10'54" (Figure 1). Field survey consists of positioning, geological data collection (coastal characteristics) and oceanographic observations, where this field survey was carried out for 28 days, starting from July 1 to July 28, 2024.

The research area can be reached either by utilizing river transportation from Riau Mainland to North Bengkalis via the Duku River Ferry Port or the Pak Ning River with a crossing frequency of 2 times a day with a travel time of approximately 5 hours. If from Batam, it can be reached in 3.5 hours with a crossing time of 3 to 4 times a day.

Research methods

The research was conducted using a survey method where direct observations were made in the field to obtain primary data including the characteristics of the beach, waves, currents and coastal protection conditions. Observation points were determined using a purposive sampling method which was determined based on the representativeness of the objects studied and ease of access

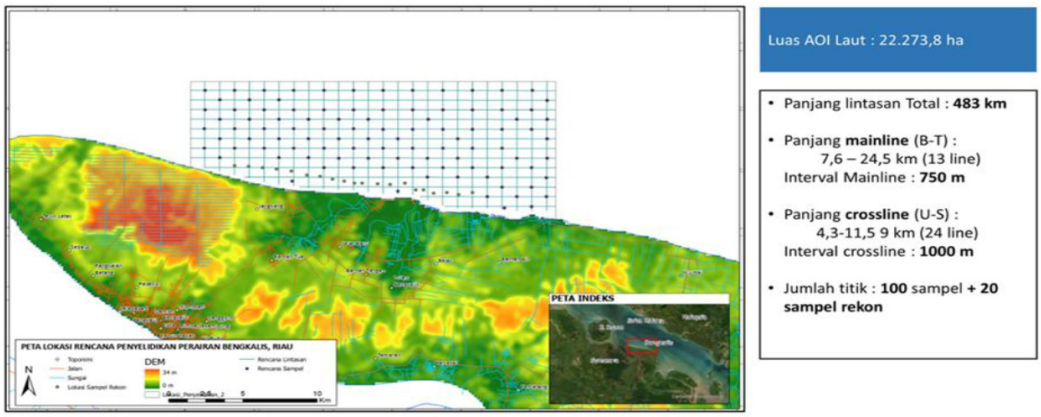

Figure 1: Location of the investigation area.

to the location. Data collection, observations, and recording of important information were carried out at the station. Data were analyzed using a descriptive analysis method through a remote sensing system which was divided into three stages, namely variable data collection, data processing, and abrasion level analysis.

RESEARCH PROCEDURE

Research location

The determination of the research location used a purposive sampling method where the research station was determined based on considerations of the representativeness of the object being studied and ease of access to the research location. There are 11 stations from which primary data will be taken.

Coastal Characteristics

Coastal protection condition

To determine the condition of the coastal protection, visual observation is carried out. Data is recorded whether the existing coastal protection is in good condition, needs repair or there is no coastal protection.

Current speed

Current speed uses secondary data (Figure 6). Wave Height (H) Wave data is measured using a scaled pole to obtain wave height. The steps for collecting wave data are by planting a scaled pole into the waters, then recording the water limit at the time of the trough and peak of the wave during a certain period of time. Data obtained in the field are used to calculate wave height using the formula in the research of Ayunarita *et al*. (2017).

DATA ANALYSIS

Data analysis was carried out using all the data obtained. The processed data was then presented in the form of a map and discussed descriptively based on various references. The analyzed data produced coastal accretion and abrasion values which were classified into 3 categories, namely high abrasion, moderate abrasion and low abrasion. Analysis of the level of abrasion can be known through analysis of coastal characteristic data using ArcGIS 10.4 software where the output data produced is in the form of scale values for each abrasion and accretion.

RESULTS AND DISCUSSION

General conditions of the research area

North Bengkalis Island is one of the sub-districts in Bengkalis Regency, Riau Province. Geographically, this area is located at 0°00 - 1°37’22” North Latitude and 101°26’4” - 102°10’54” East Longitude consisting of 9 villages and 1 sub-district. This area is directly opposite the Strait of Malacca and is adjacent to the Bengkalis Strait. There is marine tourism in the form of mangrove forest ecotourism located on Selat Baru Beach, Bantan District, which is the village that is most influenced by the Strait of Malacca because it is the closest compared to other villages/sub-districts.

Beach characteristics

Beach type

Based on field observations, the characteristics of the beaches in the research area are divided into 2 types, namely (1) Mangrove and muddy beaches (mangroves) and (2) Sandy and muddy beaches (sand beach) where each beach area is shown in the form of photos (Figure 2 and Figure 3).

Coastal abrasion is coastal erosion caused by waves and influenced by the physical conditions of the beach and its environment caused by: damage to the mangrove ecosystem/coastal plants and the characteristics of the coastal land are generally peat and alluvial which are very susceptible to erosion by ocean wave energy, so it is feared that it can cause disasters that have an impact on the lives of the people in the location. Areas that have the potential to be prone to abrasion in Bengkalis Regency are on the northern coast of Bengkalis Island facing the Malacca Strait. Abrasion that occurs in coastal areas of Bengkalis Regency has occurred.

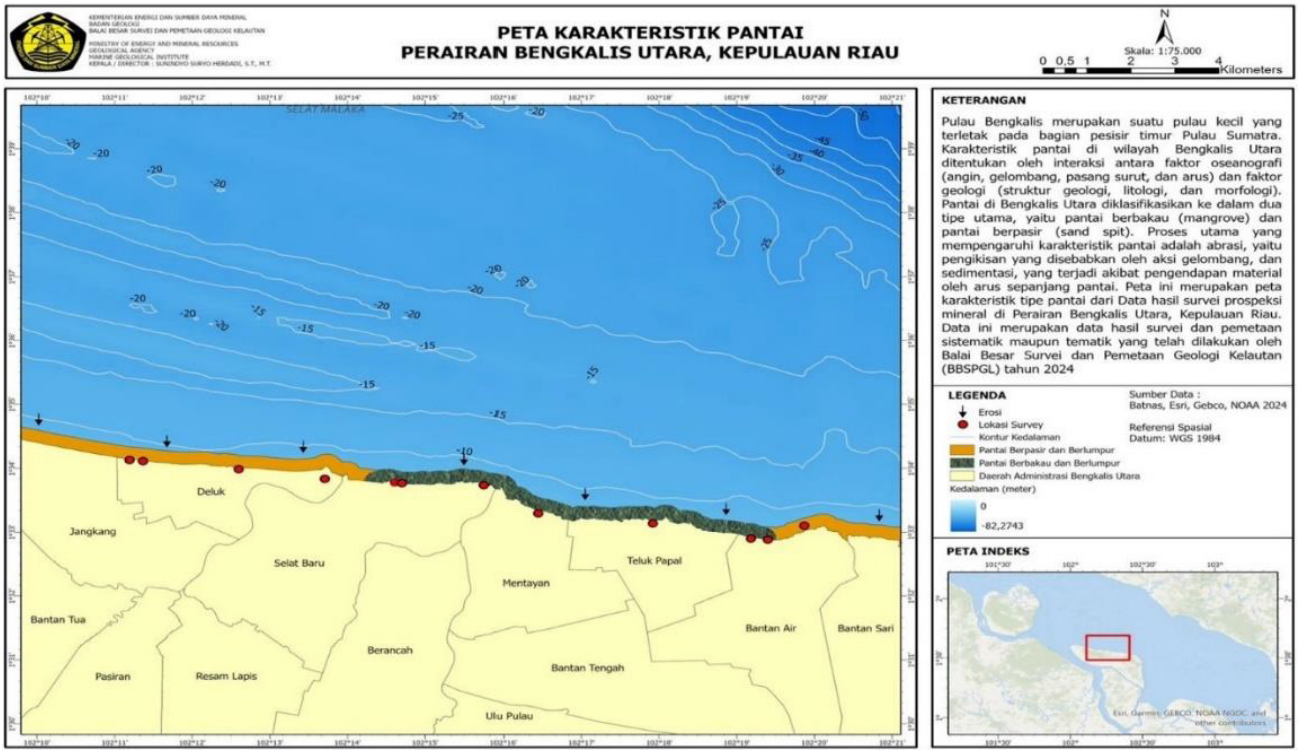

Figure 2: Map of coastal characteristics of North Bengkalis waters, Riau Islands.

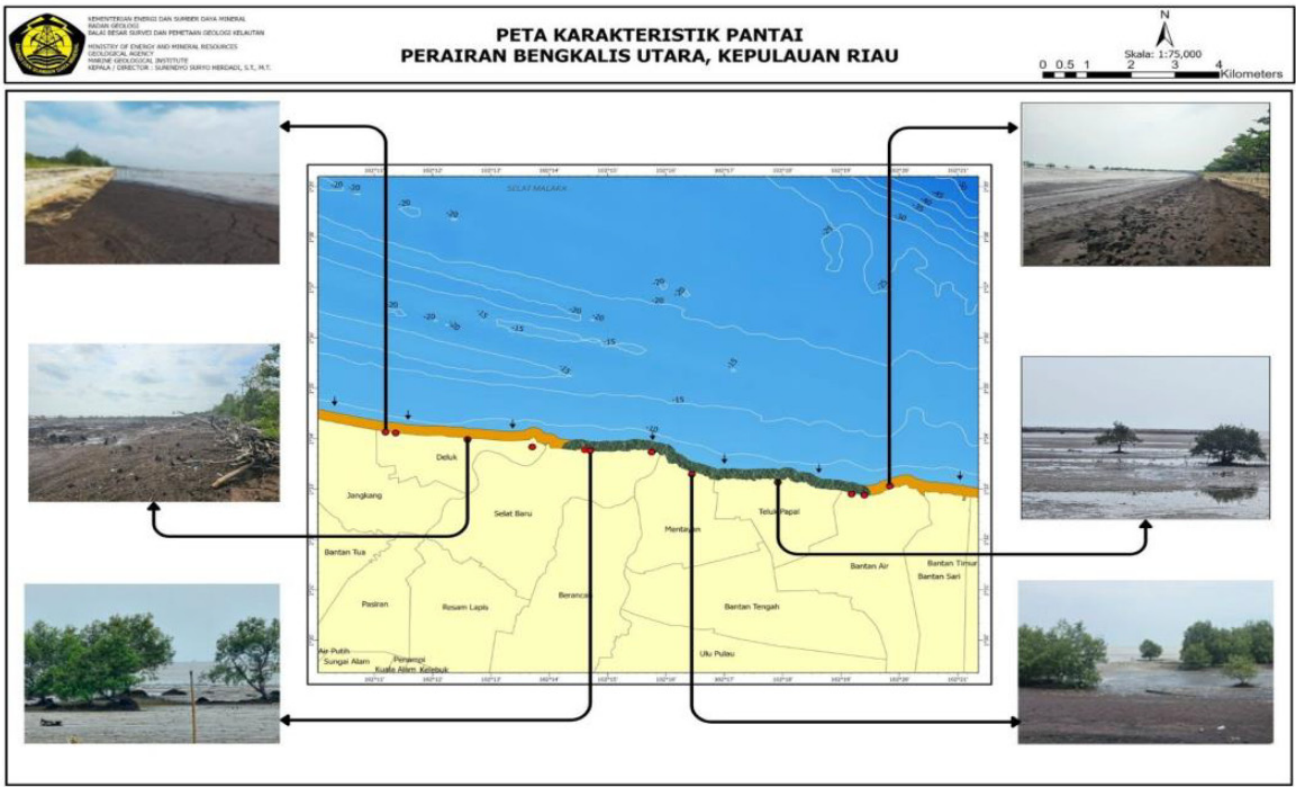

Figure 3: Fanorama of the characteristics of the North Bengkalis coast, Riau Islands.

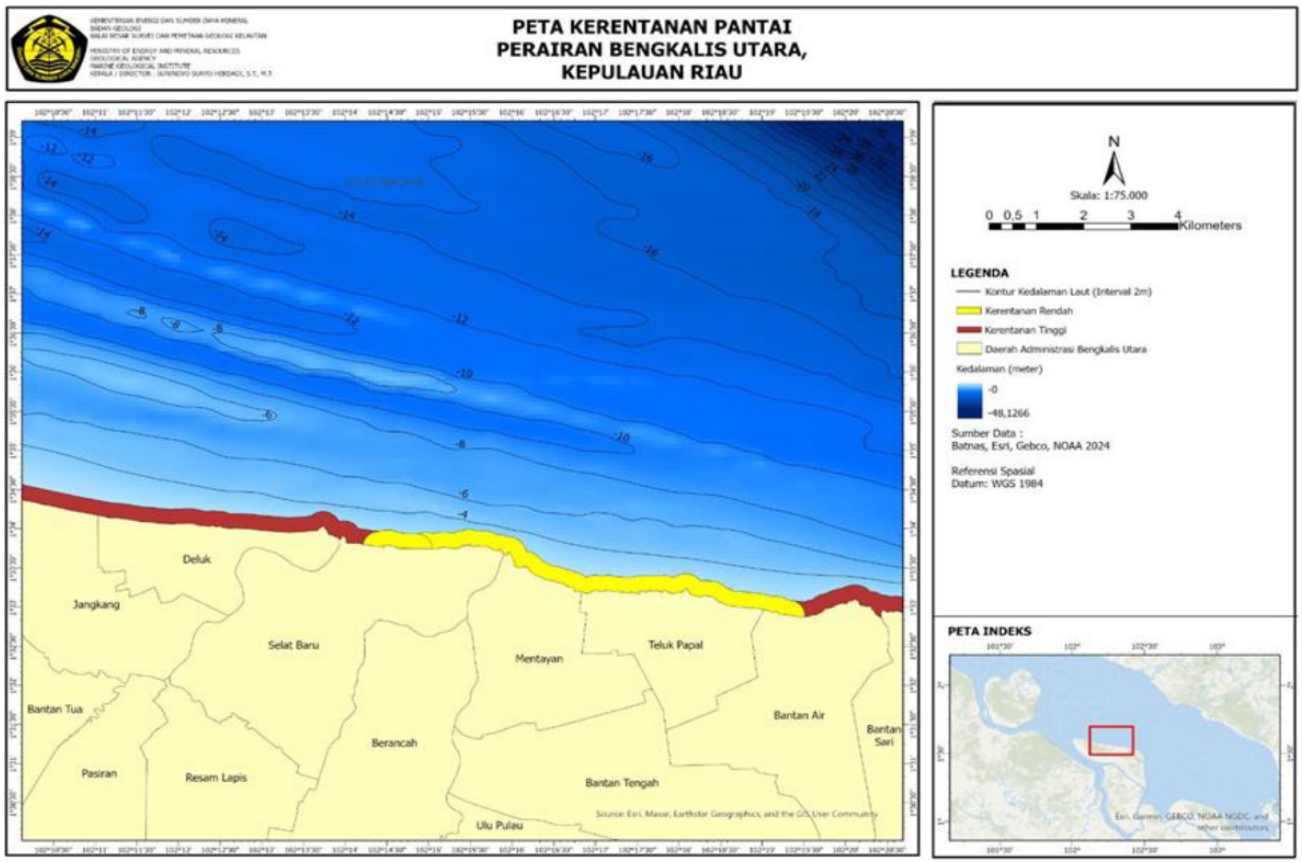

Figure 4: Condition of the beaches in Bantan Air, Teluk Papal Beach, Mentayan, Selat Baru Beach, Deluk Beach and Jangkang Beach.

Since 1988 until now, this means that the events resulting from this natural phenomenon have been going on for 32 years and many residential and plantation areas as well as community land and the coastline have collapsed due to being hit by waves, so that several areas are categorized as critical areas.

The results of the study showed that most of the northern coast of Bengkalis Island experienced abrasion with varying levels of abrasion. The western part of the northern coast of Bengkalis is the coast that experienced the most severe abrasion, while the southern part experienced sedimentation.

The northern coast of Bengkalis Island is characterized by coastal land in the form of peat sand, clay and alluvial which are very susceptible to erosion by sea waves, especially those not protected by mangrove trees. This abrasion tends to continue if no treatment is carried out. The following are the conditions of the coast in the critical abrasion area of the North Bengkalis coast.

There are three types of sea water movements that cause the gradation process on the surface of Bengkalis Regency, namely waves, currents and tides of the Malacca Strait. Wind is the cause of waves, speed, and size of waves. Waves cause erosion and re-deposition in low places and erosion of the base of the Bengkalis coast located above the base of the waves is still felt.

The coast experiences abrasion, accretion (sedimentation) or remains stable depending on the sediment that enters (supply) and leaves the coast. Most coastal problems are excessive abrasion. Coastal abrasion occurs when a beach being reviewed experiences sediment loss/reduction: meaning that the sediment transported is greater than that deposited. Several coastal areas in Bengkalis Regency experienced abrasion. Accretion or sedimentation can also reduce the function of beaches or coastal buildings, such as sedimentation in estuaries that can disrupt river flows and shipping traffic, as well as sedimentation in ports and shipping lanes.

Mangrove condition

The physical function of mangroves in relation to abrasion, has a function as a protector against coastal abrasion. The mangrove root system is very dense like an anchor and can function to soak the onslaught of sea waves. The grip of the roots that are embedded in the soil can also prevent the release of soil particles. Thus, abrasion caused by sea waves can be prevented. Distribution of mangrove forests in Bantan District.

Wave height

East of Bengkalis Regency is able to dampen the strength of the current flowing along the Malacca Strait.

The height of waves caused by wind in the open ocean depends on the strength of the wind, the distance from the wind source and the length of time the wind blows. When waves enter shallow waters and begin to experience friction and bottom resistance waters, the forward movement of the wave is hampered and the wavelength is also reduced, resulting in increased wave height and becoming steeper. At the point where the water depth is 1.3 times the wave height, the wave will break and release energy to the beach. The wave height on the North Coast of Bengkalis Regency depends on the season, usually in the northern season the wave height can reach 3 meters or more. Where the waves will hit the beach along the North Coast of Bengkalis.

Wave pattern of North Bengkalis coastal area

Based on the results of the mathematical model, the wave pattern can be seen in Figure 5 and Figure 6. Overall, the wave conditions in Bengkalis Regency are 3-4 m. The highest wave occurs at time step 234000, with a wave height of 3.4 m. While the lowest wave occurs at time step 3600 with a wave height of 0.5 m. Because of Bengkalis's very strategic location and is greatly influenced by the Malacca Strait, it is certain that the flow of waves in the waters of Bengkalis Beach is greatly influenced by the South China Sea which has a large wave type and from the Indian Ocean which flows through to Java sland.

Current speed and direction

Along the North Coast of Bengkalis and Rangsang Islands, the tidal currents are double daily and follow the path of the beach sandbars and ridges located in front of it. Changing to the east towards the southeast and to the west northwest, each around the quarter tide approximately 3 piantan after the full moon and new moon. The speed ranges from 2 knots - 3 knots, during the dead tide the current is small and the direction is uncertain.

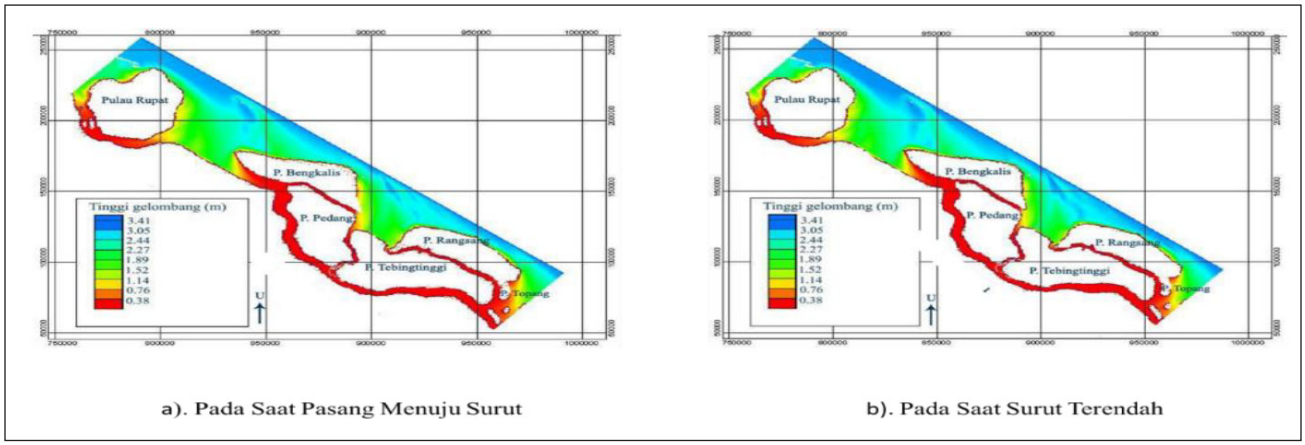

Figure 5: Wave conditions a). When the tide is going to ebb, b). When the lowest ebb.

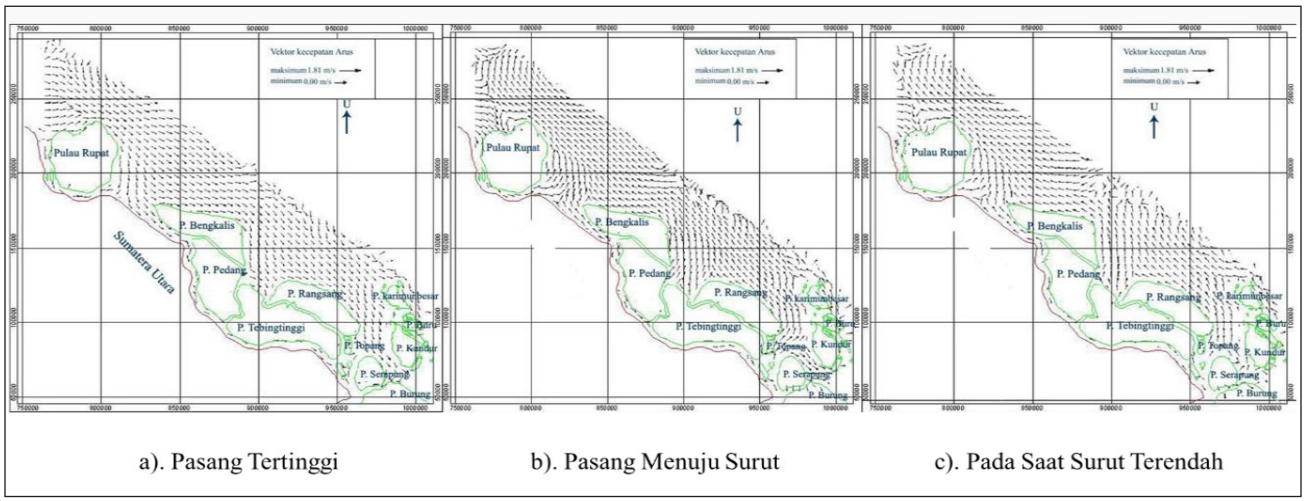

Figure 6: Tidal current conditions a). Highest tide, b). Tide towards low tide, c). At lowest tide.

Table 1: Results of visual condition analysis of coastal damage.

Visual Observation	Point for Damage	Impact in the Field
Bantan Air Beach	There is erosion and landslides which can damage facilities around the beach.	Damage to facilities and infrastructure around the beach.
Papal Bay Beach	There is erosion and landslides which can damage facilities around the beach.	Damage to facilities and infrastructure around the beach.
Mentayan Beach	There is erosion and landslides which can damage facilities around the beach.	Damage to facilities and infrastructure around the beach.
Selat Baru Beach	The coastal area experiences abrasion which can cause damage to the beach	Damage to facilities and infrastructure around the beach
Deluk Beach	There is quite severe abrasion which causes land in the area to decrease.	Land reduction
Jangkang Beach	There is quite severe abrasion and there are many collapses.	This can be dangerous for the activities of residents living around the area and land reduction

Source: Analysis (Setyanto, drr., 2024)

The current speed during the northern season in the North Coast area of Bengkalis Regency ranges from 3 - 8 knots. The maximum current speed value is 4.11 m / sec and the minimum current speed is 1.54 m / sec. The tidal conditions in Bengkalis Regency greatly affect the sea level which results in tidal currents. The tidal currents in Bengkalis are very dominant, this occurs because of the geographical location of Bengkalis which consists of large and small islands and has many rivers. Although the influence of wind can also result in currents in the sea.

The characteristics of the current in Bengkalis Regency can be seen in the image (Figure 6), where the field conditions of the maximum current speed in Bengkalis Regency range from 1.8 - 3.6 m / s. Where at the highest tide conditions the current flows from the Southeast to the Northwest through the small islands in the east of Bengkalis Regency, and in the opposite condition the current in the lowest ebb conditions combs along the large and small islands along Bengkalis Regency.

The islands in Bengkalis Regency along the east coast of Sumatra, namely Rupat Island, Bengkalis, Padang, Merbau, Tebing Tinggi, Rangsang and the small islands around them have almost the same physical oceanographic conditions. Which have mixed tidal current conditions tending to double daily. The current flows following the path of the coastal sandbar and the ridges located in front of it.

The condition of the coastal protection in Bantan District or North Bengkalis waters consists of mangrove and groin types with good conditions and need improvement. According to Jadidi *et al.* (2013), coastal protection is categorized into 3 classes, namely good, needs improvement, and does not have coastal protection. Based on visual observations in the field, the coastal protection in Bantan District, North Bengkalis waters consists of a good category and most of it needs improvement. The north coast of Bengkalis is protected by mangrove plants and groins. This is in accordance with research by Putra (2019), one of the areas experiencing abrasion in Bantan District is due to the lack of coastal protection. Based on research conducted by Purwanto *et al*. (2020), people living on the coast of Bantan District and its surroundings carry out illegal logging of mangroves which are then used as house foundation materials, raw materials for charcoal and so on. It is suspected that the reduction in mangrove plants and the remaining vegetation, most of which has been damaged, can worsen coastal damage because there are no barriers to currents and waves that occur continuously. Bantan District has a sloping coast, predominantly muddy, and there are several river estuaries. The muddy type is relatively easy to change and abrade. This is in accordance with research by Sibarani *et al*. (2019), the most dominant type of sediment fraction in Bantan District and its surroundings consists of sandy mud, while fine particles (mud) are carried by currents at relatively high speeds. Dianawati & Santosa (2016) stated that beaches with fine particles have a high level of resistance to coastal abrasion, while large particles (sand) are an important factor in the abrasion process.

CONCLUSION

The level of abrasion on the coast of North Bengkalis, Bantan District is dominated by moderate abrasion with a percentage of 35.54%, high abrasion of 27.74%, and low abrasion of 15.02%. Other changes include accretion of 8.12% and there are areas that do not experience significant changes or are in stable conditions, namely 13.58%. Waves in several areas experiencing accretion are constructive so that they tend to deposit beach material. The main factor causing abrasion on the coast of North Bengkalis, Bantan District is thought to be due to the lack of coastal protection. Although the wave height in the waters of this area is relatively low, coasts that do not have protection or coastal vegetation can experience abrasion because there are no wave dampers that occur continuously which are destructive. Destructive waves gradually sweep the coast and carry sediment particles offshore, causing abrasion. The areas affected by abrasion have currents in the moderate and fast categories and coastal protection in the form of mangroves, most of which have been damaged so that they require repair.

SUGGESTION

Based on this study, it is suspected that the main factor causing abrasion on the coast of North Bengkalis is the lack of coastal protection in several villages/sub-districts, so it is recommended for further research to analyze the condition of coastal protection and the efforts that need to be made to minimize abrasion and other supporting parameters can be added related to the analysis of the level of abrasion in coastal areas such as wind data, sediment transport, anthropogenic activities and so on so that the research results obtained are more complex.

REFERENCE

Ayunarita, S., Elizal, & M. Ghalib, 2017. Study of Current, Tidal and Wave Patterns in the Waters of Pelawan Beach, Pangke Village, Meral District, Karimun Regency, Riau Islands Province. Riau University, Pekanbaru.

Dianawati, R., & L.W. Santosa, 2016. Study of Coastal Erosion in the Muarareja Coastal Area, Tegal City, Central Java. Indonesian Earth Journal, 5(2), 4.

Guntur, M., 2017. Institutional Study of Coastal Area Management of Kiluan Bay, Lampung Province as a Tourism Area. Bogor Agricultural University, Bogor.

Jadidi, A., M.A. Mostafavi., Y. Bédard., B. Long, & E. Grenier, 2013. Using Geospatial Business Intelligence Paradigm to Design a Multidimensional Conceptual Model for Efficient Coastal Erosion Risk Assessment. Journal of Coastal Conservation, 14(1), 527-543.

Kusumaningtyas, A.I., 2020. Analysis of Coastline Changes and Evaluation of Coastal Land Use Area in Brondong District, Lamongan Regency, East Java. UIN Sunan Ampel, Surabaya.

Purwanto, W., D.M. Haryanto, & R.I. Priyambada, 2020. Study of Abration Management in Pangkalan Jambi Village, Bengkalis District. 2020 National Disaster Management Seminar, Bengkalis.

Setyanto, drr, 2024. Mineral Prospecting Report of North Bengkalis Waters, Riau Islands. Unpublished.

Sibarani, U.D., Siregar, Y.I., & Galib, M., 2019. Organic Material Content of Sediment and Abundance of Macrozoobenthos in Pakning River Waters, Bengkalis Regency. University of Riau, Pekanbaru.

Carbon sink potential in Mempawah peatland: A preliminary study

Muhammad Arief Pinandita, Fatimah*, Sigit Arso Wibisono,
Hans Elmaury Andreas Siregar, Sandi Rukhimat

Center for Mineral, Coal and Geothermal Resources – Geological Agency of Indonesia
* Email: fatimah@esdm.go.id

Abstract: Indonesia has quite extensive peatlands, especially in Sumatra and Kalimantan islands. As a coal precursor, peat has sufficient carbon content which makes it flammable. Peatland fires result in the release of greenhouse gases into the atmosphere. However, peatlands also have significant carbon sink. Peatlands store vast amounts of carbon dioxide in their waterlogged soils. Protecting and restoring peatlands is essential for achieving net zero emission, as they help carbon emission and support biodiversity. Apart from being a source of greenhouse gas emissions, peat can also become a place for carbon storage or carbon sink. These carbon repositories give significant impact to the environment and also can be an important part mitigating climate change.

The objective of this study is to identify the potential carbon sink in the peatland area in Mempawah Regency, West Kalimantan Province. Field activities in the form of geological mapping and drilling, as well as geophysical surveys using the Ground Penetrating Radar (GPR) method, were carried out to determine the area of peatland distribution and its thickness. Several laboratory analyses were carried out to determine the properties of Mempawah peat deposits, among others is carbon content.

Drilling was carried out on 2 km grid using Fikelkarp Auger. Interpretation from 50 boreholes indicates that peat deposit thickness ranges from 0 up to 9 meters. GPR measurements confirmed similar peat thickness. GPR result also shows that there are geological structures that affected rock formation beneath peat deposit.

There are 2 types of peat in the study area, namely fibric (fiber content > 67%) and hemic (fiber content 33 – 67%). The average carbon content is 63.05%, whilst the Total Organic Carbon content ranges from 45.09% up to 58.37%. The peatland in the study area covers a 15,076 hectares of peatland area. The estimated potential for carbon sink in the study area is 44.36 up to 57.42 million tons. It is such a great opportunity to turn peatland into carbon trading commodity by offering carbon credit. Further in-depth study is needed for better carbon quantification.

Keywords: carbon sink, Mempawah peatland, carbon content, total organic carbon, carbon credit

INTRODUCTION

Peatlands are unique ecosystems formed by the accumulation of partially decomposed plant material in waterlogged conditions. They play a crucial role in the carbon cycle by acting as both carbon sinks and sources (Harenda *et al.*, 2018). They are formed when organic matter accumulates faster than it decomposes in waterlogged conditions, creating a unique environment where carbon is stored for long periods (Figure 1). Peatlands play a vital role in mitigating climate change by acting as natural carbon sinks. This means they absorb and store carbon dioxide, one of the primary greenhouse gases responsible for global warming.

Indonesia has quite extensive peatlands, especially in Sumatra and Kalimantan islands (Figure 2). This peatland has the potential to be a carbon sink that helping to mitigate climate change. However, currently there is no detailed data on how much carbon is stored in Indonesia's peatlands. The objective of this study is to identify the potential carbon sink in the peatland area in Mempawah Regency, West Kalimantan Province. Mempawah peatland is one of the many Indonesian peatlands located on the tip of the western part of Kalimantan Island (Figure 3).

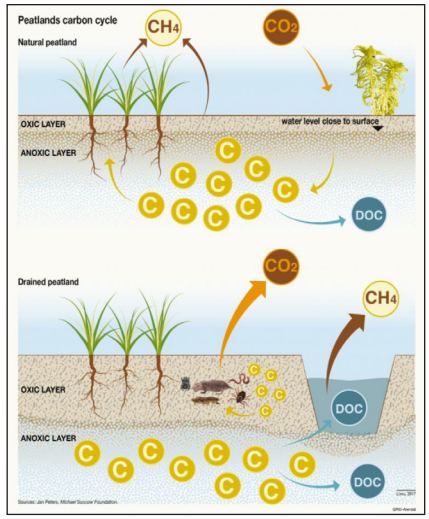

Figure 1: Peatland carbon cycle (GRID-Arendal).

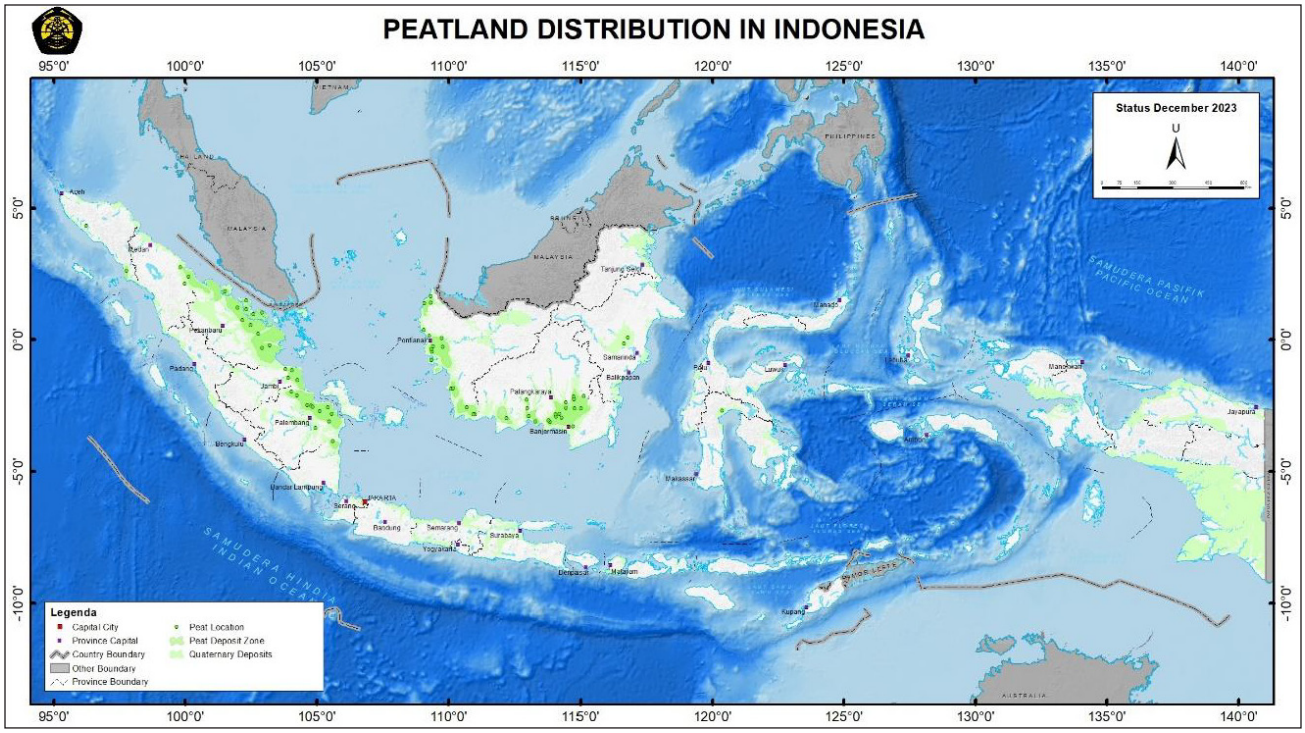

Figure 2: Peatland distribution map in Indonesia published by the Geological Agency of Indonesia. Note that peatland areas (green color) are distributed in Sumatra, Kalimantan and Papua islands.

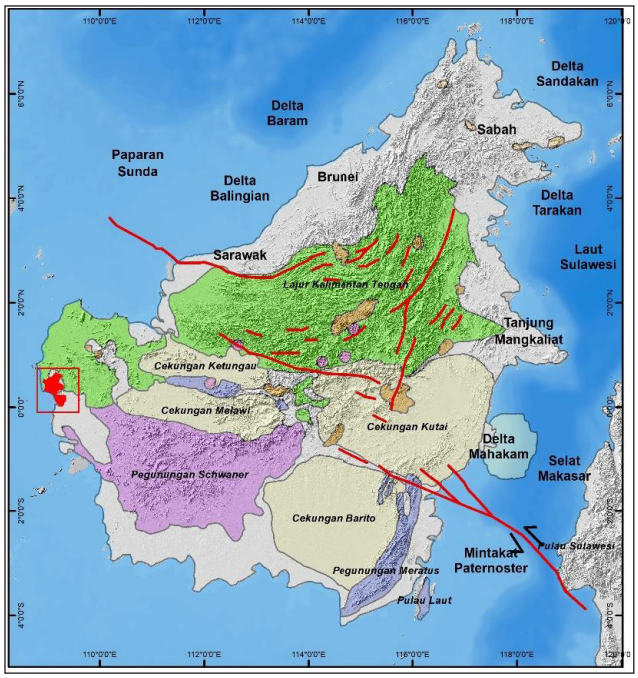

Figure 3: Study area in West Kalimantan province (red rectangle). Kalimantan map quoted from Rose & Hartono (1978).

METHODS

Field activities in the form of geological mapping and drilling, as well as geophysical surveys using the Ground Penetrating Radar (GPR) method, were carried out to determine the area of peatland distribution and its thickness (Figure 4). Peat description on fiber and ash contents as well as pH is referred to American Standard Testing Material (ASTM) 2002, while the degree of peat decay is referred to Von Post scale (1981 in Esterlee & Ferm, 1994). Several laboratory analyses were carried out to determine the properties of Mempawah peat deposits, namely chemical and physical analysis as well as combustion property. However, in regard to the objective of this study, this paper will focus on selected parameters for carbon sink estimation.

Figure 4: Peat drilling using Fikelkarp Auger (left) and Mesa Geo PDA for GPR survey (right).

RESULT AND DISCUSSION

Geological mapping was carried out on an area of 16,000 hectares. Considering this area are mostly covered by water (as it is swamp), the most effective way to identify peat deposit is by drilling using Fikelkarp Auger (hand drilling). Peat deposit data were collected from 50 drilling location on 2 km grid spacing (Figure 5).

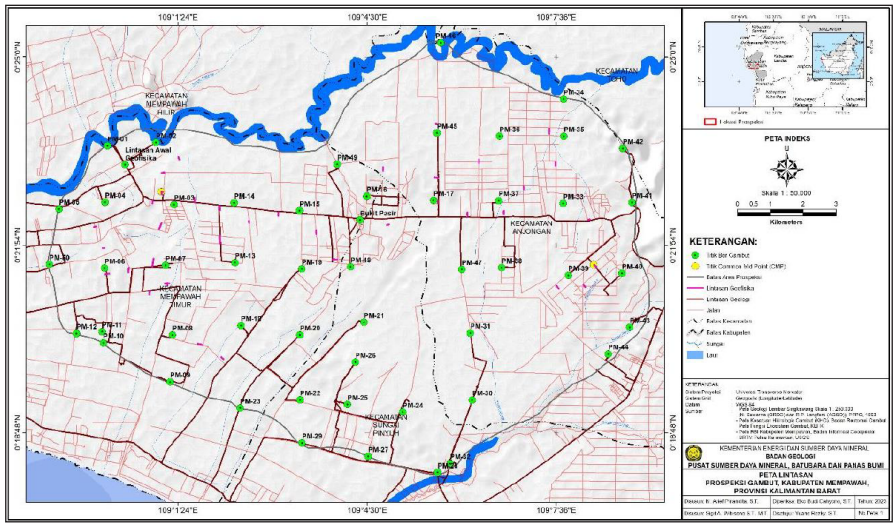

Figure 5: Drilling location map. Green points indicate drillhole location.

Peat deposits in the study area show dark brown color, composed in general of organic material from higher plants remains, i.e. plants that already have true roots, stems, and leaves (Figure 6). According to Andriesse (1998), these deposits can be categorized into fibric type (fiber content > 67%) and a hemic type (fiber content of 33% - 67%). In the study area, hemic type peat deposits are often found in peat deposit with a thickness of more than 4 meters. Acidity level was identified by testing the water on the peatland area which indicates pH value of 4.02 – 4.37. Based on ASTM D2976, peat water in the study area can be classify as highly acidic (pH < 4.5).

Referring to Van Post scale, the degree of peat decay in the study area varies between H2-H6. H2 is characterized by almost entirely undecomposed peat which, when squeezed, releases clear or yellowish water. Plant remains still easily identifiable. No amorphous material present. H6 is characterized by moderately highly decomposed peat with a very indistinct plant structure. When squeezed, about one-third of the peat escapes between the fingers. The residue is very pasty but shows the plant structure more distinctly than before squeezing.

The thickness of peat deposits ranging from 0 up to 9 meters. The peat measurement point with a thickness of 0 meters was used as a reference in determining the boundaries of the peat basin, while peat with maximum thickness is used as a reference in determining the central area of the peat deposit basin. These boundaries were used to identify the peat area which will be used in calculating the peat volume later on.

GPR survey was carried out on the same area as geological mapping area. In general, the GPR result shows a quite consistent peat thickness with drilling result. In addition, GPR result also shows that there are geological structures that affected rock formation beneath peat deposit, such as graben and fault (Figure 7).

Figure 6: Left to right: Peat from PM-13, PM-15 and PM-19 drillholes.

Twenty-five peat samples were subjected to several laboratory testing, in order to identify peat properties in the study area. Table 1 shows several parameters taken from various laboratory analysis which corelate with the objective of this study. In term of potential energy, peat deposit in the study area shows a relatively high calorific value (CV), ranging from 4354 up to 5498 cal/gr (air dried basis). Relative density (RD) ranging from 0.07 up to 0.14 gr/cm^3.

Peat carbon content can be determined through chemical analysis (proximate and ultimate analysis) as well as Total Organic Carbon analysis (TOC). In general, TOC content has a relatively small range of values, ranging from 45.09% to 58.37% with an average value of 53.21%. The range and average of TOC values of peat samples in the study area are similar to carbon concentrations in dry peatlands in general, where the carbon concentration value is around 50% (Page *et al.*, 2010) and 50% - 60% (Anshari *et al.,* 2010). Furthermore, it can be observed throughout the basin that the TOC value in the deeper zone is smaller compared to the one in the shallow area. According to Wahyunto *et al*. (2004), the hemic and sapric types of peat have lower carbon content compared to the fibric type. The result of this study confirmed this statement. It shows that almost most of the peat at the study area, in the shallow zone, was found to be peat with the fibric type.

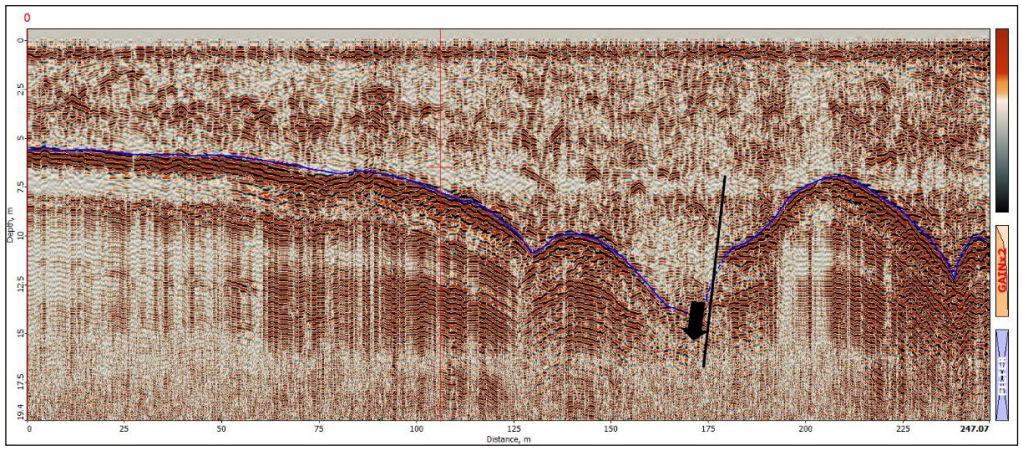

Figure 7: Fault on the basement rock – one of the geological structures that can be identified from GPR data.

Table 1: Selected peat properties from laboratory testing.

NO	SAMPLE CODE	CV cal/gr (adb)	RD gr/cm^3	TOC (%)
1	PM 2	4571	0.10	48.78
2	PM 3	4834	0.12	53.46
3	PM 7	5030	0.10	54.35
4	PM 13 (1-4 m)	5091	0.08	54.33
5	PM 14 (3-9 m)	5012	0.12	54.05
6	PM 14 Composite	5280	0.08	55.36
7	PM 15 (1-5 m)	5097	0.11	55.43
8	PM 16	5498	0.07	55.57
9	PM 17	5137	0.10	53.94
10	PM 18	4884	0.09	51.29
11	PM 19	5039	0.10	54.33
12	PM 21	5069	0.11	52.99
13	PM 24	5122	0.09	54.21
14	PM 25	4354	0.13	46.36
15	PM 30	5022	0.80	55.52
16	PM 31	5093	0.80	52.95
17	PM 33	5288	0.13	56.51
18	PM 35	4706	0.12	50.43
19	PM 36	5405	0.08	55.29
20	PM 37	5228	0.13	58.37
21	PM 38	5050	0.14	55.18
22	PM 39	4645	0.14	55.36
23	PM 45	5095	0.07	54.34
24	PM 47	5079	0.10	55.10
25	PM 48	5169	0.08	55.92

According to Page *et al*. (2010), the magnitude of the tropical peatland carbon pool or carbon sink is obtained from the following formula:

$$C_p = V_p \times BD_{be} \times C_c/10^9$$

where: C_p is the peatland carbon sink, V_p is the volume of tropical peat, BD_{be} is best estimate mean dry bulk density, and C_c is percentage carbon content.

In order to calculate the volume of peat deposits in the study area, a deposit model must first be created. This model was created based on isopach thickness from field data as can be seen on Figure 8.

Based on the peat deposit model, the volume of peat deposits in the study area is 894,363,995 m^3. Peat resources can also be estimated by multiplying peat volume by relative density (Table 1). Peat resources in the study area is 98,380,039 tons.

The minimum and maximum value of TOC (Table 1) is used in carbon sink estimation. By using Page formula as mentioned before, the minimum potential of carbon sink in the study area can be determined to be 44.36 million tons, whilst the maximum potential to be 57.42 million tons.

Peatlands can play a significant role in carbon trading by offering carbon credits. These credits represent the reduction or sequestration of greenhouse gas emissions and can be traded on international market. By participating in carbon trading, peatland owners can generate income while also contributing to climate change mitigation and biodiversity conservation. This provides a strong incentive for the protection and restoration of these valuable ecosystem.

This result on carbon sink estimation in the study area can be used as initial data for carbon trading in Indonesia. However, further in-depth study, involving various stakeholders, is needed for better carbon quantification that can be accepted by various parties.

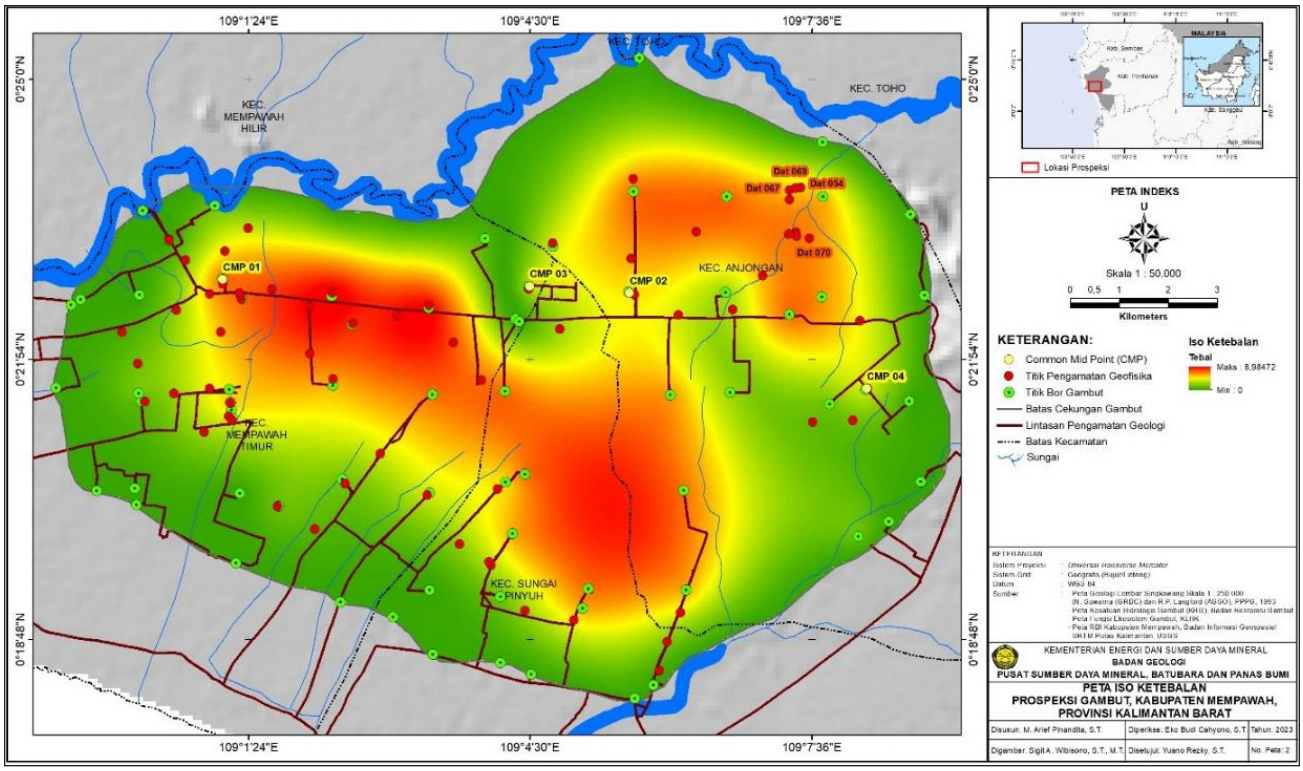

Figure 8: Peat deposit model of the study area.

CONCLUSION

Peat deposits in Mempawah area are quite widespread with hemic and fibric quality with a maximum thickness up to 9 meters. Mempawah peatlands have the ability to store very large natural carbon ranging from 44.36 million tons up to 57.42 million tons. This natural carbon storage can be used as carbon credit in anticipating climate change issues.

REFERENCES

Anshari, G., M. Afifudin, M. Nuriman, E. Gusmayanti, L. Arianie, R. Susana, R.W. Nusantara, J.S. Rahajoe, & A. Rafiastanto, 2010. Drainage and land use impacts on changes in selected peat properties and peat degradation in West Kalimantan Province, Indonesia. Biogeosciences, 7(3), 403-419.

Andriesse, J. P., 1988. Nature and Management of Tropical Peat Soils. FAO Soils Bulletin, 59. Rome.

Esterle, J. S., & Ferm, J. C., 1994. Spatial variability in modern tropical peat deposits from Sarawak, Malaysia and Sumatra, Indonesia: analogues for coal. International Journal of Coal Geology, 26, 1 – 41.

GRID-Arendal. Peatland carbon cycle. https://www.grida.no/resources/12532.

Harenda, K., Lamentowicz, M., Samson, M., & Chojnicki, B.H., 2018. The role of peatlands and Their Carbon Storage Function in the Context of Climate Change. Chapter in GeoPlanet: Earth and Planetary Sciences – January 2018.

Page, S., Rieley, J.O., & Banks C., 2010. Global and regional importance of the tropical peatland carbon pool. Global Change Biology 2010, 17(2), pp. 798.

Rose, R. & Hartono, P., 1978, Geological evolution of the Tertiary Kutei-Melawi Basin, Kalimantan, Indonesia, Proceedings Indonesian Petroleum Association, 7th Annual Convention, 225-252.

Unveiling post-burn tropical peat characteristics: Insights from Ground Penetrating Radar (GPR) analysis

Hans Elmaury Andreas Siregar*, Eko Budi Cahyono, Muhammad Abdurachman Ibrahim

Center for Mineral, Coal and Geothermal Resources, Geological Agency, Bandung, Indonesia
*Email: hans.elmaury@esdm.go.id

Abstract: Extreme weather patterns, such as drought and prolonged low-rain intensity, are becoming more frequent due to climate change and human activity, increasing the potency of peatfires in tropical regions. These fires not only burn up peatlands but also release greenhouse gases, seriously affecting the health of the people and degrading peatland ecosystems. The work of past studies in response to these increasing concerns has demonstrated that geophysical techniques, particularly Ground-Penetrating Radar (GPR), can greatly enhance our knowledge about peat structure. This work mainly focuses on the objectives of the GPR capability in delineating subsurface characteristics of peat in post-burning conditions. The GPR data were collected on the burnt peatland of West Kalimantan. Some coring has been conducted to validate the peat layer depth identified by the radargram; further, the core to radar tie is also used for the velocity calibration for time-to-depth conversion. The radargrams exhibited multiple-like signals, which were interpreted as a disturbed peat surface due to land conversion and peat burning. The characteristics of the radargram related to post-burn scar show variation in neighboring peat reflectors, which indicates changes in the bulk density and water content caused by the fire. The general outcome of this study would form significant implication, not only within the academic sector but most importantly beyond. Understanding the GPR signature that reflects changes in peatland conditions will be essential for local government, environmental organizations, and native communities in effectively preventing peat degradation caused by human activities and fires while also guiding the management of already damaged landscapes. To our knowledge, this is one of a few GPR study to offer new insights into post-burn peatland ecosystems, adding valuable knowledge to current approaches in peatland mitigation science and technology.

Keywords: GPR, peatland, peatfire, radargram, post-burn

INTRODUCTION

The phenomenon of climate change has changed the conditions of human life around the world. Shifts in rainfall frequency can be high and low in the tropics, as well as rising temperatures represent the most pronounced impacts of climate change. In addition, extreme climate events such as heat waves, droughts, and wildfires are becoming more frequent in many parts of the world (Caroline *et al*., 2017). Wildfires can become more extreme due to factors such as atmospheric conditions (Di Virgilio *et al*., 2019) and human-caused climate change (Abatzoglou & Williams, 2016). Forest fires pose a global threat and the impact is particularly severe in certain ecosystems, such as peatlands. Peatlands function as carbon sinks but become a source of greenhouse gas emissions when burned. Episodic phenomena such as El Niño, which have been observed with greater frequency due to climate change (Cai *et al*., 2014), can cause peat fires and create many hot spots in peatland areas (Yulianti *et al*., 2020). However, human-driven peatland degradation remains the main cause of the increase in fire frequency. Degraded peatland ecosystems are more susceptible to smoldering fires and make them particularly vulnerable to burning (Turetsky *et al*., 2015).

In the tropical country such as Indonesia, peat-fire occur every year especially in Kalimantan that has vast peatland area. In West Kalimantan, in one place such as Rasau Jaya has been explored to know the peat depth in March 2021 and some information from Fire Information for Resource Management System (FIRMS) application showed about burned area around Rasau Jaya village in March 2021. In another area such as Teluk Keramat, some studies about peat exploration has been conducted in May 2024 and FIRMS also depicted the latest information about burned area in March 2024.

There are several methods that have been used to measure the depth of post-burn peat such as the direct rod method in intensely burned areas (Graham *et al*., 2022) and the use of airborne lidar to calculate the depth of burned peat (Simpson *et al.*, 2016). There is also another study that provides a picture of burnt peat below the surface based on electromagnetic velocity variations at post-burning peatland using GPR analysis (Terry *et al.*, 2020). There are not many

studies that focus on the characterization of burned peat. In this study, we aim to further explore the potential of GPR with high-resolution geophysical methods. Previously, GPR applications have been used in several peat-related applications, such as identifying the subsurface morphology of peatlands (Pezdir *et al*., 2021) and internal peat structures (Pereira *et al*., 2017; Ryazantsev & Mironov, 2018). We hope that with this study we will get the results of the potential of GPR in mitigating peat fire risks.

DATA AND METHODOLOGY

We collected secondary data from NASA MODIS monthly hotspot data. The data was extracted through Fire Information for Resource Management System (FIRMS, https://firms.modaps.eosdis.nasa.gov/map/) and we selected burned area in Kubu Raya regency, West Kalimantan that overlapped with our Ground Penetrating Radar (GPR) survey. The GPR survey was conducted using the SE-150 and SE-70 unshielded antennas from Radarteam and GPS handheld on February 2020. FIRMS data from time periods close to our peatland exploration were chosen for this study. Georeferencing was used to overlay the GPR survey lines on to the burn area identified in the FIRMS data (Figure 1). Five GPR lines has been used to analysed the characteristic of post-burn peat in Kubu Raya regency.

The GPR data collected were processed using basic filters, including time-zero correction, background removal, bandpass filtering, and manual gain adjustment. For comparison, we analyzed two GPR datasets: one from the burned area and another from an unburned region. The radargrams from both areas were compared to identify distinguishing features. To convert the GPR data from time to depth, we used ground truth information from hand auger coring near the GPR survey lines.

RESULT AND DISCUSSION

Figure 2(a) shows a radargram that aligns with coring data to determine the velocity of electromagnetic (EM) waves. The calculated velocity is 0.039 m/ns allowing the conversion of the radargram from time to depth. According to the coring result, the peat depth reaches 7 meters and clay soil lies beneath it. The radargram consists of a reflection hyperbola (red arrow) and parallel reflection (red circle) (Figure 2(b)). The parallel reflection indicates the boundary between the peat and underlying sediment and the reflection hyperbola represents plant remnants such as roots and stem.

In Figure 2(c) using the same velocity assumption, a multiple-like signal (black box) appears on the radargram, highlighting two parallel reflections with similar features. This pattern occurs due to changes in the permittivity of the peat signal during the fire, resulting in two distinct reflection patterns (red and black circles). Figure 2(d) highlights the characteristics of radargram in peat medium. In addition, the analysis identifies parallel reflection patterns delineated in red and black circles and based on the 1D depth model from Huang & Rain (2014), the red circle indicates the boundary between preheated wet peat and undisturbed peat while the black circle represents the boundary between the undisturbed peat and underlain clay soil.

The GPR radargram with SE-70 shows three parallel reflections in Line E due to density and moisture changes of the peat (Benscoter *et al.*, 2011; Karušs & Bērziņš, 2015) from the peat-fire event. According to the post-burn peat model from Huang & Rain (2014), the first layer in the radargram was interpreted as char, ash, and dry peat medium. The resolution of the instrument prevents it from distinguishing between char, ash, and dry peat. The depth of the first layer varies from 60-80 cm. In the radargram from SE 150, this layer has not been identified although the resolution of SE 150 is higher than SE 70 because the thickness of this layer in the radargram from SE 150 is below the resolution of the instrument. In the second layer, preheated wet peat has been identified, showing differences in peat density and moisture compared to the first layer. The third layer is undisturbed peat. Beneath the undisturbed peat, there is clay soil and we do not have data from coring about the layer underneath the clay soil.

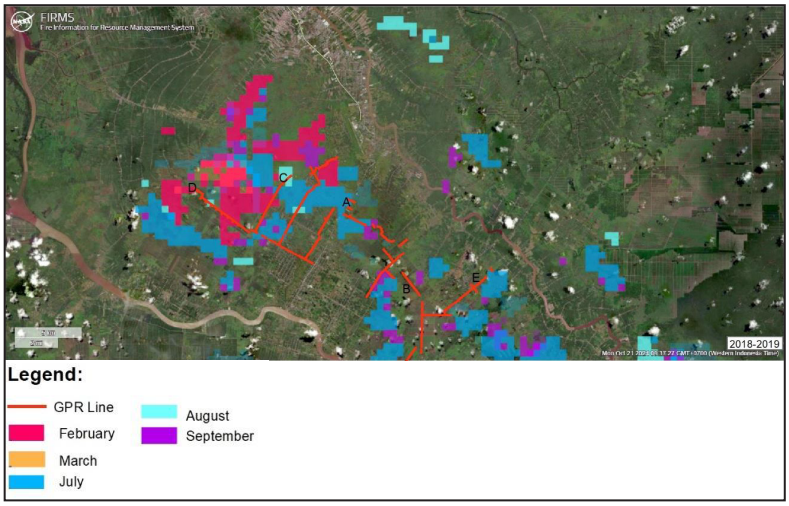

Figure 1: Distribution of burn-peat around study location from 2018-2019. The map is modified from NASA MODIS monthly hotspot data. The GPR lines were overlain with the data to identify the GPR line in burn and unburn peat. There are five GPR lines (A, B, C, D, E) that has been used in this study.

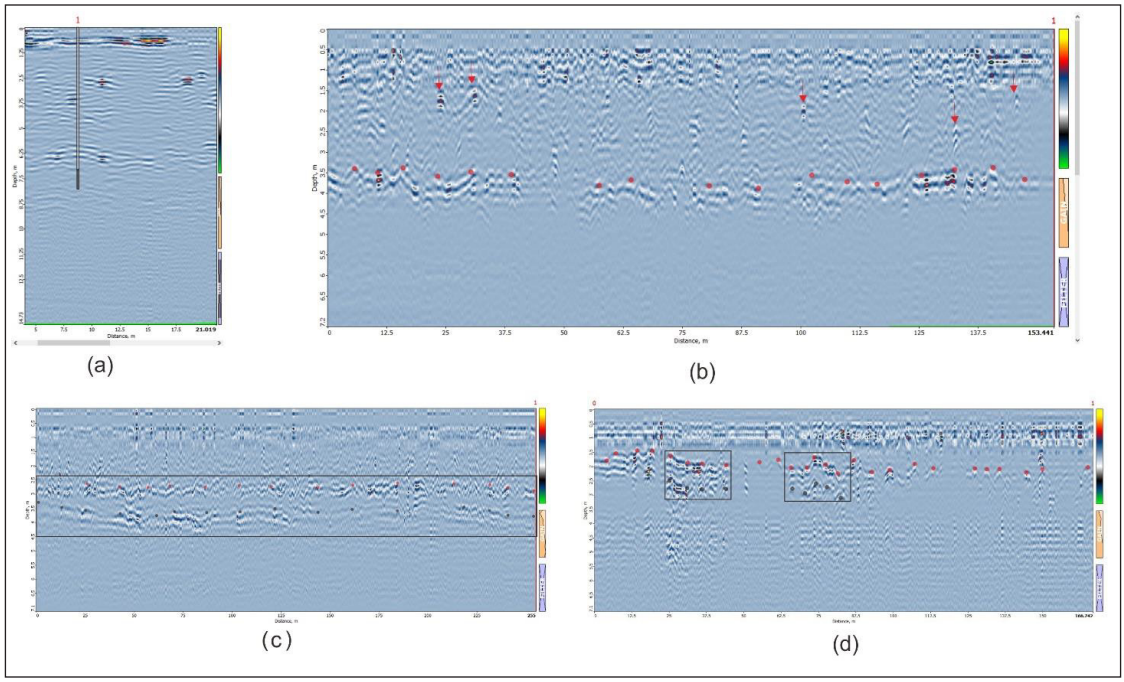

Figure 2: Processed GPR data in unburn-peat with peat coring for time-depth conversion Line A (a), Processed GPR data in unburn-peat with SE-150 antenna Line B (b), Processed GPR data in burn-peat with SE-150 antenna Line C (c) and Line D (d).

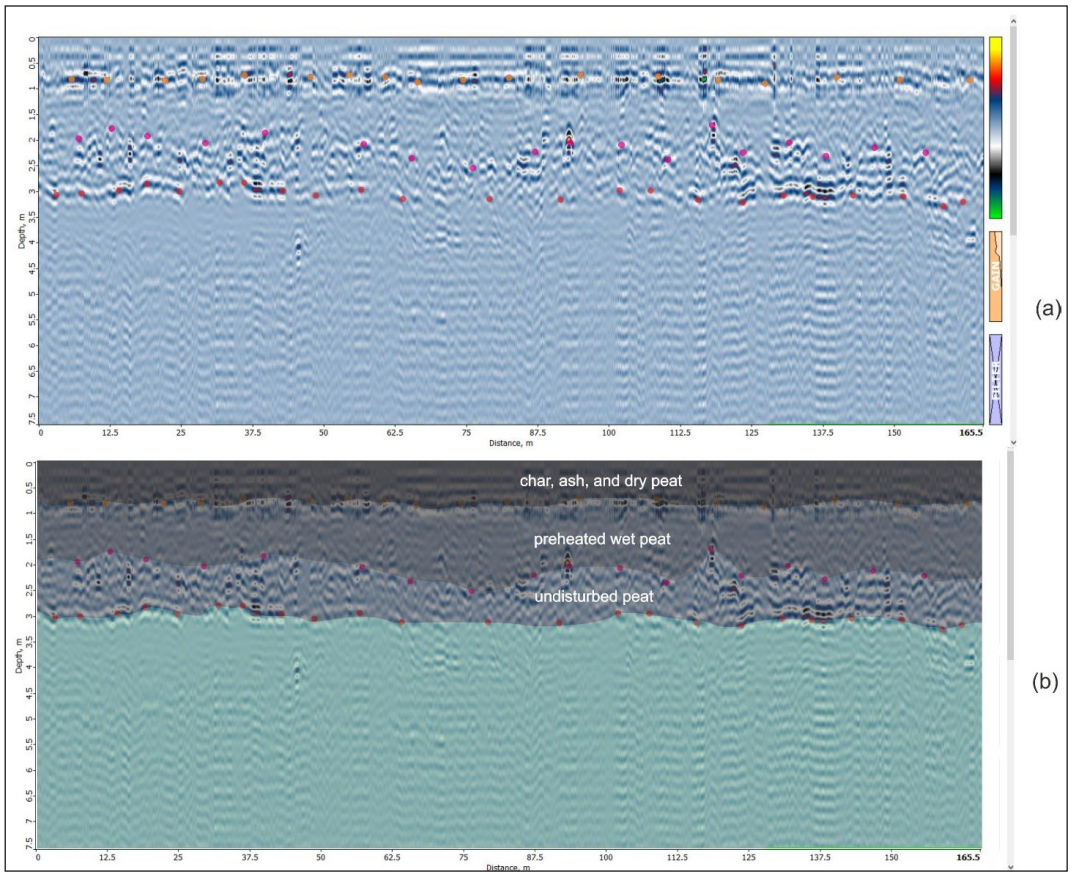

Figure 3: Processed GPR data in burn-peat with SE-70 antenna Line E (a). There are three parallel reflections in the radargram (red, pink and orange circles). Peat model based on radargram reflection in Line E (b).

CONCLUSION

This study shows the feasibility of using GPR in a post-burn peatland environment in Indonesia. A comparison between post-burn peat and unburn peat showed distinct characteristics in radargram such as horizontal parallel reflections below the 1-meter depth that can be identified in post-burn peat. The reflection is interpreted as char, ash, and dry peat, furthermore, if the thickness of this layer exceeds the GPR resolution, we can map it and maintain a constant water supply to ensure it remains undrained. Another feature such as a multiple-like signal in the peat radargram also indicates post-burn peat. The multiple-like signal can be continuous or present only in a few spots in the radar program. This feature is more than 1 meter in depth and is interpreted as preheated wet peat, as a mitigation, this layer can also be irrigated to help prevent fires in the future. It is possible to map the location of burned land and encourage the government, communities, and local people to give greater attention to these places.

The amount of emissions produced in the area specified by the radar program can be determined by simulated carbon emissions on a laboratory scale under conditions similar to natural peat fires. Furthermore, we can better assess the carbon sink in this burned area if we collect peat samples corresponding to the thickness of each characteristic of post-burn peat.

ACKNOWLEDGEMENT

This study was supported by Pusat Sumber Daya Mineral Batubara dan Panas Bumi, Badan Geologi, KESDM. We also want to thank all people who helped during field acquisition data.

REFERENCES

Abatzoglou, J.T. & Williams, A.P., 2016. Impact of anthropogenic climate change on wildfire across western US forests. PNAS, 113(42), 11770–75. doi:10.1073/pnas.1607171113.

Benscoter, B.W., Thompson, D.K., Waddington, J.M., Flannigan, M.D., Wotton, B.M., de Groot, W.J., & Turetsky, M.R., 2011. Interactive effects of vegetation, soil moisture and bulk density on depth of burning of thick organic soils. International Journal of Wildland Fire, 20, 418-429. https://doi.org/10.1071/WF08183.

Cai, W., Borlace, S., Lengaigne, M., Rensch, P.V., Collins, M., Vecchi, G., Timmermann, A., Santoso, A., McPhaden, M.J., Wu, L., England, M.H., Wang, G., Guilyardi, E., & Jin, F.F., 2014. Increasing frequency of extreme El Niño events due to greenhouse warming. Nature Climate Change, 4, 111-116.

Di Virgilio, G., Evans, J. P., Blake, S. A.P., Armstrong, M., Dowdy, A. J., Sharples, J., & McRae, R., 2019. Climate change increases the potential for extreme wildfires. Geophysical Research Letters, 46, 8517–8526. doi: 10.1029/2019GL083699.

Graham, L.L.B., Applegate, G.B., Thomas, A., Ryan, K.C., Saharjo, B.H., & Cochrane, M.A., 2022. A Field Study of Tropical Peat Fire Behaviour and Associated Carbon Emissions. Fire, 5(62). https://doi.org/ 10.3390/fire5030062.

Huang, X., & Rein, G., 2014. Smouldering Combustion of Peat in Wildfires: Inverse Modelling of The Drying and The Thermal and Oxidative Decomposition Kinetics. Combustion and Flame, 161(6), 1633-1644. DOI: 10.1016/j.combustflame.2013.12.013.

Karušs, J. & Bērziņš, D., 2015. Ground-penetrating radar study of the Cena Bog, Latvia: linkage of reflections with peat moisture content. Bull. Geol. Soc. Fin., 87, 87–98.

Pereira, D., Dias, E., & Ponte M., 2017. Investigating The Internal Structure of Four Azorean Sphagnum Bogs Using Ground Penetrating Radar. Mires and Peat, 19(13), 1-19. doi: 10.19189/MaP.2016.OMB.259.

Pezdir, V., Ceru, T., Horn, B., & Gosar, M., 2021. Investigating Peatland stratigraphy and development of the Sijec bog (Slovenia) using near-surface geophysical methods. Catena, 206, 105484.

Ryazantsev, P. & Mironov, V., 2018. Study of peatland internal structure by The Ground Penetrating Radar. 17th International Conference on Ground Penetrating Radar (GPR), pp. 1-4.

Simpson, J.E., Wooster, M.J., Smith, T.E.L., Trivedi, M., Vernimmen, R.R.E., Dedi. R., Shakti, M., & Dinata, Y., 2016. Tropical Peatland Burn Depth and Combustion Heterogeneity Assessed Using UAV Photogrammetry and Airborne LiDAR. Remote Sensing, 8(12). doi:10.3390/rs8121000.

Terry, N., Runkel, R., Werkema, D., Rutila, E., Comas, X., Warren, M., Kristiyono, A., & Murdiyarso, D., 2019. Exploring the potential of ground-penetrating radar (GPR) to measure the extent of chronic disturbance in peatlands: examples from acid mine drainage and peat fire. International Conference on Ground Penetrating Radar, 18. doi: 10.1190/gpr2020-015.1.

Turetsky, M.R., Benscoter, B., Page, S., Rein, G., van der Werf, G.R., & Watts, A., 2015. Global Vulnerability of Peatlands to Fire and Carbon loss. Nature Geoscience, 8, 11-14. doi: 10.1038/ngeo2325.

Ummenhofer, C.C. & Meehl, G.A., 2017. Extreme weather and climate events with ecological relevance: a review. Phil. Trans. R.Soc. B., 372, 20160135. doi:10.1098/rstb.2016.0135.

Yulianti, N., Kusin, K., Naito, D., Kawasaki, M., Kozan O., & Susetyo, K. E., 2020. The linkage of El Niño-induced peat fires and its relation to current haze condition in Central Kalimantan. Journal of Wetlands Environmental Management, 8(2), 100 – 116. doi: 10.20527/jwem.v8i2.221.

GSJ's commitment to building a disaster-resilient nation - Major progress in FY2023

Osamu Fujiwara* and Members of High-Precision Digital Geological Information Improvement Project for Disaster Prevention

Geological Survey of Japan, AIST, Tsukuba, Japan
*Email: o.fujiwara@aist.go.jp

Abstract: The Geological Survey of Japan (GSJ), AIST is currently implementing the "Project for the Development of High-Precision Digital Geological Information for Disaster Prevention and Mitigation" with plans for FY2022 through FY2025. This project aims to contribute to the realization of a resilient nation that can withstand natural disasters through the analysis, evaluation, aggregation, and provision of information that will be utilized in disaster prevention planning. The project encompasses two key activities: 1) accelerating the development of high-accuracy digital data on active faults, volcanoes, slope hazards, and marine geology, with enhanced spatial and temporal resolution, and 2) transforming GSJ's research outcomes into machine-readable formats, along with creating a data portal that allows users to easily access and utilize geological information, thereby advancing "geological DX." Following the outline of the project already reported in the previous fiscal year, this paper introduces the major progress of the project through FY2023.

Keywords: Active fault, geological information, slope disaster, national resilience, submarine geology, volcano, geological DX

INTRODUCTION

Located in a humid mid-latitude region and near a plate subduction boundary, Japan is prone to natural disasters such as earthquakes, volcanic eruptions, and typhoons. Implementation of measures to evaluate, consolidate, and provide information on natural disasters, which contribute to disaster prevention plans, is deemed necessary as part of national policy ("Five-Year Accelerated Measures for Disaster Prevention, Disaster Mitigation, and National Resilience," approved by the Cabinet in December 2020). In the Ministry of Economy, Trade and Industry's "Third Phase of the Intellectual Infrastructure Development Plan," the promotion of high-precision and digitization of geological information, along with the enhancement of one-stop information dissemination from the perspective of disaster prevention and mitigation, is also required.

Geological Survey of Japan (GSJ), AIST has been implementing a four-year project since fiscal year 2022 to accelerate the evaluation, consolidation, and dissemination of high-precision and digitized geological information on active faults, volcanoes, slope disasters, and marine geology, which is needed by local government disaster prevention officials. This effort is aimed at linking disaster prevention measures with geological information, utilizing the advancing digital technologies of recent years.

In this project, as shown in Table 1, we have established objectives and identified five strategic tasks to address them, forming research teams to carry out each task. Additionally, we have defined indicators to measure the progress of each task towards achieving the objectives.

MAJOR PROGRESS IN EACH STRATEGIC TASK

Active fault information

Although certain active faults are not included in the long-term evaluations by the Headquarters for Earthquake Research Promotion (HERP) or recent policy investigations, there are socially significant active faults that local governments and other entities have strongly requested to be surveyed. Therefore, we will investigate the distribution and activity of highly important active faults on land and in coastal areas. In FY2023, geophysical surveys and drilling investigations were conducted on two onshore faults distributed in Kumamoto Prefecture, Kyushu. In addition, a drilling survey was conducted for a submarine fault in the western part of the Seto Inland Sea in western Japan, and core samples were analyzed.

While GSJ has developed a nationwide active fault database at a scale of 1:200,000 (ttps://gbank.gsj.jp/activefault/), a larger scale is now required for practical use in society. Consequently, we will revise and update the positional accuracy of the data so that the active fault database can be utilized at a scale of approximately 1:50,000. In FY2023, we worked to improve the accuracy

Table 1: Project objectives and key issues.

Goal: To contribute to disaster resilient city planning and disaster prevention planning. 1. Protection of human life 2. Maintain the vital functions of the nation and society. 3. Minimize damage to property and public facilities 4. Rapid recovery and reconstruction	
Strategic Tasks	**Key Performance Indicators**
Organization of active fault information	1) Reduce the number of faults whose activity is unknown to improve the accuracy of predicting the probability and magnitude of future earthquakes. 2) Make the location and characteristics of active faults available to people briefly on the web.
Organization of volcano information	1) Reduce the number of undiscovered craters and craters with unknown eruption histories to improve the accuracy of predicting the location and magnitude of volcanic hazards. 2) Make the location and geometry of craters available to people briefly on the web.
Organization of slope disaster information	Identify geological conditions that are prone to causing slope disasters
Organization of marine geological information	Digitalization and centralized management of submarine geological information.
Promotion of geological DX (digital transformation).	Enable the automated processing of geological data and expand its distribution and advanced utilization.

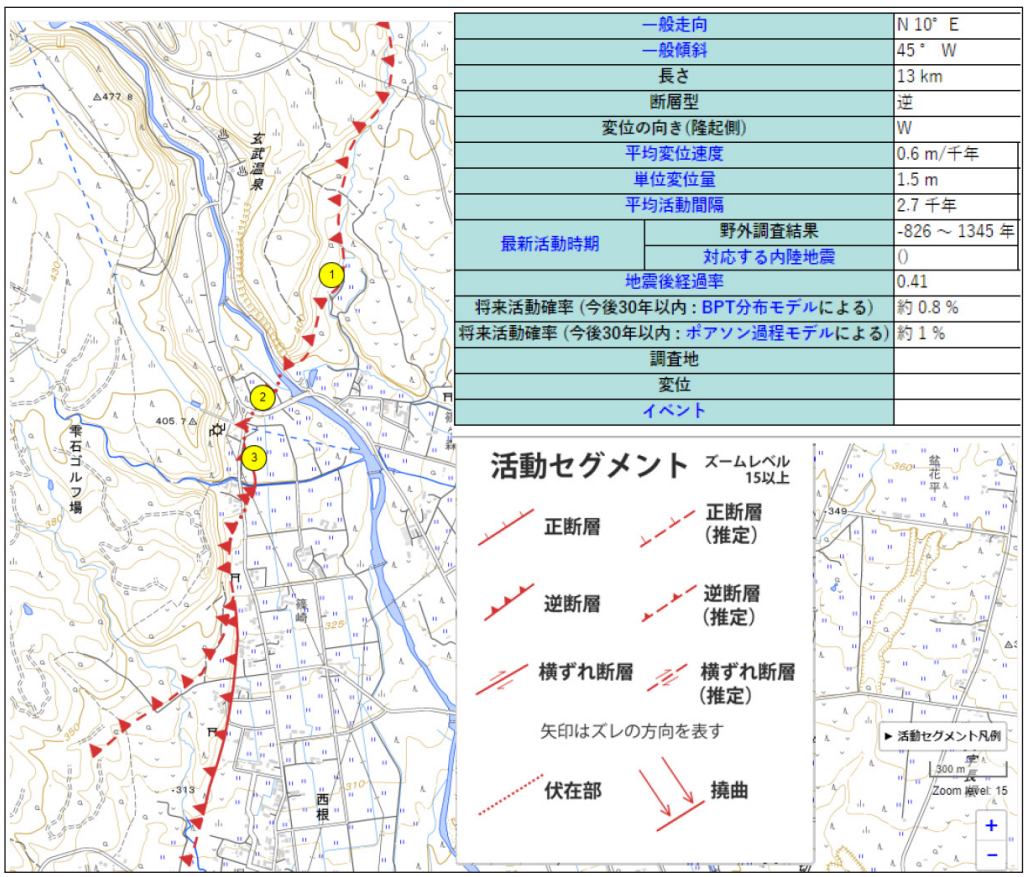

Figure 1: Example of updated active fault database display (https://gbank.gsj.jp/activefault/, cited 2024.10.2).

of the positioning of active fault data and began releasing to the public information on active faults for which work has been completed.

Volcano information

Precise location of volcanic craters and information on their activity history are fundamental data for volcanic disaster prevention. Crater maps for eight volcanoes, including Mount Fuji and Izu Ōshima Volcano, which are particularly important for disaster prevention, will be prepared as digital geological information with a scale of 1:25,000. These crater maps include data on crater locations, periods of crater activity, and eruption history. For Izu Ōshima volcano (Kawabata, 2024) and Hakoneyama volcano (Oikawa, 2023), crater maps were published (Figure 2). In addition, a crater location database will be developed for 50 volcanoes that are continuously monitored by the Japan Meteorological Agency.

Slope disaster information

The standards for slope disaster prevention and mitigation are heavily biased toward topographical elements, and the use of geological information, such as geological maps, for slope disaster risk assessment has not progressed. In this project, we will compile geological information correlated with slope disasters, including volcanic ash thickness, geophysical surveys, and satellite data, as well as information on vegetation changes. By combining this with past disaster records, we will create a risk assessment map based on geological analysis of predisposing factors.

In the 2023 fiscal year, we focused on the northern Kyushu region and conducted activities such as creating inventory datasets of topography, geology, and disaster history, as well as generating maps showing changes in forest vegetation on slopes using time-series analysis of optical satellite data. Additionally, we verified that small surface displacements can be detected through time-series interferometric analysis using synthetic aperture radar (SAR) (Mizuochi *et al.*, 2024). Furthermore, around the Aso Caldera, we investigated the thickness distribution, stratigraphy, and physical properties of wind-formed volcanic ash deposit including fallout pyroclastics and kuro-boku soil layers, which are prone to causing slope disasters.

Marine geological information

Data obtained during the process of creating a marine geological map of the waters around Japan will be digitized according to a unified standard, promoting integrated data management. Additionally, for the western area of the Nankai Trough seismogenic zone, where there is a high probability of great (Mw 8-9) earthquakes and tsunamis occurring, we will vectorize existing geological information and conduct reanalysis to develop seamless marine geological map.

In fiscal year 2023, we primarily registered digitized marine geological data from the area off the eastern coast

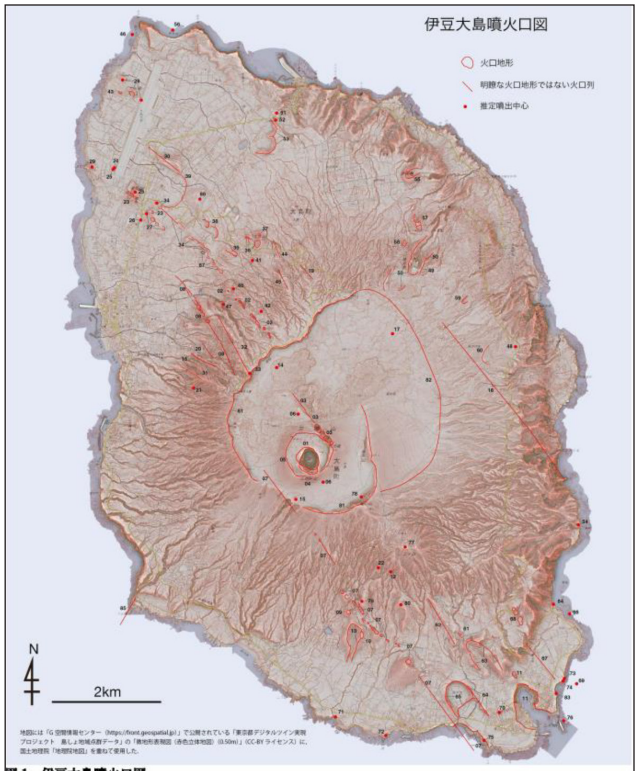

図１　伊豆大島噴火口図.
（背景地図に地理院地図（標準地図）と「東京都デジタルツイン実現プロジェクト　島しょ地域点群データ赤色立体地図」を使用）．数字は，火口 ID の数字（表１参照）．

Figure 2: Crater map of Izu Oshima volcano (Kawanabe, 2024, cited 2024.10.2).

of Shikoku to Kyushu into the newly constructed integrated management and display system, while also advancing the digitization of marine geological map data for the waters south of Kyushu and around the Noto Peninsula.

Advancing geological DX

To make it easier for industries and the public to utilize geological information necessary for disaster prevention, we are accelerating the digitization of 1:50,000 geological maps and explanatory notes, while also improving the usability of publicly available data by constructing a data catalog and data portal. 1:50,000 scale geological maps of western Japan, including the Chugoku and Shikoku regions, were vectorized and the explanatory texts of geological maps were converted to structured XML data.

We have cataloged the metadata related to the GSJ publications and initiated the trial release of the data catalog system built using CKAN (Comprehensive Knowledge Archive Network). Aiming for use in real-time hazard assessments, we have also been developing a volcanic hazard information system that allows online simulations of pyroclastic flows and tephra fallout distribution (Takada *et al.*, 2024, in this volume).

CONCLUDING REMARKS

This project is a part of GSJ's ongoing geological DX (Digital Transformation) initiative and will serve as a litmus test

for it. To effectively utilize digitized geological information, it is essential to improve disaster preparedness literacy at various levels of society (local governments, businesses, individuals, etc.), enabling people to understand disasters, prepare for them, and take actions to avoid risks. To achieve this, we will collaborate with local governments and relevant organizations.

REFERENCES

Kawanabe, Y., 2024. Volcanic craters data and Eruption events of Izu Oshima Volcano. Open-File Report of the Geological Survey of Japan, AIST, no.749, 17p. https://www.gsj.jp/data/openfile/no0749/gsj_openfile_report_749.pdf.

Mizuochi, H., Miyazaki, K., Abe, T., Hoshizumi, H., Kawabata, D., Iwao, K., Matsuoka, M. & Miyachi, Y., 2024. Detection of long-term slope displacement using time-series DInSAR and geological factor analysis for susceptibility assessment of landslides in northwestern Kyushu Island. Geomorphology, 453, 109095.

Oikawa, T., 2023. Volcanic craters data of Hakone Volcano (Hakoneyama). Open-File Report of the Geological Survey of Japan, AIST, no.745, 4p. https://www.gsj.jp/data/openfile/no0745/gsj_openfile_report_745.pdf.

Takarada, S., Bandibas, J., Kohno, Y., Kariya, E., Maitani, S., Osada, M. & Ikegami, F., 2024. Digital Transformation Activities in Geological Survey of Japan, AIST: Development of Geological Hazards Information System and Volcanic Hazards Information System. 60th Thematic Session "Geoscience in Transition".

Digital transformation activities in Geological Survey of Japan, AIST: Development of Geological Hazards Information System and Volcanic Hazards Information System

Shinji Takarada[1,*], Joel Bandibas[1], Yuhki Kohno[1], Emi Kariya[1], Shuho Maitani[1,2], Misato Osada[1,3], Fumihiko Ikegami[1,4]

[1]Geological Survey of Japan (GSJ), Tsukuba City, Japan
[2]Meiji University, Chiyoda, Tokyo, Japan
[3]Ibaraki University, Mito, Japan
[4]University of Tasmania, Hobart, Australia
*Email: s-takarada@aist.go.jp

Abstract: The Geological Survey of Japan, AIST, has implemented the new project "Development of High-Precision Digital Geological Information for Hazard Prevention and Mitigation" in 2022. Volcanic Craters DB, High-resolution Active Faults, Slope Disaster Risk Assessment, Digital Marine Geology, and Geological Digital Transformation (DX) of various geological information are project components. An outline of the Geological Hazards Information System and the Volcanic Hazards Information System developed in the DX project is introduced.

Keywords: Geoinformation, hazard, digital transformation, information system, simulation

INTRODUCTION

The new project "Development of High-Precision Digital Geological Information for Hazard Prevention and Mitigation" (2022-2026) has been developed based on "Five-years Acceleration Measures for Disaster Prevention and Mitigation, and National Resilience (Cabinet Secretariat, 2020) to protect people's lives, property, and livelihood from natural disasters, to maintain the important functions of the nation and society, to analyze, evaluate, consolidate and provide information that contributes to disaster prevention planning, and to promote the development of a resilient national land that will not succumb to natural disasters. The "Development of High-Precision Digital Geological Information for Hazard Prevention and Mitigation" project is subdivided into "Active Faults", "Volcanoes", "Slope Disasters", "Marine Geology" and "Geological Digital Transformation (DX)" projects.

GEOLOGICAL HAZARDS INFORMATION SYSTEM

The Geological DX project team is working on data distribution using API, data download service, making a viewer, and developing the Geological Hazards Information System to promote the digital transformation of various geological information based on FAIR (Findable, Accessible, Interoperable, and Reusable) data principles. The Geological Hazards Information System plans to provide data browse and search functions, data download of GIS data, and an online simulation system for real-time hazard assessment and connection with other databases to activate the digitized geoinformation. This system is designed to set up a complete geological hazards database in Japan and the East and Southeast Asia region, which will provide data view and search functions, download geospatial data, and connect with other databases to hasten the digitization of geoinformation. The Geological Hazards Information System contains not only output from the DX project but also hazard-related information from G-EVER and CCOP Geoinformation Sharing Infrastructure (GSi) projects and various publications in GSJ. About 1,280 maps (as of October 2024) are available on the System, including the 1:10M Eastern Asia Earthquake and Volcanic Hazards Information Map, the 1:200k Geological Map of Japan, and the 1:200k Seamless Geological Map of Japan, the 1:200k Geologic Map of Volcanoes in Japan, the 1:250k Distribution Map of Large-Volume Ignimbrite, Geological Map of Volcanoes, Distribution Map of Tephra Falls, Distribution Map of Earthquake Hypocenters, and 1:200k Distribution Map of Active Faults in Japan (Figure 1). The contents are categorized in map catalogs. Overlay of various contents, change orders, and transparency are possible in the system. Pop-up information is displayed by double-clicking the features on the map. GIS data, KML files, and attribute table contents are downloadable for permitted

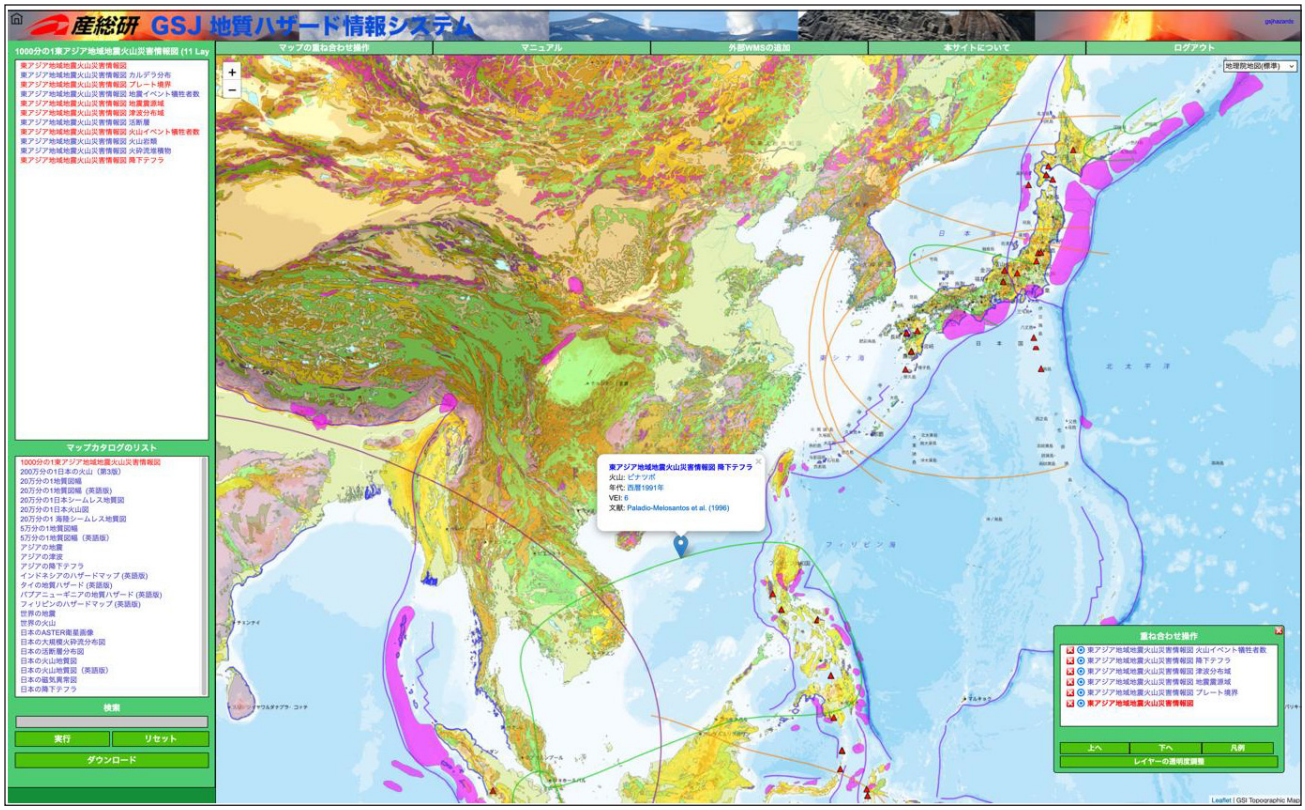

Figure 1: Geological Hazards Information System showing 1:10M Eastern Asia Earthquake and Volcanic Hazards Information Map (Takarada *et al*., 2016). The GSI Maps (Standard) published by the Geospatial Information Authority of Japan are used.

content (Figure 2). Online resource WMS parameters are shown on the Geological Hazards Information System as a new API (Application Program Interface) to display hazard-related contents directly on the other servers and GIS software (Figure 3).

VOLCANIC HAZARDS INFORMATION SYSTEM

The project of the Volcanic Hazards Information System aims to develop (1) real-time hazard assessment using online numerical simulations, (2) eruption parameter analysis at various volcanoes, (3) digitization of tephra falls, pyroclastic flows and debris avalanche distributions, (4) online tephra falls volume estimation, (5) display of volcanic crater distributions, and (6) integration of various volcano databases.

The Volcanic Hazards Information System provides functions to execute Energy Cone (Sheridan, 1980; Malin &Sheridan, 1982), Titan2D (Pitman *et al*., 2003; Sheridan *et al*., 2004), and Tephra 2 (Bonadonna *et al*., 2005; Connor, 2006) numerical simulations on about 3,000 Quaternary volcanoes worldwide using ASTER GDEM 30 m and GSI 10 m DEM. Energy Cone and Titan2D models are suitable for evaluating volcanic density flows such as pyroclastic flow and debris avalanches. Tehpra2 is made for assessing tephra falls. Its quasi-real-time volcanic hazard assessment feature sets it apart from other volcanic hazard systems, which allows for a more rapid display and comparison with previous eruption cases. The Titan2D numerical simulation is updated to version 4.2, and execute time became significantly faster (e.g., the earlier version took more than 30 min, and the new version took less than 5 min). Therefore, a more rapid volcanic hazard assessment is possible. The Titan2D numerical simulation could run not only the Coulomb model (previous version) but also TwoPhases-Pitman-Le (Pitman & Le, 2005), Pouliquen-Forterre (Pouliquen & Forterre, 2002), and Voellmy-Salm (Christen *et al*., 2010) models (Figure 4). Therefore, more detailed examination of volcanic gravity currents behaviors became possible.

Online resource WMS (Web Mapping Service) parameters are now shown on the Volcanic Hazards Information System as a new API (Application Program Interface) to display simulation results on the other servers and GIS software. Using this WMS parameter, simulation results can be shown on other calculation systems, GIS software (e.g., QGIS or ArcGIS), and Google Earth. Figure 5 shows an example of displaying the Energy Cone and Tephra2 simulation results of Mount St. Helens Volcano, Washington, USA, on the QGIS using the WMS parameter directly shown from the Volcanic Hazards Information System as a new API (Use new WMS/WMTS connection and enter the WMS parameter).

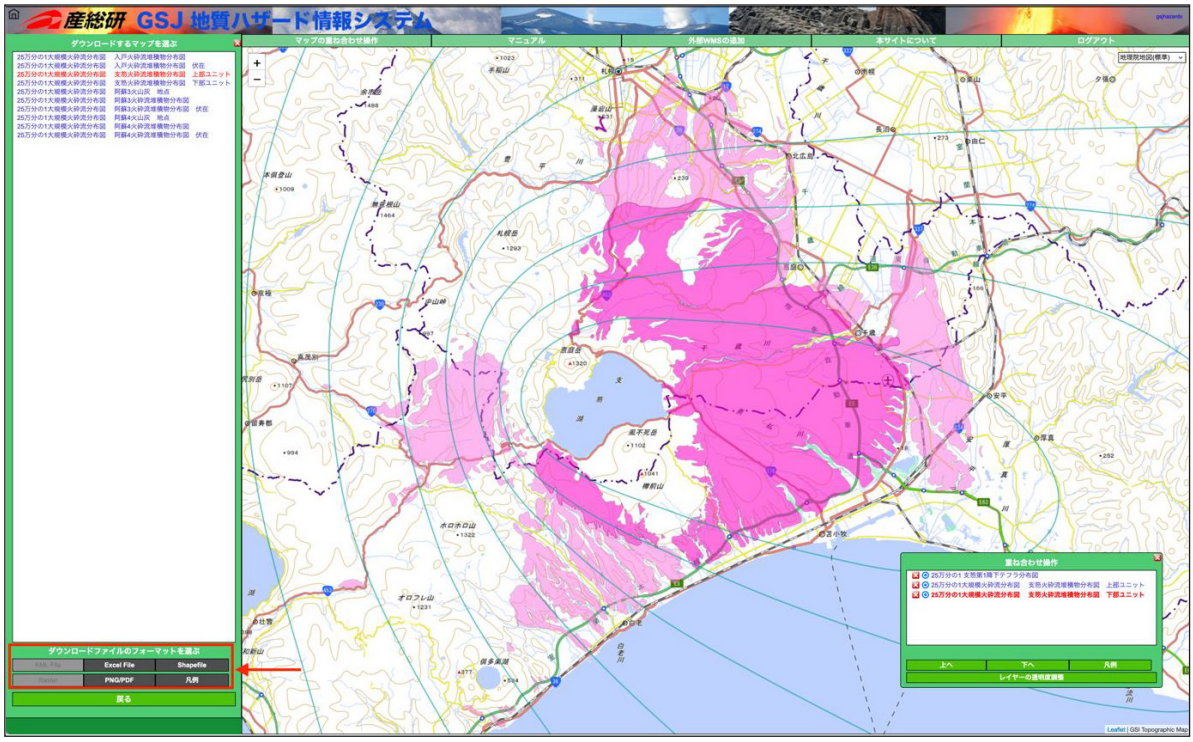

Figure 2: GIS data (Shapefile) and attribute table are downloadable in the Geological Hazards Information System. Example of Distribution Map of Shikotsu Ignimbrite and Spfa-1 Tephra Fall in SW Hokkaido, Japan. The GSI Maps (Standard) published by the Geospatial Information Authority of Japan are used.

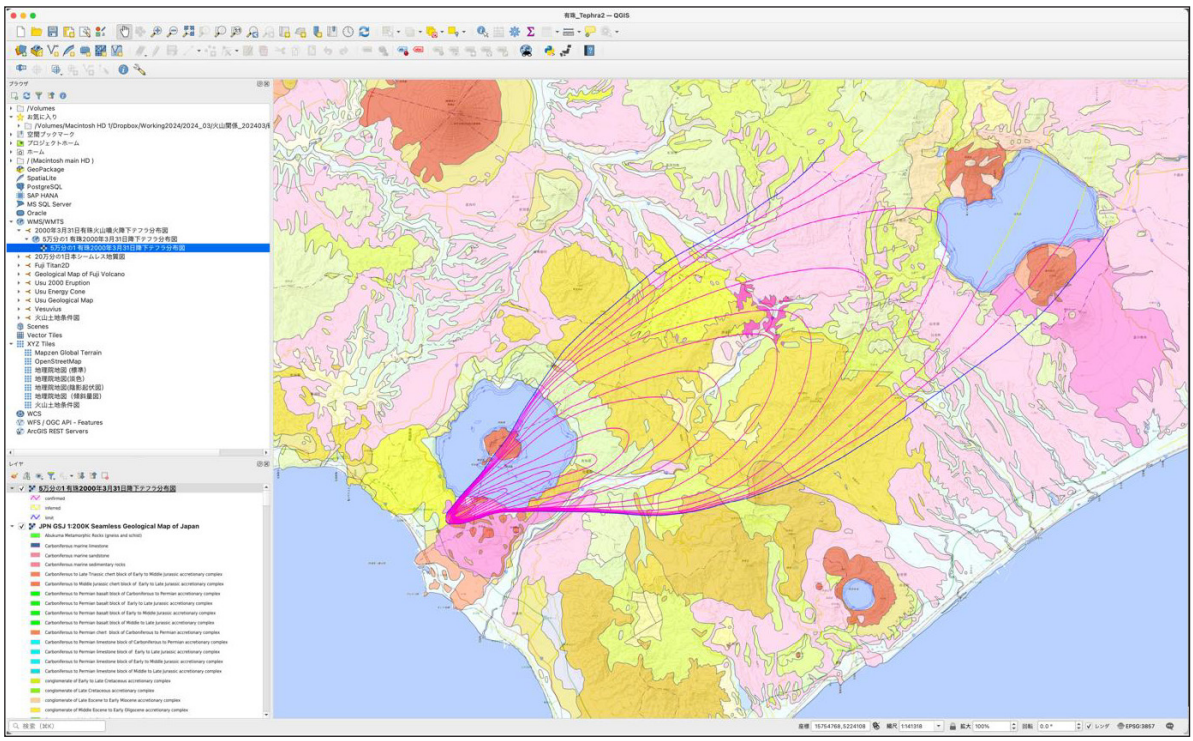

Figure 3: The contents of the Geological Hazards Information System can be displayed on the user's GIS software using WMS parameter API. The distribution map of the 31 March 2000 tephra fall deposit and the 1:200k Seamless Geological Map of Japan are shown in QGIS. The GSI Maps (Standard) published by the Geospatial Information Authority of Japan are used.

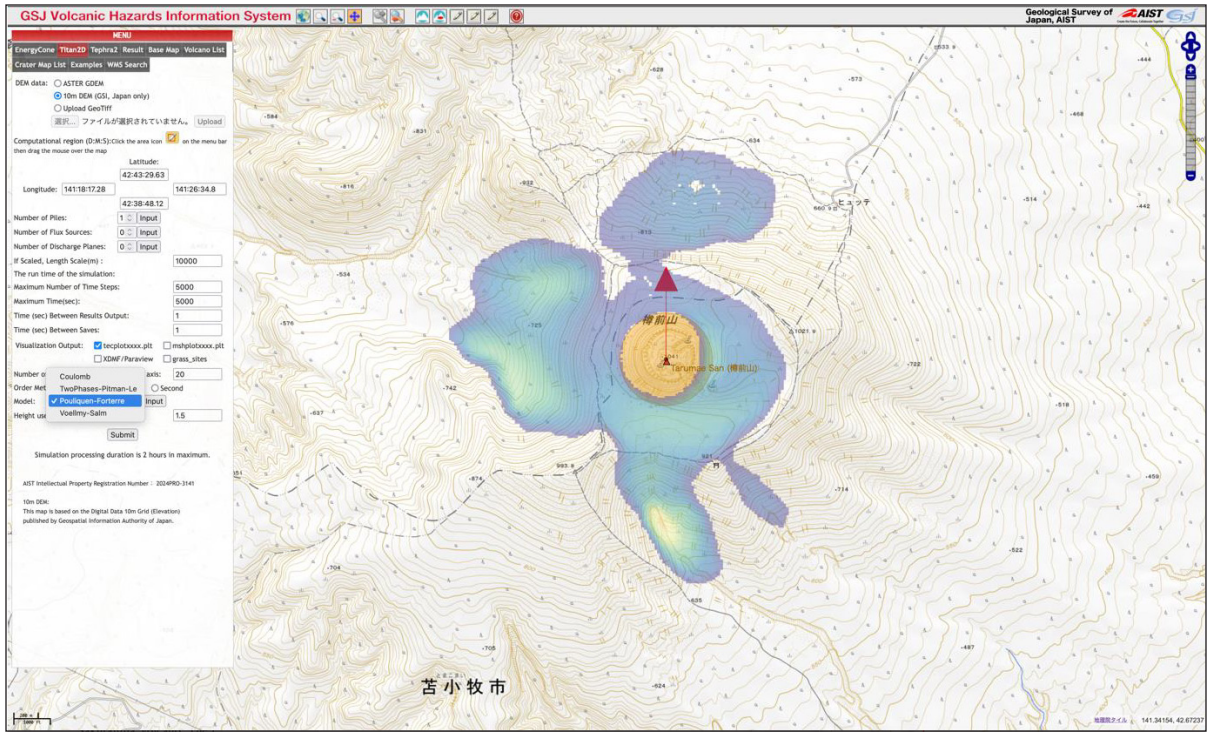

Figure 4: A Titan2D simulation result using Pouliquen-Forterre model at Tarumae Volcano in the Volcanic Hazards Information System. The GSI Maps (Standard) published by the Geospatial Information Authority of Japan are used.

The shapefiles and KML files can be downloaded from the Volcanic Hazards Information System simulation result tab and used for hazard assessments. For example, the results of the Energy Cone simulation are shown on Google Earth in 3D view. The 3D view is helpful for hazard assessment, such as understanding the relationship between the distribution of simulation results and roads and refugees, even if GIS software is inaccessible (Figure 6).

Representative eruption parameters and simulation results at major volcanoes are listed on the Volcanic Hazards Information System (Figure 7). These eruption parameters of case studies are helpful to compare with past eruptions and eruptions at other volcanoes for real-time hazards and risk assessment after starting eruptions with choosing appropriate eruption parameters. Tephra2 simulation results at Fuji Volcano, Japan, with eruption parameters: column height = 25 km, erupted mass = 1.0×10^{13} kg (about 10 km^3) is shown in Figure 7. Currently, 181 cases of Energy Cone, 76 cases of Tephra2, and 53 cases of Titan 2D models, totally 310 cases are shown on the system (as of Oct. 2024). These presentative eruption parameters and case studies on the Volcanic Hazards Information System are helpful for the hazards and risk analysis. These simulation results can be used on other servers and GIS software using WMS parameters.

Digitized GIS datasets of volcanic eruptive products such as tephra fall, pyroclastic flow, and debris avalanches and providing them to the public are essential for volcanic hazards and risk assessments. Therefore, the digitization of major eruption products at volcanoes in Japan and abroad is being processed. Currently, 246 isopach map data of tephra fall deposits at Rausu, Kutcharo, Mashu, Tokachi, Tarumae, Yotei, Usu, Toya, Hokkaido Komagatake, Hakkoda, Towada, Asama, Fuji, Aso, Kirishima, Sakurajima, Aira, Ata, Kutchinoerabujima, Calbuco, and Kelud Volcanoes are digitized (as of Oct. 2024). An example of digitized isopach maps of tephra fall deposits from the 2000 eruptions (on March 31, April 1, April 2, and April 4**)** at Usu Volcano, SW Hokkaido, Japan, are shown in Figure 8.

The online tephra fall volume estimation system (WebTephraCalc) was developed using Segment Integration (Takarada *et al.*, 2001, 2016), Exponential (Pyle, 1989; Fierstein & Nathenson, 1992), Power Law (Bonadonna & Houghton, 2005), and Weibull (Bonadonna & Costa, 2012) methods (Figure 9). The areas of each contour are calculated and the volume of each segment is estimated on the system.

FUTURE PLAN

The Volcanic Hazards Information System Project continues to develop (1) real-time hazard assessment using online numerical simulations, (2) eruption parameter analysis at various volcanoes, (3) digitization of tephra falls, pyroclastic flows and debris avalanche distributions, (4) online tephra falls volume estimation, (5) display of volcanic crater distributions, and (6) integration of various volcano databases. The interaction among the current

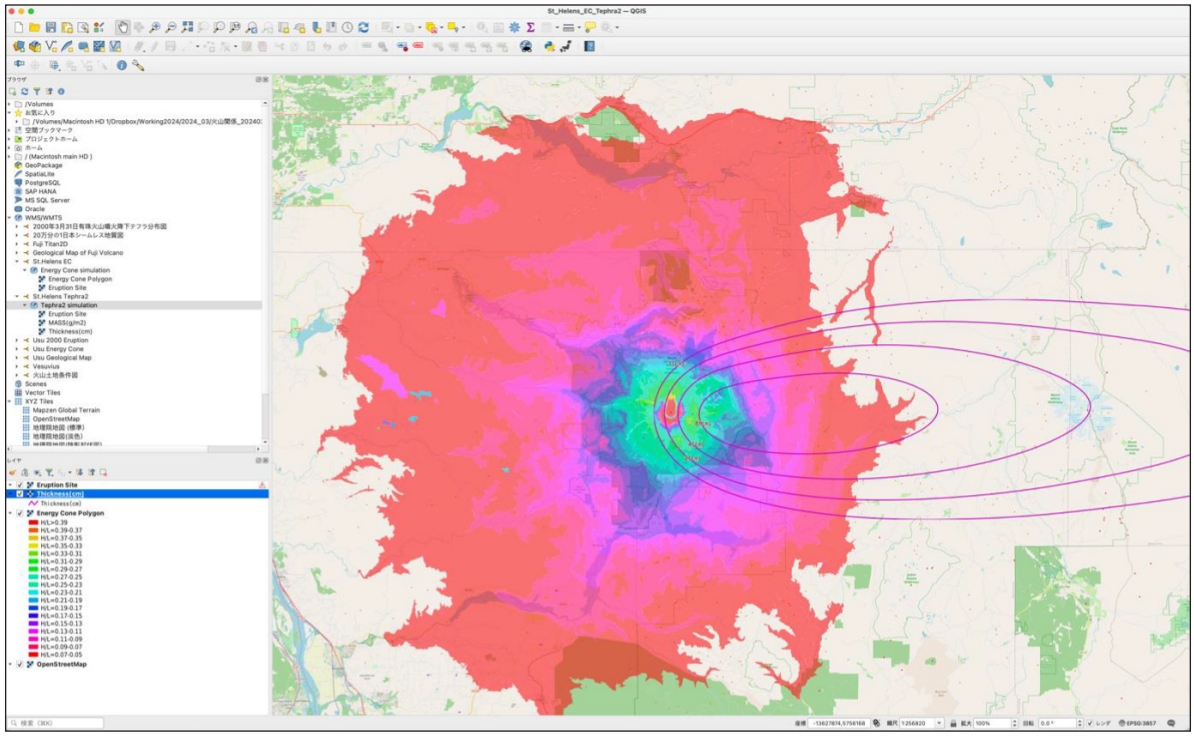

Figure 5: Energy Cone and Tephra2 simulation results at Mount St. Helens, USA, shown on QGIS software using WMS parameters. The simulation results are displayed directly from the Volcanic Hazards Information System.

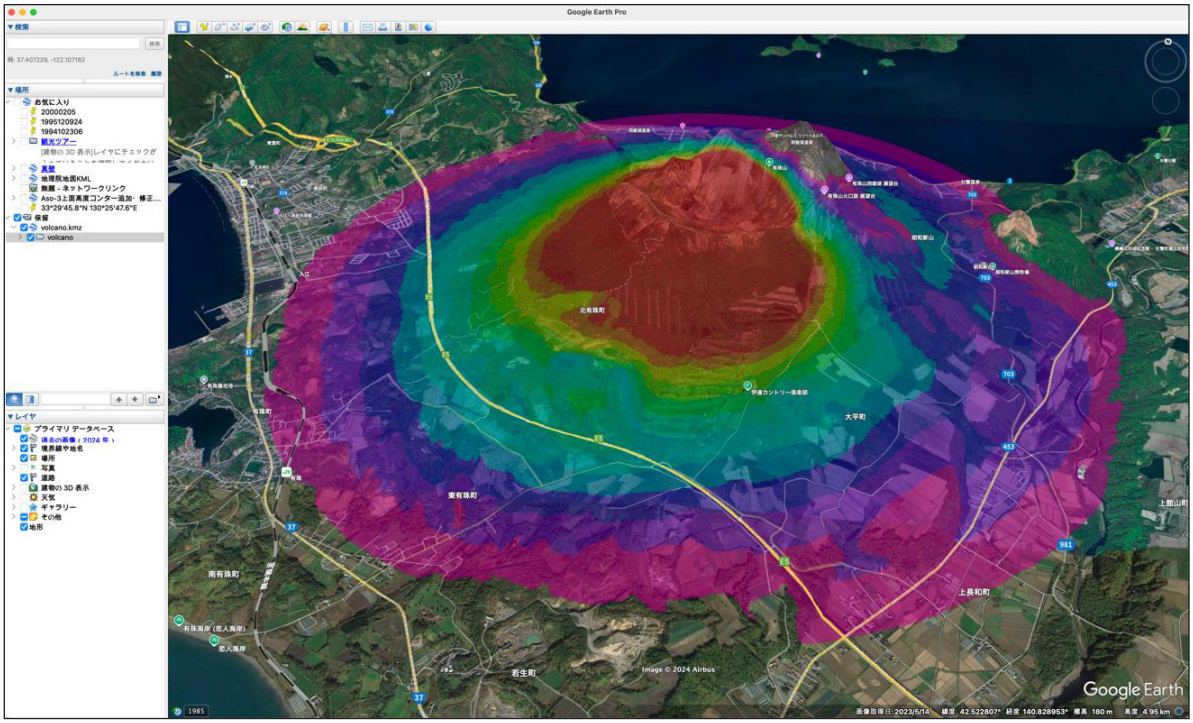

Figure 6: A 3D view of the Energy Cone simulation result at Usu Volcano, SW Hokkaido, Japan, using a KML downloaded file.

Figure 7: Simulation results for major volcanoes in the world are listed together with the results of the analysis of eruption parameters. The figure shows a tephra2 simulation result at Fuji Volcano, Japan. The GSI Maps (Standard) published by the Geospatial Information Authority of Japan are used.

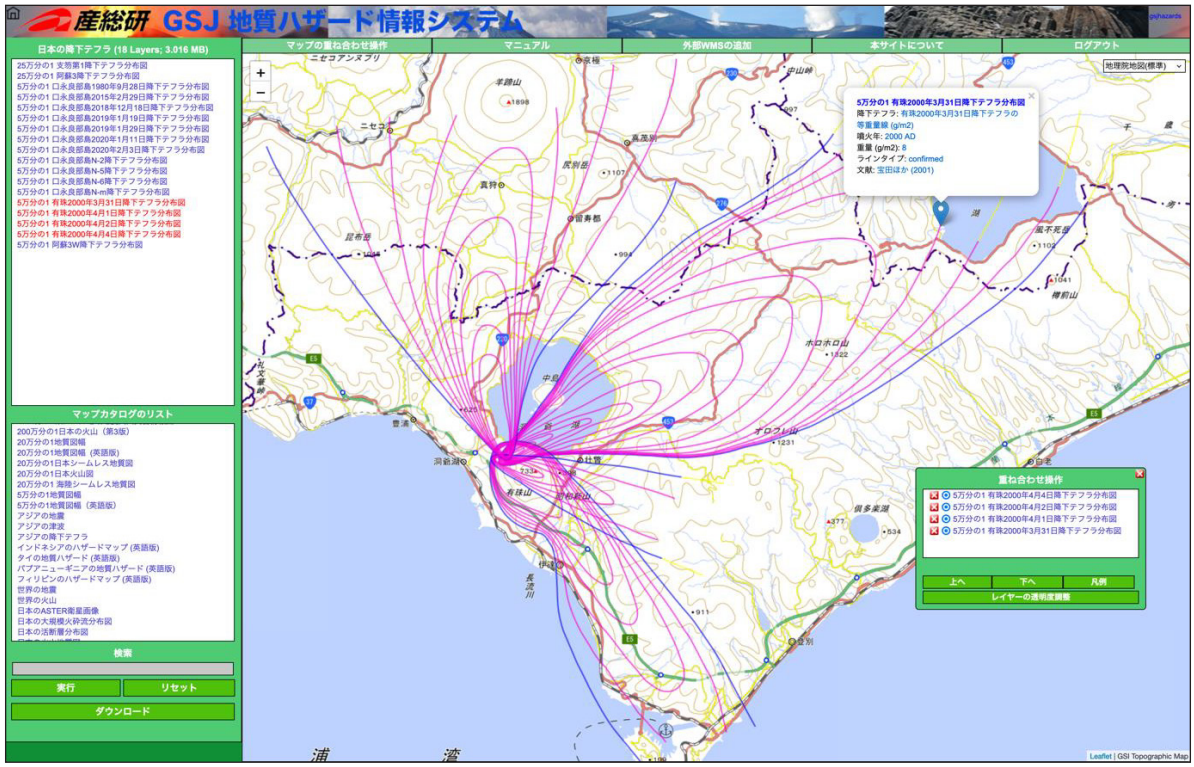

Figure 8: Digitized tephra falls distribution maps of 2000 eruptions (March 31, April 1, April 2, and April 4) at Usu Volcano, Japan, displayed on the Geological Hazards Information System. The GSI Maps (Standard) published by the Geospatial Information Authority of Japan are used.

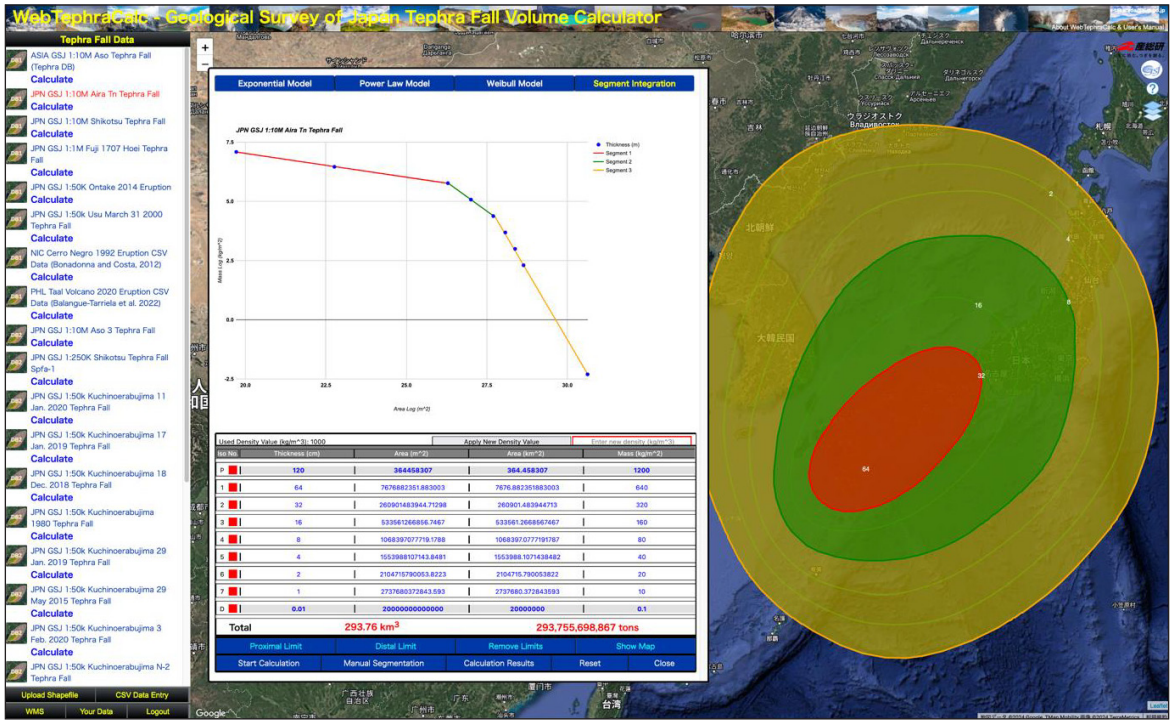

Figure 9: The online tephra fall volume calculator (WebTephraCalc). An example of tephra fall volume estimation of Aira Tn tephra fall (30ka) using the Segment Integration method (Takarada *et al*., 2016).

volcanic databases (https://gbank.gsj.jp/volcano/index_e.htm) such as Quaternary Volcanoes, Active Volcanoes, Geological Map of Volcanoes in Japan, Large-scale Eruption, Eruption Sequence, and Volcanic Ash Databases are planning. The Geological Hazards Information System and Volcanic Hazards Information System will be developed in collaboration with other projects on "Development of High-Precision Digital Geological Information for Hazard Prevention and Mitigation," such as Volcanic Craters DB, High-resolution Active Faults, Slope Disaster Risk Assessment, Digital Marine Geology, and Geological Digital Transformation projects.

The Geological Hazards Information System and the Volcanic Hazards Information System are expected to be used by many stakeholders such as researchers, students, local government workers, and Geopark staff members for their geological hazard assessments, revision of disaster prevention maps, education purposes, and other geological hazard related research undertakings.

ACKNOWLEDGMENTS

The Volcanic Hazards Information System Project has been developed with the support of the "Development of High-Precision Digital Geological Information for Hazard Prevention and Mitigation" Project since 2022.

REFERENCES

Bonadonna, C., Connor, C. B., Houghton, B. F., Connor, L., Byrne, M., Laing, A., & Hincks, T.K., 2005. Probabilistic modeling of tephra dispersal: Hazard assessment of a multiphase rhyolitic eruption at Tarawera, New Zealand. Journal of Geophysical Research: Solid Earth, 110. doi: 10.1029/2003JB002896.

Christen, M., Kowalski, J., & Bartelt, P., 2010. RAMMS: Numerical simulation of dense snow avalanches in three-dimensional terrain. Cold Regions Science and Technology, 63, 1-14.

Connor, C.B., 2006. Inversion is the solution to dispersion: understanding eruption dynamics by inverting tephra fallout. In: H.M. Mader, S. Coles, C.B. Connor, & L.J. Connor (Eds.), Statistics in Volcanology. Geological Society of London, IAVCEI1, 231–242.

Furukawa, R., & Nakagawa, M., 2010. Geological Map of Tarumae Volcano. Geological Map of Volcano no. 15, Geological Survey of Japan, AIST. 8 p.

Ishizuka, Y., Yamamoto, T., Nakano, S., & Takarada, S., 2022. Information dataset for craters of Fuji Volcano. Open-File Report of the Geological Survey of Japan, AIST, no.733.

Malin, M.C., &Sheridan, M.F., 1982. Computer-assisted mapping of pyroclastic surges. Science, 217, 637-640.

Pitman, E.B., Patra, A., Bauer, A., Sheridan, M., & Bursik, M., 2003. Computing debris flows and landslides. Physics of Fluids, 15, 3638-3646.

Pitman, E.B., & Le, L., 2005. A two-fluid model for avalanche and debris flows. Philosophical Transactions of the Royal Society A: Mathematical, Physical and Engineering Sciences,

363(1832), 1573-1601.

Pouliquen, O., & Forterre, Y., 2002. Friction law for dense granular flows: application to the motion of a mass down a rough inclined plane. Journal of fluid mechanics, 453, 133-151.

Sheridan, M.F., 1980. Pyroclastic block flow from the September 1976, eruption of La Soufrière volcano, Guadeloupe. Bulletin Volcanologique, 43, 397-402.

Sheridan, M.F., Stinton, A.J., Patra, A., Pitman, E.B., Bauer, A., & Nichita, C.C., 2004. Evaluating Titan2D mass-flow model using the 1963 Little Tahoma peak avalanches, Mount Rainier, Washington. Journal of Volcanology and Geothermal Research, 139, 89–102. doi: 10.1016/j.jvolgeores.2004.06.011.

Takada, A., Yamamoto, T., Ishizuka, Y., & Nakano, S., 2016. Geological Map of Fuji Volcano (Second Edition). Miscellaneous Map Series 12, Geological Survey of Japan, AIST, 56 p.

Takarada, S., 2017. The Volcanic Hazards Assessment Support System for the Online Hazard Assessment and Risk Mitigation of Quaternary Volcanoes in the World. Frontiers in Earth Science, 5:102. doi: 10.3389/feart.2017.00102.

Takarada, S., Yoshimoto, M., Kitagawa, J., Hiraga, M., Yamamoto, T., Kawanabe, Y., Takada, A., Nakano, S., Hoshizumi, H., Miyagi, I., Nishimura, Y., Miura, D., Hirose, W., Ishimaru, S., Kakihara Y., Endo, Y., Norota, S., Niida, K., Ishizuka, Y., Kudo, T., Aizawa, K., Honma, H., Egusa, M., Ishii, E., & Takahashi, R., 2001. Volcanic ash falls from the Usu 2000 eruption and situation at the source area. Bull. Geol. Surv. Japan, 52, 167-179.

Takarada, S., Oikawa, T., Furukawa, R., Hoshizumi, H., Itoh, J., Geshi, N., & Miyagi, I., 2016. Estimation of total discharged mass from the phreatic eruption of Ontake Volcano, central Japan, on September 27, 2014. Earth Planets and Space, 68, 1-9. doi 10.1186/s40623-016-0511-.